

พอรินที่จำเพาะต่อน้ำตาลโคโตโอลิโกแซคคาไรด์ (VhChiP) จากแบคทีเรียใน  
ทะเล *Vibrio harveyi* : การโคลน การแสดงออก  
และคุณลักษณะเฉพาะเชิงหน้าที่



นายวัชรินทร์ ชุมจันทร์

วิทยานิพนธ์นี้เป็นส่วนหนึ่งของการศึกษาตามหลักสูตรปริญญาวิทยาศาสตรดุษฎีบัณฑิต  
สาขาวิชาชีวเคมี  
มหาวิทยาลัยเทคโนโลยีสุรนารี  
ปีการศึกษา 2557

**CHITOLIGOSACCHARIDE-SPECIFIC PORIN  
(VhChiP) FROM THE MARINE BACTERIUM *VIBRIO  
HARVEYI*: CLONING, EXPRESSION AND FUNCTIONAL  
CHARACTERIZATION**

**Watcharin Chumjan**



**A Thesis Submitted in Partial Fulfillment of the Requirements for the  
Degree of Doctor of Philosophy in Biochemistry  
Suranaree University of Technology**

**Academic Year 2014**

**CHITOLIGOSACCHARIDE-SPECIFIC PORIN (*VhChiP*) FROM  
THE MARINE BACTERIUM *VIBRIO HARVEYI*: CLONING,  
EXPRESSION AND FUNCTIONAL CHARACTERIZATION**

Suranaree University of Technology has approved this thesis submitted in partial fulfillment of the requirements for the Degree of Doctor of Philosophy.

Thesis Examining Committee

---

(Assoc. Prof. Dr. Jatuporn Wittayakun)

Chairperson

---

(Assoc. Prof. Dr. Wipa Suginta)

Member (Thesis Advisor)

---

(Assoc. Prof. Dr. Albert Schulte)

Member

---

(Prof. Dr. Roland Benz)

Member

---

(Assoc. Prof. Dr. Jaruwan Siritapetawee)

Member

---

(Prof. Dr. Sukit Limpijumnong)

Vice Rector for Academic Affairs  
and Innovation

---

(Assoc. Prof. Dr. Prapun Manyum)

Dean of Institute of Science

นายวัชรินทร์ หุมจันทร์ : พอรินที่จำเพาะต่อน้ำตาลไคโตโอลิโกแซคคาไรด์ (*VhChiP*) จากแบคทีเรียในทะเล *Vibrio harveyi*: การโคลน การแสดงออกและลักษณะเฉพาะเชิงหน้าที่ (CHITOLIGOSACCHARIDE-SPECIFIC PORIN (*VhChiP*) FROM THE MARINE BACTERIUM *VIBRIO HARVEYI*: CLONING, EXPRESSION AND FUNCTIONAL CHARACTERIZATION) อาจารย์ที่ปรึกษา : รองศาสตราจารย์ ดร. วิภา สุจินต์, 224 หน้า.

การศึกษานี้รายงานถึงการแยกยีนส์ที่สังเคราะห์ไคโตพอรินที่มีชื่อว่า *VhChiP* จากจีโนมของแบคทีเรีย *Vibrio harveyi* โปรตีนไคโตพอรินที่มีในระบบของแบคทีเรียอีโคไล พบว่าเมื่อทำการแสดงออกของโปรตีนดังกล่าวสามารถทนต่อ SDS ว่องไวต่ออุณหภูมิ และมีความจำเพาะต่อแอนติบอดีชนิด anti-ChiP polyclonal antibody จากการตรวจหาคุณสมบัติการสร้างพอริน *VhChiP* ด้วยเทคนิค Planar Lipid Membrane (BLM) Reconstitution Technique แบบไม่มีตัวทำละลาย โปรตีน *VhChiP* สามารถแทรกตัวเข้าไปเพื่อฝังตัวอยู่ในผนังสองชั้นของลิปิดและมีการเปิดแบบสามหน่วยที่เสถียรด้วยค่าการนำผ่านของไอออน (Conductance, G (nS)) เท่ากับ  $1.9 \pm 0.07$  ในสารละลายบัฟเฟอร์ที่มี 1 โมลาร์ โพแทสเซียมคลอไรด์ การติดตามผลการวัดค่ากระแสในระดับ microsecond ของโปรตีนหนึ่งโมเลกุลทำให้ทราบว่ามีการแพร่ผ่านของไคโตโอลิโกแซคคาไรด์ ด้วยค่าคงที่การจับเท่ากับ  $500,000 \text{ M}^{-1}$  ซึ่งแสดงถึงการจับที่ดีที่สุดกับสับสเตรทชนิดไคโตเฮกซะไอส โดยที่ค่า On-rate ขึ้นตรงกับค่าต่างศักย์ไฟฟ้าที่ให้กับระบบ ในขณะที่เดียวกันก็ยังขึ้นอยู่กับด้านของการเติมน้ำตาล ผลดังกล่าวทำให้ทราบแน่ชัดว่าลักษณะของช่องที่อยู่ภายในโปรตีนมีลักษณะเป็นแบบไม่สมมาตร การทดลอง Liposome swelling assays แสดงให้เห็นถึงการแพร่ผ่านของน้ำตาลไคโตโอลิโกแซคคาไรด์ และยืนยันว่าไคโตพอรินเป็นช่องแพร่ผ่านที่จำเพาะต่อน้ำตาลไคโตโอลิโกแซคคาไรด์เท่านั้น

จากการศึกษาต่อไปยังแสดงให้เห็นถึงผลที่เกิดขึ้นตรงตำแหน่งภายในช่องแคบของไคโตพอรินที่ใช้สำหรับการแพร่ผ่านของไอออนและน้ำตาลไคโตเฮกซะไอส จากการเปลี่ยนตำแหน่งของ Trp136 ซึ่งเป็นกรดอะมิโนที่อยู่ตรงกลางของช่องพอรินเป็น Ala หรือ Asp ส่งผลให้เกิดการแพร่ผ่านของไอออนผ่านช่องพอรินเพิ่มสูงเล็กน้อย จากการวิเคราะห์กระแสของไอออนที่ถูกปิดกั้นด้วยโมเลกุลของน้ำตาลไคโตเฮกซะไอส ทำให้ทราบแน่ชัดว่าช่องพอรินมีลักษณะไม่สมมาตรต่อการแพร่ผ่านของน้ำตาลจากตำแหน่งของการเติมน้ำตาลและชนิดของความต่างศักย์ไฟฟ้าที่กระตุ้นเข้าไปในระบบ เมื่อเติมน้ำตาลไคโตเฮกซะไอส ที่ด้าน *Cis* พบว่าโปรตีนที่มีการเปลี่ยนแปลงของ

กรดอะมิโนตรงตำแหน่งของ Trp136 เป็น Ala และ Arg ค่า On-rate และ Off-rate ทำให้ทราบว่าเมื่อเปลี่ยนตำแหน่งของ Trp136 มีผลต่อการนำเข้าของน้ำตาลและความชอบในการจับเพิ่มขึ้นอย่างเห็นได้ชัดของช่องพอริน ยิ่งไปกว่านั้นการศึกษาด้วยการไทเทรตน้ำตาลและวัดด้วยวิธี Fluorescence spectroscopy แสดงให้เห็นว่าการแทนที่ Trp136 ส่งผลให้มีการลดลงของค่าคงที่ในการจับกับน้ำตาล ซึ่งผลกระทบมากที่สุดคือการแทนที่ด้วยหมู่ Ala (W136A) เนื่องจากโปรตีนดังกล่าวไม่สามารถจับกับน้ำตาลชนิดโคโตโอลิโกแซคคาไรด์ สายสั้นๆ ได้ เช่น GlcNAc<sub>3</sub>, GlcNAc<sub>4</sub> และ GlcNAc<sub>5</sub> ตามลำดับ จากการทดลองด้วยวิธี Liposome swelling assays แสดงให้เห็นถึงการลดลงของอัตราการแพร่ผ่านของน้ำตาลโคโตเฮกซะโอส กับชนิดของโปรตีนที่มีการเปลี่ยนตำแหน่งกรดอะมิโนของ W136 ทุกชนิดอีกด้วย *VhChiP* ยังแสดงคุณสมบัติเลือกไอออนชนิดประจุบวก (Cation selectivity) ด้วยอัตราส่วนของ  $P_{K^+}/P_{Cl^-}$  เท่ากับ 3.2 (-23 mV) ในสารละลายโพแทสเซียมคลอไรด์ ในทางตรงกันข้าม โปรตีนกลายพันธุ์ W136D มีการเปลี่ยนแปลงของการเลือกต่อไอออนและสามารถจับกับไอออนชนิดที่เป็นบวกเพิ่มมากขึ้นด้วยอัตราส่วนของ  $P_{K^+}/P_{Cl^-}$  เท่ากับ 4.2 (-28 mV) ในทางตรงกันข้าม โปรตีนกลายพันธุ์ W136R มีการลดลงของการเลือกต่อไอออนชนิดที่มีประจุเป็นบวกด้วยอัตราของ  $P_{K^+}/P_{Cl^-}$  เท่ากับ 2.74 (-20 mV) ดังนั้น จากผลการทดลองทำให้ทราบว่า Trp136 มีบทบาทสำคัญต่อการแพร่ผ่านของน้ำตาลผ่านช่องพอรินชนิด *VhChiP*

สาขาวิชาชีวเคมี  
ปีการศึกษา 2557

ลายมือชื่อนักศึกษา \_\_\_\_\_

ลายมือชื่ออาจารย์ที่ปรึกษา \_\_\_\_\_

ลายมือชื่ออาจารย์ที่ปรึกษาร่วม \_\_\_\_\_

ลายมือชื่ออาจารย์ที่ปรึกษาร่วม \_\_\_\_\_

WATCHARIN CHUMJAN : CHITOOOLIGOSACCHARIDE-SPECIFIC  
PORIN (*VhChiP*) FROM THE MARINE BACTERIUM *VIBRIO HARVEYI*:  
CLONING, EXPRESSION AND FUNCTIONAL CHARACTERIZATION  
THESIS ADVISOR : ASSOC. PROF. WIPA SUGINTA, Ph.D. 224 PP.

BLACK LIPID MEMBRANE/*VIBRIO HARVEYI*/VHCHIP/PORIN

This study reports isolation of the gene encoding chitoporin, namely *VhChiP*, from the genome of *Vibrio harveyi*. The *E. coli* expressed *VhChiP* was found to be SDS-resistant, heat-sensitive, and selectively reacting only with anti-ChiP polyclonal antibodies. The pore-forming property of *VhChiP* was investigated using solvent-free planar lipid membrane reconstitution technique. *VhChiP* inserted into artificial membranes and formed a stable trimeric channel with average single conductance of  $1.9 \pm 0.07$  nS in 1 M KCl. Single channel recordings in the presence of chitosugars with different chain lengths resolved translocation of chitooligosaccharides at microsecond time resolution. The greatest rate was observed for chitohexaose, with the binding constant of  $K = 500,000 \text{ M}^{-1}$ . The on-rates of chitosugars depend on applied voltages, as well as the side of the sugar addition, clearly indicating the inherent asymmetry of the *VhChiP* lumen. Liposome swelling assays showed only permeation of chitooligosaccharides, indicating that *VhChiP* is a chitooligosaccharide-specific channel.

Further studies reported the effect of the constriction zone on ions transport and chitohexaose translocation. Mutation of Trp136, the amino acid residue locating in the middle of the pore, to Ala or Asp slightly enhanced ion conductivity of the *VhChiP* channel. Noise analysis of the ion current in presence of chitohexaose

confirmed that the *VhChiP* channel asymmetrically responded to side of sugar addition, as well as applied electrical field. Addition of chitohexaose on the *cis* side of mutants W136A and W136R resulted in great increases in both on-rate and off-rate, suggesting that this mutation of Trp136 particularly interfered sugar accessibility, as well as binding affinity of the channel. In addition, titration measurements using fluorescence spectroscopy showed that the Trp136 substitution caused decreased in the binding constant. The highest effect was observed for the alanine mutant, for which the W136A could not bind to short chain chiooligosaccharides, including GlcNAc<sub>3</sub>, GlcNAc<sub>4</sub> and GlcNAc<sub>5</sub>, respectively. Liposome swelling assay also showed reduced permeability rate of chitohexaose with all the W136 mutants. *VhChiP* showed selectivity toward cation with the  $P_{K^+}/P_{Cl^-}$  ratio of about 3.2 (-23 mV) in a bulk solution of KCl. In contrast, with the mutant W136D, the ion selectivity was changed and attracted more cation ( $K^+$ ) with the  $P_{K^+}/P_{Cl^-}$  ratio of about 4.2 (-28 mV). On the other hand, the W136R mutant decreased selectivity towards cation with the  $P_{K^+}/P_{Cl^-}$  ratio of about 2.74 (-20 mV). Such result suggested that Trp136 played an important role for sugar translocation through the *VhChiP* channel.

School of Biochemistry

Academic Year 2014

Student's Signature \_\_\_\_\_

Advisor's Signature \_\_\_\_\_

Co-advisor's Signature \_\_\_\_\_

Co-adviser's Signature \_\_\_\_\_

## ACKNOWLEDGEMENTS

I would like to express my gratitude to both of my supervisors Assoc. Prof. Dr. Wipa Suginta and Prof. Dr. Mathias Winterhalter, for giving me the opportunity to work on this project. Their guidance, support and ideas made this work interesting and gave me high inspiration to do this research subject. Throughout the thesis, they provided their valuable time for guiding and correcting, which made Ph.D. study successful.

Furthermore, I would like to thank my co-supervisors from Suranaree University of Technology (SUT), Nakhon Ratchasima, Thailand and Jacobs University Bremen (JUB), Bremen, Germany:

- 1) Assoc. Prof. Dr. Albert Schulte from the School of Chemistry for his supervision on the knowledge and ideas on the Electrochemistry. His great support and input helped me to perform black lipid bilayer membrane experiments properly. I am also grateful for his kind support throughout my study at Suranree University of Technology, Nakhon Ratchasima, Thailand.
- 2) Prof. Dr. Roland Benz from the Department of Biophysics for passing on his great expertise in black lipid bilayer membrane. Also, he helped with data discussion about multiple insertion and sugar translocation through *VhChiP* channel.

I would like to thank all the lectures of the School of Biochemistry at SUT for passing on to me their biochemistry knowledge and biochemical lab techniques, which were later found to be useful for my Ph.D. project development.

I wish to extend warmest thanks to my colleagues at the Biochemistry-Electrochemistry Research Unit, SUT and the Biophysic Research Group, JUB for helping me to get through difficult times, and for all the emotional support, friendship, entertainment, and encouragement to carry on their provided.

I would like to express my gratitude to the Biochemistry-Electrochemistry Research Unit and the Biophysic Research group, JUB, for providing excellent research facilities, including all equipment, consumables and chemicals that were necessary to study the multiple or single channel insertions and sugar translocation through *Vh*ChiP channel. Most importantly, I would like thank the Commission of Higher Education, Ministry of University Affairs (MUA) through a grant from the Ph.D. Sandwich Scholarship Program and the Deutscher Akademischer Austausch Dienst e.V. (DAAD, German Academic Exchange Service) for the financial support during my one-year research in Germany through a DAAD scholarship.

Finally, special thanks goes to my parents for their support, their understanding and their love, that they provide through all of my life. Without them, I would not be what I am today.

Watcharin Chumjan

# CONTENTS

|   | <b>Page</b> |
|---|-------------|
| ABSTRACT IN THAI.....   | I           |
| ABSTRACT IN ENGLISH .....   | III         |
| ACKNOWLEDGEMENTS.....   | V           |
| CONTENTS.....   | VII         |
| LIST OF TABLES .....  | XI          |
| LIST OF FIGURES .....   | XIII        |
| LIST OF ABBREVIATIONS.....  | XVIII       |
| <b>CHAPTER</b>  |             |
| <b>1 INTRODUCTION.....</b>  | <b>1</b>    |
| 1.1 General introduction into Gram-negative bacteria and<br>their outer membrane proteins ..... | 1           |
| 1.2 Marine bacteria and their function in chitin uptake .....                                   | 16          |
| 1.3 Techniques for functional analysis of bacterial outer<br>membrane proteins .....            | 20          |
| 1.4 Research objectives .....   | 33          |
| <b>2 MATERIAL AND METHODS.....</b>  | <b>35</b>   |
| 2.1 Design of oligonucleotide primers .....   | 35          |
| 2.2 Expression vectors and bacterial host cells.....  | 35          |
| 2.3 Chemicals and reagents.....   | 36          |
| 2.4 Instrumentation .....   | 37          |

## CONTENTS (Continued)

|   | <b>Page</b> |
|---|-------------|
| 2.5 Methodology.....  | 37          |
| 2.5.1 Growth and maintenance of <i>V. harveyi</i> 650 strain<br>and genomic DNA isolation from <i>V. harveyi</i> type<br>strain 650.....    | 37          |
| 2.5.2 PCR amplification of the cDNA encoding <i>VhChiP</i> .....  | 38          |
| 2.5.3 Cloning of DNA encoding <i>VhChiP</i> into pET23d(+)<br>and confirmation of DNA insert .....  | 40          |
| 2.5.4 Expression and purification of recombinant <i>VhChiP</i><br>in <i>E. coli</i> BL21 (DE3) omp8 rosetta strain .....                    | 41          |
| 2.5.5 Production of anti- <i>VhChiP</i> polyclonal antibodies<br>and immunoblotting analysis .....  | 43          |
| 2.5.6 Expression of <i>VhChiP</i> porin on the native bacterial strain<br><i>Vibrio harveyi</i> 650 by induction with insoluble chitin..... | 45          |
| 2.5.7 PCR primers of mutants (W161A and W161F).....   | 45          |
| 2.5.8 Single channel conductance, voltage dependence<br>and ion selectivity analysis of wild-type and mutated<br>chitoporins.....           | 49          |
| 2.5.9 Titration experiments of <i>VhChiP</i> and its mutants via<br>intrinsic fluorescence spectroscopy.....                                | 54          |
| 2.5.10 Liposome swelling assay .....  | 56          |
| 2.5.11 Temperature measurement.....   | 57          |

## CONTENTS (Continued)

|          |   | Page |
|----------|---|------|
| <b>3</b> | <b>RESULTS</b> .....  | 59   |
|          | 3.1 Gene identification, cloning, expression and<br>protein purification .....  | 59   |
|          | 3.2 Single channel properties of <i>Vh</i> ChiP channel with<br>uncharge molecules translocation (chitooligosaccharides) .....                        | 71   |
|          | 3.3 Single channel properties of <i>Vh</i> ChiP with translocation<br>of charge molecules (chitosan hexamer) .....                                    | 87   |
|          | 3.4 Site directed mutagenesis on the constriction zone of <i>Vh</i> ChiP channel<br>for ion transport and sugar translocation .....                   | 96   |
|          | 3.5 Ion selectivity of WT and mutants .....   | 108  |
|          | 3.6 Fluorescence spectroscopy .....   | 111  |
|          | 3.7 Liposome swelling assay .....   | 116  |
|          | 3.8 Temperature dependence on the sugars translocation through<br><i>Vh</i> ChiP and its mutated channels .....                                       | 118  |
| <b>4</b> | <b>DISCUSSION</b> .....   | 125  |
|          | 4.1 Investigation of mechanism uptake of chitooligosaccharides<br>through chitoporin channel from the marine bacterium<br><i>Vibrio harveyi</i> ..... | 125  |
|          | 4.2 Binding kinetics of uncharge molecules translocation through<br><i>Vh</i> ChiP channels (chitooligosaccharides) .....                             | 126  |

## CONTENTS (Continued)

|  | Page |
|--|------|
| 4.3 Binding kinetics of charge molecules translocation<br>through <i>Vh</i> ChiP channels (chitosan hexaose) ..... | 131  |
| 4.4 Site directed mutagenesis and sugar translocation<br>(chitohexaose) .....                                      | 134  |
| 4.4 Temperature dependence on rates of sugar translocation<br>through <i>Vh</i> ChiP channel .....                 | 139  |
| <b>5 CONCLUSION</b> .....  | 141  |
| REFERENCES .....   | 144  |
| APPENDICES .....   | 161  |
| APPENDIX A COMPETENT CELL PREPARATIONS AND<br>PLASMID TRANSFORMATIONS .....  | 162  |
| APPENDIX B PREPARATION OF SOLUTIONS AND REAGENTS .....   | 164  |
| APPENDIX C CURRENT-VOLTAGE (I/V) CURVES .....  | 174  |
| APPENDIX D AMINO ACID SEQUENCES .....  | 177  |
| APPENDIX E SUPPORTING INFORMATIONS .....   | 180  |
| APPENDIX F PUBLICATIONS .....  | 192  |
| CURRICULUM VITAE .....   | 224  |

## LIST OF TABLES

| Table   | Page |
|---|------|
| 2.1 Bacterium strain and the plasmids .....   | 36   |
| 2.2 Primers for site-directed mutagenesis .....   | 46   |
| 2.3 The PCR reaction was used for site-directed mutagenesis .....   | 47   |
| 2.4 The PCR condition was used for site-directed mutagenesis .....  | 48   |
| 3.1 Substrate specificity of <i>VhChiP</i> .....  | 86   |
| 3.2 Effect of pH on the binding constant of chitoporin<br>from <i>Vibrio harveyi</i> 650 towards uncharged and<br>charged chitooligosaccharides .....                         | 92   |
| 3.3 Single channel conductance of <i>VhChiP</i> wild-type (WT) and mutant .....   | 101  |
| 3.4 Comparison of the rates and the equilibrium of binding constant ( $K$ , $M^{-1}$ )<br>of <i>VhChiP</i> wild-type (WT) and mutants for chitohexaose .....                  | 107  |
| 3.5 Ionic selectivity of WT and its mutant .....  | 110  |
| 3.6 Comparison the dissociation constants ( $K_D$ ) of <i>VhChiP</i> (WT)<br>and its mutants with chitooligosaccharides as a substrate<br>via fluorescence spectroscopy ..... | 115  |
| 3.7 Energy barrier of WT and its mutants .....  | 124  |
| 4.1 Comparison of the rates and the binding kinetics of <i>VhChiP</i><br>with those of other sugar-specific porins .....  | 130  |

**LIST OF TABLES (Continued)**

| <b>Table</b> |  | <b>Page</b> |
|--------------|--|-------------|
| S1           | The ionic selectivity of WT and its mutants. Single channel insertion was performed as described in 5.2.....   | 185         |
| S2           | The dissociation constant ( $K_D$ ) of <i>VhChiP</i> (WT) and its mutants with chitooligosaccharides (GlcNAc <sub>5</sub> -GlcNAc <sub>1</sub> ) using fluorescence spectroscopy ..... | 191         |



## LIST OF FIGURES

| Figure  | Page |
|---|------|
| 1.1 The multi-layered cell wall of a Gram-negative bacterial cell .....   | 2    |
| 1.2 Structure of an <i>E. coli</i> OmpF monomer.....  | 4    |
| 1.3 Schematic representation of the current trace of an <i>E. coli</i> OmpF .....   | 6    |
| 1.4 Typical traces of the ionic current through a single<br>trimeric OmpF protein pore .....  | 8    |
| 1.5 Cross-section of maltoporin monomer.....  | 11   |
| 1.6 Current recordings of a single maltoporin channel<br>at various maltohexaose concentrations.....  | 13   |
| 1.7 Schematic drawing of a single-sided sugar addition lipid bilayer<br>experiment with maltoporin.....   | 15   |
| 1.8 (A) Chitinase-assisted chitin degradation as driven by<br>marine bacteria for the utilization of chitin for cellular metabolism<br>and (B) the chemical structure of chitooligosaccharides products<br>of enzymatic chitin breakdown..... | 18   |
| 1.9 Model of the chitin degradation cascade of the marine<br>bacterium <i>Vibrio harvii</i> .....   | 19   |
| 1.10 Schematic representation of the electrophysiological/biophysical set-up for<br>planar lipid bilayer experiments on porin channels that were<br>isolated from outer membrane of bacterial cells.....                                      | 22   |
| 1.11 Schematic representation of the current vs. time trace .....   | 24   |

## LIST OF FIGURES (Continued)

| <b>Figure</b>   | <b>Page</b> |
|---|-------------|
| 1.12 Intrinsic biochemical fluorophores .....   | 26          |
| 1.13 Absorption and emission spectra of the fluorescent amino acids<br>in water at pH 7.0.....                      | 26          |
| 1.14 Outer membrane proteins (Omps) in detergent .....  | 28          |
| 1.15 Comparison of dynamic and static quenching .....   | 30          |
| 3.1 Alignment of the putative <i>V. harveyi</i> chitoporin sequence<br>with other sugar-specific porins.....        | 61          |
| 3.2 The Swiss-Model 3D-structure of <i>V. harveyi</i> chitoporin.....   | 63          |
| 3.3 Agarose gel electrophoresis of genomic DNA from <i>V. harveyi</i> 650 .....                                     | 65          |
| 3.4 SDS-PAGE analysis of <i>V. harveyi</i> chitoporin .....   | 67          |
| 3.5 Cross-reactivity of <i>VhChiP</i> antiserum with other outer membrane porins .....                              | 70          |
| 3.6 Single channel recordings of chitoporin in artificial lipid membranes.....                                      | 72          |
| 3.7 Effect of chitooligosaccharides on chitoporin ion currents .....  | 74          |
| 3.8 Effects of chitohexaose diffusion on subunit closure .....  | 77          |
| 3.9 Effects of transmembrane potentials and sugar concentrations<br>on ion currents.....                            | 80          |
| 3.10 Effects of transmembrane potentials and sugar concentrations<br>on ion currents.....                           | 81          |
| 3.11 Analysis of ion current blockages at various transmembrane<br>potentials and chitohexaose concentrations ..... | 83          |

## LIST OF FIGURES (Continued)

| Figure   | Page |
|--|------|
| 3.12 Binding curve of 0-10 $\mu$ M chitohexaose to <i>VhChiP</i> .....   | 85   |
| 3.13 Chemical structure of chitohexaose and chitosan hexamer .....   | 87   |
| 3.14 Influence of potential polarity on the translocation of<br>cationic chitosan hexamer .....  | 88   |
| 3.15 Binding curve for the interaction of <i>VhChiP</i> with chitosan hexamer .....  | 90   |
| 3.16 The channel current blockages at cationic chitosan hexamer .....  | 93   |
| 3.17 Voltage dependence of the on-rate ( $k_{on}$ ) and off-rate ( $k_{off}$ )<br>of chitosan hexamer through <i>VhChiP</i> channel .....  | 95   |
| 3.18 The modelled structure of the monomeric <i>VhChiP</i> and its mutant.....   | 97   |
| 3.19 Protein expression, purification and immuno-blotting analysis<br>of WT and its mutants.....   | 98   |
| 3.20 Single channel insertion of WT and its mutants .....  | 100  |
| 3.21 The effect of transmembrane potentials at various concentrations<br>of chitohexaose on single channel insertion of trimeric WT<br>and its mutants .....                               | 102  |
| 3.22 The analysis of ion current blockages at <i>cis</i> /-100 mV<br>or <i>trans</i> /+100 mV side addition of chitohexaose on<br>the single channel insertion of WT and its mutants ..... | 104  |
| 3.23 Binding curve and Lineweaver-Burk plots of WT and<br>its mutants with chitohexaose .....  | 106  |

## LIST OF FIGURES (Continued)

| Figure  | Page |
|---|------|
| 3.24 Representation of the plot between zero-current membrane potentials ( $V_m$ ) and the ratio of salt concentrations on <i>trans</i> -side of KCl bulk solution.....                               | 109  |
| 3.25 Amino acid sequence and a cross-section of the modelled structure of <i>V. harveyi</i> monomeric chitoporin .....  | 112  |
| 3.26 Comparison of the emission spectra of WT and its mutants .....   | 114  |
| 3.27 Liposome swelling assays.....  | 117  |
| 3.28 Typical ion current recordings through WT and its mutants at 10 °C (A), 15 °C (B) and 20 °C (C) in the presence of chitohexaose at <i>cis</i> -side, -100 mV .....                               | 118  |
| 3.29 Number of binding events of chitohexaose in the channel of WT and its mutants as a function of temperature from 5 °C to 20 °C .....  | 119  |
| 3.30 The residence time of chitohexaose in the channel of WT and its mutants as a function of temperature from 5 °C to 30 °C.....   | 120  |
| 3.31 The Arrhenius plot of $k_{on}$ (A ( <i>cis</i> ) and B ( <i>trans</i> )) and $k_{off}$ as function of temperature from 5 °C to 20 °C represented in a linear slope with WT and its mutants ..... | 121  |
| S1 Identification of <i>V. harveyi</i> chitoporin by mass spectrometry.....   | 180  |
| S2 Liposome swelling assays.....  | 181  |
| S3 Effects of concentrations of small chitosugars on ion current blockages ....   | 182  |

## LIST OF FIGURES (Continued)

| Figure | Page   |
|--------|--|
| S4     | Effect on ion currents of chitooligosaccharide diffusion into chitoporin ..... 183   |
| S5     | Plot between zero-current membrane potentials ( $V_m$ ) and the ratio of salt concentrations on <i>trans</i> - and <i>cis</i> -side addition of KCl bulk solution for <i>VhChiP</i> channel (WT) ..... 184 |
| S6     | Plot between zero-current membrane potentials ( $V_m$ ) and the ratio of salt concentrations on <i>cis</i> -side addition of KCl bulk solution for WT and its mutant ..... 186                             |
| S7     | The energy barriers obtained from $k_{on}$ for chitohexaose on <i>cis</i> or <i>trans</i> side addition of A) W136A and W136F and B) W136R and W136D compared to its wild type (WT) pore ..... 187         |
| S8     | The energy barriers obtained from $k_{off}$ for chitohexaose on <i>cis</i> or <i>trans</i> side addition of A) W136A and W136F and B) W136R and W136D compared to its wild type (WT) pores ..... 188       |
| S9     | The Arrhenius plot of conductance as a function of temperature from 5 °C to 30 °C gave a linear slope with an energy barrier of about 7.8 kT (-100 mV) and 7.4 kT (+100 mV) ..... 189                      |

## LIST OF ABBREVIATIONS

|                |   |  |
|----------------|---|--|
| BLM            | = | Black lipid membrane                                       |
| Omp            | = | Outer membrane proteins                                    |
| OmpF           | = | Outer membrane protein F                                   |
| OmpN           | = | Outer membrane protein N                                   |
| LamB           | = | Maltose-specific porin                                     |
| ScrY           | = | Sucrose-specific porin                                     |
| OprB           | = | Carbohydrate-selective porin <i>Pseudomonas aeruginosa</i> |
| WT             | = | Wild-type  |
| ChiP           | = | Chitoporin   |
| VhChiP         | = | <i>Vibrio harveyi</i> chitoporin                           |
| SDS-PAGE       | = | Polyacrylamide gel electrophoresis                         |
| PCR            | = | Polymerase chain reaction                                  |
| M <sub>r</sub> | = | Molecular weight   |
| Da             | = | Dalton   |
| rpm            | = | Revolutions per minute                                     |
| °C             | = | Degree celsius   |
| µg/ml          | = | Microgram per milliliter                                   |
| ng/µl          | = | Nanogram per microliter                                    |
| µl             | = | Microliter   |
| U/L            | = | Units per litre  |
| DPhPC          | = | Diphytanoyl-phosphatidylcholine                            |

**LIST OF ABBREVIATIONS (Continued)**

|                     |   |                                   |
|---------------------|---|-----------------------------------|
| GlcNAc              | = | <i>N</i> -acetyl-glucosamine      |
| GlcNAc <sub>2</sub> | = | Chitobiose                        |
| GlcNAc <sub>3</sub> | = | Chitotriose                       |
| GlcNAc <sub>4</sub> | = | Chitotetraose                     |
| GlcNAc <sub>5</sub> | = | Chitopentaose                     |
| GlcNAc <sub>6</sub> | = | Chitohexaose                      |
| IPTG                | = | Isopropyl-β-D-thiogaltopyranoside |
| BSA                 | = | Bovine serum albumin              |
| SDS                 | = | Sodium dodecyl sulphate           |
| KCl                 | = | Potassium chloride                |
| LDAO                | = | Lauryldimethylamine-oxide         |
| Octyl-POE           | = | n-Octylpolyoxyethylene            |
| PB                  | = | Phosphate buffer                  |
| PBS                 | = | Phosphate-buffered saline         |

# CHAPTER I

## INTRODUCTION

### 1.1 General introduction into Gram-negative bacteria and their outer membrane proteins

Bacteria are widespread microorganisms that, in contrast to eukaryotic cells, do not have a membrane-bound nucleus or other membrane-surrounded intracellular organelles like mitochondria and endoplasmic reticulum (Adl *et al.*, 2005). In general, a first classification of bacteria is into Gram-positive and Gram-negative bacteria. The major structural characteristic of Gram-positive bacteria is their plasma membrane covered with a thick wall of peptidoglycan. In contrast, the cytoplasm of Gram-negative bacteria is confined by a double-walled cell-envelope that is made up of inner and outer lipid bilayer membranes, and the periplasmic space sandwiched in between the two hydrophobic layers (Beveridge 1981, Nikaido and Rosenberg 1985). The cell wall of Gram-negative bacteria defines the shape of the microorganism. A further function of the cell wall is to separate physically the intracellular matrix ("cytosol") from the close cellular environment. To control the exchange of electrolytes, proteins, nutrients and metabolic products across the hydrophobic barrier has to be efficiently controlled. Accordingly, bacterial cell walls have integral protein systems incorporated to facilitate the flux of charged and uncharged hydrophilic (bio-) chemical species. Those transport units may work as carriers, pumps or channels for

ions, proteins and carbohydrates. Figure 1.1 shows the schematic illustration of typical structure of the cell wall of a Gram-negative bacterium. An important feature of the outer membrane are membrane proteins (Omp's), which form monomeric- or trimeric channels (so-called porins) used by a variety of hydrophilic compounds for translocation across into the interior of a bacterial cell.

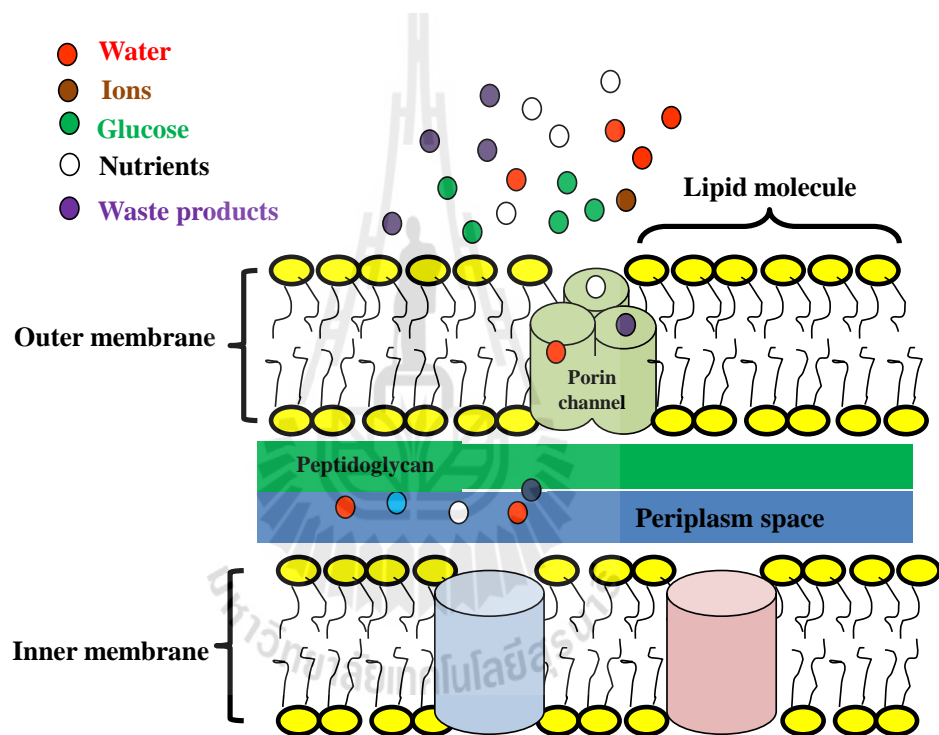


**Figure 1.1** The multi-layered cell wall of a Gram-negative bacterial cell. Characteristic for the outer membrane are trimeric outer membrane protein channels, which also are called porins. Porins allow the exchange of water soluble molecules across the outer membrane.

One important class are general diffusion porins allowing the permeation via non-specific transmembrane pores to which molecules can be shuttled via simple diffusion. The driving force for passive diffusion is a concentration gradient between the in- and out-side of the membrane. The rate limiting factors for transport across the membrane is not only the size of the traveling molecule, but depends also on the charge distribution, steric arrangement of the pore interior, Van der Waals interaction or hydrogen bonding. To date, the best studied bacterial porin is the outer membrane protein channel *E. coli* OmpF. Since OmpF is often used as a comparative standard for structural and functional analysis of other porins, a brief summary of the OmpF properties is provided in the following section.

*E. coli* OmpF is an integral membrane protein located in the outer membrane of the bacterium and considered as a non-specific pore for the diffusion of small polar molecules across the hydrophobic insulating bilayer structure of the outer membrane. Spherical species with a molecular weight up to 600 Da could pass through the OmpF pores and enter the bacterial cytoplasm and compounds shuttling between the extra- and intracellular space of the bacterium. The transported molecules includes small ions (e.g.  $K^+$ ,  $Na^+$ ,  $Ca^{2+}$ ,  $Cl^-$  etc.), glucose, ascorbate, amino acids and other nutrients as well as metabolic waste products (Cowan *et al.*, 1995; Phale *et al.*, 2001; Berkane *et al.*, 2005).

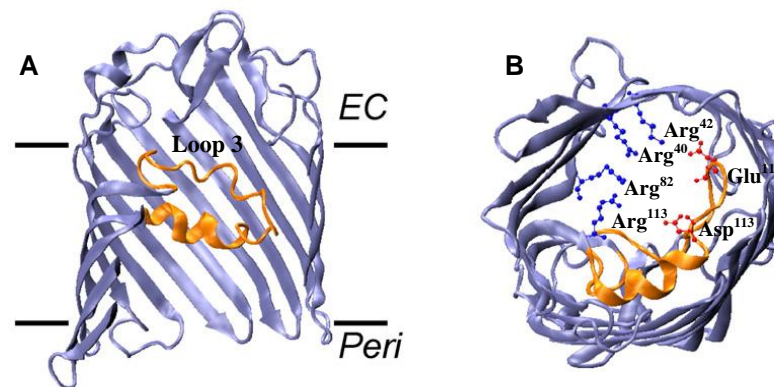


**Figure 1.2** Structure of an *E. coli* OmpF monomer. (A) Side view of a single  $\beta$ -barrel of the OmpF trimers to highlight the orientation of the protein arrangement in the outer membrane (“EC” is the extracellular side, and “Peri” the periplasmic side of the outer membrane); the front part of the strands has are not shown to make a view on the constricting L3 loop (orange) possible. (B) Cross-section of the OmpF monomer observed from the side of the periplasm; clearly visible is the narrowing of the porin channel by the internal pore residues in the constriction zone. Responsible residues the acidic residues of the L3 loop (in red) and a cluster of basic amino acids of the opposite barrel wall (in blue). (Cowan *et al.*, 1995)

The high resolution structure revealed that the active OmpF exists as trimeric subunits within the outer cell membrane (Cowan *et al.*, 1992). The individual monomers of OmpF consist of a 16-stranded  $\beta$ -barrel with a central hydrophilic pore and eight extracellular loops (Cowan *et al.*, 1992). Figure 1.2A illustrates the configuration of one of the OmpF monomers, three of the monomers will form the active trimeric agglomerate that is the functional unit in support of a cytosolic uptake

of dissolved nutrients (schematically in Figure 1.1). As seen from Figure 1.2A, the OmpF monomer has about half the way inside of the pore an internal loop, which narrows at this location the protein channel, and thus presents a hindrance for the membrane translocation of molecules. The “restriction zone” formed by the L3 loop is better observable in a cross-sectional graphical illustration of the OmpF porin (Figure 1.2B). Apparently, specific acidic amino acid residues at a certain region of loop L3 together with basic amino acid residues located at the barrel wall opposite to loop L3 are the functional entities that are responsible for the constitution of a restriction of molecular diffusion (Phale *et al.*, 2001).

Extracted and refolded trimeric OmpF can be reconstituted as functional channel into artificial lipid bilayer (so-called “black” lipid membranes, BLM’s). Reconstitution experiments are usually carried out in special BLM chambers in which the lipid bilayer spans a small hole in an insulating polymer partition and is exposed to a buffer solution (e.g. 1 M KCl) at both sides. When the voltage-induced membrane current through a freshly formed stable lipid bilayer is recorded at a given membrane potential  $V_m$  (for technical details see the later section on the BLM technique), zero current or close to zero is the indication of an intact “porin-free” lipid bilayer. The appearance of a step-like current increase upon the addition of diluted porin stock solution to the buffer electrolyte is, on the other hand, a sign of the insertion of a fully open OmpF trimeric protein channel. Interestingly, OmpF channels are prone to shut upon the exposure to higher voltage (e.g. 150-200 mV) (e.g. Mahendran *et al.*, 2009). Channel closure takes place sequentially with one of the three monomers closing after another. Figure 1.3 is a schematic representation of the predictable outcome of a BLM measurement with OmpF as the studied membrane incorporating porin. The average

single channel conductance can be calculated either from the measured magnitude of an insertion-induced current step and the known value of the membrane potential during insertion or from the slope of a plot of the membrane current as the function of the membrane potential. The literature value for the OmpF single channel conductance is about 4 nS in 1 M KCl (Kreir *et al.*, 2008). OmpF is known to be a general diffusion pore that obeys Ohm's Law, changes in the membrane potential and changes in the type and concentration of the electrolyte will of course modulate the observed single- or multiple-channel membrane currents at otherwise fixed conditions.

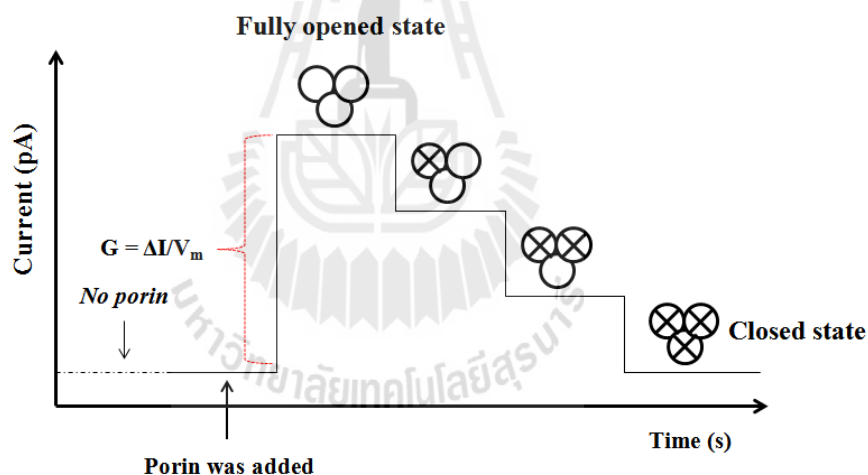


**Figure 1.3** Schematic representation of the current trace that will be obtained when a single trimeric unit of an *E. coli* OmpF inserts from a buffer solution of e.g. 1 M KCl into an artificial lipid bilayer and current flow through the membrane is recorded at a membrane potential  $V_m$  in the mV range. Ohm's law allows calculation of the porin conductance.

In a recording as schematically shown in Figure 1.3 the current through an OmpF pore is caused by the flux of the ions that are present in the measuring buffer solution. These, for example, may be hydrated potassium cations and chloride anions in the case of a 1 M KCl as electrolyte solution. The situation is very different when comparably larger molecules as for instance certain antibiotics or sugars are added at low concentration as a supplement to the measuring buffer. Large molecule will penetrate slowly thus inhibiting the flux of ions. For this reason, a decreased membrane current will be seen during the residence time of e.g. an antibiotic molecule in the pore. Figure 1.4 displays the outcome of a nice representative bacterial porin study that addressed specifically the translocation of antibiotics of different sizes and charges through single OmpF units (Mahendran *et al.*, 2010).

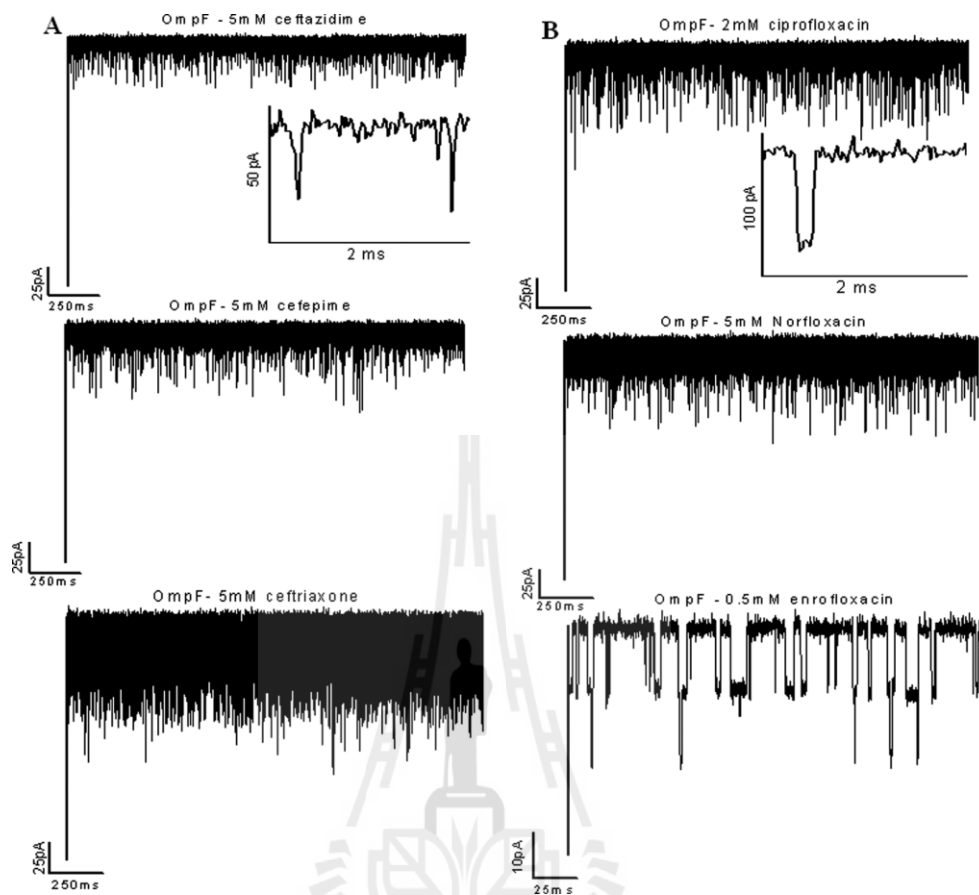


**Figure 1.4** Typical traces of the ionic current through a single trimeric OmpF protein pore in the presence of (A) selected cephalosporins and (B) selected fluoroquinolones. Insets are single-monomer blocking events at higher time resolution. Used was a DPhPC membrane in 1 M KCl (pH 6) and 5 or 0.5 mM supplement of the antibiotics. To induce current flow the transmembrane voltage was set to -50 mV (Mahendran *et al.*, 2010).

As seen in Figure 1.4 are short (sub-ms long) deflections in the membrane current traces and each of them is the reflection of an antibiotic translocation event: the current instantly decreases at the time of antibiotic channel entrance and it returns suddenly to the original level exactly when the molecule is leaving the pore. The important message here is that high-resolution membrane current measurements with reconstituted outer membrane protein channels have the power to resolve in real time the dynamics of the passage of individual penetrating and translocating (drug or other) molecules.

As outlined above, OmpF is a non-specific porin that allows molecules to pass as long as their sizes are small enough for channel passage. There are, however, also substrate-specific porins that allow access only for a certain type of molecules and not for others. Prominent reported examples of Omp's with substrate specificity are the LamB porin from *E. coli*, which is also known as the maltoporin and responsible for the membrane translocation of maltose and maltodextrins (Klebba *et al.*, 1994), and the sucrose porin ScrY from *Salmonella typhimurium* (Schmid *et al.*, 1991, Schuelein *et al.*, 1991). A brief description of the LamB porin is part of the following paragraphs in order to provide insight in the structure and function of a substrate specific porin.

*E. coli*'s LamB (maltoporin) is a specific diffusion porin that evolves in the bacterial outer membrane under special growth conditions. In fact, LamB is expressed as part of the mal-regulon upon exposure to maltose or maltodextrins. LamB is a solute-specific channel with a set of aromatic amino acid residues inside of the pore forming a substrate binding site specially designed for maltose and maltodextrins (Szmelcman *et al.*, 1976; Tommassen and Lugtenberg 1980; Hancock 1981; Brass *et al.*, 1985; Szmelcman and Hofnung, 1975).

Like non-specific general diffusion pores, also specific LamB forms trimeric pore structures in the outer membrane of bacteria. However, high-resolution crystal structures from the groups of Schirmer and Rosenbusch showed that in contrast to the 16 stranded antiparallel  $\beta$ -barrel of e.g. OmpF monomers, LamB monomers are made of an 18 stranded antiparallel  $\beta$ -barrel (Dutzler *et al.*, 1996; Meyer *et al.*, 1997; Schirmer *et al.*, 1995). Long loops protruding from the structure into the cell exterior and short turns directed towards the periplasm were also identified. As for OmpF-type porins, a constriction zone (pore narrowing) is formed by the inward folded loop L3. But with LamB, additional loops, namely the loops L1 and L6, further restrict the channel width.

The most remarkable attribute identified in the X-ray LamB structure was a successive sequence of aromatic residues including Trp<sup>74</sup>, Tyr<sup>41</sup>, Tyr<sup>6</sup>, Trp<sup>420</sup>, Trp<sup>358</sup>, Phe<sup>227</sup> that are arranged inside the channel along a left-handed helical path. This stretch of aromatic residues was named the “greasy slide” and actually is believed to be the structural element responsible for substrate binding and specificity. A chain of polar residues (namely, Arg<sup>8</sup>, Arg<sup>33</sup>, Glu<sup>43</sup>, Arg<sup>82</sup>, Arg<sup>109</sup>, Asp<sup>111</sup>, Asp<sup>116</sup>), the so-called polar track, is also situated around the constriction site and plays an important role in maltose and maltodextrin translocation. Figure 1.5 shows a cross-sectional representation of the LamB monomer that gives an idea about the relative location of its internal greasy slide and polar track.

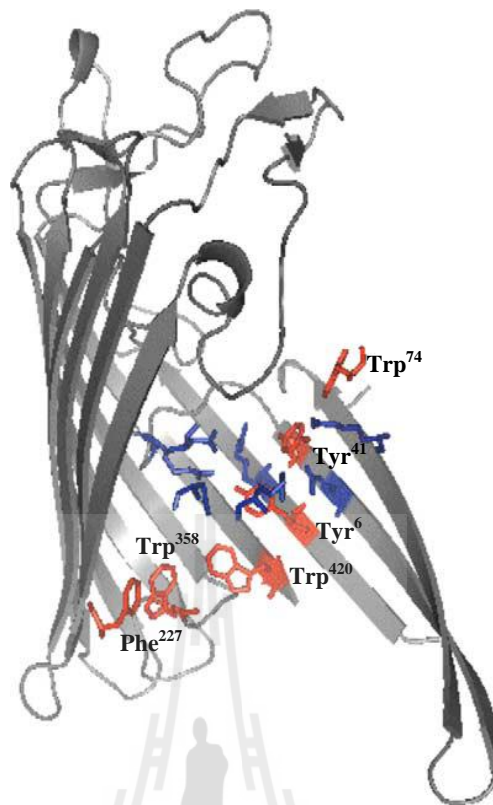


**Figure 1.5** Cross-section of maltoporin monomer. The greasy slide residues are shown in red in the following sequence: Trp<sup>74</sup> (at the top), Tyr<sup>41</sup>, Tyr<sup>6</sup>, Trp<sup>420</sup>, Trp<sup>358</sup> and Phe<sup>227</sup>. The polar tracks are shown in blue, comprising the residues: Arg<sup>8</sup>, Arg<sup>33</sup>, Glu<sup>43</sup>, Arg<sup>82</sup>, Arg<sup>109</sup>, Asp<sup>111</sup> and Asp<sup>116</sup> (Ranquin and Van Gelder, 2004).

A number of biophysical studies addressed a careful functional analysis of LamB and the assessment of the LamB channel conductance and open LamB sugar translocation rates for the protein pores that were reconstituted in artificial lipid bilayer membranes (Benz *et al.*, 1986; Benz *et al.*, 1987; Saurin *et al.*, 1995). The trimeric single channel conductance of a fully open maltoporin unit in solvent-free bilayers was found to be related only about 0.2-0.3 nS in a bulk solution that was 1 M KCl (Bezrukov *et al.*, 2000). The LamB single channel conductance is thus

significantly smaller than the one of the porin OmpF from *E. coli*. The explanation is probably the strengthening effect of loops L1 and L6 in terms of the ion flux hindrance in the area of the restriction zone that exists for LamB but not for OmpF.

Open LamB pores incorporated in solvent-free BLMs were shown to be able to effectively interact with their sugar substrates that have been added to the membrane contacting electrolyte solution. As result of the substrate binding to the binding site deep in the porin interior, the LamB channels get temporarily blocked and transient current decreases are resolvable in high-time resolution bilayer measurements. Figure 1.6 is an example of such an experiment with the wild-type *E. coli* LamB reconstituted in a DPhPC bilayer and then exposed to 0-30  $\mu\text{M}$  maltohexaose (Bezrukov *et al.*, 2000). In the absence of the maltohexaose the maximum current for the fully open channel is recorded and, with the applied membrane voltage known, allows calculation of the trimeric LamB pore conductance. The residence of the maltohexaose in individual monomer units appear as downward current deflections. At low concentrations, only individual monomer units interact at a time because of the low probability of a pore-sugar interaction and the number of penetration events (current deflection) is small and limited to the closure of one monomer unit. With increasing maltohexaose solution levels, the number of events in the current recording clearly increases and the closure of two and or even all three monomers of the LamB porin is visible.

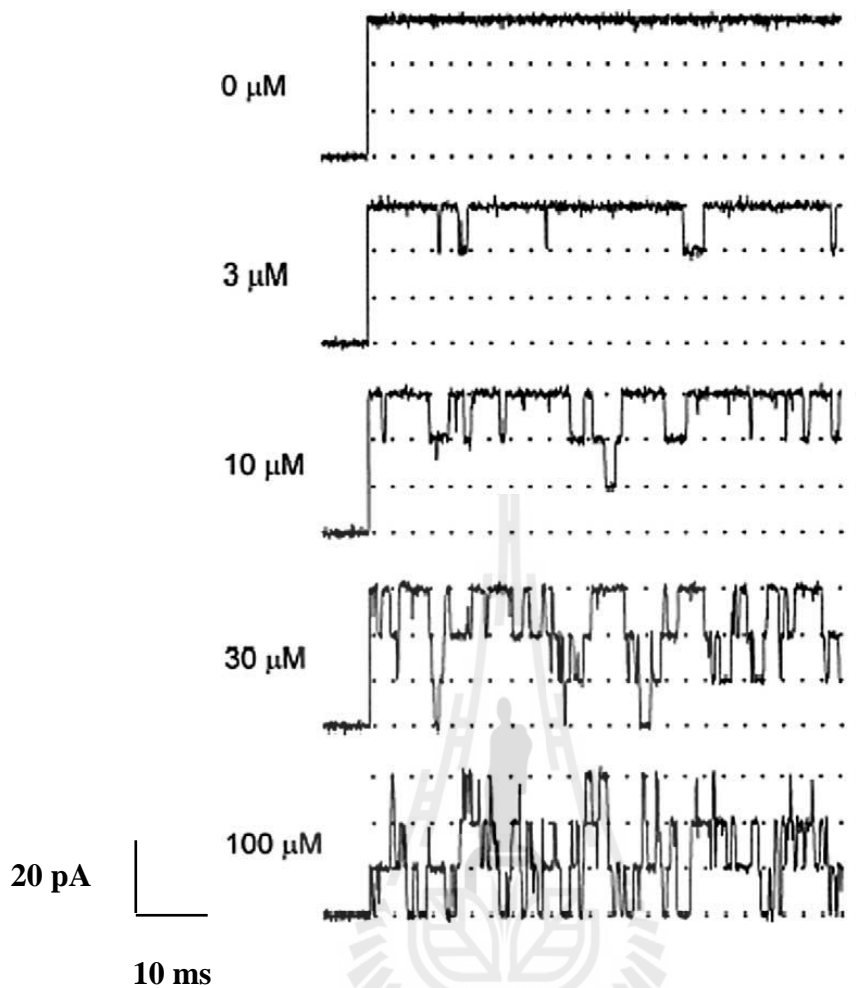


**Figure 1.6** Current recordings of a single maltoporin channel at various maltohexaose concentrations (given as numbers on the left). Deflections demonstrate time-resolved events of the reversible sugar binding/channel blockade. At small sugar concentration short interruptions in the channel current by one third of its initial value in sugar-free solution are seen. As the sugar concentration is increased, current interruptions in the different monomers comprising the trimer channel overlap displaying two thirds (10  $\mu\text{M}$  recording) or even complete (30 and 100  $\mu\text{M}$  recordings) transient blockages of the channel current. Transmembrane voltage of +200 mV is applied from the side of protein addition. Current records are presented at 50  $\mu\text{s}$  time resolution (Bezrukov *et al.*, 2000).

Note that high-time resolution lipid bilayer membrane current measurements as shown in Figure 1.6 with the specific porin channels as the LamB trimer studied in the presence and absence of the corresponding substrates and at various temperatures and concentrations allow an assessment of the binding kinetics (schematically in Figure 1.7) and the calculation of the second-order on-rate constant  $k_{\text{on}}$  ( $\text{M}^{-1}\text{s}^{-1}$ ), the first-order off-rate constant  $k_{\text{off}}$  ( $\text{s}^{-1}$ ), and the equilibrium binding constant ( $K$ ,  $\text{M}^{-1}$ ) as the ratio  $k_{\text{on}}/k_{\text{off}}$  (Nekolla *et al.*, 1994).

The kinetics of sugar-binding LamB channels was also addressed with studies of porin insertion in painted solvent-containing BLM measurements (Jordy *et al.*, 1996). The porin was actually added into the buffer electrolyte and allowed to insert until saturation of the membrane with the trimeric units was reached and a stable maximum membrane current was observed. Then, the LamB membrane conductance was titrated with maltotetraose or maltopentaose via the multiple additions of aliquots of a stock solution of the sugar of choice. The analysis of the power density spectra of the sugar-induced current noise following a procedure introduced by Nekolla *et al.* (Nekolla *et al.*, 1994) then facilitates the evaluation of the sugar binding kinetics and rate constants for carbohydrate binding to the channel interior and dissociation from there can be revealed. The study demonstrated that the wild-type maltoporin of *Salmonella typhimurium* had approximately the same sugar-binding kinetics as the wild-type LamB of the *E. coli*. The same study also demonstrated that *E. coli* LamB mutants with mutations of tyrosine residues (Tyr<sup>118</sup>) in the first transmembrane  $\beta$ -strand starting from the N terminus or in the third loop of the  $\beta$ -barrel (between  $\beta$ -strands 5 and 6) had significantly modified binding properties of sugars to the internal binding site compared to the wild-type protein (Orlik *et al.*, 2002; Orlik *et al.*, 2002).

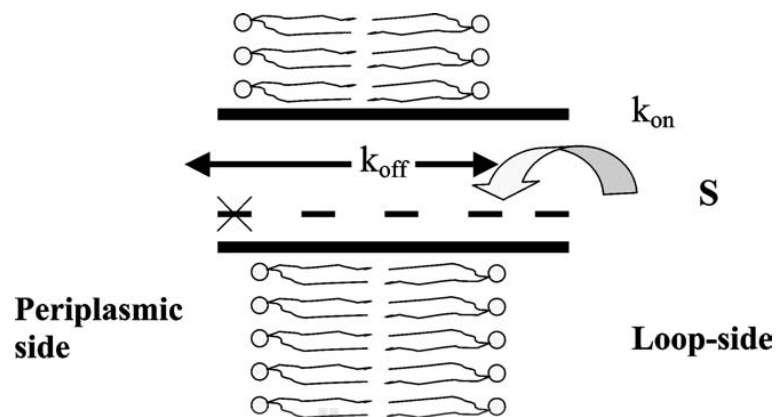


**Figure 1.7** Schematic drawing of a single-sided sugar addition lipid bilayer experiment with LamB. The chosen sugar (S) is for instance added at the loop-side of the LamB channel. Current fluctuation analysis can detect the  $k_{on}$  value. Once the sugar is bound to the binding site in the pore structure, it can leave the channel in two directions and  $k_{off}$  values of both exits can be calculated. The dashed line represents the greasy slide residues; the cross is the mutated greasy slide residue (Danelon *et al.*, 2003).

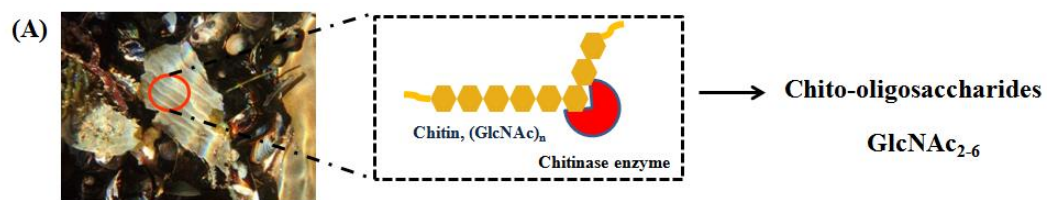
## 1.2 Marine bacteria and their function in chitin uptake

Most marine bacteria present in a seawater environment including the members of the *Vibrio* species (Keyhani and Roseman, 1999) are using chitin, or better the products of chitin hydrolysis, as a readily available energy source for supporting intracellular metabolism. Chitin is a homobopolymer that is composed of  $\beta$  1-4 linked *N*-acetyl-glucosamine (GlcNAc) residues (Li *et al.*, 2004; Park *et al.*, 2000) and is the main component of the shells of, for instance, shrimp, crab, crayfish or lobster. Marine bacteria degrade insoluble chitin into small chito-oligosaccharides, which are then transported into their cytosol. Marine bacteria have available self-produced efficient chitinases (EC 3.2.1.14), a type of enzymes that catalyze the conversion of chitin to the desired soluble chito-oligosaccharides (schematically shown in Figure 1.8). Chitinases are found in a wide range of organisms including viruses, bacteria, fungi, insects, plants and animals (Jolles and Muzzarelli, 1999; Yu *et al.*, 1991; Merzendorfer *et al.*, 2003; Herrera-Estrella *et al.*, 1999). Detailed information on the (biochemical) properties of chitinases and the mechanism of their catalytic interaction with their substrate chitin can be found in a comprehensive review article (Keyhani *et al.*, 2000)

Extracellularly synthesized chito-oligosaccharides need to get across the bacterial cell wall including the outer and inner membrane and periplasmic space in order to be transported into the cytoplasm of the marine microorganism and be available there as energy supply. The first barrier for the chito-oligosaccharides is of course the bacterial outer membrane. As illustrated in Figure 1.9, GlcNAc and (GlcNAc)<sub>2</sub> are small enough to get access to the periplasm via general diffusion pores. The higher chito-oligosaccharides ((GlcNAc)<sub>n</sub>, n = 3-6), however, are too bulky to go through a

normal unspecific (general) porin and the finding of a number of studies supported the existence of a highly specialized outer membrane protein channel that acts as specific porin for the species (GlcNAc)<sub>3-6</sub> (Hjerde *et al.*, 2008; Keyhani *et al.*, 2000; Li and Roseman, 2004; Meibom *et al.*, 2004). On account of its function, the (GlcNAc)<sub>2-6</sub> specific OMP channel of marine bacteria was termed the bacterial chitoporin (ChiP) and it is in fact the structure and function of this outer membrane protein that forms the central subject of this doctoral thesis.

An earlier microarray expression profiling and mutational analysis of *Vibrio cholera*, grown on a natural chitin surface, or with the soluble chitin oligosaccharides (GlcNAc)<sub>2-6</sub>, *N*-acetyl-glucosamine, or the glucosamine dimer (GlcN)<sub>2</sub> identified ChiS, a sensor histidine kinase as the regulated gene that is responsible for the expression a so-called (GlcNAc)<sub>2-6</sub> gene set. The gene set includes a (GlcNAc)<sub>2</sub> catabolic operon, two extracellular chitinases, a chitoporin, and a PilA-containing type IV pilus, designated ChiRP (chitin-regulated pilus) that confers a significant growth advantage to *V. cholerae* on a chitin surface (Meibom *et al.*, 2004). The regulation of the chitinolytic cascade in *Vibrios* by chitin oligosaccharides and a two-component chitin catabolic sensor kinase was also a major component of two studies from the Roseman group (Keyhani *et al.*, 2000; Li and Roseman, 2004).



$\beta$  1-4 linked:

- ❖ N-acetyl glucosamine (GlcNAc) residue
- ❖ Glucosamine (GlcN) residue

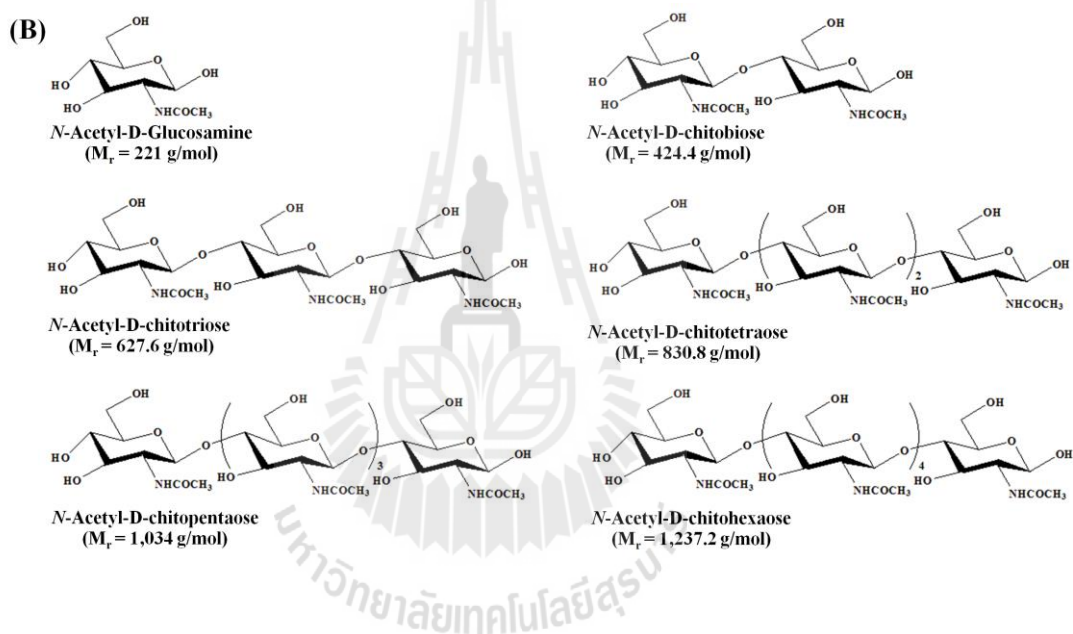


**Figure 1.8** (A) The chitinase-assisted chitin degradation as driven by marine bacteria for the utilization of chitin for cellular metabolism and (B) the chemical structure of chito-oligosaccharides products of enzymatic chitin breakdown.

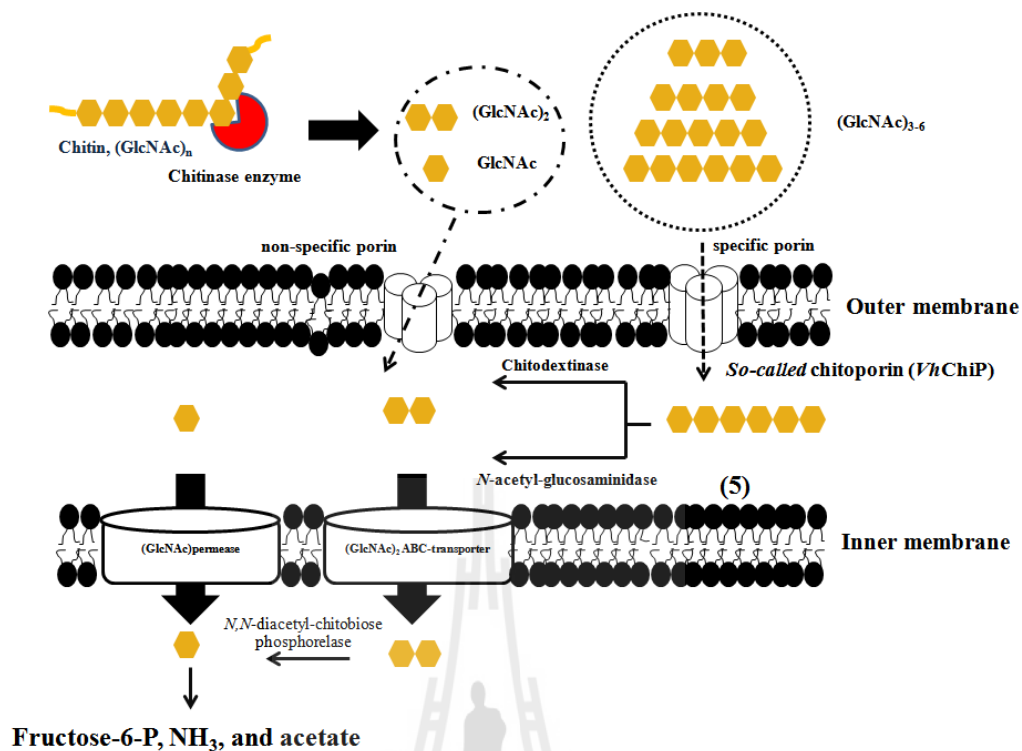


**Figure 1.9** Model of the chitin degradation cascade of the marine bacterium *Vibrio harveyi*. The model was reconstructed from the chitinolytic cascade proposed by Li and Roseman (Li *et al.*, 2004). After chitin degradation by chitinase, the chitin fragments are transported through the outer membrane by diffusion through porin or chitoporin, depending on their sizes. Further enzymatic degradation takes place in the periplasm, producing  $\text{GlcNAc}$  and  $\text{GlcNAc}_2$ . Binding of  $\text{GlcNAc}_2$  to CBD activates the ChiS sensor, producing transcription of the genes under control of the  $\text{GlcNAc}_2$  catabolic operon.  $\text{GlcNAc}$  is translocated to the cytoplasm by the  $\text{GlcNAc}$  PTS system, while  $\text{GlcNAc}_2$  is transported through the inner membrane by the  $\text{GlcNAc}_2$  ABC permease. Both products are phosphorylated, and finally converted to Fructose-6-P, acetate and  $\text{NH}_3$ .

Above-mentioned earlier molecular biology and biochemistry studies provided a clear proof that a chitoporin exists in the membrane of at least some, if not all, marine bacteria. It should be emphasized that so far there are no studies reported yet in the scientific literature that dealt and succeeded with the isolation of the ChiP components from the outer membrane fractions of suitable marine bacteria and then with a functional analysis of chito-oligosaccharide flux through these channels via the biophysical/electrophysiological measurements. Also, the structural arrangement of ChiP has not yet been revealed via the modern powerful X-ray and spectroscopic protein structure techniques. Therefore, the exact internal and external channel architecture (e.g. of ChiP's restriction zone) and the arrangement of the complex between (GlcNAc)<sub>2-6</sub> and the ChiP chito-oligosaccharide binding site currently remain to be identified.

### **1.3 Techniques for functional analysis of bacterial outer membrane proteins**

A number of sensitive analytical techniques are used for revealing the structure and function of bacterial outer membrane proteins. Best for studying OMP function in terms of flux of dissolved (ionic) species are membrane current measurements that can be achieved via the “black lipid membrane (BLM) technique. Insight in the channel-function of reconstituted Omps may also be gained by means of liposome swelling assay. In this thesis the BLM technique, the liposome swelling assay, and fluorescence spectroscopy will be the main tools for the desired functional characterization of the isolated chitoporins from *V. harveyi*. The principles behind these analytical techniques will be briefly outlined.

### 1.3.1 The “Black Lipid Membrane” (BLM) technique

BLMs are a widely-used model system for the study of membrane proteins. The principles of the BLM technique (or BLM measurements) are provided briefly in the following section. More detailed information can be found in recently published review articles and book chapters (Mueller *et al.*, 1964; Benz *et al.*, 1975; Montal *et al.*, 1972; Benz *et al.*, 1986).

The BLM experiment is a measure of the voltage-induced current through single or multiple protein channels that are incorporated in a well established bilayer. The instrumentation for the recording of ionic currents through outer membrane proteins (porins) in a freshly formed BLM is shown in Figure 1.10. Usually, a BLM set-up is placed in a Faraday cage on top of a vibration-dampening table with the main components being a low-noise two electrode patch-clamp amplifier, a special two-electrode headstage for the bilayer recordings, a two-compartment bilayer recording chamber and a computer interface for controlling the transmembrane voltage and for high-resolution, low-noise data acquisition. Special care has to be taken on the optimization of the noise properties of the set-up since the ionic currents through single outer membrane protein pores are in the pA range and only can be resolved at appropriately low noise levels in the bilayer recordings. The electrolyte for BLM measurements is usually a buffered or un-buffered solution of potassium or sodium chloride, sodium acetate, or other salts.

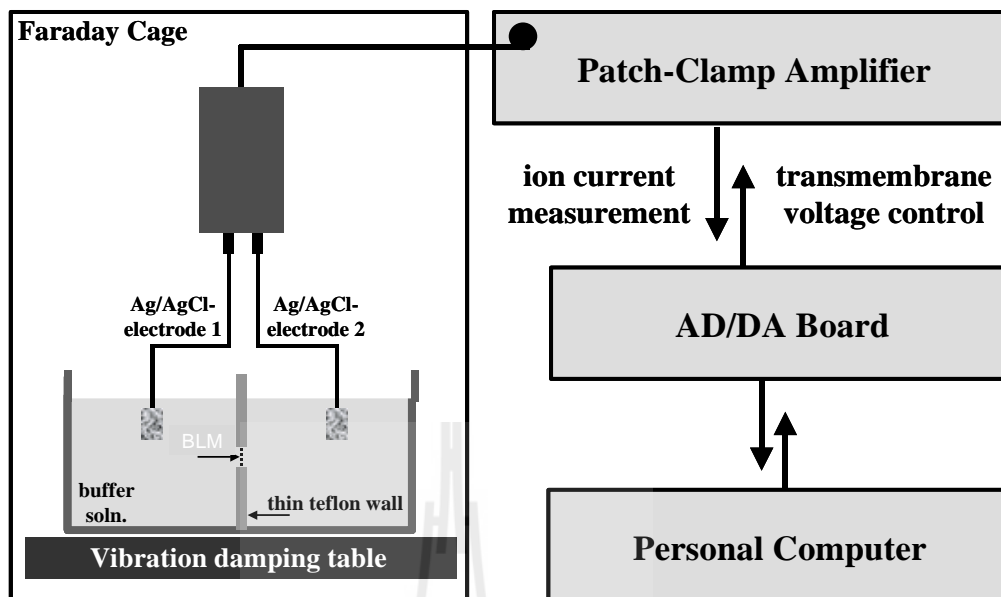


**Figure 1.10** Schematic of the electrophysiological/biophysical set-up for planar lipid bilayer experiments on porin channels that were isolated from the outer membrane of bacterial cells.

Starting material for the establishment of the required artificial lipid bilayers (BLMs) in the specially designed BLM chambers is a diluted solution of natural or synthetic lipids of choice (e.g. diphytanoyl-phosphatidylcholine, DPhPC) in a suitable organic solvent (e.g. *n*-pentane, hexane/chloroform etc.). Two different strategies are widely used for the formation of stable artificial lipid bilayer membranes on the hole in the Teflon foil that separate the two BLM electrolyte compartment:

- To establish the lipid bilayer by the painting approach (Benz *et al.*, 1975), a paint brush is soaked with a little drop of the lipid solution and a tiny amount of this mixture applied to the hole. On both side of the aperture the media is an aqueous one and lipid as well as solvent molecules as non-polar species have

the tendency to separate from that surrounding. Thinning in the centre of the aperture leads to the formation of a bilayer structure in that region. The bilayer structure is concentrically surrounded by the organic solvent and thus not 100% solvent free but contaminated with residual amounts of it.

- With the classical Montal-Mueller technique (Mueller *et al.*, 1964; Montal *et al.*, 1972), a few microliters of a solution of the lipids of choice in hexane/chloroform is dropped on top of the surface of the aqueous buffer solution that serves as electrolyte for the BLM measurement. After allowing the solvent to evaporate, a lipid monolayer is obtained on top of the buffer solution. At this stage lowering and rising of the electrolyte level below and back to above the hole in the Teflon partition is performed. Usually this action forms in straightforward fashion a stable bilayer across the aperture. Advantage of the Montal-Mueller-type of BLMs is that they are solvent-free and thus a more reproducible system for the study of membrane protein channels.

With a lipid bilayer in place as separating layer between the electrolytes in the two bilayer compartments, a membrane potential can be applied between the two Ag/AgCl electrodes to the left and the right of the BLM and the membrane current monitored at millisecond time scale and pA current resolution. As long as pore-forming porin has been added to the membrane-bathing solutions at either side of the BLM, only very small background currents should be observed. Depending on the electrical noise levels and the quality of the Ag/AgCl electrodes, the background currents may range one and a few pA. Addition of porin to one electrolyte compartment (either on the cis- or trans-side) may lead to the insertion of the protein channels into the BLM membrane. Insertion events will lead to a step-like current

increase since the cations and the anions of the buffer solution are now able to diffuse through the membrane pore under the influence of the applied voltage. Multiple sequential porin insertions will become visible in the current trace as sequential step-wise increase in signal. Figure 1.11 is a schematic representation of a current recording as it is expected when a small aliquot of a pore-forming outer membrane protein sample is added in course of a BLM experiment and membrane incorporation of a porin takes place. After addition of porin, the current will remain for a short period at background level but then multiple channels may get inserted into the BLM one after the other and the membrane current increases in sudden fashion for each porin insertion event.

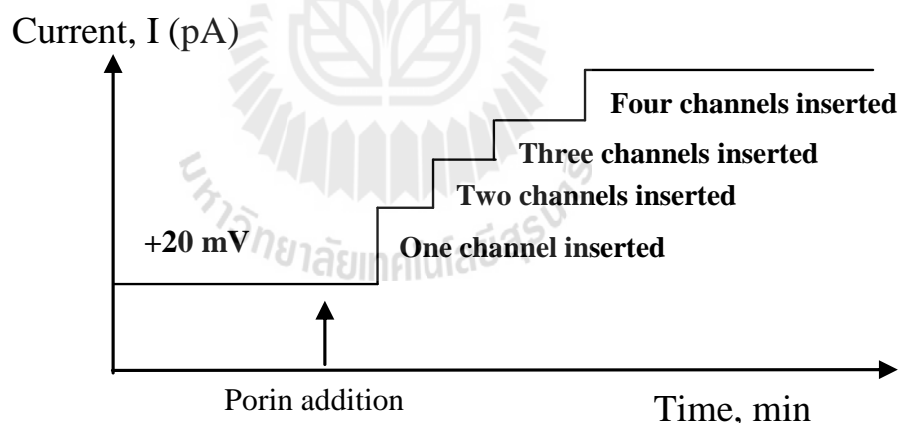


**Figure 1.11** Schematic representation of the current vs. time trace that is expected when a BLM membrane is exposed to an electrolyte containing pore-forming outer membrane proteins. In this specific case, four porin units successfully incorporated into the lipid bilayer and provided channels for ion flow at the condition of an applied membrane voltage.

For a complete understanding of the pore properties of an outer membrane protein channel/porin, the BLM measurements will be carried out under various conditions. Experimental variables are: type and concentration of salt, the side of the membrane to which the porin was added, the transmembrane potential, the type of lipid used for BLM formation, etc. The addition of large molecules revealed interaction to observe for the effect on the ion flow through the porin channels. A careful statistical analysis of the many recordings provided information on the function of bacterial outer membrane protein channel in terms of the membrane passage of charged or uncharged molecules.

### **1.3.2 Binding studies using the intrinsic fluorescence of proteins and peptides**

The fluorescence of a folded protein is from all individual aromatic residues: tryptophan (Trp), tyrosine (Try), and phenylalanine (Phe) (Demchenko, 1988; Longworth, 1971; Permyakov, 1993) (Figure 1.12). Most of intrinsic fluorescence emissions of a folded protein are due to excitation of tryptophan residues, with some emissions due to tyrosine and phenylalanine. Figure 1.13 shows excitation and emission spectra of tryptophan, tyrosine, and phenylalanine, respectively. These aromatic amino acids have for example a wavelength of maximum absorption of 240 to 280 nm and an emission wavelength ranging from 250 to 400 nm depending in the polarity of the local environment.

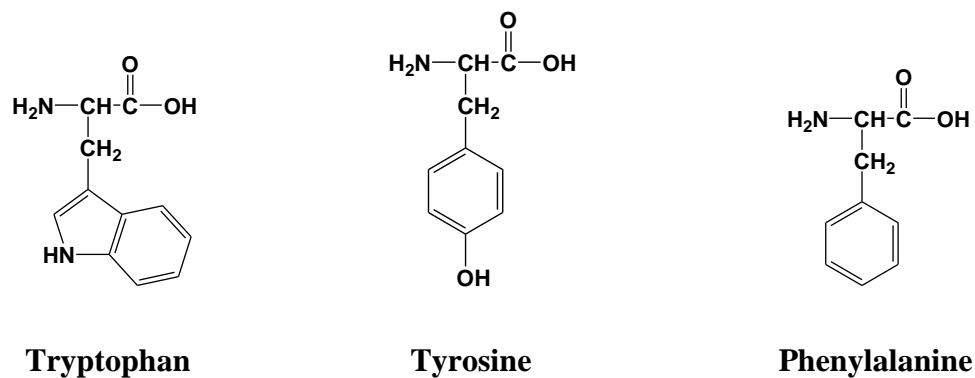


**Figure 1.12** Intrinsic biochemical fluorophores. Tryptophan (Trp), tyrosine (Try), and phenylalanine (Phe) (Lakowicz, pp. 64).

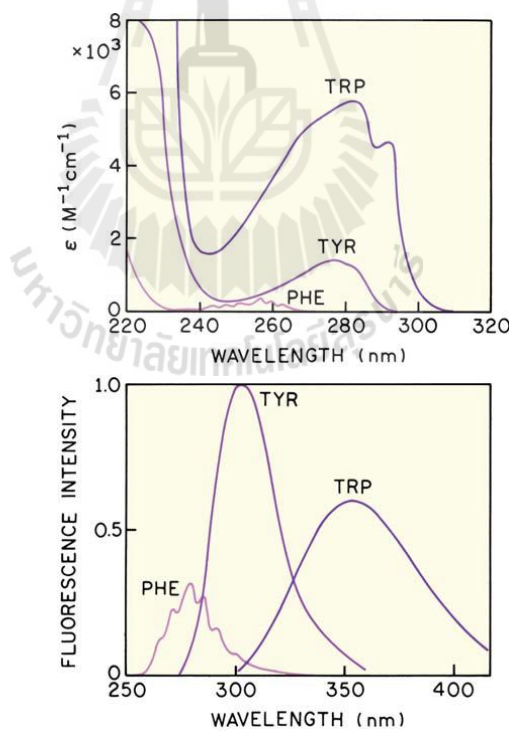


**Figure 1.13** Absorption and emission spectra of the fluorescent amino acids in water at pH 7.0 (Lakowicz, pp. 65).

Hence, protein fluorescence may be used as a diagnostic tool to determine the conformational state of a protein (Vivian and Callis, 2001). Proteins that lack tryptophan may be coupled to a fluorophore. Furthermore, tryptophan fluorescence is strongly influenced by the proximity of other residues (*i.e.*, nearby protonated groups such as Asp or Glu can cause quenching of Trp fluorescence). An energy transfer between tryptophan and the other fluorescent amino acids is possible. In addition, tryptophan is a relatively rare amino acid; many proteins contain only one or a few tryptophan residues. Therefore, tryptophan fluorescence can be a very sensitive measurement of the conformational state of individual tryptophan residues. The advantage compared to extrinsic probes is that the protein itself is not changed. The use of intrinsic fluorescence for the study of protein conformation is in practice limited to cases with few (or perhaps only one) tryptophan residues.

For example, if a protein containing a single tryptophan in its 'hydrophobic' core is denatured with increasing temperature, a red-shift emission spectrum will appear (Figure 1.14). This is due to the exposure of the tryptophan to an aqueous environment as opposed to a hydrophobic protein interior. In contrast, the addition of a surfactant to a protein which contains a tryptophan which is exposed to the aqueous solvent will cause a blue shifted emission spectrum if the tryptophan is embedded in the surfactant vesicle or micelle (Caputo and London, 2003). At 295 nm, the tryptophan emission spectrum is dominant over the weaker tyrosine and phenylalanine fluorescence. Number of processes can lead to a reduction in fluorescence intensity, *i.e.*, quenching such as collisional (dynamic) quenching and static (complex formation) quenching.

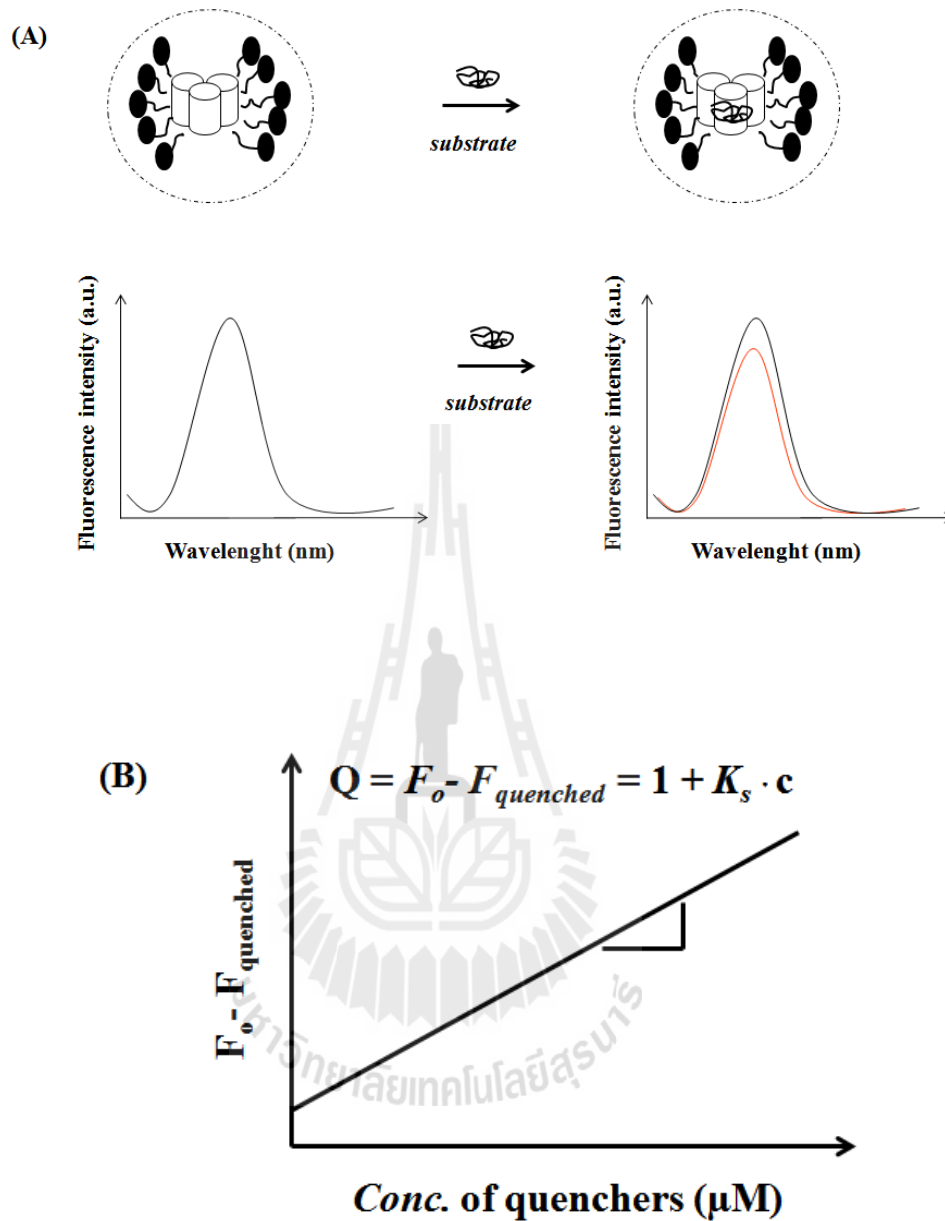


**Figure 1.14** A) An outer membrane protein (for example, Omps) is solubilized in detergent with different forms of free or interaction with its substrate. Emission spectra of Omp are shown in the black line and the red line indicated when the Omp interacted with substrate. B) Substrate quenching of Omp when bound to substrate binding protein (Neves *et al.*, 2009).

### 1.3.2.1 Theory of collisional quenching

Collisional quenching occurs when the excited fluorophore experiences contact with an atom or molecule that can facilitate non-radiative transitions to the ground state. Common quenchers include O<sub>2</sub>, I, Cs<sup>+</sup> and acrylamide (Kautsky, 1939; Kasha, 1952; Steiner and Kirby, 1969; Eftink and Ghiron, 1981; Eftink, 1991; Eftink, 1991).

Stern-Volmer equation, holds:

$$F_0/F = 1 + k_q\tau_0[Q] = 1 + K_D [Q] \quad \text{Eq. 1.1}$$

In this equation  $F_0$  and  $F$  are the fluorescence intensities in the absence and presence of quencher, respectively;  $k_q$  is the bimolecular quenching constant;  $\tau_0$  is the lifetime of the fluorophore in the absence of quencher, and  $Q$  is the concentration of quencher. The Stern-Volmer quenching constant is given by  $K_D = k_q\tau_0$ . If the quenching is known to be dynamic, the Stern-Volmer constant will be represented by  $K_D$ . Otherwise this constant will be described as  $K_{SV}$ . Quenching data are usually presented as plots of  $F_0/F$  versus  $[Q]$ . This is because  $F_0/F$  is expected to be linearly dependent upon the concentration of quencher. A plot of  $F_0/F$  versus  $[Q]$  yields an intercept of one on the y-axis and a slope equal to  $K_D$  (Figure 1.15, left).

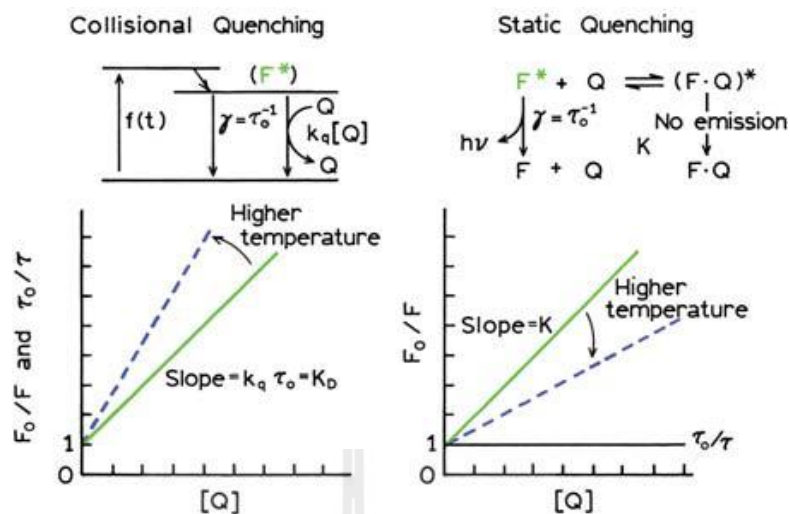


**Figure 1.15** Comparison of dynamic and static quenching (Lakowicz, pp. 280).

Quenching can also occur as a result of the formation of a nonfluorescent ground-state complex between the fluorophore and quencher (Davis, 1973; Shinitzky and Rivnay, 1977). When this complex absorbs light it immediately returns to the ground state without emission of a photon (Figure 1.15). For static quenching the dependence of the fluorescence intensity upon quencher concentration is easily derived by consideration of the association constant for complex formation.

This constant is given by:

$$K_s = [F-Q]/[F][Q] \quad \text{Eq. 1.2}$$

Where  $[F-Q]$  is the concentration of the complex,  $[F]$  is the concentration of uncomplexed fluorophore, and  $[Q]$  is the concentration of quencher. If the complexed

species is nonfluorescent then the fraction of the fluorescence that remains ( $F/F_0$ ) is given by the fraction of the total fluorophores that are not complexed:  $f = F/F_0$ . The total concentration of fluorophore  $[F]_0$  is then given by:

$$[F]_0 = [F] + [F - Q] \quad \text{Eq. 1.3}$$

substitution into Eq. 1.2 yields:

$$K_s = [F]_0 - [F]/[F][Q] = [F_0]/[F][Q] - 1/[Q] \quad \text{Eq. 1.4}$$

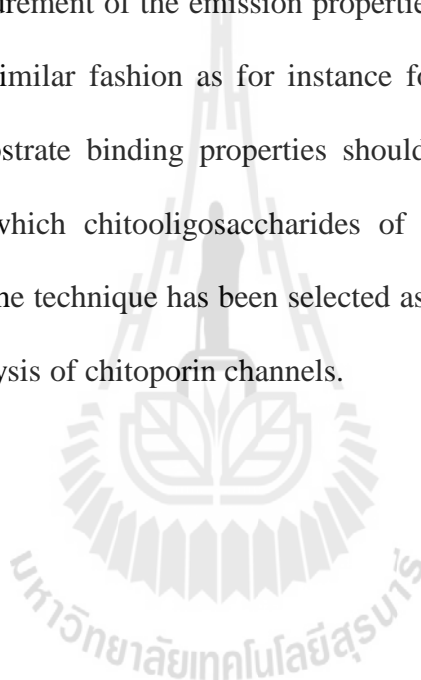
It can be substituted the fluorophore concentration for fluorescence intensities, and rearrangement of eq. 1.4 yields:

$$F_0/F = 1 + K_s[Q] \quad \text{Eq. 1.5}$$

The dependence of  $F_0/F$  is linear on  $[Q]$  and identical to that observed for dynamic quenching, except that the quenching constant is now the association constant. Static quenching removes a fraction of the fluorophores from observation. The complexed fluorophores are non-fluorescent, and the only observed fluorescence is from the uncomplexed fluorophores. The uncomplexed fraction is unperturbed, and hence the lifetime is  $\tau_0$ . Therefore, for static quenching  $\tau_0/\tau = 1$  (Figure 1.15, right).

The fluorescence spectroscopy can be used to investigate chitoporin-chitooligosaccharides interaction. It has been shown previously that fluorescent tryptophan residues inside of tubular porin channels can be selectively stimulated to emission and that the quenching of this excited fluorescence occurs through the

interaction of penetrating molecules with the inner pore structure (Neves *et al.*, 2005). First methodological studies the strategy was applied for antibiotic interactions with the *E. coli* OmpF porin (Neves *et al.*, 2009). In this Ph.D. thesis, fluorescence spectroscopy was used to study the dissociation constant ( $K_D$ ), for complex between the chitooligosaccharides and the binding sites inside the porin and how the binding characteristics and affinity constants for the pore-to-sugar interaction can be optically assessed via the measurement of the emission properties of the tryptophan (Trp<sup>136</sup>) in the pore interior. In similar fashion as for instance for OmpF the sensitive optical approach towards substrate binding properties should also work with the specific chitoporins through which chitooligosaccharides of various sizes are allowed to permeate. Therefore, the technique has been selected as one the major analytical tools for the functional analysis of chitoporin channels.



## 1.4 Research objectives

To date a clear demonstration of the function of chitoporin and chitooligosaccharide transport has not been demonstrated. The main goal of this thesis is to provide evidence of chitooligosaccharides translocation through *VhChiP* channel. For this we perform the following steps:

### 1.4.1 Cloning, expression and purification of a chitoporin from the marine bacterium *V. harveyi* 650

Hjerde *et al.* (2008) showed in an earlier study a schematic mechanism of how chito-oligosaccharides can be taken up into the periplasm space of marine bacteria, after self-secreted chitinase enzyme converted available chitin into specific substrates for the chitoporin. In first part of this PhD thesis we report how to generate recombinant plasmid pET23d(+)-*VhChiP* from *V. harveyi* 650 and use the material for a reliable and reproducible expression, isolation and purification of the target chitoporin protein.

### 1.4.2 Characterization of the function of the chitoporin

Black lipid membranes (BLMs) were used to reconstitute the native *VhChiP* porin, which is a porin type channel in the bacterial outer membrane, into artificial bilayers and the application of the BLM technique for a systematic evaluation of basic *VhChiP* properties such as its single channel conductance (G) (pore size) and voltage dependence or voltage independence to confirm of ion flux. The sugar translocation was studied in terms of membrane-incorporated chitoporin in the presence of its natural chitooligosaccharide substrates (GlcNAc)<sub>2-6</sub>.

Likewise most of outer membrane protein channels, also the chitoporin should have a specific restriction zone in the channel interior and a loop of amino acid

residues (Loop3, L3) that extends at the channel mouth into the extracellular space. The design of both the restriction zone and the external loop will influence the channel translocation activity and thus point mutations of specific amino acid residues within the named areas are an additional target of this study. Functional properties of the chitoporin mutants were assessed as performed for the wild-type variant and mutants and wild-type channel activity/specificity compared.



## CHAPTER II

### MATERIALS AND METHODS

#### 2.1 Design of oligonucleotide primers

The primers used for the generation of recombinant *VhChiP* are shown below:

Forward primer (*NcoI*) = 5'-ATACCATGGCGTCTTACCTAAAGAAAAG-3'

Reverse primer (*XhoI*) = 5'-AACCTCGAGTTAGAAGTAGTATTCAACAC-3'

Sequences underlines are cloning sites

#### 2.2 Expression vectors and bacterial host cells

pET23d(+) vector was used as the expression vector. *E. coli* DH5 $\alpha$  strain and was used as a routine host for cloning, subcloning and preparation of recombinant plasmid. *E. coli* BL21 (DE3) omp8 Rosetta strain lacking OmpF, OmpA, OmpC and LamB was used as the expression host (Table 2.1).

**Table 2.1** Bacterial strain and plasmids used in this study.

| Strains and plasmids                          | Description       | Source                             |
|---|-------------------|------------------------------------|
| <b>Strains</b>                                |                   |                                    |
| <i>V. harveyi</i> 650                         | Wild type (WT)    | This study                         |
| <i>E. coli</i> DH5 $\alpha$                   | Cloning host      | This study                         |
| <i>E. coli</i> BL21 (DE3)                     | Expression host   | Siritapetawee <i>et al.</i> (2004) |
| <i>E. coli</i> BL21 (DE3) Omp8 Rosetta strain | Expression host   | This study                         |
| <b>Plasmids</b>                               |                   |                                    |
| pGEM-T easy                                   | Cloning vector    | This study                         |
| pET23d(+)                                     | Expression vector | This study                         |

### 2.3 Chemicals and reagents

Chemicals and reagents for cloning, expression and characterization of *V. harveyi* chitopirin were analytical grades unless stated otherwise. *Pfu* DNA polymerase, dNTP mix, *Pfu* polymerase buffer, magnesium chloride, *Dpn* I restriction enzyme were products of Promega. QIA prep spin Mini prep kit, bovine serum albumin (BSA), isopropyl- $\beta$ -D-thiogaltopyranoside (IPTG), bacto tryptone, bacto yeast extract, agar, calcium chloride, potassium chloride, sodium chloride, sodium acetate, glycerol, tris-base, sodium dodecyl sulphate (SDS), acrylamide, *N,N'*-methylene bisacrylamide, TEMED, ammonium persulfate, Coomassie brilliant blue R-250, 2-mercaptoethanol, glycerol were products of Sigma-Aldrich (St. Louis, MO, USA). DNase I and RNaseA were purchased from Pacific Science Co., LTD. Ampicillin was a product of USB Corporation (Cleveland, OH, USA). Chitin from

crab shells and chito-oligosaccharides were products of Seikagaku Corporation (Tokyo, Japan)

## 2.4 Instrumentation

Instrument was required throughout the study include a Sonopuls Ultrasonic homogenizer with a 6-mm diameter probe, a PCR thermocycler, a DNA gel apparatus, a protein gel apparatus plus with a compatible power supply, a Genway UV-VIS spectrophotometer, a Gel Document system, an Axon Instrument BLM workstation for lipid bilayer experiments and a spectrofluorometer for optical *Vh*ChiP/chito-oligosaccharides binding studies.

## 2.5 Methodology

### 2.5.1 Growth and maintenance of *V. harveyi* 650 strain and genomic DNA isolation from *V. harveyi* type strain 650

The starter culture of *V. harveyi* 650 was grown in 10 ml of marine medium 2216E (MM), supplemented with an additional 5 g/L bacteriological peptone, 0.1 g/L FePO<sub>4</sub>, 5 g/L yeast extract and incubated at 30 °C, for 16-18 hr (overnight) with 250 rpm agitation. Afterwards, the bacterial cells was streaked on MM agar plate without ampicillin and incubated at 30 °C for 16-18 hr.

Single colony of *V. harveyi* 650 was grown in 5 ml of MM without ampicillin and incubated at 30 °C for 16-18 hr. Genomic DNA isolation was performed following miniprep protocol (QIAGEN, USA). Briefly, one ml of the overnight culture was transferred into 1.5 ml sterile tube, then centrifuged at 14,000 g for 2 min to remove the medium. Then, cell pellet was mixed with 600 µl of nuclei

lysis solution and gently mixed by pipetting until the cells were well resuspended. The suspension was incubated at 80 °C for 5 min, afterwards cooled down at room temperature. Three microliters of RNase solution were added into the suspension and the tube was inverted 2-5 times to mix the suspension. The lysate was incubated at 37 °C for 30 min and afterwards cooled down at room temperature. Two hundred microliters of the protein precipitation solution were added into the cell lysate and vortex vigorously at high speed for 20 second to mix the protein precipitation solution with the cell lysate and incubated the suspension on ice for 5 min and centrifuged at 14,000 g for 3 min. The supernatant containing genomic DNA of *V. harveyi* was transferred into a 1.5 µl sterile tube that contains 600 µl of iso-propanol at room temperature. Afterwards, the supernatant was gently mixed by inverting the tube until the thread-like strands of DNA form a visible mass. After that, the supernatant was centrifuged at 14,000 g for 2 min to discard the supernatant from the pellet. Then, the tube was drained on a clean absorbent paper and a pellet was washed several times with 70% of ethanol at room temperature. Finally, the DNA pellet was dissolved with 100 µl of dH<sub>2</sub>O and incubated at 65 °C for 1 hr. The size of the genomic DNA was checked using 0.8% agarose gel electrophoresis.

### **2.5.2 PCR amplification of the cDNA encoding *VhChiP***

The full-length cDNA encoding *VhChiP* was amplified by PCR reaction using the genomic DNA extracted from *V. harveyi* 650 as DNA template. The PCR reaction comprises DNA template, 10x Pfu buffer, 10 mM dNTP mix, 10 µM primer, 25 mM MgCl<sub>2</sub>, 1 unit of *Taq* DNA polymerase. Reaction mixtures were amplified in a GeneAmp® PCR system 9700 thermocycler (PE Applied Biosystems, USA). The

DNA template was denatured for 1 min at 98 °C and subjected to 30 cycles for annealing at 98 °C for 2 min, 50 °C for 30 second and extension 72 °C for 3 min, followed by a final extension for 5 min at 72 °C. PCR products were resolved on 1% agarose gel. The DNA insert of expected size (about 1.12 kb) was excised and ligated with pGEM-T cloning vector, according to the Promega Manufacturer's instruction.

Reaction comprised purified PCR, 10x buffer, 2 mM MgCl<sub>2</sub>, 10 mM ATP and Taq DNA polymerase. Ten microliters of deionized water were added to make up a final volume of 10 µl. The reaction mixture was incubated at 70 °C for 15-30 min. The amounts of DNA insert used for ligation were calculated as follow:

$$\frac{(\text{ng of vector} \times \text{kb size of insert})}{\text{kb size of vector}} \times (\text{insert} : \text{vector molar ratio}) = \text{ng of insert}$$

Ligation reactions comprised 2x T4 DNA ligase buffer, 50 ng of pGEM-T easy vector (3 kb), PCR products and 0.3 unit of T4 DNA ligase. Twenty-five microliters of deionized water were added to make up a final volume of 25 µl. The reaction mixture was incubated overnight at 4 °C.

### 2.5.3 Cloning of DNA encoding *VhChiP* into pET23d(+) and confirmation of DNA insert

Two microliters of the ligation products were transformed to 100  $\mu$ l *E. coli* DH5 $\alpha$  competent cells using a standard protocol. Single colonies, which carry the plasmid containing the *VhChiP* DNA insert were subjected to plasmid extraction using High-Speed plasmid mini kit (Geneaid Biotech Ltd., USA) and run on 1% agarose gel electrophoresis.

The purified plasmids (pGEM-T-easy/*VhChiP*) were further digested with the restriction enzymes *Xho*I and *Nco*I to obtain cohesive-end ligation. Double digestion reactions were comprised 10  $\mu$ g DNA inserts, 10x NEB buffer, 10 units of *Xho*I and *Nco*I. Sterile dH<sub>2</sub>O was added to bring the final volume up to 20  $\mu$ l. The reaction mixture was incubated at 37 °C for 3 hr and the reaction was inactivated at 65 °C for 15 min. The digestion products was separated on 1% agarose gel electrophoresis and purified by the QiaQuick gel extraction kit (QIAGEN, USA). The purified *VhChiP* cDNA was used for ligation with pET23d(+). The reaction mixture consisted of 1  $\mu$ l 10x rapid ligation buffer, 50 ng purified pET23d(+) vector, 45 ng DNA insert of DNA inserts (*VhChiP* gene), 1 unit T4 DNA ligase and sterile distilled water to bring the volume up to 20  $\mu$ l. The ligation reaction was incubated at 4 °C overnight. The total reaction mixture was transformed into *E. coli* DH5 $\alpha$  strain. The bacterial cells were grown in LB-broth contained 100  $\mu$ g/ml ampicillin and the recombinant plasmids were isolated by using the QIAPrep Spin Miniprep kit (QIAGEN, USA).

## 2.5.4 Expression and purification of recombinant *VhChiP* in *E. coli* BL21

### (DE3) Omp8 Rosetta strain

Recombinant plasmid was isolated from *E. coli* DH5 $\alpha$  strain and transformed into *E. coli* BL21 (DE3) Omp8 Rosetta strain. Recombinant plasmid was mixed with 100  $\mu$ l of the competent cells and spread onto the LB agar plate containing 100  $\mu$ g/ml ampicillin.

Single colonies of the transformed bacterial cells harboring pET23d(+)/*VhChiP* were grown in 10 ml LB-Ampicillin (100  $\mu$ g/ml) + Kanamycin (25  $\mu$ g/ml) medium, at 37 °C for 16 hr. Afterwards, the starting culture (20 ml) was transferred into 8 x 250 ml LB-Ampicillin (100  $\mu$ g/ml) + Kanamycin (25  $\mu$ g/ml) medium and shaken at 37 °C, 250 rpm until the OD<sub>600</sub> reached 0.6-0.8. Then, isopropyl thio- $\beta$ -D-galactoside (IPTG) was added into the cell culture to a final of 0.5 mM concentration for *VhChiP* induction. Incubation was continued at 37 °C by shaking at 250 rpm for additional 6 hr. After that, the cells were harvested by centrifugation at 4,500 g, 4 °C, 30 min.

For protein purification, cell pellet was re-suspension in 30 ml buffer (20 mM Tris/HCl pH 8.0, 2.5 mM MgCl<sub>2</sub>, 0.1 mM CaCl<sub>2</sub>). 300  $\mu$ l of freshly prepared RNase A (10 mg/ml) and 30  $\mu$ l DNase I (10 mg/ml) was added into the suspension and maintained on ice, it was broken by sonication for 10 min (30% duty cycle; amplitude setting 20%) using Sonopuls Ultrasonic homogenizer with a 6-mm-diameter probe. After that, 20% SDS solution stock was added into the cells suspension to obtain 2% final concentration of SDS and incubated at 50 °C for 1 hr with gentle stirring. Unbroken cells were removed by centrifugation at 22,000 rpm at 4 °C for 60 min (JA 25.50 rotor, Beckman centrifuge Avanti J-20 XP, 50 ml-NAL

GENE Oak Ridge Centrifuge Tube No. 3119-0050, 35 ml capacity). Pellet that contained *VhChiP* porin was extracted by two steps. For pre-extraction step, the pellet containing crude cell wall of the bacterial cells was washed with 15 ml of 0.125% octyl-POE in 20 mM phosphate buffer pH 7.4 (ALEXIS Biochemicals, Lausen, Switzerland). After that, the pellet was homogenized with a Potter-Elvehjem homogenizer and incubated at 37 °C, 250 rpm for 60 min. The pellet was collected by centrifugation at 40,000 rpm, 4 °C for 40 min (Type 70.1 Ti rotor, Beckman Ultracentrifuge Optima LE-80K, 10.4 ml-Beckman Centrifuge Bottles No. 355651 with Noryl 518 Cap Assembly No. 355604-9 ml capacity). For extraction step, the pellet obtained after centrifugation at 40,000 rpm was washed with 15 ml of 3% octyl-POE in 20 mM phosphate buffer pH 7.4 (ALEXIS Biochemicals, Lausen, Switzerland). After that, the pellet was homogenized with a Potter-Elvehjem homogenizer and incubated at 37 °C, 250 rpm for 60 min. The pellet was collected by centrifugation at 40,000 rpm, 4 °C for 40 min. *VhChiP* that was containing in the supernatant fraction was further purified using ion exchange chromatography (Q-column) connected to the ÄKTA prime plus FPLC system. The *VhChiP* protein was eluted with a linear gradient of 0-1 M KCl in 20 mM phosphate buffer, pH 7.4 containing 0.2% LDAO. The purified *VhChiP* was separated by 12% SDS-PAGE (120 mV voltage, 90 min). In addition, concentration of *VhChiP* was determined by BCA protein determination kit (Pierce).

### **2.5.5 Production of anti-*Vh*ChiP polyclonal antibodies and immunoblotting analysis**

Production of anti-*Vh*ChiP polyclonal antibodies was carried out using the in-gel method. Partially purified *Vh*ChiP (~2 µg per well) was separated by 8% SDS-PAGE. Following electrophoresis, the protein bands were stained with Coomassie Brilliant Blue R-250. After thorough de-staining with distilled water, the protein band ( $M_r = 38.36$  kDa) was excised from the gel. The excised band (~80 µg) was homogenized with 200 µl of 1x PBS (pH 7.2), and emulsified with 500 µl Freund's complete/incomplete adjuvant. The emulsified mixture was injected subcutaneously into a female white rabbit to produce anti-*Vh*ChiP antisera. Multiple injections were performed and bleeds were collected as described below:

**Week 0:** Collection of preimmune serum (10 ml)

**Week 1:** Following by immunization with the *Vh*ChiP antigen mixed with the complete Freund's adjuvant

**Week 3:** Collection of blood serum (1 ml), following by first boosting with the antigen (~80 µg) was mixed with the incomplete Freund's adjuvant.

**Week 4:** Collection of blood serum (1 ml), following by second boosting with the antigen (~80 µg) was mixed with the incomplete Freund's adjuvant.

**Week 5:** Collection of blood serum (1 ml), following by third boosting with the antigen (~80 µg) was mixed with the incomplete Freund's adjuvant.

**Week 6:** Collection of blood serum (20 ml)

**Week 7:** Collection of blood serum (40 ml)

**Week 8:** Collection of blood serum (40 ml)

**Week 9:** Collection of blood serum (15 ml)

The bleeds were collected from an ear vein of the immunized rabbit. The serum was obtained after centrifugation at 2,500 rpm, at 4 °C for 20 min. After centrifugation, the serum was collected and used for immunoblotting analysis.

*VhChiP-OmpN* was analyzed by Western blotting and detected with the enhanced chemiluminescence reagent. For western blotting experiment, protein *VhChiP-OmpN* samples (~4.35 µg) were mixed with one-fourth volume of the 5x SDS-gel loading buffer and heated to 100 °C for 10 min. The protein sample was loaded onto 8% SDS-PAGE. After electrophoresis, the gel was soaked in a blotting buffer containing 25 mM Tris, 192 mM glycine, and 20% methanol. The protein band was then transferred onto a nitrocellulose membrane using a semi-dry gel blotting system (Bio-Rad, USA). The transferred membrane was incubated in a blocking solution containing 1x PBS (pH 7.2), 5% non-fat milk for 1 hr at room temperature. The antisera were diluted with 2% non-fat milk into dilution of 1:10,000 to test the production of anti-*VhChiP* polyclonal antibodies. After incubation with the antiserum, the membrane was washed five times with 1x PBS containing 0.1% Tween 20 (PBS-T), followed by incubation in 1:10,000 dilution of the secondary antibody (goat anti-rabbit IgG (HRP)) in 2% non-fat milk for 1 hr at room temperature. The membranes were washed three times with PBS-T, then another two times with 1x PBS with 5 min of incubation per wash. Detection using chemiluminescence was carried out by incubating the membrane with a small volume of chemiluminescence substrate for 3 minutes at room temperature. The membrane was wrapped with Saran wrap, then exposed to an X-ray film in the dark.

### **2.5.6 Expression of *VhChiP* porin on the native bacterial strain *Vibrio harveyi* 650 by induction with insoluble chitins.**

Expression of *VhChiP* porin on the native bacterial strain *Vibrio harveyi* 650 was tested with chitin and colloidal chitin. *VhChiP* porins was induced by 1% crystalline chitin and 1% colloidal chitin. Five milliliter cells were transferred into 500 ml MM-medium, 250 rpm, at 30 °C, until OD<sub>600</sub> reached about 0.7-0.8 for 2 hr. Then 1% crystalline chitin and 1% colloidal chitin were added into the cell culture and the cells continued to grow for additional 6 hr. One milliliter of bacterial culture was collected every 1 hr after induction and centrifuged at 4,500 rpm. The induced *VhChiP* was separated by 10% SDS-PAGE, at 120 Volt voltage for 60 min. Then, induced *VhChiP* porin was checked by immunoblotting with anti-*VhChiP* polyclonal antibodies.

### **2.5.7 PCR primers of mutants (W136A, W136F, W136R and W136D)**

The oligonucleotide primers for generation of recombinant *VhChiP*-pET23d(+) mutations of :

W136 → Ala (W161A)

W161 → Phe (W161F)

W136 → Arg (W136R)

W136 → Asp (W136D)

They are shown in Table 2.2.

**Table 2.2** Primers for site-directed mutagenesis.

| <i>VhChiP</i>    | 5'-3' Primers   |
|------------------|---|
| 1) Trp136 (WT)   | (F) 5'-ataccatggcgtcttacctaaagaaaag-3' ( <i>NcoI</i> )<br>(R) 5'-aacctcgagttagaagtagtattcaacac-3' ( <i>XhoI</i> ) |
| 2) Trp136Ala     | (F) 5'-ggctaggtgatgtttacgacgcaggtggtgctatcggtggtgc-3'<br>(R) 5'-gcaccaccgatagcaccacctgcgtcgtaaacatcacctagacc-3'   |
| 3) Trp136Phe     | (F) 5'-ggctagggcgatgtttacgactttggtggtgcgattggtggtgc-3'<br>(R) 5'-gcaccaccaatcgaccaccaagtcgtaaacatcgctagacc-3'     |
| 4) Trp136Asp (-) | (F) 5'-ggctagggcgatgtttacgacgatggtggtgcgatctgtggtgc-3'<br>(R) 5'-gcaccacagatcgaccaccatcgtcgtaaacatcgctagacc-3'    |
| 5) Trp136Arg (+) | (F) 5'-ggctagggcgatgtttacgaccgtggtggtgcgatctgtggtgc-3'<br>(R) 5'-gcaccacagatcgaccaccaggtcgtaaacatcgctagacc-3'     |

**Note:** Sequences underlined indicate the mutated codons

### 2.5.7.1 Mutational design and site-directed mutagenesis

PCR products for mutations of W136A, W136F, W136R and W136D were amplified by using the recombinant plasmid pEt23d(+)-VhChiP as DNA template as description in Table 2.3 and Table 2.4.

**Table 2.3** The PCR reaction was used for site-directed mutagenesis.

| Content   | DNA template  | DNA template |
|---|---------------|--------------|
| 1. Primers                                      |               |              |
| -Forward primer<br>(W136A, W136F, W136R, W136D) | 125 ng        | 125 ng       |
| -Reverse primer<br>(W136A, W136F, W136R, W136D) | 125 ng        | 125 ng       |
| 2. DNA template                                 | 25 ng         | 50 ng        |
| 3. dNTP mix                                     | 1 $\mu$ l     | 1 $\mu$ l    |
| 4. Vi buffer (A) 10X                            | 5 $\mu$ l     | 5 $\mu$ l    |
| 5. DNA polymerase (5 U/ $\mu$ l)                | 0.5 $\mu$ l   | 0.5 $\mu$ l  |
| 6. MgCl <sub>2</sub> (50 mM)                    | 5 $\mu$ l     | 5 $\mu$ l    |
| 7. H <sub>2</sub> O                             | 36.52 $\mu$ l | 36.4 $\mu$ l |
| Total volume                                    | 50 $\mu$ l    | 50 $\mu$ l   |

**Table 2.4** The PCR condition was used for site-directed mutagenesis.

| Cycling parameters   | Cycle | Temperature (°C) | Time (min) |
|----------------------|-------|------------------|------------|
| Initial denaturation | 1     | 97               | 2          |
| Denaturation         |       | 97               | 20 second  |
| Annealing            | 16    | 55               | 1          |
| Extension            |       | 68               | 10         |

**Note:** 16 cycles for single amino acid changes

After PCR reaction, 1  $\mu$ l of the *Dpn* I restriction enzyme (10 U/L) was added directly to each amplification reaction and each reaction mixture was gently mixed by pipetting the solution up and down several times. The reaction mixtures were spin down in a microcentrifuge for 1 minute and immediately incubated each reaction at 37 °C for 1 hour to digest the parental (i.e., the non-mutated DNA) supercoiled dsDNA. After that, (10-15  $\mu$ l) *Dpn* I-treated DNA (W136A, W136F, W136R and W136D) from each control and sample reaction was transformed into XL1-blue competent cells and grown at 37 °C, for 18 hr. Recombinant plasmids of the mutants were isolated and confirmed by using DNA sequencing.

#### **2.5.7.2 Expression and purification of the mutants (W136A, W136F, W136R and W136D)**

The correctly mutated codons were verified by DNA sequencing preparation of the mutants (W136A, W136F, W136R and W136D). After transformation into BL21 (DE3) Omp8 Rosetta strain, single colonies of bacterial

cells were grown in LB-broth (containing 100 µg/ml ampicillin, 25 µg/ml kanamycin and 1% glucose) at 37 °C for overnight (18 hr). The starter culture (100 × 4 ml) was transferred into 1,000 × 4 ml of LB-amp/kana and be grown at 37 °C for 4 hr until the OD<sub>600</sub> of about 0.6 and induced with 0.5 mM IPTG for 6 hr. The cell culture was collected by centrifugation at 4,500 rpm for 30 min. The mutants were then isolated by 2% (w/v) SDS, and extracted with 3% octyl-POE (v/v) in 20 mM phosphate buffer, pH 7.4. After that, the mutated protein was incubated at 37 °C for 1 hr and centrifuged at 40,000 rpm for 40 min. The mutants contained in the supernatant fraction were further purified by using ion exchange chromatography.

#### **2.5.8 Analysis of wild-type and mutated chitoporins: Single channel conductance, voltage dependence and ion selectivity**

Both painted solvent-containing and the Montal-Mueller-type solvent free black lipid membranes were subjected to chitoporin single-channel analysis. The preparation of the aqueous electrolyte buffer solutions, the formation of solectin and DPhPC lipid bilayer membranes of the two types and the membrane reconstitution of trimeric chitoporins were employed following the procedures reported in the literature (Montal *et al.*, 1972; Mueller *et al.*, 1964; Jordy *et al.*, 1996; Kreir *et al.*, 2008). To obtain complete knowledge about ion channel properties, the biophysical measurements were performed at identical conditions:

- in different KCl-salt concentrations (e.g. 0.25 M, 0.5 M, and 1 M, etc.)
- at varying membrane potentials (voltages across the membrane)
- with various concentration of chitoporin added to *cis*-side.

At all the different conditions, the membrane current ( $I_m$ ) was recorded as a function time (t). In case of the solvent-free Montal-Mueller-type solvent depleted bilayers this was possible at a time resolution in the sub-millisecond range. The  $I_m$  vs. time traces was stored and used for the calculation of the channel conductance at the given parameters. Measurements were initially applied to the wild-type chitoporin. In further work, recordings under identical conditions were carried out for chitoporin mutants with thoughtfully introduced point mutations of amino acid residues that are likely to have an influence on the functional channel characteristics. In course of the analysis the behavior of the wild-type (WT) and mutant chitoporins were carefully compared and the effect of the mutations interpreted.

#### **2.5.8.1 Ion selectivity**

A technique widely used for measuring the ionic selectivity in the *VhChiP* channel and its mutants is its reconstitution in planar lipid membranes. This technique, introduced by Mueller et al. (Mueller *et al.*, 1962) and later improved by Montal and Mueller (Montal *et al.*, 1972), consists of forming a lipid membrane by the apposition of two lipid monolayers made from a 5 mg/ml of diphytanoyl phosphatidylcholine (DPhPC). The lipid bilayer is formed in a 50-100  $\mu\text{m}$  hole made on a 25  $\mu\text{m}$  thick Teflon film separating two solutions (Bezrukov *et al.*, 1993). The membrane was formed by raising the level of the buffer solution where a small amount of lipid dissolved in *n*-pentane has been dropped. Before the start of the experiments, the hole was pretreated with a 1% solution of hexadecane in hexane to increase membrane stability. Single channel insertion appeared by addition of 0.25-0.5  $\mu\text{l}$  of a 100 ng/ $\mu\text{l}$  solution of *VhChiP* and its mutant in a buffer solution that contains 0.25% (v/v) of LDAO in 20 mM phosphate buffer (pH 7.4) to a 2.5 ml on the

*cis*-side of the membrane (connected to ground). The membrane potential is applied across the Ag/AgCl electrodes. The ionic selectivity measurement is commonly evaluated to measure the zero-current membrane potential ( $V_m$ ).  $V_m$  is defined as the applied transmembrane voltage that yields zero electric current when there is a concentration gradient across the channel (Hille *et al.*, 2001). Firstly, a lipid membrane is formed at a ratio of salt concentrations gradient starting from 0.1 M KCl on both sides, a molecule of *VhChiP* and its mutant was inserted with highly applied potential (+/-150 mV or +/-199 mV). The channel conductance is checked by applying with any different voltages. The zero-current membrane potential reached to 0 mV. Increasing of salt concentrations with titration of 200  $\mu$ l (3 M KCl) into *trans*-side of the chamber to a final ratio of salt concentrations reached 1.5 M. Note that, with any point of salt concentrations, the ionic current through the channel is set to zero to record the zero-current membrane potential. The  $P_{K^+}/P_{Cl^-}$  values were calculated and analyzed using the Goldman-Hodgkin-Katz equation.

$$V_m = \frac{RT}{F} \ln \left[ \frac{P_{K^+} [K^+]^{cis} + P_{Cl^-} [Cl^-]^{trans}}{P_{K^+} [K^+]^{trans} + P_{Cl^-} [Cl^-]^{cis}} \right] \quad \text{Eq. 2.1}$$

Where  $V_m$  is the membrane potential (in Volts); R is the ideal gas constant (8.314 J/K/mol); T is the temperature in kelvins; F is Faraday's constant;  $P_{ion}$  is the permeability for that ion;  $[ion]^{cis}$  is the extracellular concentration of that ion and  $[ion]^{trans}$  is the intracellular concentration of that ion.

### 2.5.8.2 Single channel conductance analysis of wild-type and mutant

#### *V. harveyi* chitoporin in the presence of chitooligosaccharides

Single channel conductance and sugar translocation through the single nanopore conductance followed the methods previously described (Bezrukov *et al.*, 2000; Schwarz *et al.*, 2003; Danelon *et al.*, 2003; Kullman *et al.*, 2002; Mahendran *et al.*, 2009; Van Gelder *et al.*, 2000; Winterhalter, 2000; Berkane *et al.*, 2005). Briefly, during forming of bilayers, the cuvette consisted of two chambers separated by a 25  $\mu\text{m}$  thick Teflon film. A small aperture about 50-100  $\mu\text{m}$  in diameter was pre-treated with 1  $\mu\text{l}$  of 1% (v/v) hexadecane in hexane (Sigma-Aldrich) and dried for 10 min. 2 ml of 1 M KCl (20 mM Hepes, adjusted to pH 7.5) as a bulk solution was added into the *cis*- and *trans*-side of the chamber and Ag/AgCl electrodes immersed on either side of the Teflon film. 1, 2 Diphytanoyl-*sn*-glycero-3-phosphocholine (DPhPC) was used to form a lipid bilayer membrane. One of electrode (called *cis*-) was used to connect as the ground electrode, whereas the other (*trans*-) was connected to the input of the current amplifier. Concentration of about 50-100  $\mu\text{g}/\text{ml}$  of the trimeric molecule *VhChiP* or *its* mutants were added into the side that we assumed as *cis*-side of the lipid membrane. The single molecule of *VhChiP* or its mutant was inserted into bilayer membrane by application of high voltages (+/-199 mV). After protection of multiple insertions of other single protein molecules by dilution with a sequential addition of the working electrolyte solution, different concentration of chitohexaose (0.25 to 20  $\mu\text{M}$ ) were added into the *cis* or *trans* side to observe the diffusion of sugar molecules through the channel and the blocking events for the flow of ions were recorded for at least 60 s at transmembrane potentials of +/- 50 mV and +/-100 mV. Single channel recording measurements were performed with

an Axopach 200B amplifier in the voltage clamp mode and internal filter set at 10 kHz by using pCLAMP version 10.0 software (Molecular Devices, Sunnyvale, CA). The equilibrium binding constant ( $K$ ,  $M^{-1}$ ) was estimated from the reduction of the single channel conductance in the presence of different concentration of chitohexaose using Eq. 2.2 (Benz *et al.*, 1987; Andersen *et al.*, 1998),

$$G_{\max} - G_{[c]} / G_{\max} = I_0 - I_{[c]} / I_0 = K \cdot c / (1 + K \cdot c) \quad \text{Eq. 2.2}$$

When  $G_{\max}$  is the average conductance of the fully open *VhChiP* channel and its mutant,  $G_{[c]}$  is the average conductance at the point of a given concentration of chitohexaose ( $[c]$ ),  $I_0$  is the initial current through the fully open channel in the absence of chitohexaose and  $I_{[c]}$  is the current at the particular chitohexaose concentration. The binding constant was calculated by inverting the Eq. 2.2 into Lineweaver-Burk plot ( $((G_{\max} - G_{[c]} / G_{\max})^{-1})$  versus  $([c]^{-1})$ ). In term of binding affinity, we calculated the off-rate ( $k_{\text{off}}$ ,  $s^{-1}$ ) from the single trimeric molecule of *VhChiP* channel and its mutant after titration with different concentrations of chitohexaose that was obtained from Kullman *et al.* (Kullman *et al.*, 2002) (Eq. 2.3),

$$k_{\text{off}} = 1/\tau_c \quad \text{Eq. 2.3}$$

When the  $\tau_c$  is the average residence (dwell) time ( $s^{-1}$ ) obtained from the single molecule of chitohexaose crossing and staying in the channel. Thus, the on-rate ( $k_{\text{on}}$ ,  $M^{-1}s^{-1}$ ) is given by  $k_{\text{on}} = K \cdot k_{\text{off}}$ .

### 2.5.9 Titration experiments of *VhChiP* and its mutant via Fluorescence

#### Spectroscopy

The binding of substrates to *VhChiP* was also measured using titration experiments via Fluorescence Spectroscopy. These experiments were carried out by adding 500  $\mu\text{l}$  of 20 mM phosphate buffer, pH 7.4 containing 0.2% lauryldimethylamine oxide into the cuvette that contained a constant concentration of *VhChiP* and *its* mutants in solution (80 ng/ $\mu\text{l}$ ). Spectra were recorded at  $20 \pm 3$  °C in 1-cm quartz cuvettes. After measurement of the spectrum of *VhChiP* and *its* mutants, each chitooligosaccharide was added in defined concentration into the cuvette at increasing concentrations (5-1,000  $\mu\text{M}$ ). The spectrum was recorded for each condition with a Spectrofluorometer. The change of intrinsic tryptophan fluorescence spectra was recorded at  $20 \pm 3$  °C, under constant stirring, with a slit width of excitation and emission of 10 nm and 5 nm, at the emission length between 300 to 550 nm and the excitation of tryptophan at 295 nm. Stock solutions of each chitooligosaccharides were prepared in 20 mM phosphate buffer, pH 7.4 containing 0.2% lauryldimethylamine oxide. The fluorescence intensity data were analyzed by a non-linear regression function available in Prism version 5.0 using the following single-site binding model. To estimate the dissociation binding constants, a plot of relative fluorescence ( $F_0-F$ ) as a function of sugar concentrations yielded a well-defined hyperbolic curve, allowing the calculation of the equilibrium dissociation constant ( $K_D$ ,  $\mu\text{M}$ ) of each corresponding chitosugars using a single site binding model, as obtained from the Stern-Volmer Equation (Eq. 2.4) (Neves *et al.*, 2005 and 2009),

$$F_0 - F = 1 + k_q \tau_0 [Q] = 1 + K_D [Q] \quad \text{Eq. 2.4}$$

When  $F_0$  and  $F$  are the fluorescence intensities in the absence and presence of chitosugars,  $k_q$  is the bimolecular quenching constant;  $\tau_0$  is the lifetime of the fluorophore in the absence of chitosugars, and  $Q$  is the concentration of chitosugars. The Stern-Volmer quenching constant is given by  $K_D = k_q \cdot \tau_0$ . If the quenching is known to be dynamic, the Stern-Volmer constant was represented by  $K_D$ . Otherwise this constant was described as  $K_{SV}$ . Quenching data are usually presented as plots of  $F_0 - F$  versus  $[Q]$ . Because of the  $F_0 - F$  was expected to be linear function for the initially starting titration until saturation at high concentration dependent on the concentration of chitosugars. A plot of  $F_0 - F$  versus  $[Q]$  yields an intercept of one on the y-axis and a slope equal to be  $K_D$ . Furthermore, to obtain the Gibbs free energy, the binding constant is a special case of the equilibrium binding constant ( $K$ ,  $M^{-1}$ ). It is associated with the binding and unbinding reaction of receptor (R) and ligand (L) molecules, which is formalized as:



The reaction is characterized by the on-rate constant  $k_{on}$  and the off-rate constant  $k_{off}$ . In equilibrium, the forward binding transition  $R + L \rightarrow RL$  should be balanced by the backward unbinding transition  $RL \rightarrow R + L$ , so that is,

$$k_{on} [R] [L] = k_{off} [RL] \quad \text{Eq. 2.6}$$

Where [R], [L], and [RL] represent the concentration of unbound free receptors, the concentration of unbound free ligand and the concentration of receptor-ligand complexes.

The binding constant or the association constant  $K_a$  is defined by:

$$K_a = k_{\text{on}}/k_{\text{off}} = [\text{RL}]/[\text{R}] [\text{L}] \quad \text{Eq. 2.7}$$

An often considered quantity is the dissociation constant  $K_D = 1/K_a$ . For the binding of receptor and ligand molecules in solution, the molar Gibbs free energy ( $\Delta G$ ), or the binding affinity is related to the dissociation constant  $K_D$  via,

$$\Delta G_{\text{binding}} = RT \ln [K_D] \text{ or } \Delta G_{\text{binding}} = 2.303RT \log_{10} [K_D] \quad \text{Eq. 2.8}$$

Where R is the ideal gas constant (8.314 J/K/mol) and T is the absolute temperature (T = 298 K).

#### 2.5.10 Liposome swelling assay

The liposome swelling assay was carried out to verify permeability of chitohexaose through *VhChiP* (WT) and its mutants. *E. coli* total lipid extract (Avanti) (20 mg/ml in chloroform) was used to form multi-lamellar liposomes and 17% (w/v) dextran ( $M_r = 40,000$  Da) was entrapped in the liposomes. The purified WT (100 ng) or its mutant were reconstituted into liposomes as described previously (Luckey and Nikaido, 1980; Yoshimura and Nikaido, 1985). *E. coli* total lipid extract was used to form liposomes and 17% (w/v) dextran ( $M_r = 40,000$  Da) was entrapped in the

liposomes. The isotonic solute concentration was determined with 40 mM D (+)-raffinose solution (prepared in 20 mM Hepes buffer, pH 7.5) added into the proteoliposome suspension. The value obtained for isotonic concentration of D (+)-raffinose was used as an approximation to facilitate the adjustment of isotonic concentrations for different solutes. Thirty microliters of liposome or proteoliposome solution was diluted into 600  $\mu$ l of the isotonic test solution in a 1 ml cuvette and mixed manually. The initial swelling rate upon addition of the isotonic sugar solutions was monitored using a UV-Vis spectrophotometer with the wavelength set at 500 nm. The absorbance change over the first 60 sec was used to estimate the swelling rate (per second,  $s^{-1}$ ) using the equation:  $\Phi = (1/A_i)dA/dt$ , in which  $\Phi$  is the swelling rate,  $A_i$  the initial absorbance, and  $dA/dt$  the rate of absorbance change during the first 60 s. The swelling rate of 750  $\mu$ M chitohexaose was normalized by setting the rate of D (+)-arabinose ( $M_r = 150$  g/mol) to 100%. Protein-free liposomes and proteoliposomes without sugars were used as negative controls.

### 2.5.11 Temperature measurement

Lipid bilayer of temperature measurements and single channel analysis were performed as following to the technique developed by Montal and Mueller with a modification (Chimerel *et al.*, 2008; Jung *et al.*, 2006; Kang *et al.*, 2005; Mahendran *et al.*, 2009). Briefly, a cell with a 50-100  $\mu$ m diameter aperture in a 25- $\mu$ m-thick Teflon partition provided a two compartment black lipid membrane (BLM) chamber and two Ag/AgCl electrodes at either side of dividing wall allowed voltage control of solvent-depleted planar lipid bilayers that were formed using a solution of DPhPC in pentane. Low concentration about 50-100  $\mu$ g/ml of the trimeric molecule of *VhChiP*

or its mutants were added into *cis* side of the lipid membrane. The single channel inserted into bilayer membrane at high voltages ( $\pm 199$  mV). After protection of the multiple insertion from another single molecule of protein by dilution with a sequential addition of the working electrolyte solution, one concentration of chitohexaose was added on *cis* or *trans* side to observe the sugar diffusion through the channel and the blocking event of ions flow and record for at least 60-120 s at transmembrane potentials of  $\pm 50$  mV and  $\pm 100$  mV. Starting with the trials of the temperature dependence for sugar translocation, the temperature was lowered to 5 °C and the temperature measurement started. The temperature was increased and adjusted to different point of temperatures. A Peltier element (Dagan Corporation, Minneapolis, MN, USA) was used for accurate temperature regulation of the BLM chamber. Single channel measurements were recorded by using an Axopatch 200B amplifier (Molecular Devices, Sunnyvale, CA, USA) in the voltage clamp mode and the internal filter at 10 kHz and analyzed by using pClamp v.10.0 software (Molecular Devices).

## CHAPTER III

### RESULTS

#### 3.1 Gene identification, cloning, expression and protein purification

The availability of the complete genome sequence of *V. harveyi* type strain ATCC BAA-1116 BB120 in the GenBankH database enabled to identify an open reading frame that encodes a hypothetical chitoporin (ChiP). To isolate the gene encoding ChiP from the genome of the closely related species *V. harveyi* type strain 650, specific oligonucleotide primers were designed, based on the identified ChiP gene from the BAA-1116 BB120 strain. The full-length ChiP cDNA was amplified by the PCR technique. The nucleotide sequence of the identified gene comprises 1,125 bps, which was translated to a putative polypeptide of 375 amino acids, including the 25-aa signal sequence. The theoretical mass of the full-length *VhChiP* was 41,089.10 Da, with a predicted pI of 4.09. BLAST searching of the translated *VhChiP* sequence gave high score hits with putative chitoporin of several species in the family *Vibrionaceae* in the SwissProt/UniProtKB database. *VhChiP* shows low sequence identity (< 20%) with other functionally already characterized outer membrane porins, such as *E. coli* OmpF (P02931), *E. coli* OmpC (P06996), *E. coli* OmpA (P0A910), *E. coli* OmpN (P47747), *Pseudomonas fluorescens* OprD (Q3LAG8), and *Neisseria gonorrhoeae* PorB (Q5XKX0). Figure 3.1 presents an amino acid sequence alignment of *VhChiP* with chitoporin from *V. furnissii* (accession number 09KK91) (Keyhani *et*

*al.*, 2000), *E. coli* LamB or maltoporin (maltose-specific porin, P02943) (Clément *et al.*, 1981), and *Salmonella typhimurium* ScrY (sucrose-specific porin, P22340) (Forst *et al.*, 1998). The sequence identity of *VhChiP* with *V. furnissii* chitoporin is 40%, while it shows remarkably low identity with other sugar-specific porin: LamB (15.3%), and ScrY (12.9%). It is also only 15.7% identical to a carbohydrate-selective porin *Pseudomonas aeruginosa* OprB (Wylie *et al.*, 1994; Trias *et al.*, 1988). In LamB, six aromatic residues (Y6, Y41, W74, F229, W358 and W420) located in the pore lumen form a polar track, which facilitates ion and sugar transport (Schirmer *et al.*, 1995; Dumas *et al.*, 2000; Dutzler *et al.*, 2002; Denker *et al.*, 2005). Y118, on the other hand, controls the central constriction of the LamB channel (Orlik *et al.*, 2002; Orlik *et al.*, 2002).

Sequence alignment (Figure 3.1) shows that the residues Y6, Y41, W74, W358 and W420 of LamB are well aligned with Y78, Y118, W151, F435 and W482, respectively, of ScrY. In marked contrast, *VhChiP* displays substantial sequence dissimilarities with both LamB and ScrY. Only two residues in LamB (W74 and W358) are aligned with F64 and Y310 of *VhChiP*. Furthermore, Y118 of LamB shows no match with any aromatic residue of *VhChiP*, which indicates that the functionality of pore constriction by Y118, as found in LamB, is governed by a different residue located elsewhere in the *VhChiP* sequence. Submission of the putative sequence of *VhChiP* through the Swiss-Model database generated a structural model of *VhChiP* (Figure 3.2) using *Delftia acidovorans* Omp32 as template (pdb 2GFR) (Zeth *et al.*, 2000).

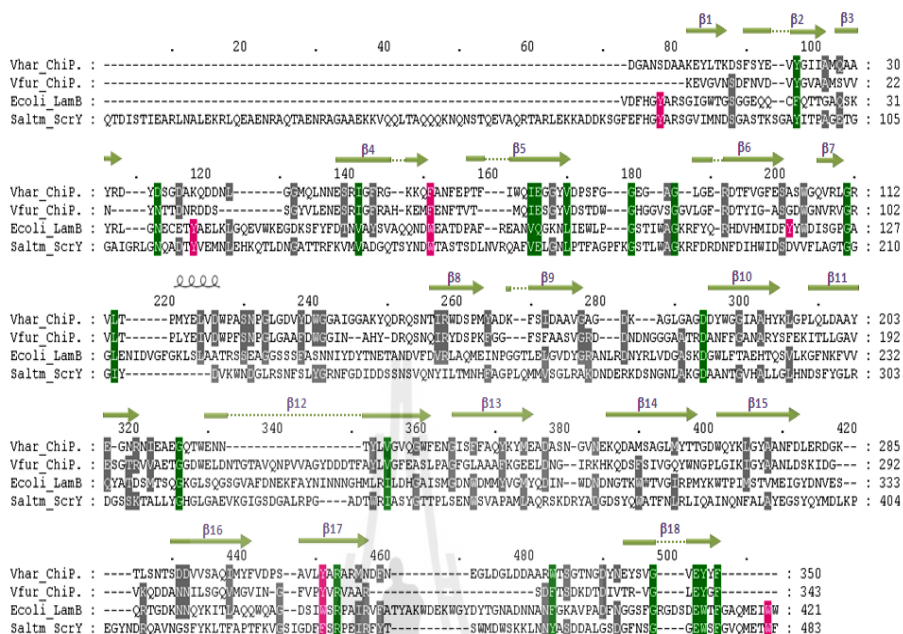


**Figure 3.1** Alignment of the putative *V. harveyi* chitoporin sequence with other sugar-specific porins. Amino acid sequences of *V. furnissii* chitoporin (Q9KK91), *E. coli* LamB or maltoporin (P02943), and *S. typhimurium* ScrY (P22340) were retrieved from the SwissProt/UniProtKB protein databases, aligned using “CLUSTALW” algorithm in the DNASTAR package, and displayed in Genedoc. The secondary structure of *VhChiP* was constructed by ESPript v. 2.2 according to the structure of *Delftia acidovorans* Omp32 (pdb 2GFR) (Zeth *et al.*, 2000). The residues that are aligned with Y6, Y41, Y118, W74, W358, and W420 of *E. coli* LamB are shaded in magenta. Green shading refers to amino residues conserved within the four sequences.  $\beta$ -strands are represented as green lines with an arrow.

Compared with porins with known 3D-structures, *VhChiP* is closest to Omp32 with a sequence identity of 20.5%. Figure 3.1 shows the secondary structural features of *VhChiP*, which are similar to those of most Gram negative bacterial porins, with 18  $\beta$ -strands forming a barrel structure (Figure 3.2A). These predicted 18 anti-parallel  $\beta$ -strands make up only 16 putative membrane-spanning domains, as strand  $\beta$ 2 is connected with  $\beta$ 3 and forms the first transmembrane domain, whereas strand  $\beta$ 1 with  $\beta$ 18 are part of the last domain (Figure 3.1 and Figure 3.2A). The predicted transmembrane topology (Figure 3.2C) indicates considerable irregularity of the extracellular loops (L1-L8), while the eight periplasmic turns are short and of similar length. The longest extracellular loop (L3), comprising 41 amino acids (G111 to N151), lies between strands  $\beta$ 7 and  $\beta$ 8. A typical right-handed  $\alpha$ -helix is found at the early part of L3 at positions P116 to W123 (Figure 3.2B). This loop, known as a pore-confined loop, is responsible for the size-selectivity of sugar-specific porins (LamB and ScrY) (Forst *et al.*, 1998; Schirmer *et al.*, 1995) and general diffusion porins (Koebnik *et al.*, 2000; Nikaido *et al.*, 1992).

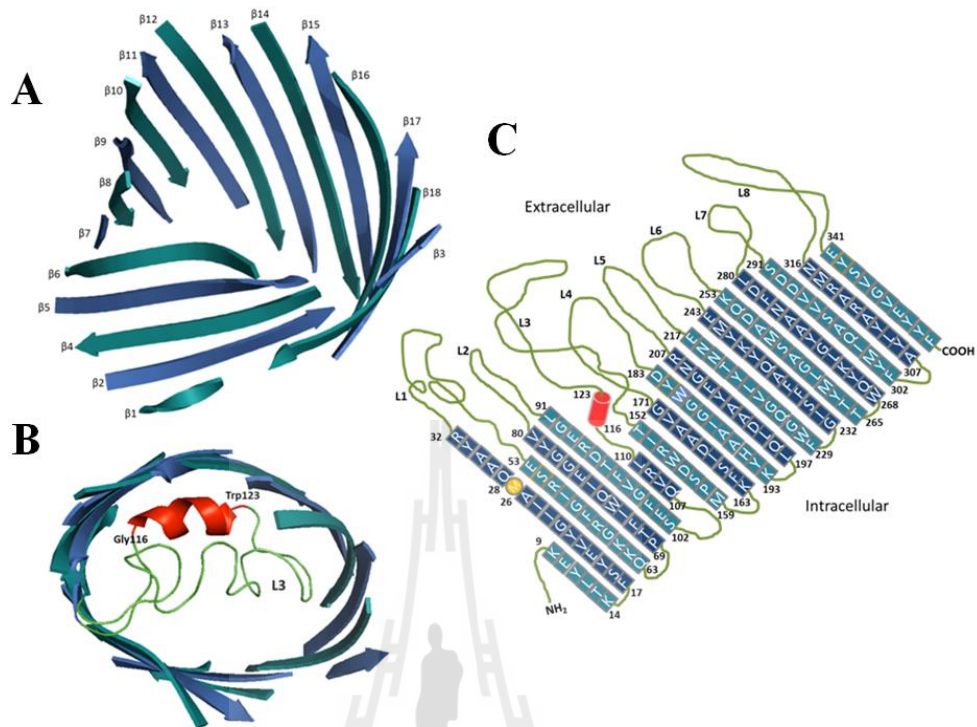


**Figure 3.2** The Swiss-Model 3D-structure of *V. harveyi* chitoporin. A) Side view of a ribbon representation of *VhChiP*. The homology structure was constructed by the SWISS-MODEL program using an automated mode (<http://swissmodel.expasy.org/>). The x-ray structure of *D. acidovorans* Omp32 (pdb 2GFR) was selected as structure template. B) Top view of the modeled structure, showing L3 as the pore-confining loop with a short helix consisting 8 amino acids (G116-W123) presented in red. C) Transmembrane domains of *VhChiP* were depicted based on the homology structure (Figure 3.2A–B) and the structure-based alignment (Figure 3.1) (Zeth *et al.*, 2000).

A BlastP search using chitoporin from *V. furnisseyi* (UniProtKB/TrEMBL entry: Q9KK91 and Keyhani *et al.*, 2000) as protein template identified putative chitoporins from several marine bacteria in family *Vibrionaceae*, including a hypothetical protein VIB-HAR\_01269 (accession number YP\_001444474) from *V. harveyi* type strain ATCC BAA-1116 BB120. Therefore, specific oligo-nucleotides were designed from the hypothetical gene of the BAA-1116 BB120 strain in order to obtain the gene encoding chitoporin from our laboratory strain (*V. harveyi* type strain 650). Figure 3.3A was shown the Genomic DNA from the bacterium of *V. harveyi* type strain 650 using PureLink™ Genomic DNA Kits (Invitrogen, Gibthai Company Ltd., Bangkok, Thailand) and used as the DNA template for PCR amplification.

Both the oligonucleotides 5'-ATACCATGGCGTCTTACCTAAAGAAAAG-3' (forward primer) and 5'-AACCTCGAGTTAGAAGTAGTATTCAACAC-3' (reverse primer) were used for PCR amplification. The PCR product was of the expected size about 1.12 kbp (Figure 3.3B) and was firstly cloned into pGEMt easy vector (Figure 3.3C) and further sub-cloned into pET23d(+) expression vector using *Nco* I and *Xho* I cloning sites (sequences underlined) following the protocol supplied by the manufacturer (Figure 3.3D). Nucleotide sequences of sense and anti-sense strands of the PCR fragment were determined by automated sequencing (First BASE Laboratories Sdn Bhd, Selangor Darul Ehsan, Malaysia).

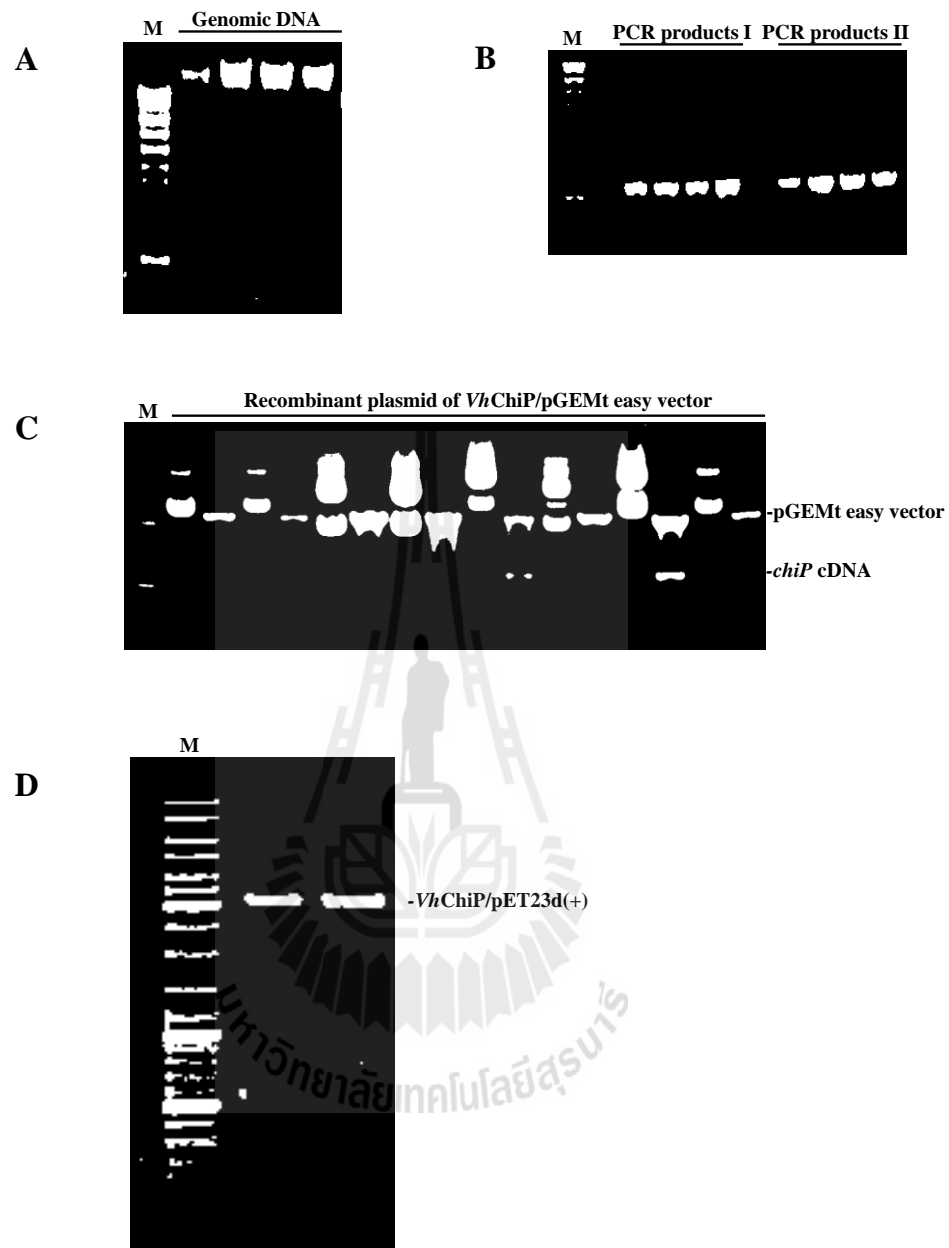


**Figure 3.3** Agarose gel electrophoresis of Genomic DNA (A) were isolated from *V. harveyi* 650; PCR products (B); recombinant plasmid *VhChiP/pGEMt* easy vector (C); *VhChiP/pET23d(+)* (D) obtained by cloning into both pGEMt easy vector and pET23d(+) (Suginta *et al.*, 2013).

After the correct nucleotide sequence was confirmed, the full-length *chiP* DNA obtained from PCR amplification was cloned into pET23d(+) expression vector, which was ready to be expressed in *E. coli* BL21(DE3) Omp8 Rosetta strain. The recombinant protein was expressed with the 25-amino acid *N*-terminal signal sequence attached, to aid protein targeting to the bacterial cell envelope. After proteolytic removal of the signal sequence, the mature *VhChiP* contains 350 amino acid residues and has a predicted  $M_r$  of 38,508.97 Da.

Firstly, the *VhChiP* was isolated with the contamination OmpN protein. The SDS-PAGE analysis displayed that the upper band migrated close to 40 kDa and the lower band migrated to slightly lower than 40 kDa (Figure 3.5A). Identification of tryptic peptides by high resolution ESI MS gave a primary hit with gi|3273514 porin OmpN from *E. coli* for the higher MW band, while the lower protein band was identified as gi|28897534 putative chitoporin from *V. parahaemolyticus* RIMD 2210633, as well as gi|153834464 outer membrane protein from *V. harveyi* HY01, and gi|156973567 hypothetical protein from *V. harveyi* ATCC BAA-1116. Given that no functionally-identified chitoporin of the *V. harveyi* species is available in the NCBI database and assume that the identified peptides of the lower MW protein were derived from chitoporin.

Figure 3.4 shows further cells induction by 0.5 mM IPTG for 6 hr and cell-wall extraction by SDS, following 0.125% (v/v), and then 3% (v/v) octyl-POE in 20 mM phosphate buffer (pH 7.4), the solubilized fraction contained enriched *VhChiP*. SDS-PAGE analysis revealed a several protein bands. To obtain highly purified *VhChiP* for functional characterization, the detergent-extracted *VhChiP* was further purified by ion exchange chromatography using a HiTrap Q resin column.

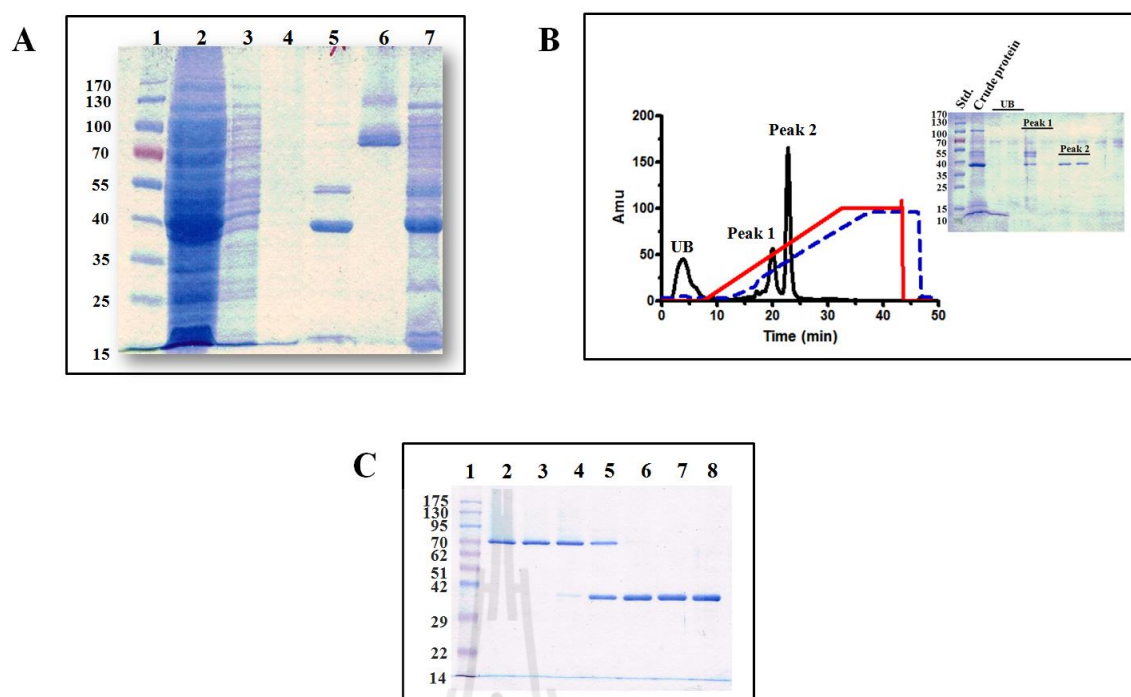


**Figure 3.4** SDS-PAGE analysis of *V. harveyi* chitoporin. A) SDS-PAGE of outer membrane proteins extracted with 2% (w/v) SDS (lane 2), washed with 0.125% octyl-POE (lane 3-4), followed by 3% (v/v) octyl-POE (lane 5-6, heated (5) or unheated (6)) and the pellet after 3% Octyl-POE extraction (lane 7). *E. coli* OmpN and *VhChiP* bands were identified by mass spectrometry. B) Chromatographic profile of *VhChiP* purification with a Hitrap Q HP prepacked column ( $5 \times 1$  ml) connecting to an ÄKTA Prime plus FPLC system. The column was eluted with a linear gradient of 0-1 M KCl. SDS-PAGE analysis of unbound (UB) and bound fractions P1 and P2 is shown in an inset. C) Heat stability of *VhChiP*. The purified ChiP was subjected to different temperatures 0 (lane 2), 40 (lane 3), 50 (lane 4), 60 (lane 5), 70 (lane 6), 80 (lane 7) and 100 °C (lane 8) and then run on a 10% polyacrylamide gel (Suginta *et al.*, 2013).

Figure 3.4B shows a chromatographic profile of *VhChiP* purification. After removal of the unbound fraction ('UB'), the bound proteins were then eluted in two peaks ('P1' and 'P2') when a linear gradient of 0-1 M KCl was applied. SDS-PAGE analysis shows that *VhChiP* was in the second peak (P2) and the protein was pooled and run check on SDS-PAGE (Figure 3.4B; see in an inset). After purification by using ion-exchange chromatography, *VhChiP* becomes homogeneity. The pooled sample from peak P2 was heat-treated at different temperatures for 10 min, and then analyzed by SDS-PAGE. Figure 3.4C shows migration of the purified *VhChiP* to above 95 kDa, corresponding to the trimeric form, when unheated (lane 2). The trimer remained intact when the temperature was raised to 40 °C, but began to dissociate at 50 °C. At 60 °C, more than half of the *VhChiP* trimers were dissociated to monomers and at 70 °C or above, no trimers remained. These results indicate that *VhChiP* is a heat-sensitive, SDS-stable trimer; each subunit has apparent MW of approximately 38.5 kDa, consistent with the predicted MW of the translated polypeptide lacking the signal sequence.

To ensure that the recombinant protein obtained was chitoporin and not contaminating OmpN, which was co-expressed by the *E. coli* host strain Omp8 Rosetta, polyclonal antibodies against OmpN and *VhChiP* were raised independently. Figure 3.5A shows a Coomassie Blue stained gel of different porins, corresponding to the immunoblot with anti-*VhChiP* antiserum (Figure 3.5B). It is clear that the antibody recognized only the *VhChiP* band (Figure 3.5A, lane 1: lower band and lanes 2 and 3), but not *E. coli* OmpN (lane 1, upper band and lane 4), *E. coli* OmpF (lane 5) and *B. pseudomallei* Omp38 (lane 6). The results suggest no cross reactivity of anti-*VhChiP* antibody with other porins. Figure 3.5C–E further confirmed that there was no cross-reactivity of the anti-*VhChiP* serum with OmpN and anti-*E. coli* OmpN serum with *VhChiP*. Anti-*VhChiP* serum recognized only *VhChiP* (Figure 3.5D, lanes 1 and 2), and correspondingly, anti-OmpN serum reacted only with OmpN (Figure 3.5E, lane 3).

To determine whether expression of native chitoporin in *V. harveyi* type strain 650 was controlled by the chitin-induced operon, expression profiles of *VhChiP* were evaluated after the bacterial cells were grown in the presence of chitin. Figure 3.5F shows a Coomassie stained gel of the cell lysates prepared at different times of induction, while Figure 3.5G shows the corresponding immunoblot with anti-*VhChiP* antibody. It is seen that the antibody reacted with the protein bands in the position of purified *VhChiP* when the cells were exposed to 1% (w/v) colloidal chitin for 1 h or more. No positive signal was detected in the lysate prepared from the cells grown in the absence of chitin. The chitoporin expression was also observed in the *V. harveyi* cells after induction with crystalline a chitin, but the signals were not as strong as when colloidal chitin was used (data not shown).

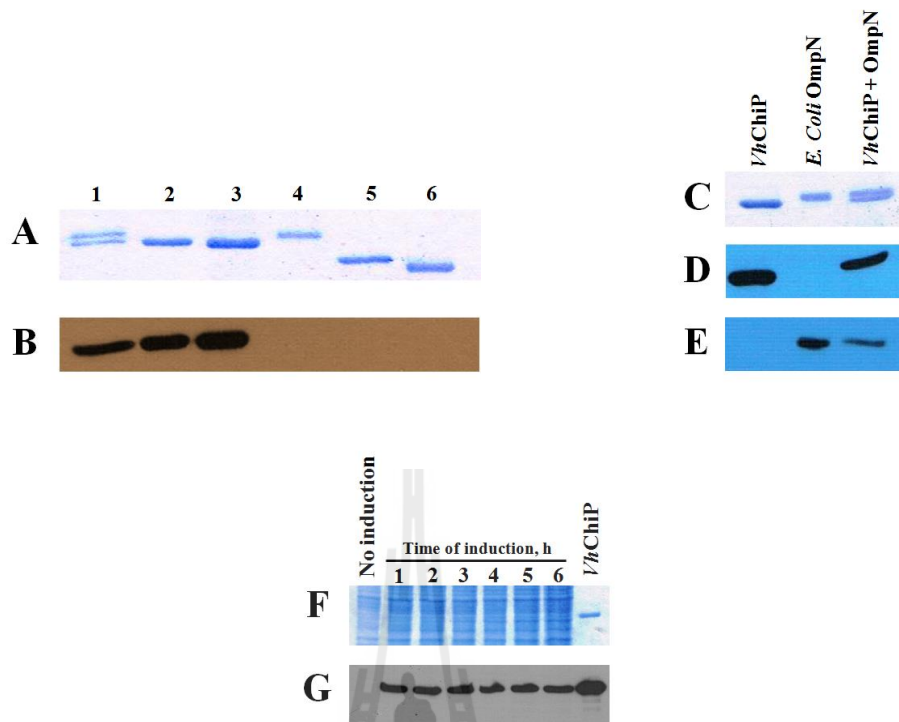


**Figure 3.5** Cross-reactivity of *VhChiP* antiserum with other outer membrane porins. A) Coomassie blue-stained 8% SDS-polyacrylamide gel and B) the corresponding immunoblot detected with anti *VhChiP* antibody. The *VhChiP*+OmpN (lane 1, *VhChiP*, lower band and OmpN, upper band), *VhChiP*-preparation I (lane 2), *VhChiP*-preparation II (lane 3) *E. coli* OmpN (lane 4), *E. coli* OmpF (lane 5) and *B. pseudomallei* Omp38 (lane 6). C-D: cross-reactivity of *VhChiP* and *E. coli* OmpN with anti *VhChiP* and anti OmpN antibodies. C) Coomassie blue-stained SDS-polyacrylamide gel, the corresponding immunoblots showing cross-reactivity with anti *VhChiP* antiserum, and D-E) anti OmpN antiserum, respectively. F) Endogenous expression of chitoporin in *V. harveyi*, F) Coomassie blue-stained SDS-polyacrylamide gel and immunoblot of cell lysate of *V. harveyi* cultured in the presence of 1% (w/v) colloidal chitin at various time of 1-6 h (Suginta *et al.*, 2013).

### **3.2 Single channel properties of *VhChiP* channel with uncharge molecules translocation (chitooligosaccharides)**

The pore-forming properties of *VhChiP* were investigated at the molecular level using a planar lipid bilayer (BLM) set-up for ion current recordings. The signals for functional analysis were acquired on application of a small potential across two Ag/AgCl wires, one either side of an artificial bilayer of diphytanoyl phosphatidylcholine (DPhPC) in 1 M KCl/20 mM Hepes (pH 7.5), and the subsequenced measurement of the electrostatically driven ion (current) flow through the normally non-conducting lipid membrane, on the inclusion of single pore-forming units. Reconstitution of trimeric *VhChiP* into a previously formed lipid bilayer membrane was obtained through the addition of a small amount of the purified protein to the bulk phase of the membrane-bathing KCl solution on one or other side of the bilayer. Typically addition of a diluted protein (<1 ng/ml) resulted in the incorporation of a single protein molecule in more constantly open state and this was the favored situation for inspecting the *VhChiP* single channel conductance and chitooligosaccharide translocation. Figure 3.6A-B are characteristic examples of membrane current recordings (500 ms out of 60 s measuring time) from individual *VhChiP* trimers inserted in a DPhPC bilayer in 1 M KCl under applied transmembrane potentials of +/-100 mV, respectively. The traces in Figure 3.6A and B indicate that the inserted *VhChiP* channel is fully open, with a stable ionic current over the time of recording. Occasionally transient current deflections occur as one of the three subunits apparently closes and opens rapidly in a stochastic manner. In multiple measurements, single reconstituted trimeric *VhChiP* channels showed an average conductance of  $1.89 \pm 0.07$  nS ( $n = >50$ ) in 1 M KCl/20 mM Hepes (pH 7.5).

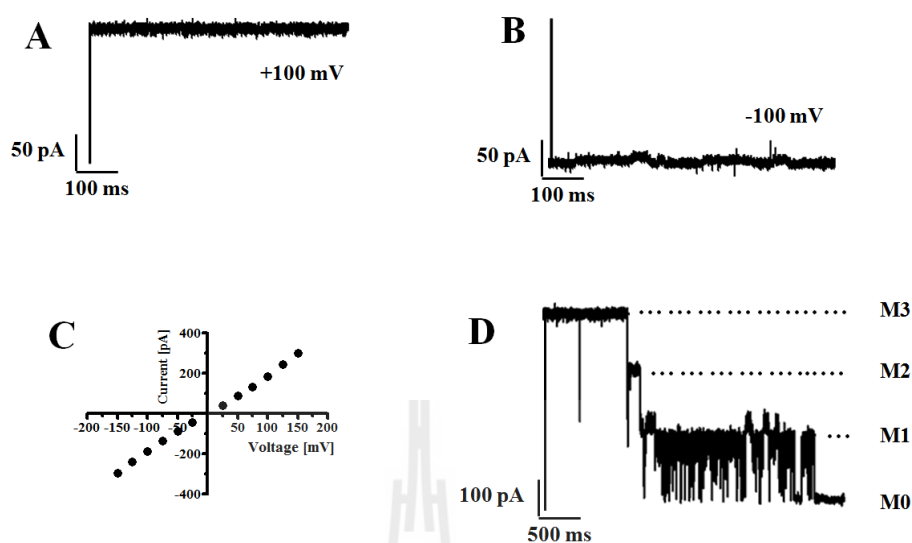


**Figure 3.6** Single channel recordings of chitoporin in artificial lipid membranes. A) Typical ion current trace of a single channel at fully-open state of *VhChiP* at applied voltage of +100 mV; B) at -100 mV; C) The ion currents were normally recorded for a period of 120 s. Analysis of current/voltage (I/V) relationship. The average current values were obtained by stepwise ramping of the potential, performed in an average of >50 single channels. D) Three-step closure, induced by increasing the applied voltage to +200 mV (Suginta *et al.*, 2013).

As with many other bacterial porins, currents through DPhPC-incorporated *VhChiP* pores can be approximated by Ohm's Law, being directly proportional to the applied voltage over the range +/-150 mV (Figure 3.6C). Finally, *VhChiP* channels showed the typical voltage gating properties of bacterial porins and closed in a characteristic three-step fashion upon abrupt application of higher voltages (Figure 3.6D). The threshold potential (critical voltage) inducing the trimeric closure of the channels was found to be +/-150 mV, while at less than or equal to +/-100 mV the channels were not affected by gating perturbations and so were suitable for studies on chito-oligosaccharides translocation through the *VhChiP* channel.

Chitoporin has been proposed to facilitate the movement of chitin degradation products from the extracellular into the periplasmic space of marine *Vibrios* (Keyhani *et al.*, 2000; Meibom *et al.*, 2004) before they are further transported to the cytoplasm and used as an energy source. To test this function we performed experiments to investigate the effects of chito-oligosaccharides of various sizes on fully-open pores of *VhChiP* in artificial phospholipid bilayer membranes. Figure 3.7 shows current recordings from single *VhChiP* channels with all the tested chito-oligosaccharides (Figure 3.7A–F) as well as those acquired in comparative trials with the structurally related maltopentaose (Figure 3.7G) and maltohexaose (Figure 3.7H). In absence of chitosugars, the ion current ( $I$ , pA) of a fully open *VhChiP* trimer was stable. Figure 3.7A shows a typical ion current trace of ~180 pA at +100 mV.

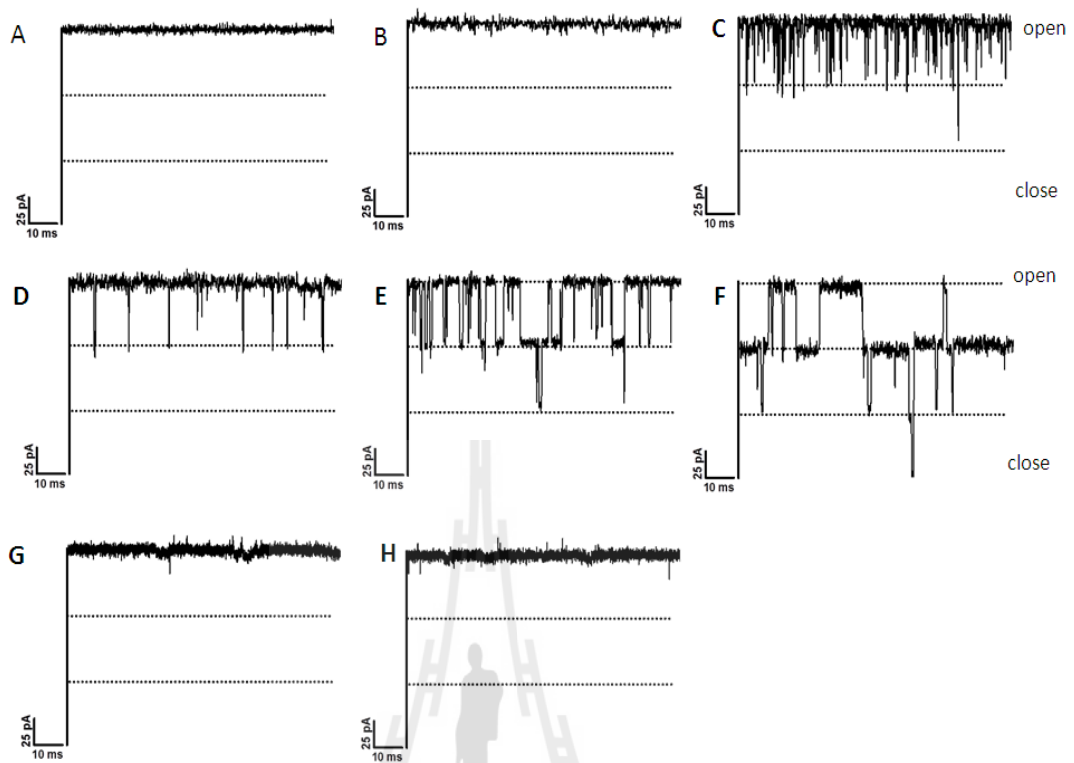


**Figure 3.7** Effect of chitooligosaccharides on chitoporin ion currents. A fully open state of a single channel of *VhChiP* was inserted in the artificial membrane (A). Then, chitooligosaccharide: chitobiose (B), -triose (C), -tetraose (D), -pentaose (E), and -hexaose (F) were added on the *cis* side of the chamber to a final concentration of 80  $\mu\text{M}$ . Control recordings were made with maltopentaose (G) and maltohexaose (H) at a concentration of 400  $\mu\text{M}$ . Ion current fluctuations were monitored for 120 s at applied voltages of  $\pm 100$  mV. Here, only ion traces for +100 mV are presented (Suginta *et al.*, 2013).

The response of the system to the addition of the set of chitosugars was diverse. For example, no transient decreases were observed when the reconstituted *VhChiP* was exposed to chitobiose (Figure 3.7B). The current traces obtained had, however, slightly greater noise levels than controls without added solute. In marked contrast, the presence of higher MW chitosugars (GlcNAc<sub>4,5,6</sub>) in the solution on the *cis* side of the membrane produced clear short-lived downward current deflections (Figure 3.7C-F). These correspond to the time-resolved blockade of the trimeric pores of *VhChiP* by individual chitoooligosaccharide molecules that physically obstruct the channels in course of contact. Occlusion of ion flow during sugar diffusion apparently occurred as a reversible process by which each of the brief current decreases was caused by a single sugar molecule entering the *VhChiP* channel and leaving it very shortly later. Characteristic current traces for 80 mM chitotriose and chitotetraose showed that no more than one of the three subunits of a *VhChiP* trimer was blocked by such chitosugars (Figure 3.7C-D). The frequency of the single subunit blockades was considerably higher for the triose than for the tetraose. At the same concentration, diffusion of chitopentaose also caused two-subunit blockage (Figure 3.7E) and with chitohexaose, even blockage of all three channel subunits could be observed (Figure 3.7F). In a follows, series of experiments we added chitoooligosaccharides into the solution on the *trans*-side of the bilayer membrane. Sugar addition on the *cis* side, resulted in distinct channel blockades in the corresponding membrane current recordings; however, for the same solute concentration the blocking effect was slightly less pronounced (not shown). To elucidate the specificity, the exposure of single *VhChiP* channels to maltopentaose and maltohexaose did not cause the transient drops of ion flow that were observed with the chitosugars, even when five

times higher concentrations (400 mM) of the maltosugars were used (Figure 3.7G-H, respectively).

BLM recording with different chitosugars suggested chitohexaose to be most potent in terms of pore obstruction (Figure. 3.7F). Chitohexaose was thus chosen for evaluating the concentration dependence of chitosugar-induced *VhChiP* blockade. Membrane current recordings were taken for the same single channel, while the chitohexamer concentration was progressively increased from 0 mM to 1, 120 and 400  $\mu$ M, respectively. Figure 3.8 shows the original membrane current measurements (A-D, left panel) together with a statistical analysis of the raw data as current magnitude histograms (A-D, right panel). Clearly, the open probability of the channel decreased with increasing concentrations of the sugar. By addition of 1.0 mM chitohexaose to the *cis* side of the chamber, the protein channel instantaneously transformed from being constantly fully open (Figure 3.8A) to a state in which one subunit of *VhChiP* was temporarily occluded (Figure 3.8B). This is shown by a decrease of the channel conduction by one-third of the full conductance. As its concentration was raised to 120  $\mu$ M (Figure 3.8C), the sugar began to occupy two subunits, decreasing the conductance by two-thirds. At this concentration, occupation of the third subunit was periodically observed, with the channel conductance reduced to zero. At 400 mM chitohexaose (Figure 3.8D), two of the three subunits were constantly blocked, and the effect of increased chitohexaose concentration on the third subunit was apparent. The probability of complete closure of the trimeric channel was approx. 0.8, indicating that the *VhChiP* channel was nearly saturated by chitohexaose at this concentration.

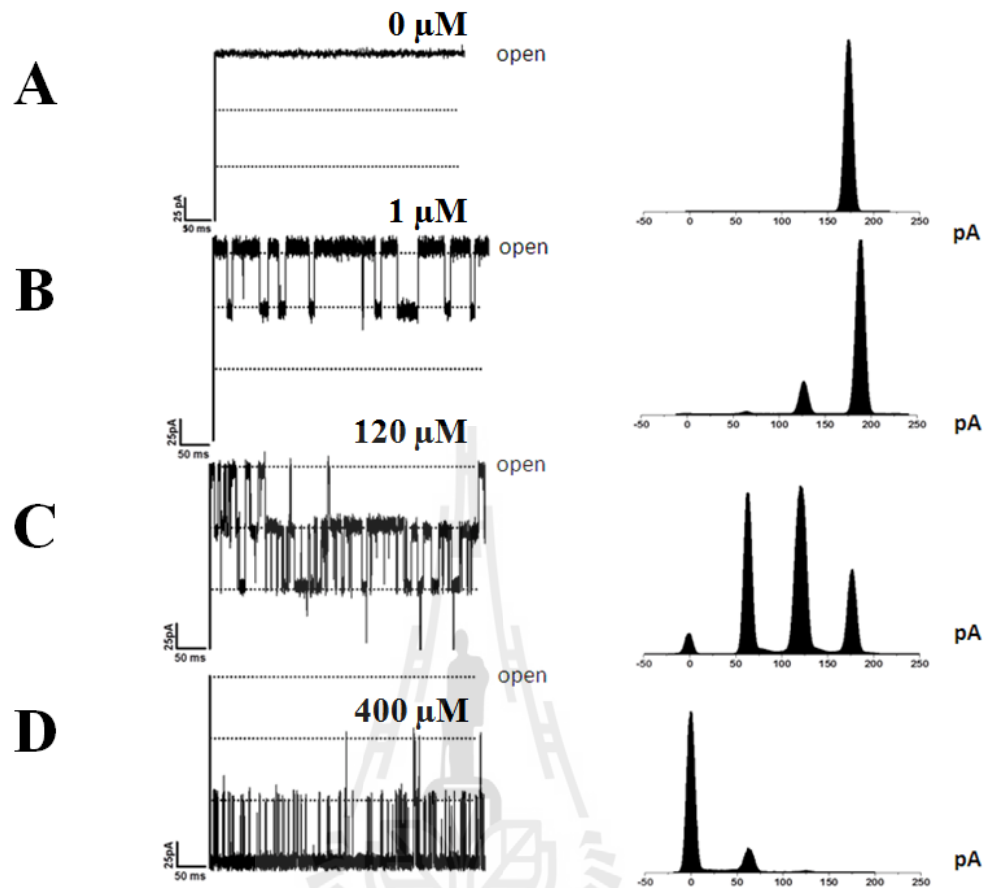
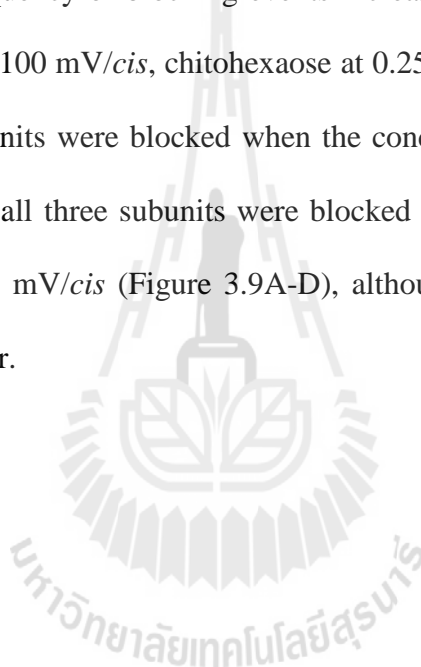


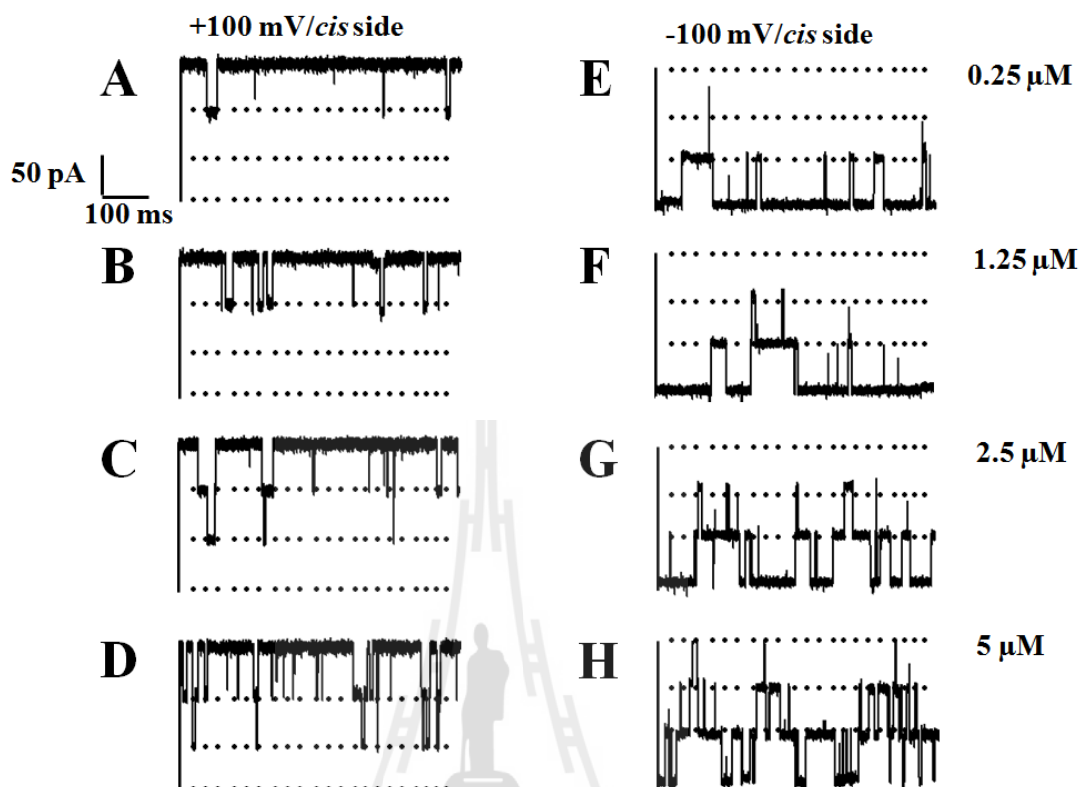
**Figure 3.8** Effects of chitohexaose diffusion on subunit closure. The fully open *VhChiP* channel was exposed to different concentrations of chitohexaose (A-D). Right panel: the original traces displaying ion current blockade. Left panel: the corresponding frequency/current histograms, reflecting discrete changes in the subunit conductance upon sugar diffusion through the channel (Suginta *et al.*, 2013).

Chitooligosaccharides of various sizes were added on either side of the chamber, and their ability to block ion current was quantified. Number blockage was visible when chitobiose was varied up to 400  $\mu\text{M}$  on either the *cis* or *trans*-side or when the channel was exposed to maltodextrins (maltopentaose and maltohexaose) or raffinose (not shown). In marked contrast, after the addition of 5  $\mu\text{M}$  chitosugars, we observed ion current blockages, which depended on the size of the sugar and the side of sugar addition. The ionic current blockages were observed at much greater frequency when the sugar was added on the *cis* side compared with the *trans*-side. For instance, current blockage by chitotriose was rarely visible with addition on the *trans*-side, whereas significant blocking events were detected when same concentration of chitotriose was added on the *cis* side (not shown).

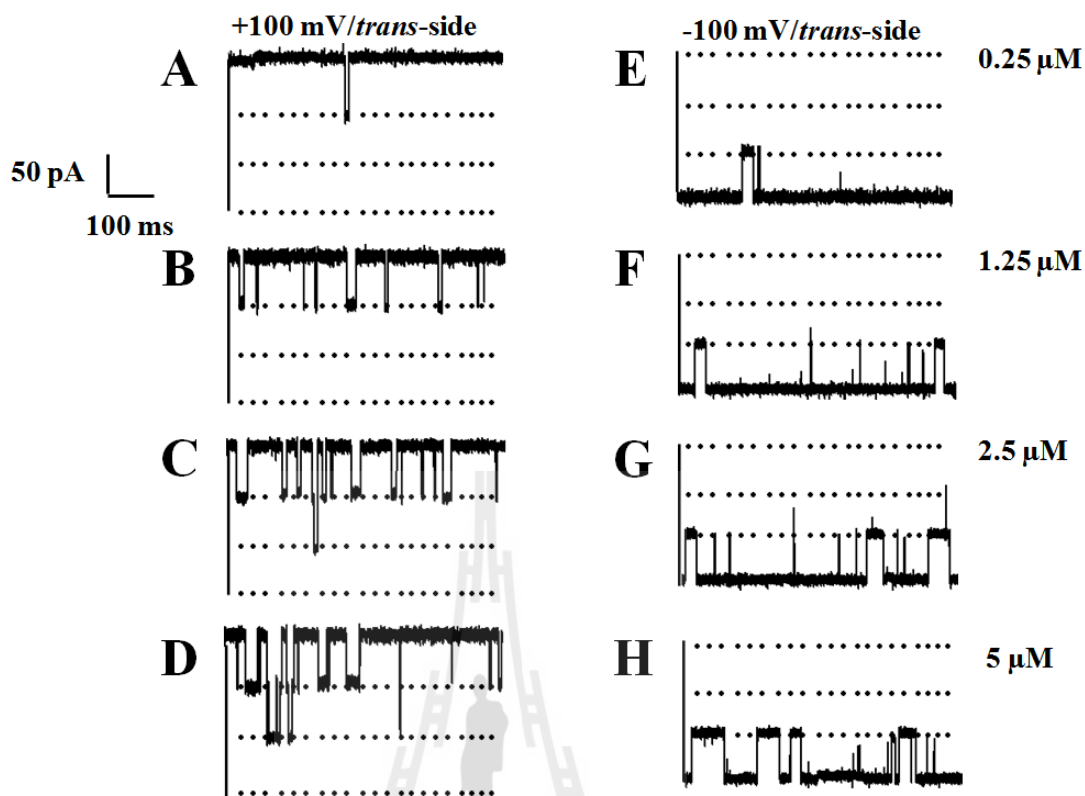
Starting with the *cis* side addition, chitotriose was found to partially interrupt the flow of ions, visible by statistical transient reduction of the channel conductance by one-third. Chitotriose, chitotetraose, and chitopentaose blocked one monomer of the single trimeric channel, whereas increasing the sugar length to hexamer resulted in the double and triple blocking of the single trimeric channel. Furthermore, chitohexaose exhibited the longest residence time, during which each sugar molecule remained entrapped before leaving the pore. This was clear from single channel analysis, which yielded an average residence time of  $6.0 \pm 0.7$  ms for the chitohexaose. This value decreased rapidly as the number of GlcNAc units in the polymer decreased from five ( $2.4 \pm 0.2$  ms) to four ( $0.33 \pm 0.08$  ms) and three ( $0.11 \pm 0.05$  ms).

We further investigated the effect of applied voltages on sugar translocation from both the *cis*- and *trans*-sides at various concentrations. As shown in Figure 3.9, channel blockage by chitohexaose occurred to a much greater extent for *cis*-side addition compared with *trans*-side addition. Considering *cis* side addition, the number of blocking events was obviously higher at -100 mV (Figure 3.9E-H) than at +100 mV (Figure 3.9A-D). This result was reversed with *trans*-side addition (Figure 3.10). In both cases, the frequency of blocking events increased with concentration. Figure 3.9E-H shows that at -100 mV/*cis*, chitohexaose at 0.25  $\mu\text{M}$  blocked only one subunit on average. Two subunits were blocked when the concentration was increased up to 1.25  $\mu\text{M}$ , and finally, all three subunits were blocked at 5  $\mu\text{M}$ . Similar observations were made with +100 mV/*cis* (Figure 3.9A-D), although the frequency of blocking events was much lower.



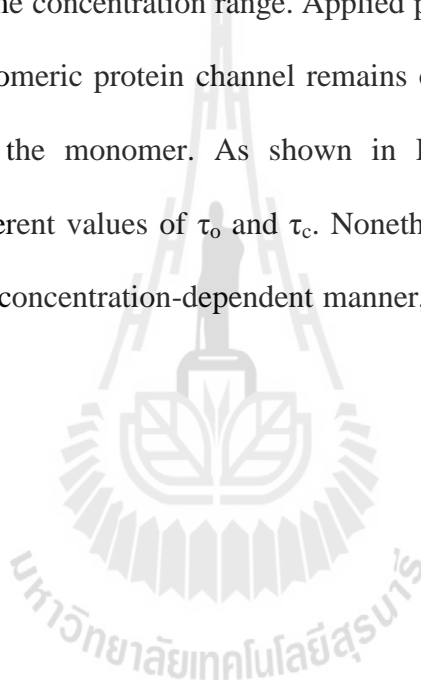


**Figure 3.9** Effects of transmembrane potentials and sugar concentrations on ion currents. The fully open *VhChiP* trimeric channel was exposed to different concentrations of chitohexaose. Ion current blockages at +100 mV (A-D) and -100 mV (E-H) are shown. The chitohexaose was titrated on the *cis*-side (Suginta *et al.*, 2013).



**Figure 3.10** Effects of transmembrane potentials and sugar concentrations on ion currents. The fully open *VhChiP* trimeric channel was exposed to different concentrations of chitohexaose. Ion current blockages at +100 mV (A-D) and -100 mV (E-H) are shown. The chitohexaose was titrated on the *trans*-side (Suginta *et al.*, 2013).

Plots of the number of blockade events/s (reflecting translocation rate) over a selected range of chitohexaose concentrations were examined for *cis* and *trans*-side additions at +/-100 mV. The on-rates for chitohexaose moving through open pores decreased as follows: -100 mV/*cis* > +100 mV/*cis* > +100 mV/*trans* >> -100 mV/*trans* (Figure 3.11A). The rates versus sugar concentrations from *cis*-to-*trans* yielded saturable curves, but the rates for *trans*-to-*cis* translocation did not reach saturation over the same concentration range. Applied potentials also affected both  $\tau_o$ , the time that the monomeric protein channel remains open, and  $\tau_c$ , the time that the sugar resides within the monomer. As shown in Figure 3.11B-C, each setting condition yielded different values of  $\tau_o$  and  $\tau_c$ . Nonetheless, all conditions showed a linear decay of  $\tau_c$  in a concentration-dependent manner, but  $\tau_c$  does not depend on the concentration.



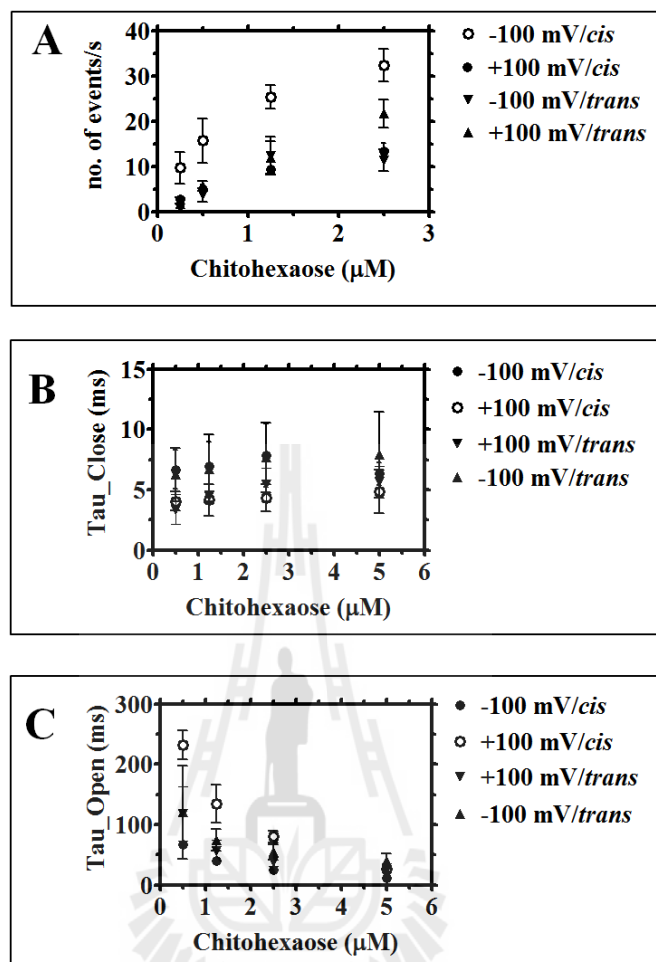


**Figure 3.11** Analysis of ion current blockades at various transmembrane potentials and chitohexaose concentrations. Plot of the number of binding events versus sugar concentrations, comparing both the +100 mV and the -100 mV and *cis/trans* side potential application (A). Plot of open times ( $\tau_o$ ) versus sugar concentrations (B). Plot of residence times ( $\tau_c$ ) versus sugar concentrations (C) (Suginta *et al.*, 2013).

The characteristic substrate-specific channel activity of *VhChiP* was confirmed by enhancement of the on-rate of chitohexaose, relative to that of other oligosaccharides, and by its concentration dependence. In our measurement we observed signal of blockages above at 0.1  $\mu\text{M}$  with increase blocking events at high concentration (Figure 3.11A). Chitohexaose blocked the ion flow very efficiently even at nanomolar concentrations. A conductance histogram shows a continuous increase in the level of monomeric blockage as the channel was titrated with chitohexaose from 0.125 up to 2.5  $\mu\text{M}$  (not shown). The amplitudes of sugar-induced noise levels were elevated in proportion to the concentration of chitohexaose and correlated well with the levels of monomeric blockage (not shown).

Further quantitative analysis of the binding constants was carried out to study the channel affinity. Figure 3.12A shows the binding curves of various concentrations of chitohexaose at  $\pm 100$  mV from *cis*- or *trans*-side of sugar addition. Fitting the curves using a nonlinear regression function derived from Eq. 2.2 yielded typical Michaelis-Menten plots (Nikaido *et al.*, 1992). The plot for chitohexaose is hyperbolic, as described above, and saturation was reached above 5  $\mu\text{M}$ . On the other hand, the binding curves of chitotriose, chitotetraose, and chitopentaose did not approach saturation even at 40  $\mu\text{M}$  (not shown). Transformation of these binding curves yielded linear double reciprocal plots (Lineweaver-Burk plots) as shown in Figure 3.12B. These Lineweaver-Burk plots allowed the binding constants ( $K$ ,  $\text{M}^{-1}$ ) to be determined as shown in Table 3.1. As shown in Table 3.1, the binding constant of chitohexaose was found to be larger than those of other chitosugars at both the +100 and the -100 mV. The value of  $K$  decreased by several orders of magnitude as the polymer length decreased from  $\text{GlcNAc}_6$  to  $\text{GlcNAc}_5$  and  $\text{GlcNAc}_4$ . Surprisingly, the

greater binding affinity of the *VhChiP* channel for chitohexaose was under the -100 mV/*cis* condition ( $K$  is  $\geq 500,000 \text{ M}^{-1}$ ; see in Table 3.1 and Table 3.4). These kinetic data consistently show chitohexaose to be the best substrate for the *VhChiP* channel.

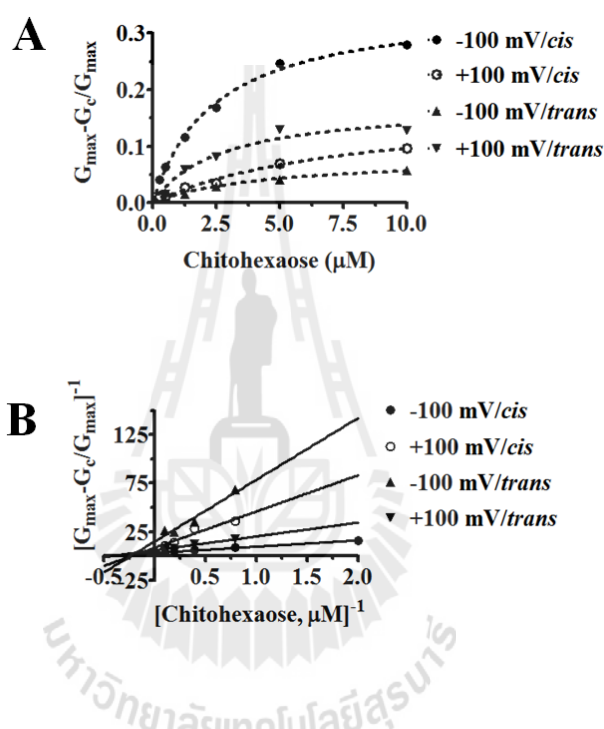


**Figure 3.12** Binding curve of 0.25-10  $\mu\text{M}$  chitohexaose to *VhChiP*. The Michaelis-Menten plots were evaluated from the data acquired on the *cis*- or *trans*-side at  $\pm 100$  mV (A). The values are averaged from the BLM data obtained in triplicate. The plots of  $(G_{\max} - G_{[c]}) / G_{\max}$  versus sugar concentrations (micromolar) were derived from Eq. 2.2. Lineweaver-Burk plots of chitohexaose at both the +100 mV and the -100 mV, at *cis*- or *trans*-side addition (B). The equilibrium binding constant ( $K$ ,  $\text{M}^{-1}$ ) can be obtained directly by fitting the curves with a linear regression function as described in the text (Suginta *et al.*, 2013).

**Table 3.1** Substrate specificity of *VhChiP*.

| Substrates    | Rate constant at <i>cis</i> -side addition of chitosugars             |   |                                       |   |   |                                       |
|---------------|---|---|---------------------------------------|---|---|---------------------------------------|
|               | +100 mV   |   |                                       | -100 mV   |   |                                       |
|               | $k_{\text{on}}^{\text{b}}$<br>$10^6$ ( $\text{M}^{-1}\text{s}^{-1}$ ) | $k_{\text{off}}^{\text{b}}$<br>$10^3$ ( $\text{s}^{-1}$ ) | $K^{\text{a}}$<br>( $\text{M}^{-1}$ ) | $k_{\text{on}}^{\text{b}}$<br>$10^6$ ( $\text{M}^{-1}\text{s}^{-1}$ ) | $k_{\text{off}}^{\text{b}}$<br>$10^3$ ( $\text{s}^{-1}$ ) | $K^{\text{a}}$<br>( $\text{M}^{-1}$ ) |
| Chitobiose    | ND <sup>c</sup>   | -   | ND <sup>c</sup>                       | ND <sup>c</sup>   | -   | ND <sup>c</sup>                       |
| Chitotriose   | $2.0 \pm 0.2$   | $9.0 \pm 2.0$   | $220 \pm 100$                         | $5.0 \pm 0.4$   | $12.5 \pm 2.5$  | $400 \pm 150$                         |
| Chitotetraose | $10.0 \pm 0.1$  | $3.7 \pm 0.11$  | $2,700 \pm 700$                       | $15 \pm 0.3$  | $3.0 \pm 0.40$  | $5000 \pm 850$                        |
| Chitopentaose | $25.5 \pm 0.4$  | $1.7 \pm 0.13$  | $15,000 \pm 3000$                     |   |   |                                       |
| Chitohexaose  | $78.8 \pm 29.4$   | $0.21 \pm 0.02$   | $370,000 \pm 140,000$                 | $85.0 \pm 1.4$  | $0.17 \pm 0.02$   | $500,000 \pm 68,000$                  |

<sup>a</sup>The equilibrium binding constants ( $K$ ,  $\text{M}^{-1}$ ) was estimated from the reduction of the single channel conductance in the titration of different concentrations of chitosugars using Equation 1.

<sup>b</sup>The on-rate ( $k_{\text{on}}$ ,  $\text{M}^{-1}\text{s}^{-1}$ ) is given by  $k_{\text{on}} = K \cdot k_{\text{off}}$ , and the off-rate ( $k_{\text{off}}$ ,  $\text{s}^{-1}$ ) from the single trimeric molecule of *VhChiP* channel after titration with different of chito-oligosaccharides that was obtained from Kullman *et al.* (Kullman *et al.*, 2002) refer to equation of  $k_{\text{off}} = 1/\tau_c$ .

<sup>c</sup>ND, no detectable blocking events with this sugar.

### 3.3 Single channel properties of *VhChiP* with respect to the translocation of charged molecules (chitosan hexamers)

Single-channel experiments were performed with different sugars to demonstrate the effect of sugar side chains on permeation through *VhChiP*. Figure 3.13A-B shows the chemical structures of chitohexaose (A) and chitosan hexaose (B). The difference between both sugars is the chemical character of the nitrogen in C<sub>2</sub>-position of monomers. It is in chitin derivatives an *N*-acetamido group (-NHCOCH<sub>3</sub> or -NHAc) and in chitosan an unmodified amino (-NH<sub>2</sub>) group. In chitosan sugar, this amino group can be protonated, with a *pK*<sub>a</sub> of about 6.7.

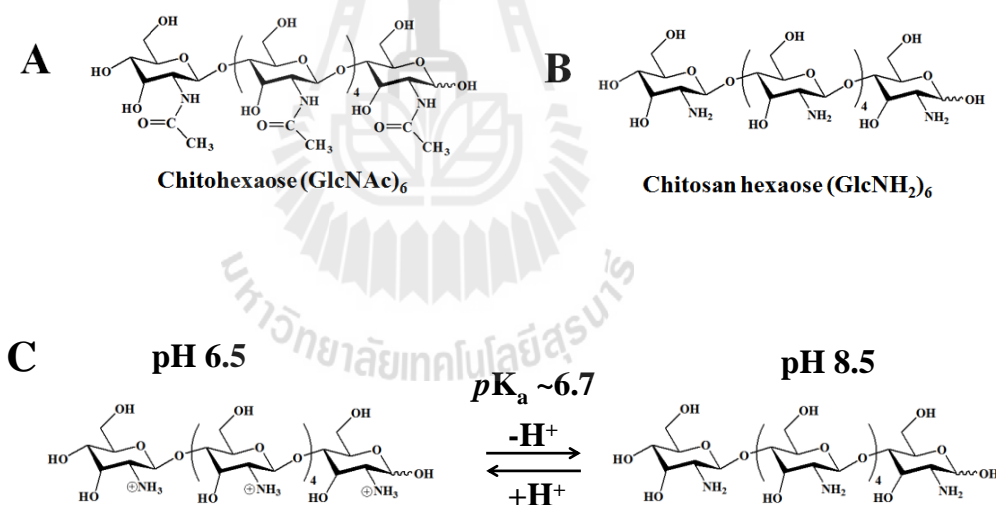


**Figure 3.13** Chemical structures of A) chitohexaose and B) chitosan hexaose. C) The pH change from 8.5 to 6.5 causes protonation of the chitosan hexaose to the cationic (ammonium) form. The two structures were created and displayed using ChemDraw v.9 (Perkin Elmer, Waltham, MA, USA).

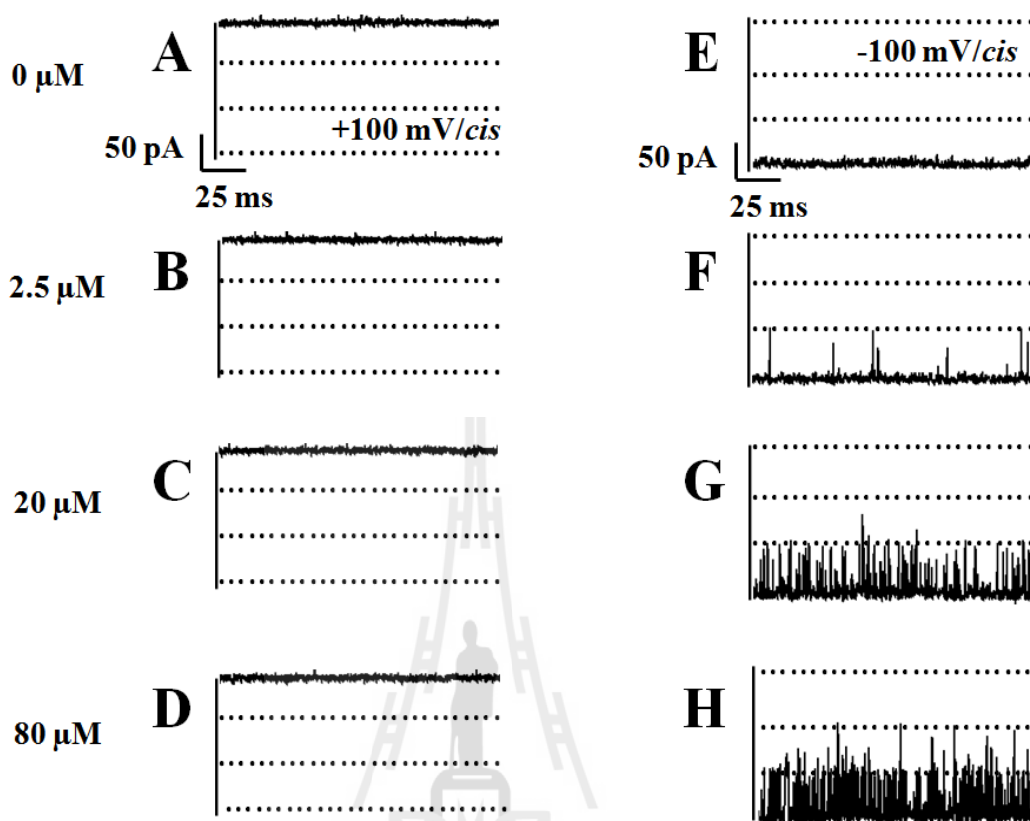


**Figure 3.14** Influence of the polarity of the membrane potential on the translocation of cationic chitosan hexaose through *VhChiP*. Single channel current recordings of one *VhChiP* channel incorporated in a planar lipid bilayer from the *cis* side and exposed to 1 M KCl, 20 mM potassium acetate (pH 6.5), at +100 mV (A-D) and -100 mV (E-H). Chitosan hexaose was added at various concentrations to the *cis* side of the lipid bilayer.

To study the effect of protonation of chitosan the pH of the measuring solution was lowered to 6.5 below the  $pK_a$  of chitosan hexaose, so that the amino groups of the chitosan hexaose became predominately cationic through protonation. Providing that the *trans* Ag/AgCl electrode was negative (e.g. -100 mV), the protonation state of the chitosugar molecules (Figure 3.13C), produce cationic groups along the glucosyl chain, resulting in time-resolved ion current blockages (Figure 3.14E-H) at 2.5, 20 and 80  $\mu\text{M}$ . Each of these blocking events represented the rapid channel entry and exit of a charged molecule with the estimated dwell time obtained from the data acquired over 120 sec and was about 0.08 ms (pH 6.5) (Mahendran *et al.*, 2009; Mahendran *et al.*, 2013; Lamichhane *et al.*, 2013). Note that the dwell time of chitosan hexaose was about >50 fold faster than that of chitohexaose mentioned earlier, suggesting that the chitosan hexaose-*VhChiP* interaction was much weaker than the chitohexaose-*VhChiP* interaction. At condition of low pH and under an external field the electrostatic driving force on the protonated amino sugars appeared to be strong enough to compensate for their poor channel affinity, hence causing sugar permeation. At pH 7.5, the blocking events were much less frequent and the dwell time of the partially-protonated sugars was smaller than at pH 6.5 (Table 3.2), indicating weaker electrostatic force and affinity. Note that at pH 8.5 (not shown) where chitosan hexaose was essentially uncharged, the blocking events were short and rare, assuming almost no affinity of interaction between the sugar and the *VhChiP* at this condition.

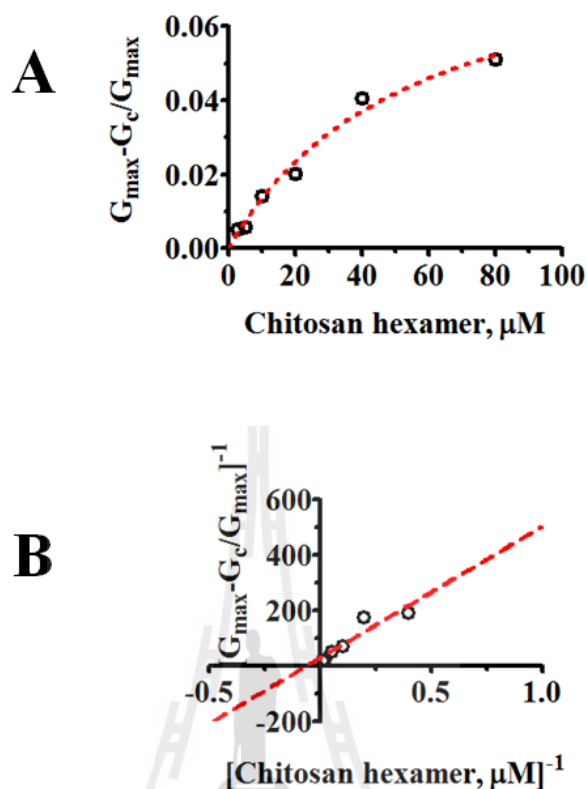


**Figure 3.15** Binding curve for the interaction of *VhChiP* with chitosan hexaose. Reconstituted *VhChiP* channels were titrated with increasing concentration of chitosan hexaose (from 2.5  $\mu\text{M}$  to 80  $\mu\text{M}$ ) at pH 6.5 using Eq. 2.2. The chitoporin was inserted from the *cis* side of the lipid bilayer as well as the sugar; the applied transmembrane potential was -100 mV. The buffer contained 1 M KCl, 20 mM potassium acetate, pH 6.5 plus the volumes of 1 M KOH required for pH adjustments. A) The binding curve was obtained plotting  $[G_{\text{max}} - G_c] / G_{\text{max}}$  vs. sugar concentrations ( $\mu\text{M}$ ). The results represent averages are from at least three independent single channel current measurements. B) The binding constant was estimated from Lineweaver-Burk plots.

Figure 3.15A-B, a binding curve shows the concentration dependency of chitosan hexaose with the *VhChiP* channel at pH 6.5. Figure 3.15A shows the binding curves of chitosan hexaose acquired at pH 6.5, while Figure 3.15B shows Lineweaver-Burk plots to determine the binding constants ( $K$ ). The binding curve of chitosan hexaose was strongly dependent on pH of the bulk solution, being strongest at pH 6.5 at where chitosan hexaose is predominantly cationic. At pH 8.5, the chitosan hexaose was in its neutral form ((GlcNH<sub>2</sub>)<sub>6</sub>) and the electrostatically-triggered channel obstruction was almost absent. Table 3.2 summarizes the various rates. At pH 8.5, the binding constant for chitohexaose of 340,000 M<sup>-1</sup> was extremely high, whereas at this pH the chitosan hexaose interaction was too low to be quantified. At pH 6.5, the binding constant of the chitohexaose was more than a hundred fold larger than the one of the protonated chitosan variant. This strongly underlines the essential role of the *N*-acetyl moieties in defining the sugar specificity of *VhChiP*. In addition, Table 3.2 also shows a marked contrast in the effect of pH on the binding constants of both chitosugars. Although the affinity of *VhChiP* for chitohexaose does not change significantly with pH, the corresponding value for chitosan hexaose is too small to be meaningfully assessable at pH 8.5. For chitosan hexaose, changes of pH caused a drastic increase in the on-rate ( $k_{\text{on}}$ ), but the off-rate ( $k_{\text{off}}$ ) remained virtually unaffected. In contrast, both the on-rate and off-rate for chitohexaose were found to be pH independent. Our BLM measurements also indicated that the translocation rate increased with increasing external field. With protonated chitosan oligosaccharides present on the *cis*-side, changes of electrode polarity on the *trans*-side drastically affected the channel penetration and the passage of the oligosaccharides.

**Table 3.2** Effect of pH on the binding constant of chitoporin from *Vibrio harveyi* 650 towards uncharged and charged chitosugars.

| pH  | Chitohexaose (GlcNAc <sub>6</sub> ), -100 mV/cis                                      |   |   | Chitosan hexaose (GlcN <sub>6</sub> ), -100 mV/cis                                    |   |   |
|-----|---|---|---|---|---|---|
|     | On-rate constant<br>10 <sup>6</sup> (M <sup>-1</sup> · s <sup>-1</sup> ) <sup>b</sup> | Off-rate constant<br>10 <sup>3</sup> (s <sup>-1</sup> ) | Binding constant<br>(M <sup>-1</sup> ) <sup>a</sup> | On-rate constant<br>10 <sup>6</sup> (M <sup>-1</sup> · s <sup>-1</sup> ) <sup>c</sup> | Off-rate constant <sup>b</sup><br>10 <sup>3</sup> (s <sup>-1</sup> ) <sup>e</sup> | Binding constant<br>(M <sup>-1</sup> ) <sup>a</sup> |
| 6.5 | 69 ± 0.5  | 0.21 ± 0.01   | 330,000 ± 47,000                                    | 15.6 ± 2.5<br>(0.09 ± 0.02)   | 6.8 ± 1.5<br>(0.047 ± 0.3)  | 2,300 ± 1,700<br>(1,900 ± 72)                       |
| 7.5 | 58 ± 0.6  | 0.17 ± 0.02   | 340,000 ± 51,000                                    | 3.3 ± 1.0   | 8.2 ± 0.8   | 350 ± 150   |
| 8.5 | 65 ± 0.6  | 0.19 ± 0.01   | 340,000 ± 56,000                                    | -   | ND <sup>f</sup>   | -   |

<sup>a</sup> The equilibrium binding constants ( $K$ , M<sup>-1</sup>) was estimated from the titration method according to Eq. 2 as described in the text.

<sup>b</sup> The on-rate ( $k_{on}$ , M<sup>-1</sup>s<sup>-1</sup>) of chitohexaose is given by  $k_{on} = K \cdot k_{off}$ .

<sup>c</sup>  $k_{on}$  of the cationic chitosan was estimated from number of blocking events/sec.

<sup>d</sup> Values in brackets represent the extrapolated values at 0 mV. These values were obtained from the plots shown in Fig. 3.17.

<sup>e</sup> off-rate ( $k_{off}$ , s<sup>-1</sup>) of charged chitosan hexaose was estimated from  $k_{off} = k_{on}/K$ .

<sup>f</sup> N.D , no detectable blocking events with this sugar.

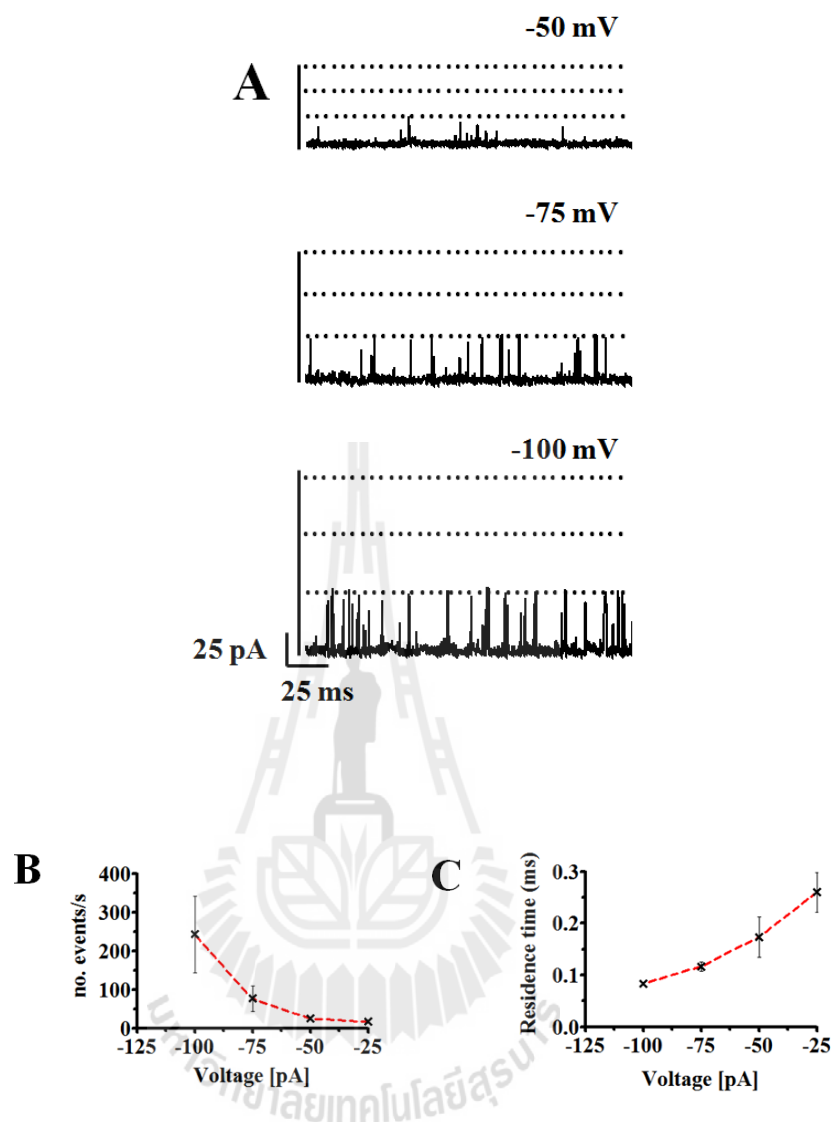


**Figure 3.16** The channel current blockages at cationic chitosan hexaose. Single channel current recordings of one *VhChiP* molecule incorporated in a planar lipid bilayer from the *cis* side and exposed to 1 M KCl in 20 mM potassium acetate pH 6.5. A) 5  $\mu$ M cationic chitosan hexaose was added on the *cis* side at negative transmembrane potential of -50 mV, -75 mV and -100 mV. B) Plot of number of events vs.  $V_m$ , while C) represents the plot of residence (dwell) time vs.  $V_m$ .

To observation of the effect of applied voltages on sugar translocation through *VhChiP* channel at various concentrations of chitosan hexaose. We added sugar on the *cis*-side and with the *trans* electrode either kept at +100 mV (Figure 3.14, left panel) or -100 mV (Figure 3.14, right panel). As expected, no channel current blockages were observed when the *trans* electrode was positive since the repelling electrostatic force opposed the movement of cationic sugar from *cis* to *trans* (Figure 3.14A-D). At -100 mV, however, the *trans* electrode imposed a force of attraction on the sugar molecules, triggering chitoporin entry and transient current trace deflections (Figure 3.14E-H) and we even observed double monomer blocking at high concentrations of the cationic sugar (i.e. at 20 and 80  $\mu\text{M}$ ).

Figure 3.16A shows the channel current blockages at 5  $\mu\text{M}$  cationic chitosan hexaose on the *cis* side at negative transmembrane potential of -50 mV, -75 mV and -100 mV. At the negative transmembrane potential from -25 mV to -100 mV, the number of events were increased (Figure 3.16B), while the residence (dwell) time were decreased (Figure 3.16C). Moreover, both on-rate ( $k_{\text{on}}$ ) and off-rate ( $k_{\text{off}}$ ) increased as the magnitude of the transmembrane potential was adjusted from -25 mV to -100 mV (Figure 3.17A-B). To elucidate the voltage effect, we extrapolated the plots of  $\ln [k_{\text{on}}]$  vs.  $V_m$  (Figure 3.17A) and  $\ln [k_{\text{off}}]$  vs.  $V_m$  (Figure 3.17B) to 0 mV, thus yielding virtual values of the on-rate ( $0.089 \times 10^{-6} \text{ M}^{-1} \text{ s}^{-1}$ ) and the off-rate ( $0.043 \times 10^{-3} \text{ s}^{-1}$ ) (Table 3.2). These values reflected a chitosan hexaose *VhChiP* channel binding and release that occurred entirely by diffusion. Also, increasing in the off-rate (decreasing dwell time) with increasing in the voltage indicates translocation (Figure 3.17B) that helps to distinguish binding and translocation as suggested elsewhere (Lamichhane *et al.*, 2013). Figure 3.17C presents the plot of  $\ln [K]$  vs.  $V_m$ . It is noted

that the voltage dependence for the on and off rates are different, giving a voltage dependent binding constant that suggests a possible structural change of the affinity site(s) caused by transmembrane voltages. The extrapolated value should ideally represent the intrinsic chemical affinity between the sugar molecule and the affinity site(s) inside the channel. Unlike the charged chitosan sugar, chitohexaose exhibited different binding behavior. Both the on- and the off-rates of chitohexaose were slightly modulated by the applied voltage (not shown). As constant  $k_{\text{on}}$  and  $k_{\text{off}}$  values would be expected for an entirely neutral molecule, this correlation indicates the influence of partial polarity of the  $\text{C}_2\text{-NHCOCH}_3$  groups on the chitohexaose molecule.

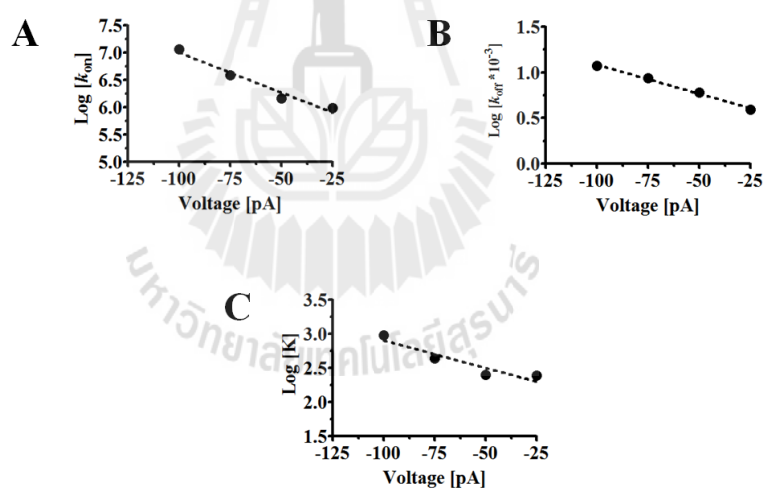


**Figure 3.17** Voltage dependence of the on-rate ( $k_{\text{on}}$ ) and off-rate ( $k_{\text{off}}$ ) of chitosan hexaose through *VhChiP* channel. All data were obtained with *VhChiP* inserted from the *cis* side of lipid bilayer in 1 M KCl supplemented 20 mM potassium acetate buffer (pH 6.5). The values are from triplicate measurements at each potential. Logarithmic plots of A) the on-rate ( $\times 10^{-6} \text{ M}^{-1} \text{ s}^{-1}$ ), B) off-rate ( $\times 10^{-3} \text{ s}^{-1}$ ) and C) the binding constant ( $K, \text{ M}^{-1}$ ) for chitosan hexaose.

### **3.4 Site directed mutagenesis on the constriction zone of *VhChiP* channel for ion transport and sugar translocation**

The modelling structure of *VhChiP* had built based on the x-ray structure of *D. acidovorans* Omp32 (pdb 2GFR) and compared with the maltooligosaccharide-specific maltoporin from *E. coli* to predict the position of the amino acids. (Schirmer *et al.*, 1995). The external loop 3 in maltoporin is controlled by a numbers of different amino acids, in particularly tyrosine 118 was identified as the constriction element. The homology model of the *VhChiP* channel was shown the pore size after mutation from tryptophan to alanine and phenylalanine. Figure 3.18 showed the model of three-dimensional structure of *VhChiP* wild-type (WT) and its mutant (W136A, W136F, W136R and W136D). In agreement with the ion conductance the model reveals a pore size somewhat larger compared to maltoporin. Mutation of the W opens putative constriction to provide more space for ions and sugar molecule to pass through the channel. Here in part of this study we consider the Tryptophan 136 (Trp136) and characterize ion conductance as well specificity of sugar translocation compared to WT.

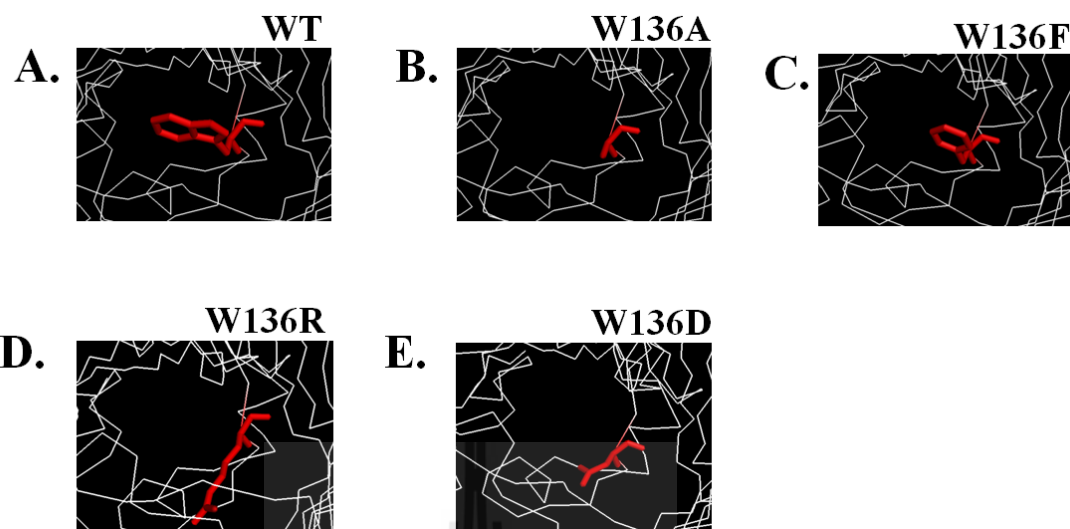


**Figure 3.18** The modelling structure of A) the monomeric *VhChiP* (WT) from *Vibrio harveyi* and its mutant such as B) W136A, C) W136F, D) W136R and E) W136D). The modelling structure of *VhChiP* had built based on the X-ray structure of *D. acidovorans* Omp32 (pdb 2GFR).

To study the functional activity behavior in the bilayer membrane, the recombinant plasmid containing the gene of mutated *VhChiP* was transferred and expressed in *E. coli* BL21 (DE3) omp8 Rosetta strains. After two step purification using Hitrap Q HP prepacked column, all proteins displayed a single band of molecular weight of above 100 kDa (native trimeric form) and 40 kDa (denatured monomeric form) as shown in Figure 3.4C. Figure 3.19A shows the monomeric form of WT and its mutants and all mutants had been confirmed using immuno-blotting detection using anti-*VhChiP* (Figure 3.19B) and anti-OmpN polyclonal antibody (Figure 3.19C). The results demonstrated that the protein is not contaminated of *E. coli* OmpN and its identity to its WT.

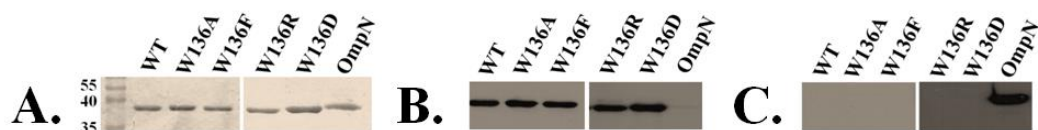


**Figure 3.19** Protein expression, purification and immuno-blotting analysis of WT and its mutant. A) shows 10% SDS-PAGE of purified WT and its mutant. After expression by 0.5 mM IPTG for 6 hr and then extracted with 2% SDS, followed with 3% octyl-POE in 20 mM phosphate (pH 7.4), further purified using Hi-trap Q column chromatography. B) Purified proteins were confirmed by immuno-blotting detection using anti-*VhChiP* and C) anti-OmpN polyclonal antibody.

In a first series we characterize the single channel conductance of WT and its mutant. Figure 3.20 shows the typical examples of the single and multiple insertions of WT and its mutant at transmembrane potential +100 mV. Figure 3.20A-E shows the single channel trace of WT and its mutant in solvent free membrane at transmembrane potential +100 mV and the histograms displayed the fully opened subunit without the sugar diffusion through the channel (Figure 3.20F-J). The multiple insertions of a small ion current channel demonstrated in a solvent containing bilayer membrane as shown in Figure 3.20K-O. The single channel conductance of alanine and aspartate were slightly increased which observed in both solvent free (Figure 3.20B and E) and solvent containing bilayer membrane (Figure 16L and O) and decreased with the replacement of arginine (Figure 3.20D and N). Table 3.3 shows summaries of single channel conductance for WT and its mutant, the single channel conductance were obtained using both the solvent containing and the solvent

free lipid bilayer membrane. The single channel conductance was obtained from 1 M KCl in 20 mM Hepes (pH 7.5). Replacing tryptophan by alanine and aspartate, the single channel conductance was slightly increased. In contrast, the smaller effect was observed when the phenylalanine replacement on W136. It means that may be caused in part of the bulky side chains of tryptophan 136 is similarly affected on the ion transport of *its* wild-type pore channel.



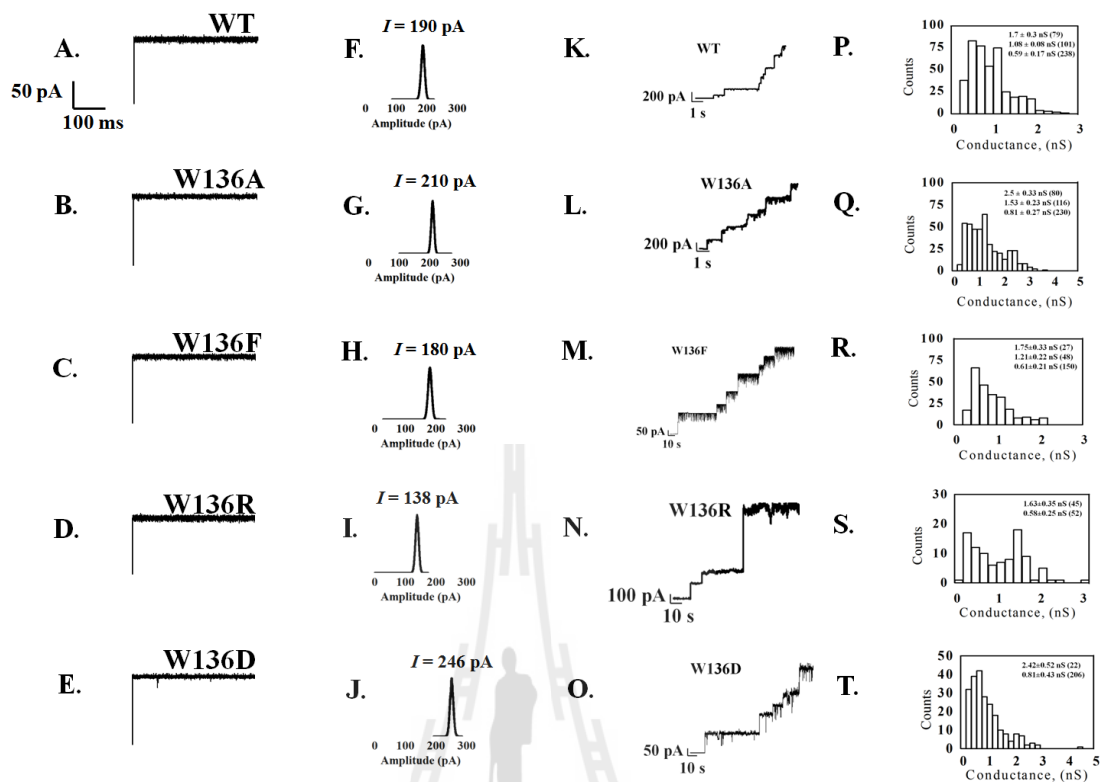


**Figure 3.20** Single channel insertion of DPhPC-bilayer membrane dissolved in *n*-pentane in the presence of WT and its mutant (W136A, W136F, W136R and W136D). The single channel recordings (A-E) and histogram represent the fully open state (F-J) of WT and its mutant, at transmembrane potential +100 mV. The stepwise insertion of WT and its mutant in solvent containing DPhPC-bilayer membrane were recorded (K-O) and histogram represent an average conductance, at +100 mV (P-T). The aqueous phase bulk solution contained 1 M KCl in 20 mM Hepes (pH 7.5) and a few solution of WT and its mutant were added. The temperature to carry out of the experiment was at  $20 \pm 3$  °C.

**Table 3.3** Single channel conductance of *VhChiP* (WT) and its mutants.

| 1 M KCl<br>(20 mM Hepes, pH 7.5) | Conductance, G (nS) |                  |                  |                 |                  |
|----------------------------------|---------------------|------------------|------------------|-----------------|------------------|
|                                  | WT                  | W136A            | W136F            | W136D           | W136R            |
| 1) Solvent free membrane         | 1.9 ± 0.03 (17)     | 2.17 ± 0.05 (16) | 1.94 ± 0.02 (18) | 2.3 ± 0.03 (22) | 1.75 ± 0.03 (12) |
| 2) Solvent containing membrane   | 1.7 ± 0.3 (79)      | 2.5 ± 0.3 (80)   | 1.7 ± 0.3 (27)   | 2.4 ± 0.5 (22)  | 1.6 ± 0.3 (45)   |
|                                  | 1.1 ± 0.1 (101)     | 1.5 ± 0.2 (116)  | 1.2 ± 0.2 (48)   | 0.8 ± 0.4 (206) | 0.6 ± 0.2 (52)   |
|                                  | 0.6 ± 0.2 (238)     | 0.8 ± 0.3 (230)  | 0.6 ± 0.2 (150)  |                 |                  |

The membranes were formed from DPhPC dissolved in *n*-pentane or *n*-decane. The aqueous phase contained 1 M KCl in 20 mM Hepes (pH 7.5). The voltage was applied at ±25 to ±150 mV and the temperature was 20 ± 3 °C.

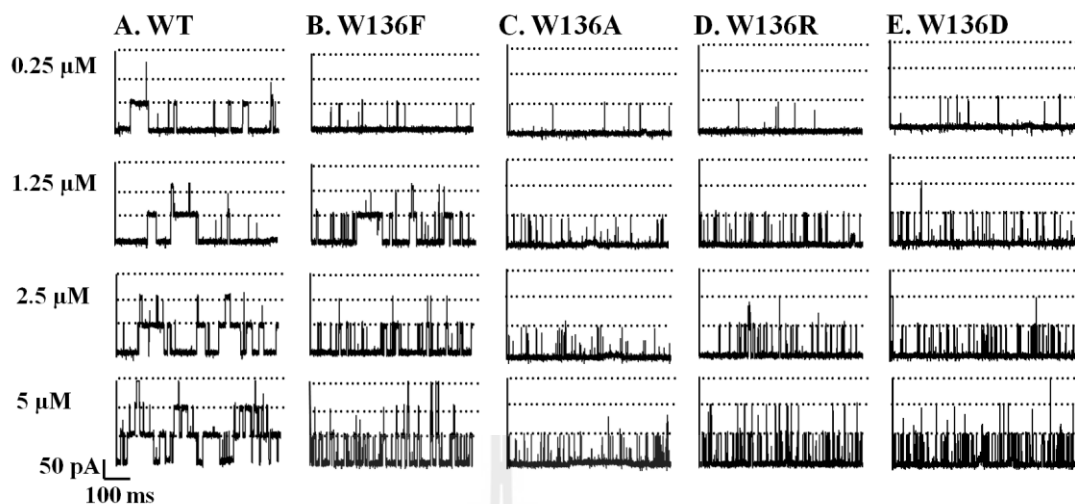


**Figure 3.21** The effect of transmembrane potentials at various concentration of chitohexaose on the single channel conductance of trimeric *VhChiP* (WT) and its mutants. The single channel insertion of WT (A) and its mutants (B-E) were reconstituted into solvent-free lipid membrane bath in 1 M KCl, 20 mM Hepes (pH 7.5) and exposed to addition of various concentrations of chitohexaose (0.25, 1.25, 2.5, and 5  $\mu\text{M}$ ) to the *cis* side at a transmembrane potential of -100 mV.

To study the constriction zone inside the *VhChiP* pore, single channel reconstitution of the trimeric *VhChiP* was performed to study the effect on the conductance fluctuation compared to the different mutants. Various concentrations of chitohexaose (0.25 to 5  $\mu\text{M}$ ) were titrated into to the *cis* or *trans* sides of the chamber to investigate the blocking events of ion current. Figure 3.21 shows a 500-ms-long recordings of *VhChiP* (Figure 3.21A) and its mutants (Figure 3.21B, W136A, 3.21C, W136F, 3.21D, W136R and 3.21E, W136D) demonstrating the chitohexaose induced ion current fluctuations by *cis* side addition at transmembrane potential -100 mV. In comparison to WT, the mutation of W136 to alanine caused less blocking events. At

the same concentration of chitohexaose (2.5  $\mu\text{M}$ ), two subunit block events were observed at the single nanopore of the trimeric *VhChiP* channel and W136F mutant. In contrast, only rare single monomer blocking events were observed by the replacement of W136 by alanine, arginine and aspartate, respectively. The number of blocking events per second under the various concentrations of chitohexaose on *cis* or *trans* side addition at transmembrane potential +100 mV and -100 mV were counted and analyzed to obtain an average residence (dwell) time from the single channel conductance of *VhChiP* and its mutants. These measurements were performed after addition of various concentrations of chitohexaose on the *cis* or *trans* sides and at different transmembrane potential +100 mV and -100 mV. The numbers of events were counted and the residence (dwell) times were estimated. Figure 3.22A-D shows both Tau-close ( $\tau_c$ ) and Tau-open ( $\tau_o$ ) times from *cis* or *trans* side addition also known as  $\tau_c$ , the times that sugar molecule stayed within the monomers, and  $\tau_o$ , the times that monomeric protein channels remained open or sugar left the monomers. The results indicated that  $\tau_o$  showed a rapidly decreased dependence on the concentration of chitohexaose. Interestingly,  $\tau_c$  did not show a dependence on chitohexaose concentration. The longest residence (dwell) time was observed at transmembrane potential -100 mV reached the value  $\sim 6.7$  ms for *VhChiP*. This time decreased rapidly upon replacement of W136 by alanine ( $\sim 0.32$  ms), phenylalanine ( $\sim 2.3$  ms), arginine ( $\sim 0.34$  ms), and aspartate ( $\sim 0.5$  ms).

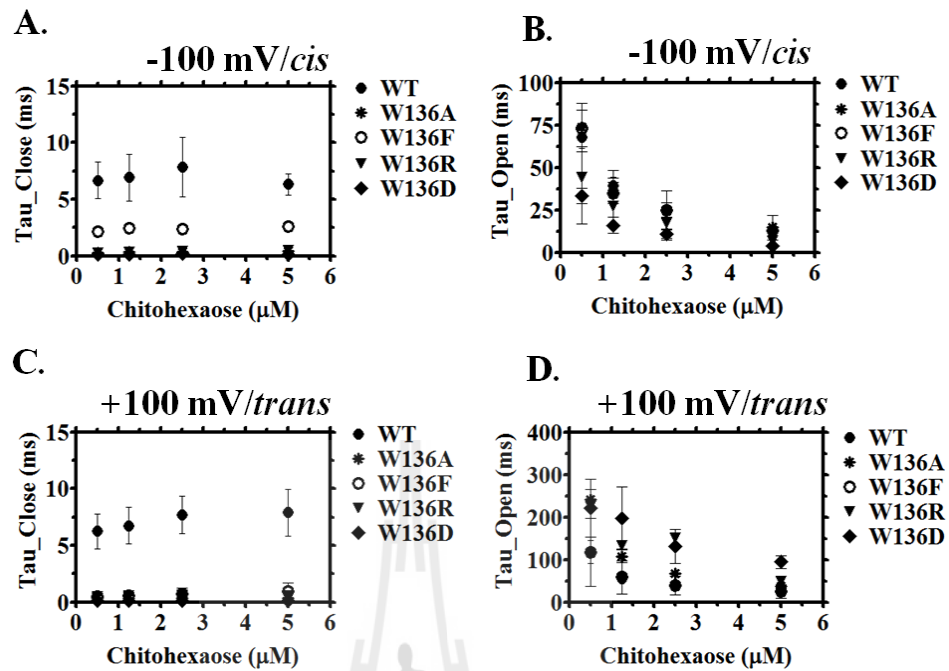


**Figure 3.22** Analysis of ion current blockades at *cis*/ $-100 \text{ mV}$  or *trans*/ $+100 \text{ mV}$  side addition of chitohexaose on the single channel conductance of *VhChiP* (WT) and its mutants. Plot of residence (dwell) time ( $\tau_c$ ) (A and C) and open time ( $\tau_o$ ) (B and D) versus various concentration of chitohexaose.

The rate of binding affinity was obtained from Lineweaver-Burk plots ( $(G_{\text{max}} - G_{[\text{c}]})/G_{\text{max}}$ )<sup>-1</sup> vs. ( $[\text{c}]^{-1}$ ) to estimate the equilibrium binding constant ( $K$ ,  $\text{M}^{-1}$ ) of *VhChiP* and its mutants with chitohexaose as its best substrate. Figure 3.23 shows the binding curves of *VhChiP* and its mutants with various concentrations of chitohexaose at  $-100 \text{ mV}/\text{cis}$  (Figure 3.23A) and  $+100 \text{ mV}/\text{trans}$  (Figure 3.23C). Fitting curves using a nonlinear regression function derived from Eq. 2.2 yielded to typical Michaelis-Menten plots (Nikaido *et al.*, 1992) and the plots with different concentrations of chitohexaose is reached saturation for *VhChiP* only, at both the  $-100 \text{ mV}/\text{cis}$  and the

+100 mV/*trans*, whereas all mutants did not reach saturation within the same range of chitohexaose concentrations (0.25 to 20  $\mu$ M). In case of *VhChiP*, saturation was reached within 5 to 20  $\mu$ M. The binding curve was transformed to Lineweaver-Burk plots ( $((G_{\max} - G_{[c]})/G_{\max})^{-1}$  vs.  $([c]^{-1})$ ) to obtain the binding constants. Figure 3.23B shows Lineweaver-Burk plots for *VhChiP* and its mutants for binding with chitohexaose at both -100 mV/*cis* and +100 mV/*trans* (Figure 3.23D). Table 3.4 shows the binding constant ( $K$ ,  $M^{-1}$ ) obtained from *cis* or *trans* side addition of chitohexaose at transmembrane potential -100 mV and +100 mV. Here, at -100 mV/*cis*, we found the highest of binding affinity ( $K$ ,  $M^{-1}$ ) for *VhChiP* ( $0.7 \times 10^6 M^{-1}$ ). This constant decreased slightly when W136 was replaced with arginine ( $0.37 \times 10^6 M^{-1}$ ), phenylalanine ( $0.33 \times 10^6 M^{-1}$ ), alanine ( $0.16 \times 10^6 M^{-1}$ ) and aspartate ( $0.1 \times 10^6 M^{-1}$ ). In contrast to this, on-rates ( $k_{\text{on}}$ ,  $M^{-1}s^{-1}$ ) increased. The results indicated that the binding constants were related to the conductance change when W136 was replaced by alanine and aspartic acid.

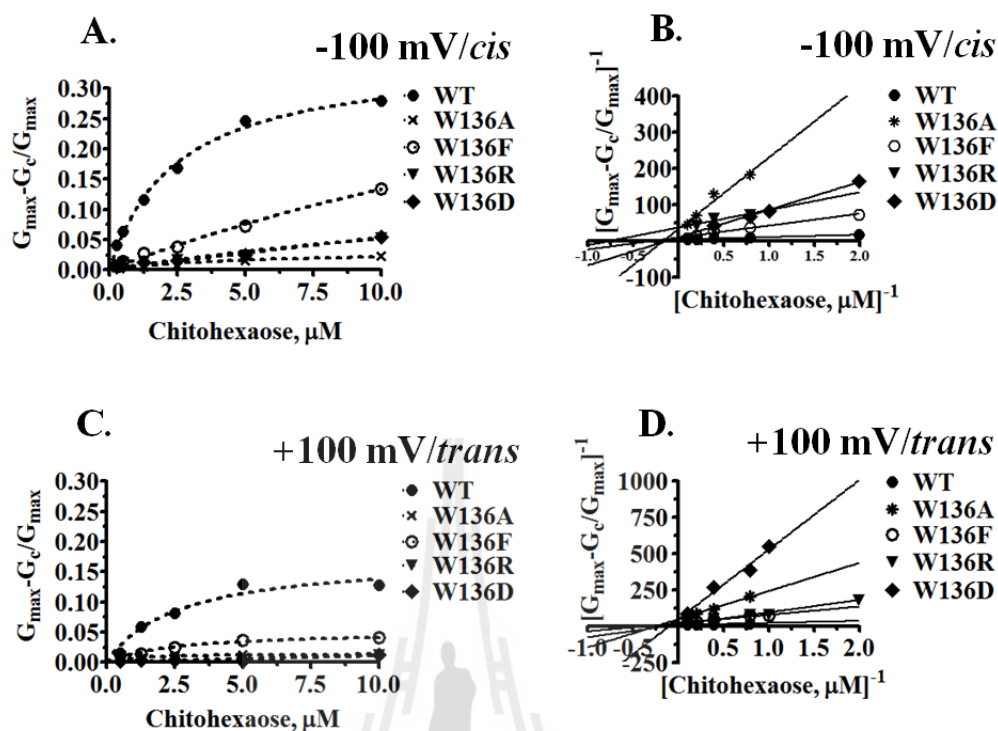


**Figure 3.23** Binding curve (Langmuir adsorption isotherms) and Lineweaver-Burk plots of *VhChiP* and its mutants with chitohexaose. The Michaelis-Menten plots were performed from the data on the *cis*/-100 mV (A) or *trans*/+100 mV (C) side addition. The plot of  $(G_{\max} - G_{[c]})/G_{\max}$  versus various concentrations of chitohexaose (0.25 to 20  $\mu\text{M}$ ) were derived from Eq. 2. Lineweaver-Burk plots of *VhChiP* and its mutants were obtained from the various concentrations of chitohexaose (0.25 to 10  $\mu\text{M}$ ), at -100 mV/*cis* (B) or +100 mV/*trans* (D) side addition.

**Table 3.4** Comparison of the rates and the equilibrium binding constants ( $K$ ,  $M^{-1}$ ) of *VhChiP* (WT) and its mutants for chitohexaose.

| Protein | <i>cis</i> -side addition                 |                                      |                                |   |                                      |                                | <i>trans</i> -side addition               |                                      |                                |   |                                      |                                |
|---------|---|--------------------------------------|--------------------------------|---|--------------------------------------|--------------------------------|---|--------------------------------------|--------------------------------|---|--------------------------------------|--------------------------------|
|         | +100 mV                                   |                                      |                                | -100 mV                                   |                                      |                                | +100 mV                                   |                                      |                                | -100 mV                                   |                                      |                                |
|         | $k_{on} \cdot 10^6$<br>( $M^{-1}s^{-1}$ ) | $k_{off} \cdot 10^3$<br>( $s^{-1}$ ) | $K \cdot 10^6$<br>( $M^{-1}$ ) | $k_{on} \cdot 10^6$<br>( $M^{-1}s^{-1}$ ) | $k_{off} \cdot 10^3$<br>( $s^{-1}$ ) | $K \cdot 10^6$<br>( $M^{-1}$ ) | $k_{on} \cdot 10^6$<br>( $M^{-1}s^{-1}$ ) | $k_{off} \cdot 10^3$<br>( $s^{-1}$ ) | $K \cdot 10^6$<br>( $M^{-1}$ ) | $k_{on} \cdot 10^6$<br>( $M^{-1}s^{-1}$ ) | $k_{off} \cdot 10^3$<br>( $s^{-1}$ ) | $K \cdot 10^6$<br>( $M^{-1}$ ) |
| WT      | 55  | 0.25                                 | 0.22                           | 105                                       | 0.15                                 | 0.70                           | 63  | 0.15                                 | 0.42                           | 46  | 0.2                                  | 0.23                           |
| W136A   | 500                                       | 5                                    | 0.10                           | 500                                       | 3.12                                 | 0.16                           | 760                                       | 3.3                                  | 0.23                           | 504                                       | 3.6                                  | 0.14                           |
| W136F   | 544                                       | 1.7                                  | 0.32                           | 142                                       | 0.43                                 | 0.33                           | 495                                       | 1.5                                  | 0.33                           | 510                                       | 3.4                                  | 0.15                           |
| W136R   | 540                                       | 2                                    | 0.27                           | 1,110                                     | 3                                    | 0.37                           | 153                                       | 1.7                                  | 0.09                           | 175                                       | 2.5                                  | 0.07                           |
| W136D   | 308                                       | 7.7                                  | 0.04                           | 200                                       | 2                                    | 0.10                           | 693                                       | 7.7                                  | 0.09                           | 250                                       | 6.25                                 | 0.04                           |

The equilibrium binding constants ( $K$ ,  $M^{-1}$ ) was estimated from the reduction of the single channel conductance in the titration of different concentrations of chitohexaose using Equation 1.

The on-rate ( $k_{on}$ ,  $M^{-1}s^{-1}$ ) is given by  $k_{on} = K \cdot k_{off}$ , and the off-rate ( $k_{off}$ ,  $s^{-1}$ ) from the single trimeric molecule of *VhChiP* channel and its mutant after titration with different concentrations of chitohexaose that was obtained from Kullman *et al.*

(Kullman *et al.*, 2002) refer to equation of  $k_{off} = 1/\tau_c$ .

### 3.5 Ion selectivity of *VhChiP* (WT) and its mutants

To study the ion selectivity, the single channel insertion was used to approve a reversal potential measurement. Here, KCl bulk solution was chosen in this study to compare the cationic selectivity between *VhChiP* (WT) and its mutants. The experiments were done with single salt solutions starting from 0.1 M KCl supplemented with 20 mM Hepes, pH 7.5 on *cis*- (connected to ground) and *trans*-side of the bilayer chamber. The insertion of *VhChiP* or its charged residues mutants W136D and W136R was performed into black lipid bilayer membrane with applied high potential (+/-199 mV). The channel conductance was checked by applying different voltages. Then instrumentation was switched to the measurement of zero-current membrane potentials. Increasing amounts of concentrated KCl solution were added to the *trans*-side of the membrane and the zero-current potentials were recorded (as show in Figure 3.24). Table 3.5 shows the results of the selectivity measurements of *VhChiP* and its arginine (W136R) and aspartic acid (W136D) mutants. The  $P_{K^+}/P_{Cl^-}$  values were calculated and analyzed using the Goldman-Hodgkin-Katz equation as described in the methods section. The results show a slight increase of cation selectivity for W136D with the ratio  $P_{K^+}/P_{Cl^-}$  of about 4.2 ( $V_m = -28$  mV), while the *VhChiP* showed a cation selectivity of  $P_{K^+}/P_{Cl^-} = 3.20$  ( $V_m = -23$  mV). In contrast to this, cation selectivity of the mutant W136R decreased to  $P_{K^+}/P_{Cl^-} = 2.74$  ( $V_m = -20$  mV). The results suggested that the mutation of tryptophan by arginine reduces cation selectivity with the ratio  $P_{K^+}/P_{Cl^-}$  to be about 2.74.

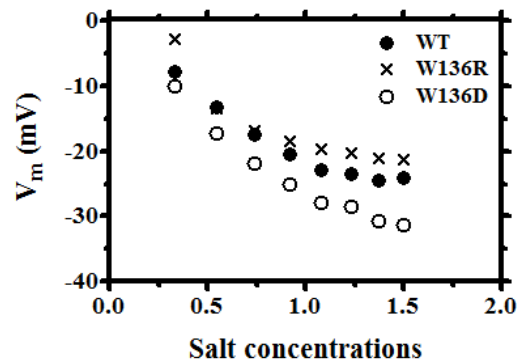


**Figure 3.24** Representation of the plot between zero-current membrane potentials ( $V_m$ ) and the ratio of salt concentrations on *trans*-side of KCl bulk solution. Low concentrations of 0.1 M KCl were kept on the *cis*-side of the chamber. Increasing KCl concentrations were applied to the *trans*-side by addition of small amounts of 3 M KCl. The curves were fitted to the equation of Goldman-Hodgkin-Katz.

**Table 3.5** Ionic selectivity of *VhChiP* WT and its charged mutants.

| Protein  | Ratio of salt concentrations (KCl, M) | $V_m$ , (mV) | $e^x$       | $e^x$ | $P_{K^+}/P_{Cl^-}$ |
|----------|---------------------------------------|--------------|-------------|-------|--------------------|
| 1) WT    | 0.1 : 1                               | -23          | $e^{-0.9}$  | 0.4   | 3.20               |
| 2) W136R | 0.1 : 1                               | -20          | $e^{-0.79}$ | 0.45  | 2.74               |
| 3) W136D | 0.1 : 1                               | -28          | $e^{-1.1}$  | 0.33  | 4.20               |

The single channel insertion of *VhChiP* WT and its mutants were performed in DPhPC lipid bilayer membrane dissolved in *n*-pentane. The bulk solution contained 1 M KCl (*trans*) and 0.1 M KCl (*cis*) supplemented with 20 mM HEPES, pH 7.5. The temperature was  $20 \pm 3$  °C to carry out of the experiment.

### 3.6 Fluorescence spectroscopy

To study the dissociation binding constants ( $K_D$ ,  $\mu\text{M}$ ) using Fluorescence Spectroscopy, the intrinsic fluorescence was used to assess the binding affinity with chitosugars as a substrate towards WT and its mutant. Firstly, the amino acid alignment are revealed and shown under line of ten aromatic residues, including W73, W105, W123, W136, W157, W188, W220, W233, W275, and W338 (Figure 3.25A). Figure 3.25B represented the modeling of the three-dimensional structure of *VhChiP* channel based on the X-ray structure of *D. acidovorans* Omp32 (pdb 2GFR). Only three tryptophan residues (W123, W136, and W338) were found to be exposed inside the pore. The intrinsic fluorescence intensity (assumes to come from tryptophan 136) of *VhChiP* and its mutants was measured at excitation wavelength of 295 nm and emission spectrum wavelength between 300-500 nm as shown in Figure 3.25C. Decrease of fluorescence intensity were found to occur by replacement of W136 by alanine, arginine and aspartate (Figure 3.25C) at 40 ng/ $\mu\text{l}$  of protein concentration.

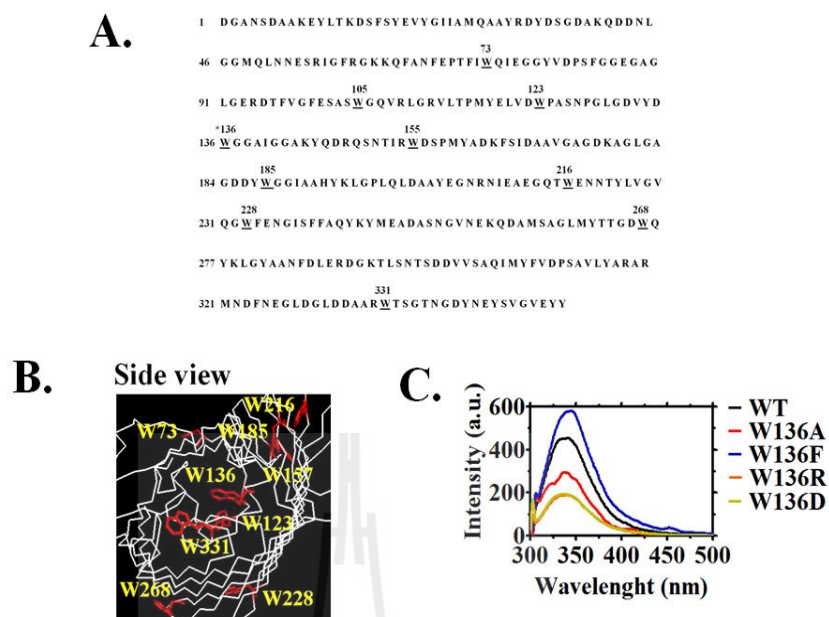


**Figure 3.25** Amino acid sequence and a cross-section of the modelling structure of *V. harveyi* monomeric chitoporin. A) Amino acid sequence of chitoporin, underline indicated ten tryptophan residues including W73, W105, W123, W136, W157, W188, W220, W233, W275, and W338. Loop 3 (white line) and B) amino acid residues (donated with their numbers from the mature N-terminal end) that are relevant for passage of ions and chitosugars transport through the constriction zone of chitoporin channel. C) Example of the emission spectra from WT and its mutant via tryptophan fluorescence intensity of WT and its mutants (40 ng/ $\mu$ l). The emission spectra were obtained from fluorescence recording in a solution containing 20 mM phosphate (pH 7.4), 0.2% LDAO and were collected at wave lengths between 300-550 nm. The excitation wave length was 295 nm (excitation slit, 5 nm and emission slit, 10 nm).

The fluorescence intensity measured with WT and its mutants allowed the titration of chitosugars at various concentrations to obtain the dissociation constants. The decreased fluorescence intensity was found to correspond to an increase in the concentrations of chitooligosaccharides. Figure 3.26A-E showed decreased and increased fluorescence intensity profiles of WT and its mutants dissolved in 0.2% LDAO during titration with chitohexaose in phosphate buffer (pH 7.4) for fit of the binding curve for *VhChiP* and its mutants,  $F_0 - F$  or  $F - F_0$  were plotted versus  $[c]$  to obtain the dissociation constants. Moreover, *VhChiP* was tested with GlcNAC<sub>2</sub> and GlcNAC<sub>1</sub>, but we could not detect any decreased fluorescence intensity. The titration experiments of *VhChiP* and its mutants with chitohexaose were used to calculate the dissociation constant ( $K_D$ ,  $\mu\text{M}$ ) from Lineweaver-Burke plots or Langmuir adsorption isotherms. The results are given in Table 3.6. The strongest binding affinity was observed for *VhChiP* (0.09  $\mu\text{M}$  for chitohexaose). The dissociation constants slightly decreased when the number of GlcNAc molecules in the chain length was reduced to five (0.29  $\mu\text{M}$ ), four (1.16  $\mu\text{M}$ ), and three (1.91  $\mu\text{M}$ ), respectively. Binding of GlcNAC<sub>2</sub> and GlcNAC<sub>1</sub> to *VhChiP* was not detectable (included in Table S4). The mutation of W136 resulted in decreased binding affinity for chitohexaose. Replacement of W136 by alanine, phenylalanine, arginine and aspartate resulted in an increase of the half saturation constant to 0.14  $\mu\text{M}$ , 0.25  $\mu\text{M}$ , 0.53  $\mu\text{M}$  and 2.99  $\mu\text{M}$ , respectively. In addition, Gibbs free energy ( $\Delta G$ ) calculated according to Eq. 2.8 slightly decreased dependent on the numbers of GlcNAc units in the chain length of chitosugars. Similarly, Gibbs free energy ( $\Delta G$ ) was reduced for binding of chitohexaose to mutants.

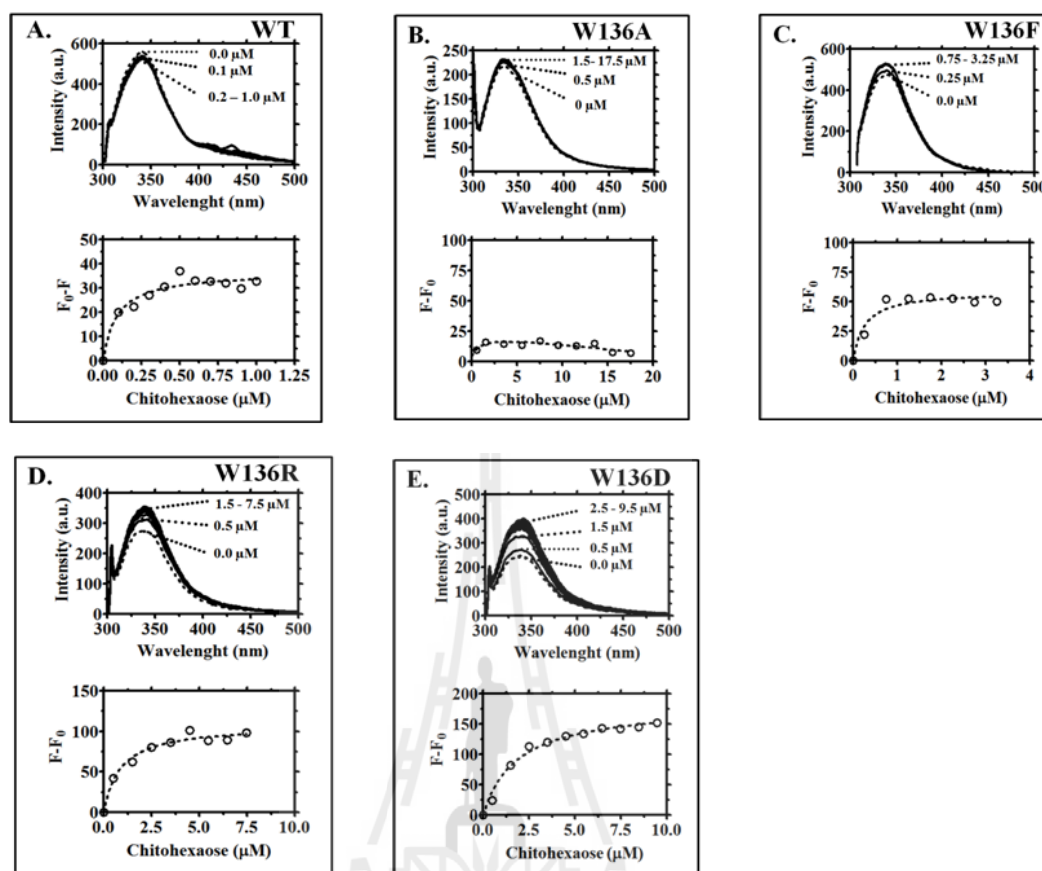


**Figure 3.26** Comparison of the emission spectra from A) *VhChiP* and B-E) its mutants. 40 ng/ $\mu\text{l}$  proteins were titrated with various concentrations of chitohexaose. All emission spectra were recorded in 20 mM phosphate (pH 7.4) contains 0.2% LDAO and collected from 300-550 nm upon excitation at 295 nm (excitation slit, 5 nm and emission slit, 10 nm). The temperature was  $20 \pm 3$  °C.

**Table 3.6** The dissociation constant ( $K_D$ ) of *VhChiP* (WT) and its mutants with chitohexaose (GlcNAc<sub>6</sub>) using Fluorescence Spectroscopy.

| Ligand              | Protein  | Nonpolar, Hydrophobic   |        |         |                                   |           |            |                     |        |        |
|---------------------|----------|-------------------------|--------|---------|-----------------------------------|-----------|------------|---------------------|--------|--------|
|                     |          | $K_D$ ( $\mu\text{M}$ ) |        |         | $K$ ( $1/K_D$ , $\text{M}^{-1}$ ) |           |            | $\Delta G$ (kJ/mol) |        |        |
|                     |          | pH 4.0                  | pH 6.0 | pH 7.4  | pH 4.0                            | pH 6.0    | pH 7.4     | pH 4.0              | pH 6.0 | pH 7.4 |
| GlcNAc <sub>6</sub> | 1) WT    | -                       | 1.25   | 0.09    | -                                 | 800,000   | 11,000,000 | -                   | -33    | -39.4  |
|                     | 2) W136A | -                       | -      | 1.1     | -                                 | -         | 909,000    | -                   | -      | -33.3  |
|                     | 3) W136F | -                       | -      | 0.25    | -                                 | -         | 4,000,000  | -                   | -      | -36.9  |
|                     | 4) W136D | Polar Acidic            |        |         |                                   |           |            |                     |        |        |
|                     |          | $K_D$ ( $\mu\text{M}$ ) |        |         | $K$ ( $1/K_D$ , $\text{M}^{-1}$ ) |           |            | $\Delta G$ (kJ/mol) |        |        |
|                     |          | pH 4.0                  | pH 6.0 | pH 7.4  | pH 4.0                            | pH 6.0    | pH 7.4     | pH 4.0              | pH 6.0 | pH 7.4 |
|                     |          | 3.13                    | 2.99   | 1.88    | 320,000                           | 330,000   | 530,000    | -30.7               | -30.8  | -31.9  |
|                     | 5) W136R | Polar Basic             |        |         |                                   |           |            |                     |        |        |
|                     |          | $K_D$ ( $\mu\text{M}$ ) |        |         | $K$ ( $1/K_D$ , $\text{M}^{-1}$ ) |           |            | $\Delta G$ (kJ/mol) |        |        |
|                     |          | pH 4.0                  | pH 6.0 | pH 7.4  | pH 4.0                            | pH 6.0    | pH 7.4     | pH 4.0              | pH 6.0 | pH 7.4 |
|                     | 1.49     | 0.53                    | 0.87   | 670,000 | 1,900,000                         | 1,150,000 | -32.5      | -35                 | -33.9  |        |

The dissociation binding constants ( $K_D$ ,  $\mu\text{M}$ ) obtain from the Stern-Volmer of the Eq. 2.4 and converted to the equilibrium binding constants ( $K$ ,  $\text{M}^{-1}$ ) as inversion as  $1/K_D$ . The Gibbs free energy ( $\Delta G$ ) was calculated from the Eq. 2.8, where R is the ideal gas constant ( $8.1315 \times 10^{-3}$  kJ/mol); T is temperature (T = 298 K).

### 3.7 Liposome swelling assay

High resolution ion conductance measurements were complemented by proteoliposome swelling assays, which determined the permeation of sugar molecules through WT and its mutant reconstituted into proteoliposomes. Diffusion rates of sugars through WT channels and its mutant determined by these assays indicate influx of solutes into the proteoliposomes. Figure 3.27 represent the illustration of the swelling of proteoliposomes reconstituted with WT and its mutant exposed to chitohexaose, which sugar found to be the most potent channel blocker in membrane current measurements. In the previous section, the swelling rates in raffinose, sucrose, maltose, maltopentaose and maltohexaose were also tested in comparison (Figure S2). When normalized to the swelling rate of arabinose (set to 100%), only chitohexaose at concentrations of 750  $\mu\text{M}$  was found to permeate through *VhChiP* and its mutants. The rate of permeation through its mutant was decreased. It means that the tryptophan 136 played the role important for chitosugars permeation through *VhChiP* channel.

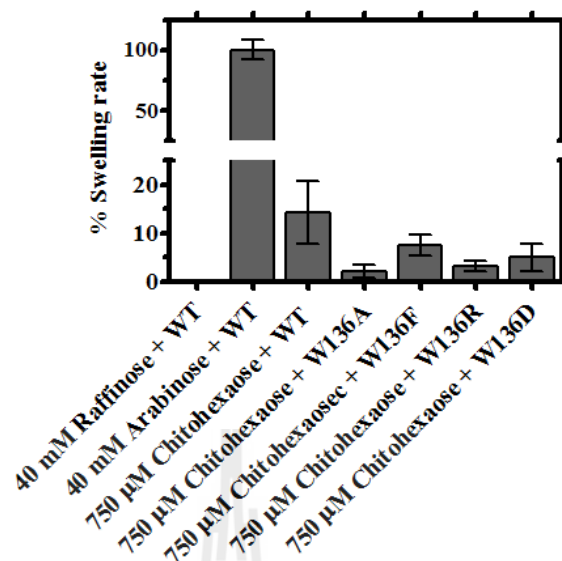


**Figure 3.27** Liposome swelling assays. Multilamellar liposomes, prepared as described in the text, were reconstituted with purified *VhChiP* (100 ng). The isotonic concentration was defined as the concentration of raffinose added into the proteoliposome suspension that did not cause change in absorbance at 500 nm for a period of 60 s. Permeation of different types of sugars through *VhChiP* and its mutant reconstituted liposomes were then tested. The swelling rates were normalized, with the rate of swelling in arabinose set to 100%. Values presented are averages of triplicate experiments. The isotonic concentration of 40 mM raffinose and 750 μM chitohexaose was added.

### 3.8 Temperature dependence on the sugars translocation through *VhChiP* and its mutant channel

To reveal energy barriers involved in sugars translocation through the *VhChiP* channel (WT) and its mutant. In this study used the single channel insertion reconstituted into black lipid bilayer membrane to characterize the effect of the temperature on the translocation of chitohexaose through WT and its mutant. Chitohexaose is the best substrate and strong interaction for WT channel. At low concentration of chitohexaose (between 0.5  $\mu\text{M}$  to 1.25  $\mu\text{M}$ ) was chosen to test with WT and its mutant on *cis*- or *trans*-side, one monomeric blockage events were observed and different temperatures were applied. Figure 3.28 shows an example of one monomeric blockage on *cis*-side addition of chitohexaose with three different temperatures at 10 °C (Figure 3.28A), 15 °C (Figure 3.28B) and 20 °C (Figure 3.28C) for WT and its mutant (W136A, W136F, W136R, and W136D).

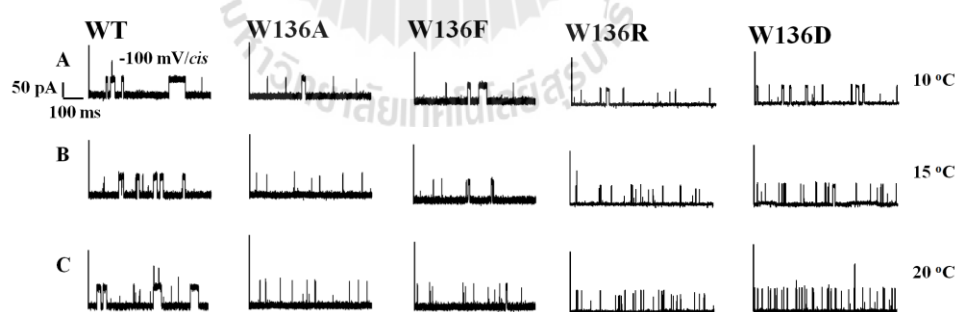


**Figure 3.28** Typical ion current recordings through WT and its mutant at 10 °C (A), 15 °C (B) and 20 °C (C) in the presence of chitohexaose at *cis*-side, -100 mV. The experiment was carried out in 1 M KCl in 20 mM Hepes (pH 7.5) and the concentration of chitohexaose was added with different concentrations (in range between 0.5 to 1.25  $\mu\text{M}$ ).

When increasing the temperature from 5 to 20 °C, the opened channel conductance was increased. As expected the no. of events were increased (Figure 3.29A (*cis*-) and Figure 3.29B (*trans*-)). The results suggested that *VhChiP* showed the voltage and temperature dependent channel closure, at high voltage and temperature, more gating occurs with increasing temperature, which observed only one side of transmembrane potential applied through the channel from *cis*- or *trans*-side. It means that the number of events increased which indicates that the electric field pulled the molecule of the chitohexaoses from the bulk solution of 1 M KCl on the bath into the binding site inside the channel.

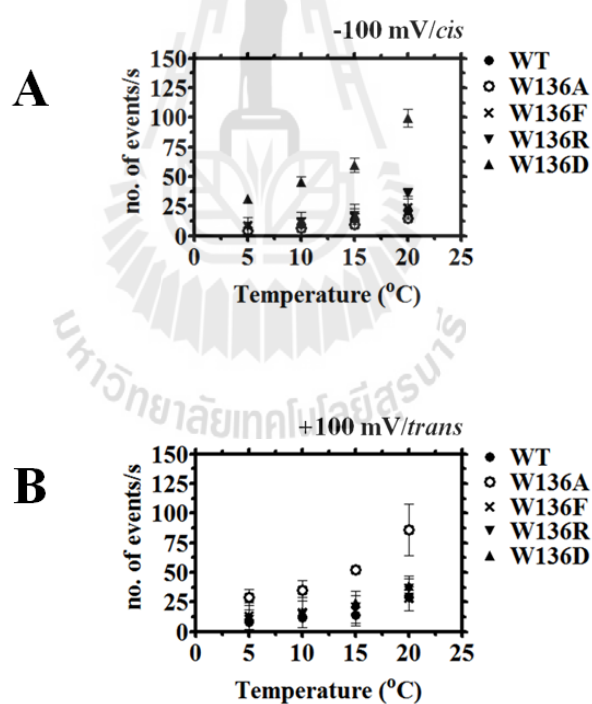


**Figure 3.29** The number of binding events of chitohexaose in the channel of WT and its mutants as a function of temperature from 5 °C to 20 °C at *cis*- (-100 mV, (A)) and *trans*- (+100 mV, (B)) side of chitohexaose addition. The bulk solution is 1 M KCl in 20 mM Hepes (pH 7.5).

The statistical analysis of the ion trace at temperature of 5 to 30 °C obtained the average residence time of chitohexaose translocation through WT and its mutant pores. Figure 3.30 shows the average residence time from *cis*- (Figure 3.30A) or *trans*-side (Figure 3.30B) addition of chitohexaose. With increasing temperature from 5 to 30 °C, the averages residence time slightly decreased, which could be observed for WT and its mutant. Observation of residence time for WT at 5 °C, a few ion current blockages were detected with the residence time above 50 ms (*cis*-), while at *trans*-side addition of chitohexaose were found to be above 10 ms. As expected the residence time is reduced about 60 folds (*cis*-side) and 5 folds (*trans*-side) with its mutant.

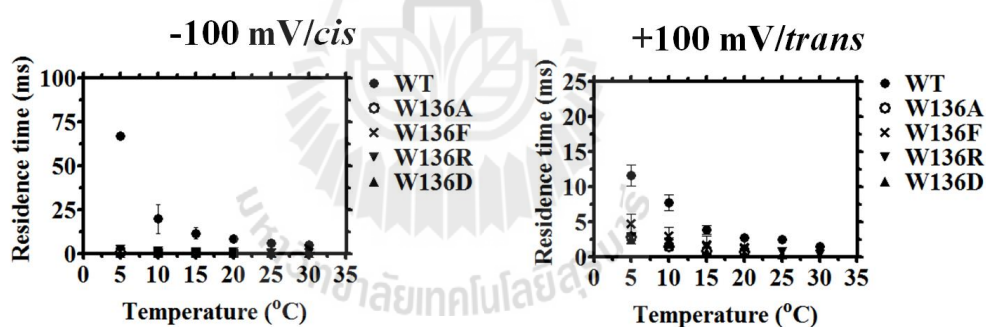


**Figure 3.30** The residence time of chitohexaose in the channel of WT and its mutant as a function of temperature from 5 °C to 30 °C at *cis*- (-100 mV, (A)) and *trans*- (+100 mV, (B)) side of chitohexaose addition. The bulk solution is 1 M KCl in 20 mM Hepes (pH 7.5).

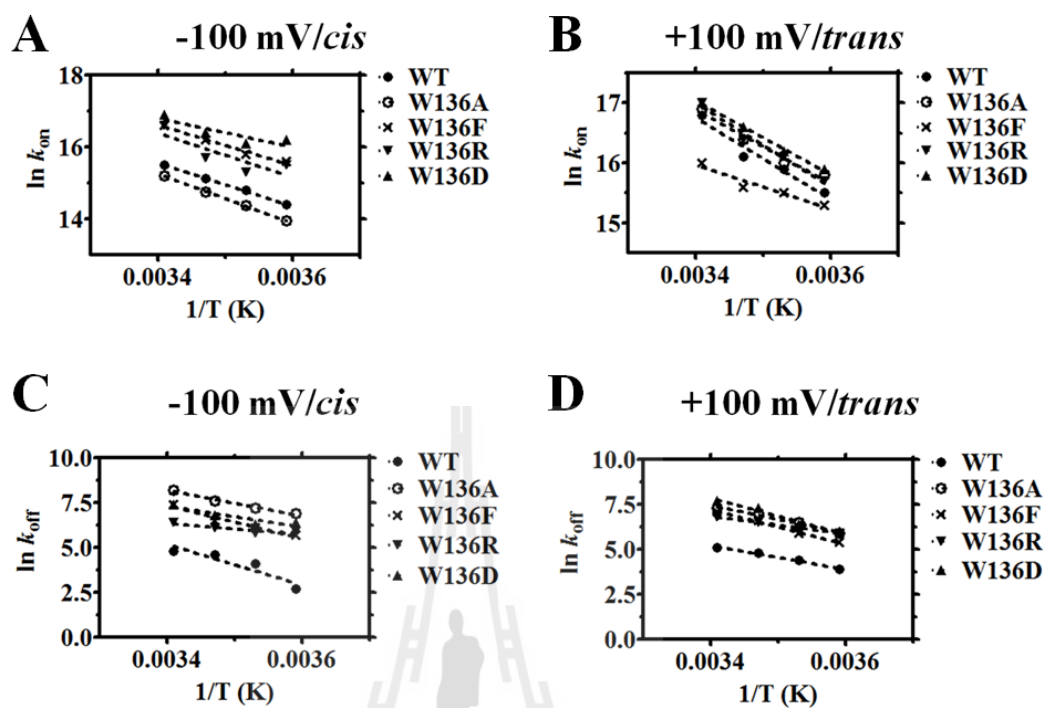


**Figure 3.31** Arrhenius plot of  $k_{\text{on}}$  (A (*cis*-side) and B (*trans*-side)) and  $k_{\text{off}}$  as function of temperature from 5 °C to 20 °C represented in a linear slope with WT and its mutant. The bulk solution contained 1 M KCl in 20 mM Hepes (pH 7.5).

An energy barrier is calculated from an Arrhenius plot obtained from the number of events and residence times are related to the on- and off-rates of chitohexaose translocation through WT and its mutant channels. The number of events ( $\nu$ ) obtained from the on-rate at a given concentration  $[c]$  of chitohexaose is followed the equation of  $k_{\text{on}} = \nu/3[c]$  and the off-rate  $k_{\text{off}} = 1/\tau$  is the inverse of the residence time ( $\tau$ ). The exponential increase of the number of events from 5 to 20 °C (Figure 3.31A-B) suggested the correlation of  $k_{\text{on}}$  with the activation barriers, while high temperature (25 or 30 °C) was observed with more gating the channel behavior. Figure 3.31A-B represent the Arrhenius plot from  $k_{\text{on}}$  at both the -100 mV (*cis*-side, Figure 3.31A) and the +100 mV, (*trans*-side, Figure 3.31B) of sugar addition and Figure 3.31C-D show the Arrhenius plot from  $k_{\text{off}}$  at *cis*-side (Figure 3.31C) and *trans*-side (Figure 3.31D) of sugar addition, both are obtained from the fitting region of Figure 3.29A-B. The energy barrier for the chitohexaose translocation through channel of WT and its mutant calculated from the Arrhenius plot. The logarithm of both  $k_{\text{on}}$  and  $k_{\text{off}}$  showed a linear dependence in  $1/T$  yields  $E_a$ .  $E_a$  is calculated from the slope times with the ideal gas constant.  $E_a$  required for the chitohexaose permeate through the channel from the *cis*-side ( $E_a, \text{cis}$ ) to *trans*-side ( $E_a, \text{trans}$ ) to the internal affinity at the binding site in the channel as shown in the Table 3.7. When the chitohexaose was added on *cis*-side, the energy barriers required for sugar translocation from *cis*- to *trans*-side across the affinity site of the *VhChiP* channel is asymmetry yields an energy barrier about 17.7 kT (+100 mV) and 19 kT (-100 mV). While high asymmetry is observed when chitohexaose was added on the *trans*-side gave an energy barrier about 19.2 kT (+100 mV) and 27.5 kT (-100 mV). With mutations, high energy barriers and the channel behavior became more asymmetry are

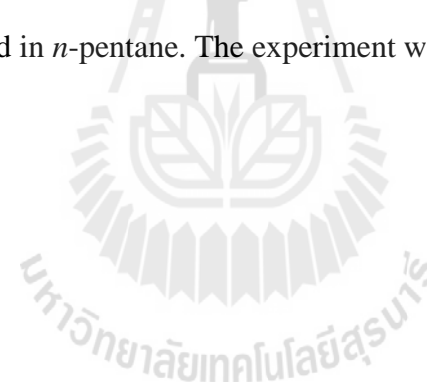
observed when replacement of tryptophan 136 with charged residue groups (arginine and aspartate) as shown in the Table 3.7. The result indicated that at internal affinity site in the *VhChiP* channel requires for different activation energy from *cis*- or *trans*-side addition of chitohexaose.



**Table 3.7** Energy barrier of *VhChiP* WT and its mutants.

| Proteins     | $\ln k_{\text{on}}$ |         |                       |         | $\ln k_{\text{off}}$ |         |                       |         |
|--------------|---------------------|---------|-----------------------|---------|----------------------|---------|-----------------------|---------|
|              | Ea (kT)/ <i>cis</i> |         | Ea (kT)/ <i>trans</i> |         | Ea (kT)/ <i>cis</i>  |         | Ea (kT)/ <i>trans</i> |         |
|              | +100 mV             | -100 mV | +100 mV               | -100 mV | +100 mV              | -100 mV | +100 mV               | -100 mV |
| <b>WT</b>    | 17.7                | 19      | 19.2                  | 27.5    | 31                   | 29.2    | 21.4                  | 22.2    |
| <b>W136A</b> | 16.2                | 23      | 20.6                  | 18.9    | 27.8                 | 23.8    | 26.2                  | 21      |
| <b>W136F</b> | 27.3                | 18.9    | 12.1                  | 29      | 20.6                 | 30.6    | 32.3                  | 16.5    |
| <b>W136R</b> | 19.7                | 17.3    | 27                    | 24.2    | 16.9                 | 22.6    | 26.6                  | 26.2    |
| <b>W136D</b> | 34.7                | 27      | 20                    | 19.7    | 26.2                 | 22.6    | 21.4                  | 21.8    |

The membranes were formed from DPhPC dissolved in *n*-pentane. The experiment was carried out in 1 M KCl in 20 mM Hepes (pH 7.5).



## CHAPTER IV

### DISCUSSION

#### 4.1 Investigation of the uptake mechanism of chitooligosaccharides through *VhChiP* channel

The gene encoding chitoporin from *Vibrio harveyi* (so called *VhChiP*) was successfully cloned and the recombinant *VhChiP* was expressed in the Omp-deficient *E. coli* BL21 (Omp8) strain. Detection of endogenous expression of chitoporin was seen when the *V. harveyi* cells were grown on chitin-containing medium, suggesting that the *ChiP* gene was regulated by the chitin-induced regulation, known as the ChiS regulon (Li *et al.*, 2004; Meibom *et al.*, 2004). Single channel recordings revealed that the recombinant *VhChiP* inserted readily into the artificial membranes and behaved as a pore-forming component with a characteristic trimeric closure when high external membrane potentials were applied. Structural homology with other porins suggested that *VhChiP* had 16  $\beta$ -stranded transmembrane domains, 8 extracellular loops and 8 periplasmic turns, similar to most bacterial porins (Koebnik *et al.*, 2000; Nikaido *et al.*, 1992; Schirmer *et al.*, 1998).

High time resolution BLM current measurements were used to demonstrate the interaction of chitooligosaccharides with *VhChiP*. Such sugar-protein interaction is, by some mean, interpreted as oligosaccharide translocation. The channel was found to interact with the chitosugars to various extents, depending on sizes and types of the

chitosugars. The absence of current fluctuation upon addition of chitobiose (GlcNAc<sub>2</sub>) suggested no interaction. This may be due to that this small sugar did not permeate or it may permeate so fast that the residence time of blocking events was too small to be resolved. In contrast, the *VhChiP* channel was much more responsive against higher-MW of chitosugars (GlcNAc<sub>3-6</sub>). Channel blocking by chitosugar also reflected a common characteristic of substrate-specific channel, especially when higher-MW oligosaccharides were preferred substrates (Dumas *et al.*, 2000; Hilty *et al.*, 2001). Similar channel blocking behaviors were previously observed in maltoporin (LamB) with maltooligosaccharides (Bezrukov *et al.*, 2000). Current noise analysis revealed no response of *VhChiP* to maltopentaose and maltohexaose even at a concentration five-fold greater than that of chitosugars, indicating that *VhChiP* was a chitooligosaccharide-specific porin. The results of liposome swelling assays additionally confirmed insignificant permeation of other sugars, including raffinose, maltose and sucrose (APPENDIX E, Figure S2). These data indicated high specificity of the *VhChiP* porin towards chitooligosaccharides. These findings were not astonishing, since *VhChiP* showed unusually low sequence identity with other sugar-specific porins (less than 20%).

## **4.2 Binding kinetics of uncharged molecules translocation through *VhChiP* channel (chitooligosaccharides)**

To quantify sugar translocation, *VhChiP* was reconstituted into BLM and the ion fluctuation was exposed to various types of sugars. The channel responded only to chitooligosaccharides, with increasing level of response for longer molecular weight (MW), especially strongest interaction was seen with chitohexaose. This observation

was analogous to maltoporin-binding maltooligosaccharides, for which the most effective ligand was seen with the longest sugar: maltoheptaose (Andersen *et al.*, 1995; Benz *et al.*, 1986). Note that analysis of the sugar-induced blockages provides information on the presence of sugar in the channel with a residence time limit of 100  $\mu$ s of events/s. Faster events are not resolvable by this technique. Throughout BLM recording, the probability for ion current blockade increased with concentrations of the chitosugars. For example in APPENDEX E, Figure S3 represents selected current time I(t) traces showing that, at 10  $\mu$ M, chitotriose (Figure S3A), chitotetraose (Figure S3B), and chitopentaose (Figure S3C) blocked only the *VhChiP* monomer. The second and third subunits were subsequently blocked when the sugar concentration was raised to 80  $\mu$ M. The results suggested that *VhChiP* responded in a concentration-dependent manner not only toward chitohexaose, but also toward lower molecular weight chitosugars. However, much higher concentrations of short-chain sugars were required to induce multiple blockages due to their poor affinity as shown in Table 3.1.

The rate of sugar interaction (Figure 3.11A) with *VhChiP*, the residence time within the channel (Figure 3.11B), and its binding affinity (Table 3.1) were found to be highly dependent on the polarity of the applied potential. Voltage-dependent sugar permeation through the *VhChiP* pore were caused by dipole moments, arising from impaired electron distribution on the *N*-acetamido (-NHCOCH<sub>3</sub>) groups of the multiple GlcNAc units that compose a chitooligosaccharide chain. As a result, the sugar chains seem to orient themselves favorably for channel entrance with a negative potential on the *cis* side and an opposite potential on the other side. The much higher rate of sugar permeation from *cis*-to-*trans* over *trans*-to-*cis* clearly indicated intrinsic asymmetry of the channel. In the case of maltoporin, channel asymmetry was also

observed; however, the effect was opposite from that seen for *VhChiP*. The frequency of sugar diffusion into maltoporin from *trans*-to-*cis* was significantly higher than from *cis*-to-*trans* (Schwarz *et al.*, 2003; Danelon *et al.*, 2003; Kullman *et al.*, 2002). Such results indicated that the molecular arrangement contributing to GlcNAc-binding subsites within the *VhChiP* lumen was completely different from that in maltoporin. Kinetic analysis indicated that *VhChiP* interacted with chitooligosaccharides in a concentration-dependent manner. However, there is a discrepancy regarding the size of the sugars. On-rates increased almost linearly for chitotriose and chitotetraose as their concentrations increased. Diffusion through the *VhChiP* channel in these cases was driven entirely by the concentration gradient, with weak interactions between the sugar and protein molecules. However, the binding affinity significantly increased when the sugar chain was longer. Binding of chitopentaose to chitoporin was of particular interest because of its strong interaction yields a permanent reduction of the channel conductance to one-third of the full conductance when its concentrations exceeded 5  $\mu\text{M}$  (see APPENDEX E, Figure S4C as a representative trace at 5  $\mu\text{M}$ ). As a result, we could not evaluate the binding constant of chitopentaose under this particular condition (Table 3.1). We do not yet completely understand why negative potentials strongly affected the permeation of chitopentaose. This will be a subject of our further investigation. Translocation of chitohexaose particularly involved specific substrate-protein interactions, resulting in Michaelis-Menten transport kinetics resembling those of previously reported sugar-specific porins, including maltoporin (LamB) (Andersen *et al.*, 1995; Benz *et al.*, 1986; Van Gelder *et al.*, 2002; Klebba *et al.*, 2002), sucrose porin (ScrY) (Andersen *et al.*, 1998; Van Gelder *et al.*, 2001), glucose-inducible porin (OprB) (Saravolac *et*

*al.*, 1991; Wylie *et al.*, 1993), and cyclodextrin porin (CymA) (Pajatsch *et al.*, 1999; Orlik *et al.*, 2003). Our study revealed that chitohexaose is the most potent substrate of the *VhChiP* channel, as it blocked the ion flow even at nanomolar concentrations, and the monomeric subunit was already saturated below 1  $\mu\text{M}$ . In Table 4.1, we summarize the rate constants: the on-rate ( $k_{\text{on}}$ ) is by far the highest for chitohexaose, whereas the off-rate ( $k_{\text{off}}$ ) is the lowest. Consequently, the resultant binding constant ( $K$ ) of  $500,000 \pm 68,000 \text{ M}^{-1}$  is 1-5 orders stronger than the reported values for other analogs (Andersen *et al.*, 1998; Andersen *et al.*, 1995; Van Gelder *et al.*, 2001; Saravolac *et al.*, 1991; Wylie *et al.*, 1993; Pajatsch *et al.*, 1999; Orlik *et al.*, 2003; Hilty *et al.*, 2001). According to the kinetic data in Table 4.1, *VhChiP* is the most active sugar-specific channel reported to date. Highly effective sugar transport machinery is considered to be crucial for *V. harveyi* to maintain the homeostatic balance that enables the bacterium to survive and thrive in extreme marine environments with a scarcity of the usual nutrients.

**Table 4.1** Comparison of the rates and the binding kinetics of *VhChiP* with those of other sugar-specific porins.

| Channel type  | Substrate     | $K$<br>$M^{-1}$ | $k_{on}$<br>$\times 10^6 M^{-1}s^{-1}$ | $k_{off}$<br>$\times 10^3 s^{-1}$ | Ref.                     |
|---|---------------|-----------------|--|-----------------------------------|--------------------------|
| 1. <i>VhChiP</i>  | Chitohexaose  | 500,000         | 85.0                                   | 0.17                              | This study               |
| 2. <i>E. coli</i> maltoporin (LamB)                             | Maltotriose   | 4,300           | 8.4                                    | 1.95                              | Refs. 25, 33, 35, and 40 |
|   | Maltotetraose | 8,100           | 6.1                                    | 0.77                              | ”                        |
|   | Maltopentaose | 13,000          | 5.3                                    | 0.43                              | ”                        |
|   | Maltohexaose  | 20,000          | 4.8                                    | 0.24                              | ”                        |
|   | Maltoheptaose | 31,000          | 5.6                                    | 0.18                              | ”                        |
| 3. <i>Salmonella typhimurium</i> sucrose porin (ScrY)           | Sucrose       | 80              | 0.004                                  | 0.05                              | Ref. 25                  |
| 4. <i>Klebsiella oxytoca</i> cyclodextrin porin (CymA)          | Cyclodextrin  | 31,300          |  |                                   | Ref. 38                  |
| 5. <i>Pseudomonas putida</i> glucose-inducible porin (OprB)     | Glucose       | 9.1             |  |                                   | Ref. 36                  |
| 6. <i>Pseudomonas aeruginosa</i> glucose-inducible porin (OprB) | Glucose       | 2.6             |  |                                   | Ref. 37                  |

### **4.3 Binding kinetics and translocation of charge molecules through *VhChiP* channels (chitosan hexamer)**

We performed BLM measurements of the open state of *VhChiP* in the pH range that allowed switching from protonated (cationic) to deprotonated (neutral) state of deacetylated chitooligosaccharide or chitosan hexamer. The relevant sets of the membrane current recordings of single *VhChiP* channels were performed at transmembrane potential ( $V_m$ ) of  $\pm 100$  mV and at four relevant pH values (5.0, 6.5, 7.5, and 8.5) in the bathing electrolyte (not shown). In agreement with earlier observations (Suginta *et al.*, 2013), the ion current that passed through the fully-open trimeric chitoporin yielded the conductance of 1.8 nS and did not vary significantly over the studied pH range. The channel was found to be fully open below  $\pm 100$  mV and at pH 8.5 or 7.5. At pH 6.5, the channel was open for most of the time for  $\pm 100$  mV and infrequently gated (not shown). Lowering the pH further to 5.0 caused a dramatic change in the ionization of the amino acid side chains lining the *VhChiP* lumen, thereby leading to frequent channel closure. Low pH causing channel closure was observed previously for *E. coli* maltoporin or LamB (Andersen *et al.*, 2002) and other general diffusion porins, including OmpF, OmpC, and PhoE (Xu *et al.*, 1986; Todt *et al.*, 1992). From an electrophysiological point of view, understanding the *VhChiP* channel behaviors at different pH values may explain the local habitats of the *Vibrio* species mainly on sea surface. This is because deep water carries more CO<sub>2</sub>, which undergoes acidification (<http://www.whoi.edu/OCB-OA>) that could perturb metabolic activity of the bacteria. In addition, ongoing ocean acidification due to high concentration of CO<sub>2</sub> derived from global warming is predicted to affect the ecosystems of marine organisms (Joint *et al.*, 2011; Krause *et al.*, 2012), including the

*Vibrio* species responsible for chitin turnover in the marine ecosystem. As shown, external transmembrane potential affects the gating behavior of *VhChiP* with the threshold potential for gating of  $\pm 150$  mV (Suginta *et al.*, 2013). To avoid intrinsic channel gating at high voltages ( $>150$  mV), we restricted our analysis to lower voltages.

To elucidate the interaction of the chitin/chitosan sugars with the *VhChiP* channel, the ion current fluctuations were recorded at pH 8.5 for which both oligosaccharides are uncharged. Addition of chitohexaose on the *cis* side caused long, infrequent sugar blocking events with the average dwell time of about  $5.7 \pm 0.2$  ms. Moreover the dwell time of chitohexaose blockages was invariant at different pH. Increasing concentrations caused multiple blockages, and at 10  $\mu$ M the sugar occasionally blocked of all three monomeric *VhChiP* subunits. In contrast, if chitosan hexaose was added on the *cis* side with various concentrations (Figure 3.14B-D, left panel), blocking events were almost undetectable. Note that this could imply negligible sugar penetration or extremely fast events beyond the time resolution of our BLM instrument. The remarkable difference in the interaction of chitoporin with chitohexaose (GlcNAc)<sub>6</sub> and chitosan hexamer (GlcNH<sub>2</sub>)<sub>6</sub> suggested that the C<sub>2</sub>-NHCOCH<sub>3</sub> groups were crucial for the interaction with the affinity sites lining the *VhChiP* pore, and that such C<sub>2</sub>-NHCOCH<sub>3</sub> groups defined high specificity of *VhChiP* for chitooligosaccharides. This interpretation is also supported by our earlier findings from both BLM measurements and liposome swelling trials that maltohexaose, with its chemical structure related to chitohexaose but with the C<sub>2</sub>-OH substituent, were inactive in terms of the channel entry and the membrane current blockage (Suginta *et al.*, 2013).

To prove permeability of chitin/chitosan sugars through *VhChiP*, we carried out liposome swelling assay. In our previous work, we observed that the swelling rates were charge-dependent and worked only with neutral species (Suginta *et al.*, 2013). Therefore, the condition for liposome swelling assay was intentionally set at high pH (pH 8.5) to secure the neutral state of both chitohexaose and chitosan hexaose. The results obtained suggested that chitohexaose and other neutral chitooligosaccharides (chitobiose, and chitotriose, and chitotetraose) could permeate through *VhChiP*-reconstituted liposomes at significant rates even at a low concentration of 1 mM, while uncharged chitosan hexaose was unable to enter the proteoliposomes. Nevertheless, lowering the pH, which favors protonation of the amino group, facilitates the sugar translocation under the presence of strong transmembrane potential as seen in our BLM measurements.

In a further series of experiments we elucidated the asymmetry with respect to sugar addition. The BLM data clearly indicated that the number of blocking events by chitosan hexaose was dependent on the side of sugar addition and the polarity of the applied transmembrane potential. Addition of chitosan hexaose on *cis* and *trans* sides, while placing the cationic sugar and the negative electrode on opposite sides of the porin, caused noticeable channel entry and blockage. In contrast, with the exception of very rare, random events, the protonated chitosan hexaose did not enter chitoporin pores when the cationic sugar and the negative electrode were in the same compartment, and at the same side of the porin. This set of experiments at high pH may not mimic the native conditions, but the data clearly demonstrated that the *VhChiP* channel is highly asymmetric, due to charge distribution of the interior polar side chains of amino acids contributing to bias (cationic) ion conductivity of this

channel. Although we observed the asymmetric feature when the channel was exposed to its natural substrate (Suginta *et al.*, 2013), the results were much more pronounced when the charged/uncharged sugar was used. For structural point of view, topology modeling suggested that each subunit of trimeric *VhChiP* has eight long amino-acid loops on the extracellular side and eight short loops on the periplasmic side of the protein barrel (Suginta *et al.*, 2013). This basic structural design is analogous to that reported for maltoporin. For maltoporin channel, the preferred mode of bilayer insertion results in the long loops being on the *cis* side, with the short loops predominantly in the *trans* compartment (Danelon *et al.*, 2003). Chitoporin apparently inserts similarly; easier access of the chitosan sugar cations to the channel from the long loop flank, with larger structural flexibility, is probably the reason for the higher frequency of voltage-driven chitooligosaccharide channel entry from the *cis* side, just as was detected for the interactions of maltooligosaccharids with maltoporin.

#### **4.4 Site directed mutagenesis for chitohexaose translocation through *VhChiP* pore**

*VhChiP* is known for exceptionally high affinity to chitooligosaccharides (Suginta *et al.*, 2013). Similarly to maltoporin, the affinity increased with the longer chain chitooligosaccharides. Strong binding affinity is expected to correlate with enhanced rate of sugar transport. Homology modeling revealed previously Trp136 to be at the top of the constriction zone. To quantify the role of this aromatic residue, we performed four different point mutations of Trp136 to alanine, phenylalanine, arginine, and aspartate, and the rate constants of the newly-generated W136 variants

(so called W136A, W136F, W136R, and W136D, respectively) in the transport of chitohexaose were compared with that of the native *VhChiP*. When W136A and W136F mutants were reconstituted into solvent free membrane, the single channel conductance of the W136A mutant was slightly increased, due to the less bulky side chain that replaced the tryptophan ring. In contrast, the single channel conductance of W136F mutant was not much changed as compared to the native conductance, suggesting that the Phe side chain had similar steric effect with the Trp side chain on the constriction site for ion transport through the *VhChiP* channel. Moreover, the effect of the charge residues on ion transport was studied by replacing the aromatic side chain of Trp136 with aspartic acid (W136D) or arginine (W136R). A slightly increased single channel conductance was observed for W136D. As expected from the cationic selective preference of this channel, the single channel conductance decreased with the replacement of the positively charged residue (R), most likely due to charge repulsion. On the other hand, introduction mutation of Trp136 with other amino acid residues led to a slight change in the single channel conductance, depending on the side chain of the amino acid that was used to replace. The results suggested that the aromatic side chain of Trp136 located at the central part of the channel lumen took part in controlling the ions transport through *VhChiP*. This finding was in analogy to maltoporin. Orlik and co-workers (Orlik *et al.*, 2002), also reported changes in the channel conductance when Try118, locating at the constriction zone of maltoporin, was mutated to various amino acids. The highest conductance change was observed for Ala (850 pS) and Asp (1050 pS), as compared to the conductance of the native channel (155 pS). Moreover, mutations of the polar track residues were also reported to cause a strong decrease in the rate of sugar

transport, as compared to maltoporin wild-type (Danelon *et al.*, 2003). Effects of mutations of the amino acid residues locating on the pore-controlling loop L3 on ion conductivity were also reported for the sucrose-specific channel ScrY. Single mutants (D201Y, N192R, F204D) showed decreases of channel conductance, as well as narrowed the sucrose passage of the ScrY channel (Ulmke *et al.*, 1999; Kim *et al.*, 2002).

Increased or decreased conductance with the replacement of the positively or negatively charged residues also led to changes in the ionic selectivity of *VhChiP* pore. Native *VhChiP* pore was cationic selective with the  $P_{K^+}/P_{Cl^-}$  ratio of about 3.2 (see in Table 3.5). Such results indicated that the net charge inside the *VhChiP* channel was slightly negative, so as the channel attracted more cations than anions. For maltoporin, the channel showed stronger cationic selective than the *VhChiP* channel, with the  $P_{K^+}/P_{Cl^-}$  ratio of about 5.5 (Orlik *et al.*, 2002), similar with OmpF that showed cationic selective with the  $P_{K^+}/P_{Cl^-}$  ratio of about 5.0 (López *et al.*, 2010). In contrast, mutation of Trp136 to neutral amino acid residues (Ala or Phe) slightly decreased or even promoted the channel selectivity towards anions ( $Cl^-$ ). Moreover, the ionic selectivity of the W136D mutant attracted even more cations ( $K^+$ ), due to an increase in the negative charge distribution inside the pore, which seemed to repel the  $Cl^-$  anions. This result was in line with the ion selectivity of the W136R mutant that showed less attraction towards cations with the  $P_{K^+}/P_{Cl^-}$  ratio of 2.74. Similar observation was seen with maltoporin (Orlik *et al.*, 2002).

Translocation of chitohexaose through the *VhChiP* channel was performed using single channel recordings. The *VhChiP* channels (both WT and W136A/F/R/D

mutants) were titrated with low concentrations of chitohexaose until the fully-open state of a channel single subunit was saturated. With native *VhChiP*, a number of blocking events increased linearly with increasing concentrations of chitohexaose, and then became saturated when chitohexaose of 5  $\mu\text{M}$  or above was added on the *cis* side under -100 mV, indicating strong affinity of the *VhChiP* channel towards this substrate. In contrast, the same concentration of chitohexaose did not saturate the channel when sugar addition was done on the *trans* side. This again provided the evidence of the asymmetric property of the *VhChiP* channel (Suginta *et al.*, 2013). With all W136 mutants, a number of blocking events did not reach saturation at high concentration of chitohexaose up to 10  $\mu\text{M}$ . The mutant channels seemed to close when high concentrations of chitohexaose were added. Furthermore, we analyzed the data with respect to residence (dwell) times ( $\tau_c$ ), the sugar molecules were found to stay at shorter time in the pore as indicated by decrease in the average residential time as compared to the residential time of the WT channel for the same sugar. Strong effects were observed with the alanine, aspartate, and arginine substitutions (mutants W136A, W136D, and W136R, respectively), whereas the phenylalanine substitution caused only a slight change in the residential time. The results suggested that the steric property of the aromatic side chain of the mutated residue played an important role in the channel-sugar interaction.

When the kinetics of chitohexaose translocation were analyzed, all the mutants showed significant decreases in the values of the equilibrium binding constant ( $K$ ,  $1/\text{M}$  or  $\text{M}^{-1}$ ) (Table 3.3). Such changes in the binding constant were essentially caused by the mutation of Trp136 that affected both on-rate and off-rate. Increases in the on-rate indicated more molecules of chitohexaose enabled to enter the *VhChiP* pore in a

concentration-dependent manner. Increases in the off-rate indicated that the sugar molecules also left the channel quickly, signifying weakened interactions due to the loss of the binding affinity due to mutations of the important interacting amino acid residue. When compared to maltoporin and sucrose-specific ScrY, the on-rate was opposite. The replacement of Tyr118 of maltoporin to alanine (mutant Y118A), resulted in decreased on-rate, but increased off-rate. (Orlik *et al.*, 2002; Jordy *et al.*, 1996; Kim *et al.*, 2002; Denker *et al.*, 2005). When Tyr118 of maltoporin was mutated to Phe and Trp (mutants Y118F and Y118W), the mutations were shown to decrease the off-rate constant. Such results suggested that the aromatic property of the 118 residue was essential for maltooligosaccharides-maltoporin interactions, just similar to Trp136 in *VhChiP*. In agreement of liposome swelling assay, rates of chitohexaose permeation through bulk reconstitution of *VhChiP* mutants into multi-lamellar liposomes decreased dramatically as compared to the rate of the non-mutated channel (Figure 3.6).

In addition, we performed the titration experiment using fluorescence spectroscopy to determine the strength of binding between *VhChiP* and chitosugars. Changes in the fluorescence intensity upon titrating a fix amount of porin with different concentrations of chitohexaose gave rise to the quantitative values of the dissociation binding constant ( $K_D$ ,  $\mu\text{M}$ ), and the Gibbs free energy of binding ( $\Delta G$ ). For the titration experiment with *VhChiP* (WT), the binding affinity decreased, when the number of GlcNAc in the chain length was reduced from six to five, four, and three, respectively, while the binding affinity was not detectable for GlcNAc<sub>2</sub> and GlcNAc. These results were in complete agreement with our BLM data that yielded reduced binding constant ( $K$ ) when shorter chain chitin-oligosaccharides (GlcNAc<sub>3,4,5</sub>)

were tested as compared to GlcNAc<sub>6</sub>, and no detectable translocation of chitobiose was observed (Suginta *et al.*, 2013). The data reflected obvious characteristic substrate-specific channel. For *VhChiP*, the channel was most effective for translocation for a long chain sugar with six sugar rings. Our data that showed no permeability of chitosan hexamer, with the -NH<sub>2</sub> existing in a neutral form, clearly indicating the acetamido substituent (-NHC=OCH<sub>2</sub>) on the C<sub>2</sub> position of each sugar ring dictates the sugar specificity of this chitooligosaccharide-specific porin.

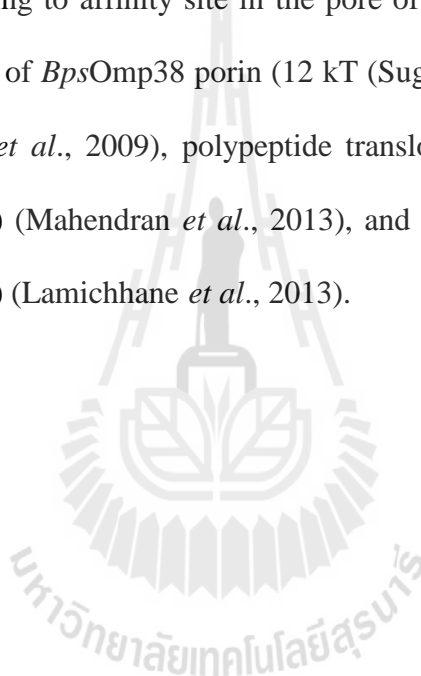
#### **4.5 Temperature dependence rates on the sugars translocation through *VhChiP* channel**

BLM measurements with *VhChiP* were performed at various temperatures. As expected, the channel conductance exhibited temperature dependence characteristic. The conductance increased, with increasing temperature. Increasing on-rates, but decreasing off-rates were seen, when the temperature of measurement increased from 5 to 30 °C. It is known that temperature directly influence the kinetic energy for molecular movement, according to the Arrhenius's law ( $k = Ae^{-E_a/RT}$ ).

When the temperature measurements were performed with *VhChiP* mutants, the residence time for chitohexaose translocation was reduced about 60 folds (for *cis* addition) and 5 folds (for *trans* addition) compared to the residence time for the non-mutated porin. It means that the sugar molecules moved and stayed a shorter time on the mutated pore, due to reduced affinity up on Trp136 mutation. For native porin, the energy barrier estimated for *cis* and *trans* side addition of chitohexaose were not distinguishable, give the value of about 19 kT for both -100 mV (*cis*) and +100 mV (*trans*). In contrast, all mutants (W136A/F/R/D mutants) different activation energy

required for chitohexaose translocation (Table 3.11), indicating that the mutation impaired the transport process, by interfering the energetic process of translocation.

Translocation of antibiotic molecule through *BpsOmp38* protein had been reported as well as symmetry for energy barrier required for binding and releasing of chemical molecules (Suginta *et al.*, 2011), while, OmpF porin showed asymmetric with activation energy barrier (Mahendran *et al.*, 2009). The energy barrier required for chitohexaose binding to affinity site in the pore of *VhChiP* was seen higher than antibiotic accessibility of *BpsOmp38* porin (12 kT (Suginta *et al.*, 2011), OmpF porin (13 kT) (Mahendran *et al.*, 2009), polypeptide translocation through mitochondrial TOM channel (15 kT) (Mahendran *et al.*, 2013), and peptides translocation through OmpF channel (18 kT) (Lamichhane *et al.*, 2013).



## CHAPTER V

### CONCLUSION

In this research, the gene encoding an outer membrane protein, namely chitoporin or *VhChiP*, was isolated from the genome of the marine bacterium *Vibrio harveyi*. The recombinant *VhChiP* was successfully cloned into pET23d(+) vector, which was suitable to be expressed in the Omp-deficient *E. coli* BL21 (Omp8) rosetta host strain. The *VhChiP* expressed in the cell wall of the *E. coli* host cells, was extracted by SDS, and then further purified to homogeneity using ion exchange chromatography. Similar to other bacterial porins, the recombinant *VhChiP* was functionally expressed in trimeric form, with an approximate MW of 110 kDa. The protein was tested to be a SDS-resistant, heat-sensitive trimer. Basic channel-forming properties were further investigated using black lipid membrane (BLM) reconstitution technique. The *VhChiP* reconstituted into solvent-free phospholipid membrane could form stable trimeric channel, with average single conductance of  $1.9 \pm 0.07$  nS ( $n = >50$ ) in 1 M KCl, prepared in 20 mM HEPES, pH 7.5. In contrast, in solvent containing membrane, *VhChiP* frequently formed flickering channels, with three sub-conductances of  $1.7 \pm 0.3$  nS,  $1.08 \pm 0.08$  nS, and  $0.59 \pm 0.17$  nS, corresponding to trimer, dimer, and monomer, respectively.

*VhChiP* was confirmed by BLM technique to act as a sugar-specific porin, responsible for the transport of chitooligosaccharides. The on-rate of chitosugars depend on applied voltages, as well as the side of the sugar addition, clearly indicating

the inherent asymmetry of the *VhChiP* lumen. *VhChiP* displayed exceptionally high affinity for chitohexaose ( $K = 500,000 \text{ M}^{-1}$ ), but low affinity for chitosan hexaose ( $K = 2,300 \pm 1,700$ ). On the other hand, protonation of the primary amine in the chitosan hexaose under low pH created positive charges which was highly responsive with the transmembrane voltage. Liposome swelling assay confirmed that chitooligosaccharides through *VhChiP* pores, except other oligosaccharides, including maltose, sucrose, maltopentaose, maltohexaose and raffinose, indicating that *VhChiP* is a highly-specific channel for chitooligosaccharides. The binding affinity of *VhChiP* for chitohexaose is larger than that of other known sugar-specific porins for their respective preferred substrates.

We further reported the effects of mutation of Trp136, locating at the constriction zone of the *VhChiP* lumen, on ion transport and chitohexaose translocation. Homology modelling suggested that Trp136 was in the position to act as the major binding site. Mutation of Ala and Asp resulted in increased ion conductivity. Noise analysis of the ion current in presence of chitohexaose as well as tryptophan fluorescence quenching revealed an asymmetry of the channel with respect to sugar translocation, as well as an asymmetry with respect to the channel response to the applied electrical field. Mutations in Trp136 and sugar addition on the putative extracellular (*cis*) side resulted in increasing on-rate, and off-rate. Increased in the on-rate indicated enhanced sugar accessibility, whereas increased off-rate indicated lower binding affinity. Lowered binding affinity for all mutants may be caused by partial local structural changes inside the *VhChiP* lumen. In addition, the titration measurements using fluorescence spectroscopy showed a slight decrease in the dissociation constant ( $K_D$ ). The highest effect was observed for the Ala mutation,

since the mutated protein could not bind to the short chain length chitooligosaccharides, including GlcNAc<sub>5</sub>, GlcNAc<sub>4</sub> and GlcNAc<sub>3</sub>. Liposome swelling assay also showed significantly reduced diffusion rate of chitohexaose, with all W136 mutant. Thus, we assume that Trp136 on the pore lumen played an important role in sugar translocation through the *VhChiP* channel.

The pore conductance on the lumen of *VhChiP* showed cation selectivity with the  $P_{K^+}/P_{Cl^-}$  ratio of about 3.2 (-23 mV). Mutation of Trp to Asp (mutant W136D) particularly changed the ion selectivity to attract more cation ( $K^+$ ) (the  $P_{K^+}/P_{Cl^-}$  ratio of about 4.2), while mutation of Trp136 to Arg (mutant W136R) reduced the cation selectivity (the  $P_{K^+}/P_{Cl^-}$  ratio of about 2.74).

Temperature measurement was used to determine the energy required for sugar translocation through the *VhChiP* channel. The energy barrier required for sugar translocation from *cis-* to *trans* was not the same as from *trans-* to *cis*, indicating the channel asymmetry. Mutations increased the asymmetry of the energy barrier and the channel behavior change to high asymmetry with replacing Trp136 to the charged residues of arginine and aspartic acid. This indicated that binding and releasing from the internal affinity site of the *VhChiP* channel required different activation energy from *cis-* to *trans*-side and *trans-* to *cis*-side addition of chitohexaose.



## **REFERENCES**

## REFERENCES

- Adl, S.M., Simpson, A.G., Farmer, M.A., Andersen, R.A., Anderson, O.R., Barta, J.R., Bowser, S.S., Brugerolle, G., Fensome, R.A., Fredericq, S., James, T.Y., Karpov, S., Kugrens, P., Krug, J., Lane, C.E., Lewis, L.A., Lodge, J., Lynn, D.H., Mann, D.G., McCourt, R.M., Mendoza, L., Moestrup, O., Mozley-Standridge, S.E., Nerad, T.A., Shearer, C.A., Smirnov, A.V., Spiegel, F.W. and Taylor, M.F. (2005). The new higher level classification of eukaryotes with emphasis on the taxonomy of protists. **J. Eukaryot. Microbiol.** 52: 399-451.
- Andersen, C., Cseh, R., Schülein, K., and Benz, R. (1998). Study of sugar binding to the sucrose-specific ScrY channel of enteric bacteria using current noise analysis. **J. Membr. Biol.** 164: 263-274.
- Andersen, C., Jordy, M., and Benz, R. (1995). Evaluation of the rate constants of sugar transport through maltoporin (LamB) of *E. coli* from the sugar-induced current noise. **J. Gen. Physiol.** 105: 385-401.
- Andersen, C., Schiffler, B., Charbit, A., and Benz, R. (2002). pH-induced collapse of the extracellular loops closes *Escherichia coli* maltoporin and allows the study of asymmetric sugar binding. **J. Biol. Chem.** 277: 41318-41325.
- Bassler, B.L., Gibbons, P.J., Yu, C., and Roseman, S. (1991). Chitin utilization by marine bacteria. Chemotaxis to chitin oligosaccharides by *Vibrio furnissii*. **J. Biol. Chem.** 266: 24268-24275.

- Benz, R., Fröhlich, O., Läuger, P., and Montal, M. (1975). Electrical capacity of black lipid films and of lipid bilayers made from monolayers. **Biochim. Biophys. Acta.** 394: 323-334.
- Benz, R., and Hancock, R.E. (1987). Mechanism of ion transport through the anion-selective channel of the *Pseudomonas aeruginosa* outer membrane. **J. Gen. Physiol.** 89: 275-295
- Benz, R., Schmid, A., and Vos-Scheperkeuter, G.H. (1987). Mechanism of sugar transport through the sugar-specific LamB channel of *Escherichia coli* outer membrane. **J. Membr. Biol.** 100: 21-29.
- Benz, R., Schmid, A., Nakae, T., and Vos-scheperkeuter, G.H. (1986). Pore formation by LamB of *Escherichia coli* in Lipid Bilayer Membranes. **J. Bacteriol.** 165: 978-986.
- Berkane, E., Orlik, F., Charbit, A., Danelon, C., Fournier, D., Benz, R., and Winterhalter, M. (2005). Nanopores: maltoporin channel as a sensor for maltodextrin and lambda-phage. **J. Nanobiotech.** 3: 3.
- Beveridge, T.J. (1981). Ultrastructure chemistry and function of the bacterial wall. **Int. Rev. Cytol.** 72: 229-317.
- Bezrukov, S.M., Kullman, L., and Winterhalter, M. (2000). Probing sugar translocation through Maltoporin at the single channel level. **FEBS Lett.** 476: 224-228.
- Bezrukov, S.M., and Vodyanoy, I. (1993). "Probing alamethicin channels with water-soluble polymers. Effect on conductance of channel states" **Biophys. J.** 64: 16-25.

- Brass, J.M., Bauer, K., Ehmann, U., and Boos, W. (1985). Maltose-binding protein does not modulate the activity of maltoporin as a general porin in *Escherichia coli*. **J. Bacteriol.** 161: 720-726.
- Bouma, C.L., and Roseman, S. (1996). Sugar transport by the marine chitinolytic bacterium *Vibrio furnissii*. Molecular cloning and analysis of the glucose and *N*-acetylglucosamine permeases. **J. Biol. Chem.** 271: 33457-33467.
- Caputo, G.A., and London, E. (2003). Cumulative effects of amino acid substitutions and hydrophobic mismatch upon the transmembrane stability and conformation of hydrophobic alpha-helices. **Biochem.** 42: 3275-3285.
- Chimerel, C., Movileanu, L., Pezeshki, S., Winterhalter, M., and Kleinekathöfer, U. (2008). Transport at the nanoscale: temperature dependence of ion conductance. **Eur. Biophys. J.** 38: 121-125.
- Clément, J.M., and Hofnung, M. (1981). Gene sequence of the lambda receptor, an outer membrane protein of *E. coli* K12. **Cell.** 27: 507-514.
- Connelly, P.R., Aldape, R.A., Bruzzese, F.J., Chambers, S.P., Fitzgibbon, M.J., Fleming, M.A., Itoh, S., Livingston, D.J., Navia, M.A., Thomson, J.A., and Wilson, K.P. (1994). Enthalpy of hydrogen bond formation in protein-ligand binding reaction. **Proc. Natl. Acad. Sci.** 91: 1964-1968.
- Cowan, S.W., Garavito, R.M., Jansonius, J.N., Jenkins, J.A., Karlsson, R., König, N., Pai, E.F., Paupit, R.A., Rizkallah, P.J., Rosenbusch, J.P., Rummel, G., and Schirmer, T. (1995). The structure of OmpF porin in a tetragonal crystal form. **Structure.** 3: 1041-1050.

- Cowan, S.W., Schirmer, T., Rummel, G., Steiert, M., Ghosh, R., Pauptit, R.A., Jansonius, J.N., and Rosenbusch, J.P. (1992). Crystal structures explain functional properties of two *E. coli* porins. **Nature**. 358: 727-733.
- Danelon, C., Brando, T., and Winterhalter, M. (2003). Probing the orientation of reconstituted maltoporin channels at the single-protein level. **J. Biol. Chem.** 278: 35542-35551.
- Davis, G.A. (1973). Quenching of aromatic hydrocarbons by alkylpyridinium halides. **J. Chem. Soc., Chem. Commun.** 728-729.
- Demchenko, A.P. (1988). Red-edge-excitation fluorescence spectroscopy of single-tryptophan proteins. **Eur. Phys. J.** 16: 121-129.
- Denker, K., Orlik, F., Schiffler, B., and Benz, R. (2005). Site-directed mutagenesis of the greasy slide aromatic residues within the LamB (maltoporin) channel of *Escherichia coli*: effect on ion and maltopentaose transport. **J. Mol. Biol.** 352: 534-550.
- Dumas, F., Koebnik, R., Winterhalter, M., and Van Gelder, P. (2000). Sugar transport through maltoporin of *Escherichia coli*. Role of polar tracks. **J. Biol. Chem.** 275: 19747-19751.
- Dutzler, R., Schirmer, T., Karplus, M., and Fischer, S. (2002). Translocation mechanism of long sugar chains across the maltoporin membrane channel. **Structure**. 10: 1273-1284.
- Dutzler, R., Wang, Y.F., Rizkallah, P.J., Rosenbusch, J.P., and Schirmer, T. (1996). Crystal structure of various malto-oligosaccharides bound to maltoporin reveal a specific sugar translocation pathway. **Structure**. 4: 127-134.

- Eftink, M.R., and Ghiron, C. (1981). Fluorescence quenching studies with proteins. **Anal. Biochem.** 114: 199-227.
- Eftink, M.R. (1991). Fluorescence quenching reactions: probing biological macromolecular structures. In biophysical and biochemical aspects of fluorescence spectroscopy. pp. 1-41. Ed TG Dewey. Plenum Press, New York, U.S.A.
- Eftink, M.R. (1991). Fluorescence quenching: theory and applications. In Topics in fluorescence spectroscopy. Ed JR Lakowicz. Plenum Press, New York, U.S.A. 2: 53-126.
- Forst, D., Welte, W., Wacker, T., and Diederichs, K. (1998). Structure of the sucrose-specific porin ScrY from *Salmonella typhimurium* and its complex with sucrose. **Nat. Struct. Biol.** 5: 37-46.
- Hancock, R.E. (1981). Aminoglycoside uptake and mode of action-with special reference to streptomycin and gentamicin. I. Antagonists and mutants. **J. Antimicrob. Chemother.** 8: 249-276.
- Herrera-Estrella, A., and Chet, I. (1999). Chitinases in biological control. **Science.** 87: 171-184.
- Hille, B. (2001). Ion Channels of Excitable Membranes, Sinauer Associates, Sunderland, Mass, USA.
- Hilty, C., and Winterhalter, M. (2001). Facilitated substrate transport through membrane proteins. **Phys. Rev. Lett.** 86: 5624-5627.
- Hjerde, E., Lorentzen, M.S., Holden, M.TG., Seeger, K., Paulsen, S., Bason, N., Churcher, C., Harris, D., Norbertczak, H., Quail, M.A., Sanders, S., Thurston, S., Parkhill, J., Willassen, N.P., and Thomson, N.R. (2008). The genome sequence of

- the fish pathogen *Aliivibrio salmonicida* strain LFI1238 shows extensive evidence of gene decay. **BMC Biochem.** 616: 2164-2179.
- Hunt, D.E., Gevers, D., Vahora, N.M., and Polz, M.F. (2008). Conservation of the chitin utilization pathway in the *Vibrionaceae*. **Appl. Environ. Microbiol.** 74: 44-51.
- Jolles, P., and Muzzarelli, R.A.A. (1999). Chitin and Chitinase. Basel; Boston; Berlin: Birkhauser, Germany. pp. 111-125. ISBN 3-7643-5815-7.
- Joint, I., Doney, S.C., Karl, D.M. (2011). Will ocean acidification affect marine microbes? **ISME J.** 5: 1-7.
- Jordy, M., Andersen, C., Schulein, K., Ferenci, T., and Benz, R. (1996). Rate Constants of Sugar Transport Through Two LamB Mutants of *Escherichia coli*: Comparison with Wild-type Maltoporin and LamB of *Salmonella typhimurium*. **J. Mol. Biol.** 259: 666-678.
- Jung, Y., Bayley, H., and Movileanu, L. (2006). Temperature-responsive protein pores. **J. Am. Chem. Soc.** 128: 15332-15340.
- Kautsky, H. (1939). Quenching of luminescence by oxygen. **Trans Faraday Soc.** 35: 216-219.
- Kang, X.F., Gu, L.Q., Cheley, S., and Bayley, H. (2005). Single protein pores containing molecular adapters at high temperatures. **Angew. Chem. Int. Ed.** 44: 1495-1499.
- Keyhani, N.O., Li, X.B., and Roseman, S. (2000). Chitin catabolism in the marine bacterium *Vibrio furnissii*. Identification and molecular cloning of a chitoporin. **J. Biol. Chem.** 275: 33068-33076.

- Keyhani, N.O., Li, X., and Roseman, S. (2000). Chitin catabolism in the marine bacterium *Vibrio furnissii*. **J. Biol. Chem.** 275: 33068-33076.
- Keyhani, N.O., and Roseman, S. (1996). The chitin catabolic cascade in the marine bacterium *Vibrio furnissii*. Molecular cloning, isolation, and characterization of a periplasmic beta-*N*-acetylglucosaminidase. **J. Biol. Chem.** 271: 33425-33432.
- Keyhani, N.O., and Roseman, S. (1999). Physiological aspects of chitin catabolism in marine bacterial. **Biochim. Biophys. Acta.** 1473: 108-122.
- Kim, B.H., Andersen, C., Kreth, J., Ulmke, C., Schmid, K., and Benz, R. (2002). Site-directed mutagenesis within the central constriction site of ScrY (sucroseporin): effect on ion transport and comparison of maltooligosaccharide binding to LamB of *Escherichia coli*. **J. Membr. Biol.** 187: 239-53.
- Klebba, P.E. (2002). Mechanism of maltodextrin transport through LamB. **Res. Microbiol.** 153: 417-424.
- Klebba, P., Hofnung, M., and Charbit, A. (1994). A model of maltodextrin transport through the sugar-specific porin, LamB, based on deletion analysis. **EMBO J.** 13: 4670-4675.
- Kreir, M., Farre, C., Beckler, M., George, M., and Fertig, N. (2008). Rapid screening of membrane protein activity: electrophysiological analysis of OmpF reconstituted in proteoliposomes. **Lab Chip.** 8: 587-595.
- Koebnik, R., Locher, K.P., and Van Gelder, P. (2000). Structure and function of bacterial outer membrane proteins: barrels in a nutshell. **Mol. Microbiol.** 37: 239-253.

- Krause, E., Wichels, A., Giménez, L., Lunau, M., Schilhabel, M.B., and Gerdts, G. (2012). Small changes in pH have direct effects on marine bacterial community composition: a microcosm approach. **PLoS One**. 7: e47035.
- Kullman, L., Winterhalter, M., and Bezrukov, S.M. (2002). Transport of maltodextrins through maltoporin: a single-channel study. **Biophys. J.** 82: 803-812.
- Lakowicz, J.R. Principle of Fluorescence Spectroscopy. pp. 64, 65, and 280, Third Edition, University of Maryland School of Medicine Baltimore, Maryland, USA.
- Lamichhane, U., Islam, T., Prasad, S., Weingart, H., Mahendran, K.R., and Winterhalter, M. (2013). Peptide translocation through mesoscopic channel: Binding kinetics at single molecule level. **Eur. Biophys. J.** 42: 363-369.
- Li, X., and Roseman, S. (2004). The chitinolytic cascade in *Vibrios* is regulated by chitin oligosaccharides and a two-component chitin catabolic sensor/kinase. **Proc. Natl. Acad. Sci.** 101: 627-631.
- Longworth, J.W. (1971). Luminescence of polypeptides and proteins. In Excited states of proteins and nucleic acids. Springer Science + Business Media, LLC, 223 Spring street, New York, NY 10013 (U.S.A.). pp. 319-484. e-ISBN-13: 978-0-387-46312-4.
- Luckey, M., and Nikaido, H. (1980). Diffusion of solutes through channels produced by phage lambda receptor protein of *Escherichia coli*: inhibition by higher oligosaccharides of maltose series. **Biochem. Biophys. Res.** 93: 166-171.
- Lovelle, M., Mach, T., Mahendran, K.R., Weingart, H., Winterhalter, M., and Gameiro, P. (2011). Interaction of cephalosporins with outer membrane channels

- of *Escherichia coli*. Revealing binding by fluorescence quenching and ion conductance fluctuations. **Phys. Chem. Chem. Phys.** 13: 1521-1530.
- López, M.L., García-Giménez, E., Aguilera, V.M., and Alcaraz, A. (2010). Critical assessment of OmpF channel selectivity: merging information from different experimental protocols. **J. Phys. Condens. Matter.** 22: 454106 (7pp).
- Mahendran, K.R., Chimere, C., Mach, T., and Winterhalter, M. (2009). Antibiotic translocation through membrane channels: temperature-dependent ion current fluctuation for catching the fast events. **Eur. Biophys. J.** 38: 1141-1145.
- Mahendran, K.R., Kreir, M., Weingart, H., Fertig, N., and Winterhalter, M. (2010). Permeation of antibiotic through *Escherichia coli* OmpF and OmpC Porins: Screening for Influx on a single-molecule level. **J. Biol. Sys.** 15: 302-307.
- Mahendran, K.R., Lamichhane, U., Romero-Ruiz, M., Nussberger, S., and Winterhalter, M. (2013). Polypeptide translocation through mitochondrial TOM channel: Temperature dependent rates at single molecule level. **J. Phys. Chem. Lett.** 4: 78-82.
- Meibom, K., Li, X., Nielsen, A., Wu, C.Y., Roseman, S., and Schoolnik, G.K. (2004). The *Vibrio cholerae* chitin utilization program. **Proc. Natl. Acad. Sci.** 101: 2524-2529.
- Merzendorfer, H., and Zimoch, L. (2003). Chitin metabolism in insects: structure, function and regulation of chitin synthases and chitinase. **J. Exp. Biol.** 206: 4393-4412.
- Meyer, J.E.W., Hofnung, M., and Schulz, G.E. (1997). Structure of maltoporin from *Salmonella typhimurium* ligated with a nitrophenyl-maltotrioxide. **J. Mol. Biol.** 266: 761-775.

- Modi, N., Singh, P., Mahendran, K.R., Schulz, R., Winterhalter, M., and Kleinekathöfer, U. (2011). Probing the transport of ionic liquids in aqueous solution through nanopores. **J. Phys. Chem. Lett.** 2: 2331-2336.
- Montal, M., and Mueller, P. (1972). Formation of bimolecular membranes from lipid monolayers and a study of their electrical properties. **Proc. Natl. Acad. Sci.** 69: 3561-3566.
- Mueller, P., Rudin, D.O., Tien, H.T., and Wescott, W.C. (1964). Formation and properties of bimolecular lipid membrane. **Recent. Prog. Surf. Sci.** 1: 379-393.
- Mueller, P., Rudin, D.O., Tien, H.T., and Wescott, W.C. (1962). Reconstitution of excitable cell membrane structure in vitro. **Circulation.** 26: 1167-1171.
- Nekolla, S., Andersen, C., and Benz, R. (1994). Noise analysis of ion current through the open and the sugar-induced closed state of the LamB channel of *Escherichia coli* outer membrane: evaluation of the sugar binding kinetics to the channel interior. **Biophys. J.** 66: 1388-1397.
- Neves, P., Berkane, E., Gameiro, P., Winterhalter, M., and Castro, B. (2005). Interaction between quinolone antibiotics and bacterial outer membrane porin OmpF. **Biophys. Chem.** 113: 123-128.
- Neves, P., Sousa, I., Winterhalter, M., and Gameiro, P. (2009). Fluorescence quenching as a tool to investigate quinolone antibiotic interactions with bacterial protein OmpF. **J. Membr. Biol.** 227: 133-140.
- Nikaido, H. (1992). Porins and specific channels of bacterial outer membranes. **Mol. Microbiol.** 6: 435-442.

- Nikaido, H., and Rosenberg Emiko, Y. (1983). Porin channels in *Escherichia coli*: studies with liposomes reconstituted from purified proteins. **J. Bacteriol.** 153: 241-252.
- Nikaido, H., and Vaara, M. (1985). Molecular basis of bacterial outer membrane permeability. **Microbiol. Rev.** 49: 1-32.
- Nitzan, Y., Orlovsky, K., and Pechatnikov, I. (1999). Characterization of porins isolated from the outer membrane of *Serratia liquefaciens*. **Microbiol.** 38: 71-79.
- Orlik, F., Andersen, C., Danelon, C., Winterhalter, M., Pajatsch, M., Böck, A., and Benz, R., (2003). CymA of *Klebsiella oxytoca* outer membrane: binding of cyclodextrins and study of the current noise of the open channel. **Biophys. J.** 85: 876-885.
- Orlik, F., Andersen, C., and Benz, R. (2002). Site-directed mutagenesis of tyrosine 118 within the central constriction site of the LamB (maltoporin) channel of *Escherichia coli*. I. Effect on ion transport. **Biophys. J.** 82: 2466-2475.
- Orlik, F., Andersen, C., and Benz, R. (2002). Site-directed mutagenesis of tyrosine 118 within the central constriction site of the LamB (maltoporin) channel of *Escherichia coli*. II. Effect on maltose and maltooligosaccharide binding kinetics. **Biophys. J.** 83: 309-321.
- Pajatsch, M., Andersen, C., Mathes, A., Böck, A., Benz, R., and Engelhardt, H. (1999). Properties of a cyclodextrin-specific, unusual porin from *Klebsiella oxytoca*. **J. Biol. Chem.** 274: 25159-25166.
- Park, J.K., Keyhani, N.O., and Roseman, S. (2000). Chitin catabolism in the marine bacterium *Vibrio furnissii*. **J. Boil. Chem.** 275: 33077-33083.

- Park, J.K., Wang, L.X., and Roseman, S. (2002). Isolation of a glucosamine-specific kinase, a unique enzyme of *Vibrio cholera*. **J. Biol. Chem.** 277: 15573-15578.
- Permyakov, E.A. (1993). Luminescent spectroscopy of proteins. CRC Press, London.
- Phale, S., Philippsen, A., Widmer, C., Phale, V., Rosenbusch, J., and Schirmer, T. (2001). Role of charged residues at the OmpF porin channel constriction probed by mutagenesis and simulation. **J. Biochem.** 40: 6319-6325.
- Ranquin, A., and Van Gelder, P. (2004). Maltoporin: sugar for physics and biology. **Microbiol.** 155: 611-616.
- Saravolac, E.G., Taylor, N.F., Benz, R., and Hancock, R.E. (1991). Purification of glucose-inducible outer membrane protein OprB of *Pseudomonas putida* and reconstitution of glucose-specific pores. **J. Bacteriol.** 173: 4970-4976.
- Saurin, W.E., Francoz, P., Martineau, A., Charbit, E., Dassa, P., Duplay, E., Gilson, A., Schirmer, T., Keller, T.A., and Rosenbusch, J.P. (1995). Structure basis for sugar translocation through maltoporin channels at 3.2 Å resolution. **Science.** 267: 512-514.
- Schirmer, T. (1998). General and specific porins from bacterial outer membranes. **J. Struct. Biol.** 121: 101-109.
- Schirmer, T., Keller, T.A., Wang, Y.F., and Rosenbusch, J.P. (1995). Structure basis for sugar translocation through maltoporin channel at 3.1 Å resolution. **Science.** 267: 473-474.
- Schülein, K., Schmid, K., and Benz, R. (1991). The sugar-specific outer membrane channel ScrY contains functional characteristics of general diffusion pores and substrate-specific porins. **Mol. Microbiol.** 5: 2233-2241.

- Schmid, K., Ebner, R., Jahreis, K., Lengeler, J.W., and Titgemeyer, J. (1991). A sugar- specific porin, ScrY, is involved in sucrose uptake in enteric bacteria. **Mol. Microbiol.** 5: 941-950.
- Shinitzky, M., and Rivnay, B. (1977). Degree of exposure of membrane proteins determined by fluorescence quenching. **J. Biochem.** 16: 982-986.
- Schwarz, G., Danelon, C., and Winterhalter, M. (2003). On translocation through a membrane channel via an internal binding site: kinetics and voltage dependence. **Biophys. J.** 84: 2990-2998.
- Siritapetawee, J., Prinz, H., Krittanai, C., and Suginta, W. (2004). Expression and refolding of Omp38 from *Burkholderia pseudomallei* and *Burkholderia thailandensis*, and its function as a diffusion porin. **J. Biochem.** 384: 609-617.
- Steiner, R.F., and Kirby, E.P. (1969). The interaction of the ground and excited states of indole derivatives with electron scavengers. **J. Phys. Chem.** 73: 4130-4135.
- Songsiriritthigul, C., Pantoom, S., Aguda, A.H., Robinson, R.C., Suginta, W. (2008). Crystal structures of *Vibrio harveyi* chitinase A complexed with chitooligosaccharides: implications for the catalytic mechanism. **J. Struct. Biol.** 162: 491-499.
- Suginta, W. (2007). Identification of chitin binding proteins and characterization of two chitinase isoforms from *Vibrio alginolyticus* 283. **Enzyme Microb. Technol.** 41: 212-220.
- Suginta, W, Chuenark, D, Mizuhara, M, and Fukamizo, T. (2010). Novel  $\beta$ -N-acetylglucosaminidase from *Vibrio harveyi* 650: cloning, expression, enzymatic properties, and subsite identification. **BMC Biochem.** 11: 40.

- Suginta, W., Chumjan, W., Mahendran, K.R., Janning, P., Schulte, A., and Winterhalter, M. (2013). Molecular uptake of chitooligosaccharides through chitoporin from the marine bacterium *Vibrio harveyi*. **PLoS ONE**. 8: e55126.
- Suginta, W., Chumjan, W., Mahendran, K.R., Schulte, A., and Winterhalter, M. (2013). Chitoporin from *Vibrio harveyi*: a channel with exceptional sugar specificity. **J. Biol. Chem.** 288: 11038-11046.
- Suginta, W., Robertson, P.A., Austin, B., Fry, S.C., and Fothergill-Gilmore, L.A. (2000). Chitinases from *Vibrio*: activity screening and purification of chiA from *Vibrio carchariae*. **J. Appl. Microbiol.** 89: 76-84.
- Suginta, W., Songsiriritthigul, C., Kobdaj, A., Opassiri, R., and Svasti, J. (2007). Mutations of Trp275 and Trp397 altered the binding selectivity of *Vibrio carchariae* chitinase A. **Biochim. Biophys. Acta.** 1770: 1151-1160.
- Suginta, W., Vongsuwan, A., Songsiriritthigul, C., Prinz, H., Estibeiro, P., Duncan, R.R., Svasti, J., and Fothergill-Gilmore, L.A. (2004). An endochitinase A from *Vibrio carchariae*: cloning, expression, mass and sequence analyses, and chitin hydrolysis. **Arch. Biochem. Biophys.** 424: 171-180.
- Suginta, W., Vongsuwan, A., Songsiriritthigul, C., Svasti, J., and Prinz, H. (2005). Enzymatic properties of wild-type and active site mutants of chitinase A from *Vibrio carchariae*, as revealed by HPLC-MS. **FEBS J.** 272: 3376-3386.
- Sytnik, A., and Litvinyuk, I. (1996). Energy transfer to a proton-transfer fluorescence probe: Tryptophan to flavonol in human serum albumin. **Proc. Natl. Acad. Sci.** 93: 12959-12963.
- Szmelcman, S., and Hofnung, M. (1975). Maltose transport in *Escherichia coli* K-12: involvement of the bacteriophage lambda receptor. **J. Bacteriol.** 124: 112-118.

- Szmelcman, S., Schwartz, M., Silhavy, T.J., and Boos, W. (1976). Maltose transport in *Escherichia coli* K12: A comparison of transport kinetics in wild-type and  $\lambda$ -resistant mutants with the dissociation constants of the maltose-binding protein as measured by fluorescence quenching. **Eur. J. Biochem.** 65: 13-19.
- Todt, J.C., Rocque, W.J., and McGroarty, E.J. (1992). Effects of pH on bacterial porin function. **J. Biochem.** 31: 10471-10478.
- Tommassen, T., and Lugtenberg, B. (1980). Outer membrane protein of *Escherichia coli* K-12 is co-regulated with alkaline phosphatase. **J. Bacteriol.** 143: 151-157.
- Trias, J., Rosenberg, E.Y., and Nikaido, H. (1988). Specificity of the glucose channel formed by protein D1 of *Pseudomonas aeruginosa*. **Biochim. Biophys. Acta.** 938: 493-496.
- Ulmke, C., Kreth, J., Lengeler, J.W., Welte, W., and Schmid, K. (1999). Site-directed mutagenesis of loop L3 of sucrose porin ScrY leads to changes in substrate selectivity. **J. Bacteriol.** 181: 1920-1923.
- Van Gelder, P., Dumas, F., Bartoldus, I., Saint, N., Prilipov, A., Winterhalter, M., Wang, Y., Philippsen, A., Rosenbusch, J.P., and Schirmer, T. (2002). Sugar transport through maltoporin of *Escherichia coli*: role of the greasy slide. **J. Bacteriol.** 184: 2994-2999.
- Van Gelder, P., Dutzler, R., Dumas, F., Koebnik, R., and Schirmer, T. (2001). Sucrose transport through maltoporin mutants of *Escherichia coli*. **Protein Eng.** 14: 943-948.
- Van Gelder, P., Dumas, F., and Winterhalter, M. (2000). Understanding the function of bacterial outer membrane channels by reconstitution into black lipid membranes. **Biophys. Chem.** 85: 153-167.

- Vivian, J.T., and Callis, P.R. (2001). "Mechanisms of tryptophan fluorescence shifts in proteins". **Biophys. J.** 80: 2093-2109.
- Winkelmann, G. (2001). Microbial transport systems. Betz-Druck GmbH, D-67269 Grunstadt, Germany. pp. 231. ISBN 3-527-30304-9.
- Winterhalter, M. (2000). Black lipid membranes. **Curr. Opin. Colloid Interface Sci.** 5: 250-255.
- Winterhalter, M. (1999). Sugar transport through channels reconstituted in planar lipid membranes. **Phys. Eng.** 149: 547-551.
- Wylie, J.L., Bernegger-Egli, C., O'Neil, J.D., and Worobec, E.A. (1993). Biophysical characterization of OprB, a glucose-inducible porin of *Pseudomonas aeruginosa*. **J. Bioenerg. Biomembr.** 25: 547-556.
- Wylie, J.L., and Worobec, E.A. (1994). Cloning and nucleotide sequence of the *Pseudomonas aeruginosa* glucose-selective OprB porin gene and distribution of OprB within the family *Pseudomonadaceae*. **Eur. J. Biochem.** 220: 505-512.
- Xu, G.Z., Shi, B., McGroarty, E.J., and Tien, H.T. (1986). Channel-closing activity of porins from *Escherichia coli* in bilayer lipid membranes. **Biochim. Biophys. Acta.** 862: 57-64.
- Yoshimura, F., and Nikaido, H. (1985). Diffusion of beta-lactam antibiotics through the porin channels of *Escherichia coli* K-12. **Antimicrob. Agents Chemother.** 27: 84-92.
- Yoshimura, F., Zalman, L.S., and Nikaido, H. (1983). Purification and properties of *Pseudomonas aeruginosa* porin. **J. Bacteriol.** 258: 2308-2314.

Yu, C., Lee, A.M., Bassler, B.L., and Roseman, S. (1991). Chitin utilization by marine bacteria. A physiological function for bacterial adhesion to immobilized carbohydrates. **J. Biol. Chem.** 266: 24260-24267.

Zeth, K., Diederichs, K., Welte, W., and Engelhardt, H. (2000). Crystal structure of Omp32, the anion-selective porin from *Comamonas acidovorans*, in complex with a periplasmic peptide at 2.1Å resolution. **Structure.** 8: 981-992.





**APPENDICES**

# APPENDIC A

## COMPETENT CELL PREPARATIONS AND PLASMID TRANSFORMATIONS

### 1. Preparation of calcium chloride competent cells

The *E. coli* DH5 $\alpha$  and omp8 Rosetta strain are bacterial strain used for the competent cell preparations. The single colony was picked up from LB agar plate and grown in 5 ml of LB broth and incubated at 37 °C for overnight (18 hr) at 200 rpm. Then 1 ml the overnight cell cultured was subjected into 100 ml of LB broth (ratio 1:100) and grown at 37 °C until OD<sub>600</sub> reached about 0.4-0.5. The cell cultured was transferred into a pre-chilled polypropylene tube, chilled on ice for 10 min, and the cell pellets were collected by centrifugation at 4,500 rpm at 4 °C for 10 min. The cell pellets were gently resuspended in 10 ml of pre-chilled CaCl<sub>2</sub> solution (100 mM CaCl<sub>2</sub> and 15% glycerol) on ice, then centrifuged at 4,500 rpm at 4 °C for 10 min. then, the cell pellets were gently resuspended again in 10 ml of pre-chilled CaCl<sub>2</sub> solution. The cell pellets were collected as describe above, then resuspended in 4 ml of pre-chilled CaCl<sub>2</sub> and kept on ice for 10 min. aliquot 100  $\mu$ l of suspension competent cells into 1.5 ml eppendroft tube. The competent cells were frozen using snap-freeze technique under liquid nitrogen and store at -80 °C.

## 2. Plasmid transformation (Heat shock method)

The frozen competent cells were gently thawed on ice and then added 50-100 ng recombinant plasmid DNAs of *VhChiP* into 100  $\mu$ l of the competent cells and kept on ice. The mixture were immediately placed at 42 °C for 45 second and then rapidly placed on ice again for 10 min. adding 900  $\mu$ l of pre-warmed LB broth at 37 °C into the transformed cells and incubated at 37 °C for 60 min. centrifugation at 4,500 rpm for 5 min, the 900  $\mu$ l of supernatant were removed. The 100  $\mu$ l of cells were spread on an LB agar plate containing the appropriate antibiotic and then incubated at 37 °C overnight.



## APPENDIC B

### PREPARATION OF SOLUTIONS AND REAGENTS

#### 1. Reagents for bacterial culture and competent cell transformation

##### 1.1 Luria-Bertani (LB) broth containing 100 µg/ml of ampicillin

Dissolve 10 g Bacto tryptone, 5 g Bacto yeast extract and 10 g NaCl in 950 ml distilled water. Stir until the solutes have been dissolved. Adjust the volume of the solution to 1,000 ml with distilled water. The solution is then sterilized by autoclaving at 121 °C for 15 min. the medium is allowed to cool down to 50 °C before ampicillin is added to the final concentration of 100 µg/ml. The medium is freshly used or store at 4 °C until used.

##### 1.2 LB broth containing 100 µg/ml of ampicillin and 25 µg/ml of kanamycin

Dissolve 10 g Bacto tryptone, 5 g Bacto yeast extract and 10 g NaCl in 950 ml distilled water. Stir until the solutes have been dissolved. Adjust the volume of the solution to 1,000 ml with distilled water. The solution is then sterilized by autoclaving at 121 °C for 15 min. The medium is allowed to cool down to 50 °C before ampicillin and kanamycin were added to the final concentration of 100 µg/ml and 25 µg/ml. The medium is freshly used or store at 4 °C until used.

### 1.3 LB agar medium containing 100 µg/ml of ampicillin

Dissolve 10 g Bacto tryptone, 5 g Bacto yeast extract and 10 g NaCl and 15 g Bacto agar in 950 ml distilled water. Stir until the solutes have been dissolved. Adjust the volume of the solution to 1,000 ml with distilled water. The solution is then sterilized by autoclaving at 121 °C for 15 min. the medium is allowed to cool down to 50 °C before adding ampicillin to the final concentration of 100 µg/ml. Pour medium into petri-dishes and allowed the agar to harden and store at 4 °C.

### 1.4 LB agar medium containing 100 µg/ml of ampicillin and 25 µg/ml of kanymycin

Dissolve 10 g Bacto tryptone, 5 g Bacto yeast extract and 10 g NaCl and 15 g Bacto agar in 950 ml distilled water. Stir until the solutes have been dissolved. Adjust the volume of the solution to 1,000 ml with distilled water. The solution is then sterilized by autoclaving at 121 °C for 15 min. the medium is allowed to cool down to 50 °C before adding ampicillin to the final concentration of 100 µg/ml and 25 µg/ml, respectively. Pour medium into petri-dishes and allowed the agar to harden and store at 4 °C.

### 1.5 Antibiotic stock solutions

#### 1.5.1 Ampicillin stock solution (100 mg/ml)

Dissolve 1 g of ampicillin in 10 ml of sterile distilled water. Filter sterile solution with 0.2 µm filtration, then ampicillin solution is aliquoted and stored at -20 °C until used.

### 1.5.2 Kanamycin stock solution (50 mg/ml)

Dissolve 50 g of kanamycin in 10 ml of sterile distilled water.

Filter sterile solution with 0.2  $\mu\text{m}$  filtration, then kanamycin solution is aliquoted and stored at  $-20\text{ }^{\circ}\text{C}$  until used.

### 1.6 Isopropyl thio- $\beta$ -D-galactoside (IPTG) stock solution (1 M)

Dissolve 2.38 g of IPTG in distilled water and make up to a final volume of 10 ml. The stock solution is filtered to sterilization and aliquoted to small volume and stored at  $-20\text{ }^{\circ}\text{C}$ .

## 2. Reagents for competent *E. coli* cell preparation

### 2.1 $\text{CaCl}_2$ solution (100 mM $\text{CaCl}_2$ contains 15% (v/v) glycerol)

Preparation of 100 ml  $\text{CaCl}_2$  working solution, mixed the stock solution as follows:

- 10 ml of 1 M  $\text{CaCl}_2$  (14.7 g/100 ml, filtered to sterilization)
- 15 ml of 100% (v/v) sterilized glycerol (autoclaved at  $121\text{ }^{\circ}\text{C}$ , for 15 min)

Adding sterile distilled water to bring a volume to 100 ml. Store the solution at  $4\text{ }^{\circ}\text{C}$ .

## 3. Reagent for agarose gel electrophoresis

### 3.1 50x TAE buffer

Mix 242 g Tris-base, 57.1 ml glacial acetic acid, and 100 ml of 0.5 M EDTA (pH 8.0). Adjust the final volume to 1,000 ml with distilled water. Store the solution at room temperature.

### 3.2 6x DNA loading solution (10 ml)

Mix 0.025 g Bromophenol blue and/or 0.025 g xylene cyanol and 3 ml of 100% (v/v) of glycerol. Adjust to the final volume of 10 ml with distilled water and store at 4 °C.

## 4. Solutions for protein expression and purification

### 4.1 200 mM Lysis buffer (200 mM Tris-HCl, 25 mM MgCl<sub>2</sub>, 1 mM CaCl<sub>2</sub>)

Dissolve 4.84 g of Tris-base, 1 g of MgCl<sub>2</sub>, and 29.4 mg of CaCl<sub>2</sub> in 100 ml of distilled water. Adjust pH to 8.0 with 6 M HCl and make up the volume to 200 ml with distilled water and stored the solution at 4 °C.

### 4.2 0.2 M Na<sub>2</sub>HPO<sub>4</sub> (M<sub>r</sub> = 358.14 g/mol)

Dissolve 71.63 g of Na<sub>2</sub>HPO<sub>4</sub> in 500 ml of distilled water and make up the volume to 1,000 ml with distilled water.

### 4.3 0.2 M Na<sub>2</sub>H<sub>2</sub>PO<sub>4</sub> (M<sub>r</sub> = 136 g/mol)

Dissolve 27.2 g of NaH<sub>2</sub>PO<sub>4</sub> in 500 ml of distilled water and make up the volume to 1000 ml with distilled water.

### 4.4 0.1 M phosphate buffer (PB), pH 7.4

Preparation of 100 ml of 0.1 M PB, pH 7.4 working solution, mixed the stock solution as follows:

- 40.5 ml of 0.2 M Na<sub>2</sub>HPO<sub>4</sub>
- 9.5 ml of 0.2 M NaH<sub>2</sub>PO<sub>4</sub>

Adjust the volume to 100 ml with distilled water and stored the solution at room temperature.

### 4.5 DNase I (10 mg/ml)

Dissolve 0.001 g of DNase I in 20 mM PB (pH 7.4) to the final volume of 100  $\mu$ l and kept at -20 °C before used.

#### 4.6 RNase A (10 mg/ml)

Dissolve 0.01 g of RNase A in 20 mM PB (pH 7.4) to the final volume of 1,000  $\mu$ l and kept at -20 °C before used.

#### 4.7 20% SDS stock solution

Dissolve 20 g of SDS in distilled water to final volume of 100 ml and stored at room temperature.

#### 4.8 3% Octyl-POE

Dilute 3 ml of octyl-POE in 20 mM PB (pH 7.4) to the final volume of 100 ml and stored at 4 °C before used.

#### 4.9 0.125% Octyl-POE

Dilute 0.125 ml of octyl-POE in 20 mM PB (pH 7.4) to the final volume of 100 ml and stored at 4 °C before used.

#### 4.10 0.2% LDAO

Dilute 0.6 ml of LDAO in 20 mM PB (pH 7.4) to the final volume of 100 ml and stored at 4 °C before used.

#### 4.11 SDS-gel loading buffer (3x stock) contains 0.15 M Tris-HCl (pH 6.8), 6% SDS, 0.1% bromophenol blue and 30% glycerol

Dissolve 6 g of SDS, 0.1 g bromophenol blue, 30 ml of glycerol and add 0.15 M Tris-HCl (pH 6.8) to the final volume of 100 ml. Store the solution at -30 °C. Before used, add 20  $\mu$ l of 2-mercapthoethanal to the final volume of 40  $\mu$ l of the solution mixture.

## 4.12 1.5 M Tris-HCl (pH 8.8)

Dissolve 18.17 g of Tris-base in 80 ml distilled water. Adjust pH to 8.8 with 6 M HCl and bring the volume up to 100 ml with distilled water and stored at 4 °C.

## 4.13 1.0 M Tris-HCl (pH 6.8)

Dissolve 12.10 g of Tris-base in 80 ml distilled water. Adjust pH to 6.8 with 6 M HCl and bring the volume up to 100 ml with distilled water and stored at 4 °C.

## 4.14 30% (w/v) Acrylamide solution

Dissolve 29 g of Acrylamide and 1 g N, N'-methylene-bis-acrylamide in distilled water to a final volume of 100 ml. Mix the solution by stirring for 1 hr until the solution is homogeneous and filter through a whatman filter paper membrane No. 1. Store the solution in the dark bottle at 4 °C.

## 4.15 Tris-glycine electrode buffer (5x stock solution)

Dissolve 30.29 g of Tris-base, 144 g of glycine, 5 g of SDS in distilled water. Adjust pH to 8.3 with 6 M HCl and bring the final volume up to 1 liter with distilled water.

## 4.16 Staining solution with Coomassie Brilliant Blue for protein

Mix 1 g of Coomassie Brilliant Blue R-250, 400 ml methanol, 500 ml distilled water and 100 ml glacial acetic acid and filter through a whatman filter paper membrane No. 1 and Store the solution in the dark bottle at room temperature.

## 4.17 Destaining solution for Coomassie stain

Mix 400 ml methanol, 100 ml glacial acetic acid, and then add distilled water to the final volume of 1,000 ml.

## 4.18 10% (w/v) Ammonium persulfate

Dissolve 100 mg of ammonium persulfate in 1 ml of distilled water. Store the solution at -20 °C.

## 4.19 12% (w/v) Separating SDS-PAGE gel

Mix the solution as follows:

|                               |          |
|-------------------------------|----------|
| 1.5 M Tris-HCl (pH 8.8)       | 2.5 ml   |
| Distilled water               | 3.3 ml   |
| 10% (w/v) SDS                 | 0.1 ml   |
| 30% (w/v) Acrylamide solution | 4.0 ml   |
| 10% (w/v) Ammonium persulfate | 0.1 ml   |
| TEMED                         | 0.004 ml |

Adjust the volume with distilled water to 10 ml

## 4.20 5% (w/v) Stacking SDS-PAGE gel

Mix the solution as follows:

|                               |          |
|-------------------------------|----------|
| 0.5 M Tris-HCl (pH 6.8)       | 0.63 ml  |
| Distilled water               | 3.4 ml   |
| 10% (w/v) SDS                 | 0.05 ml  |
| 30% (w/v) Acrylamide solution | 0.83 ml  |
| 10% (w/v) Ammonium persulfate | 0.05 ml  |
| TEMED                         | 0.005 ml |

## 5. Buffer solutions for black lipid bilayer membrane

### 5.1 0.5 M Hepes ( $M_r = 238.31$ g/mol, pH 7.5)

Dissolve 59.6 g of Hepes in 250 ml of distilled water. Adjust pH to 7.5 with 1 M KOH and bring the volume up to 500 ml with distilled water and stored at room temperature.

### 5.2 1 M KCl (pH 7.5)

Dissolve 74.56 g of KCl in 850 ml of distilled water supplemented with 40 ml of 0.5 M Hepes (pH 7.5) to the final concentration of 20 mM. Adjust pH to 7.5 with 1 M KOH and bring the volume up to 1,000 ml with distilled water.

### 5.3 1 M KCl (pH 6.5)

Dissolve 74.56 g of KCl in 850 ml of distilled water supplemented with 40 ml of 0.5 M potassium acetate to the final concentration of 20 mM. Adjust pH to 6.5 with 1 M KOH and bring the volume up to 1,000 ml with distilled water.

### 5.4 0.1 M KCl (pH 7.5)

Dissolve 7.456 g of KCl in 850 ml of distilled water supplemented with 40 ml of 0.5 M Hepes (pH 7.5) to the final concentration of 20 mM. Adjust pH to 7.5 with 1 M KOH and bring the volume up to 1,000 ml with distilled water.

### 5.5 1 mM Stock of chitohexaose ( $M_r = 1237.2$ g/mol, GlcNAc<sub>6</sub>)

Dissolve 0.0012 g of GlcNAc<sub>6</sub> in 1 ml of 1 M KCl in 20 mM Hepes (pH 7.5) and store at -20 °C before used.

5.6 5 mM Stock of chitopentaose ( $M_r = 1034$  g/mol, GlcNAc<sub>5</sub>)

Dissolve 0.0052 g of GlcNAc<sub>5</sub> in 1 ml of 1 M KCl in 20 mM Hepes (pH 7.5) and store at -20 °C before used.

5.7 10 mM Stock of chitotetraose ( $M_r = 830.78$  g/mol, GlcNAc<sub>4</sub>)

Dissolve 0.0083 g of GlcNAc<sub>4</sub> in 1 ml of 1 M KCl in 20 mM Hepes (pH 7.5) and store at -20 °C before used.

5.8 10 mM Stock of chitotriose ( $M_r = 627.6$  g/mol, GlcNAc<sub>3</sub>)

Dissolve 0.0063 g of GlcNAc<sub>3</sub> in 1 ml of 1 M KCl in 20 mM Hepes (pH 7.5) and store at -20 °C before used.

5.9 50 mM Stock of chitobiose ( $M_r = 424.4$  g/mol, GlcNAc<sub>2</sub>)

Dissolve 0.021 g of GlcNAc<sub>2</sub> in 1 ml of 1 M KCl in 20 mM Hepes (pH 7.5) and store at -20 °C before used.

5.10 50 mM Stock of *N*-acetylglucosamine ( $M_r = 221.208$  g/mol, GlcNAc)

Dissolve 0.011 g of GlcNAc in 1 ml of 1 M KCl in 20 mM Hepes (pH 7.5) and store at -20 °C before used.

5.11 5 mg/ml Diphytanoyl phosphatidylcholine (DPhPC)

Dissolve 5 mg of DPhPC in *n*-pentane and store at -20 °C.

5.12 1% Hexadecane in *n*-hexane

Dilute 10 µl of hexadecane in 990 µl of *n*-hexane and store at -20 °C.

## 6. Buffer solutions for liposome swelling assay

6.1 20 mM Hepes (pH 7.5)

Dilute 40 ml of 0.5 M Hepes (pH 7.5) in distilled water to the final volume of 1,000 ml.

6.2 D (+) Arabinose ( $M_r = 150.13 \text{ g/mol}$ )

Dissolve 1.5 g of D (+) Arabinose in 50 ml of 20 mM Hepes (pH 7.5).

6.3 D (+) Raffinose ( $M_r = 594.53 \text{ g/mol}$ )

Dissolve 5.94 g of D (+) Raffinose in 50 ml of 20 mM Hepes (pH 7.5).

6.4 1 mM Stock of chitohexaose ( $M_r = 1237.2 \text{ g/mol}$ ,  $\text{GlcNAc}_6$ )

Dissolve 0.0012 g of  $\text{GlcNAc}_6$  in 1 ml of 20 mM Hepes (pH 7.5).

6.5 17% (w/v) Dextran ( $M_r = 40,000 \text{ Da}$ )

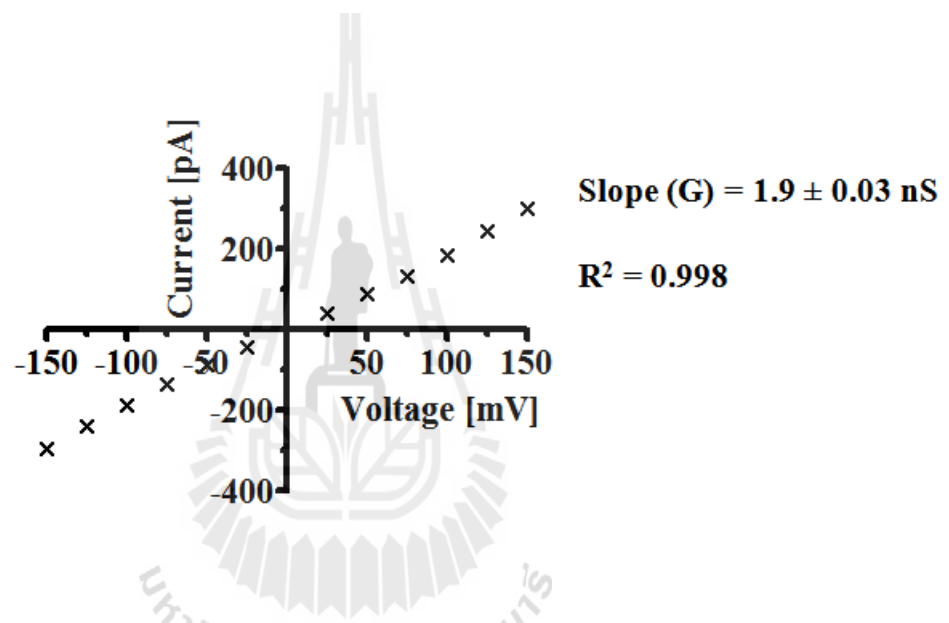
Dissolve 17 g of Dextran in 100 ml of 20 mM Hepes (pH 7.5).



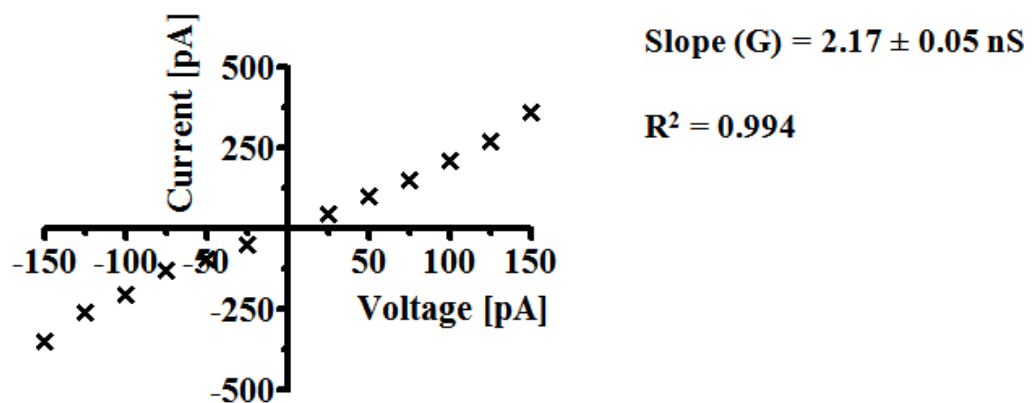
## APPENDIC C

### CURRENT-VOLTAGE (I/V) CURVES

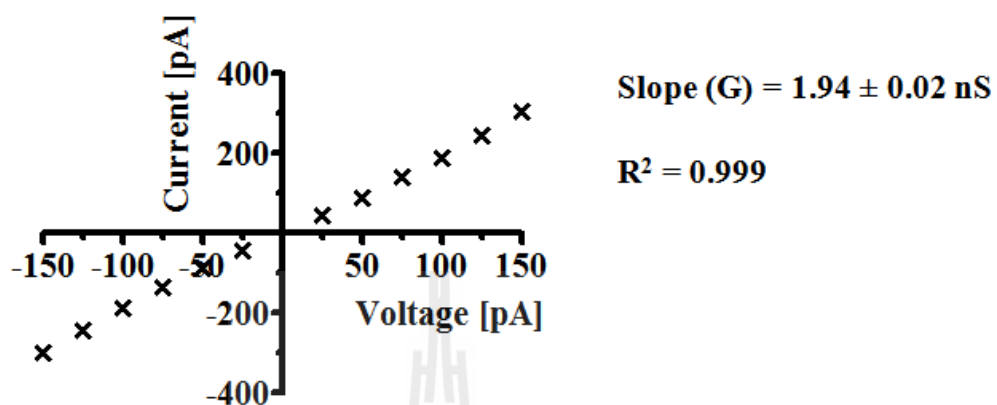
#### 1. Current/voltage (I/V) relationship of *VhChiP* (WT)



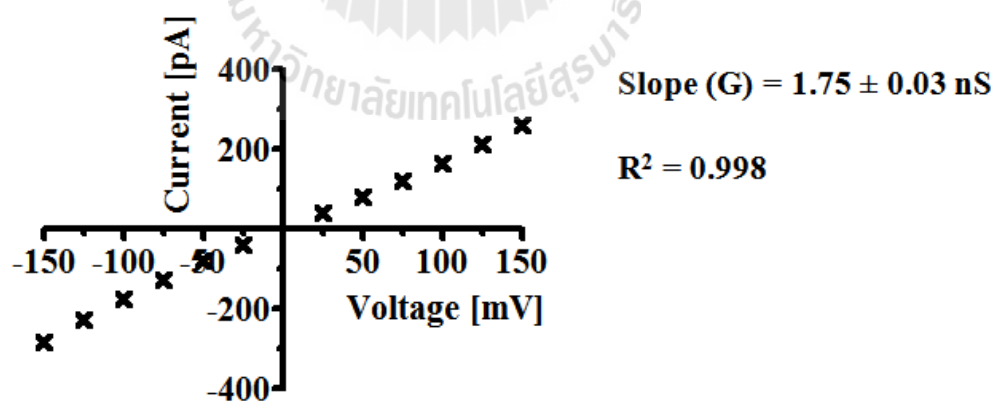
#### 2. Current/voltage (I/V) relationship of W136A



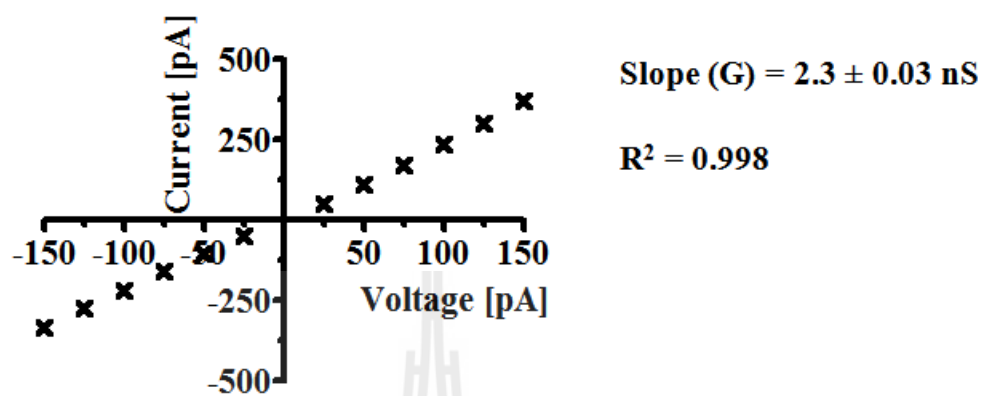
### 3. Current/voltage (I/V) relationship of W136F



### 4. Current/voltage (I/V) relationship of W136R



### 5. Current/voltage (I/V) relationship of W136D



# APPENDIC D

## AMINO ACID SEQUENCES

### 1. Amino acid sequences of *VhChiP* (WT)

1 DGANSDAAKEYLTKDSFSYEVYGIAMQAAYRDYDSGDAKQDDNL  
46 GGMQLNNE SRIGFRGKKQFANFEPTFIWQIEGGYVDPSFGGEGAG  
91 LGERDTFVGFESASWGQVRLGRVLTMPYELVDWPASNPLGDDVYD  
\*136  
136 WGGAIGGAKYQDRQSNTIRWDSPMYADKFSIDAAVGAGDKAGLGA  
184 GDDYWGGIAAHYKLGPLQLDAAYEGNRNIEAEGQTWENNTYLVGV  
231 QGWFENGISFFAQYKYMEADASNGVNEKQDAMSAGLMYTTGDWQ  
277 YKLGAAANFDLERDGGKTLNNTSDDVVSQAQIMYFVDPSAVLYARAR  
321 MNDFNEGLDGLDDAARWTSGTNGDYNEYSVGVEYY

### 2. Amino acid sequences of W136A

1 DGANSDAAKEYLTKDSFSYEVYGIAMQAAYRDYDSGDAKQDDNL  
46 GGMQLNNE SRIGFRGKKQFANFEPTFIWQIEGGYVDPSFGGEGAG  
91 LGERDTFVGFESASWGQVRLGRVLTMPYELVDWPASNPLGDDVYD  
\*136  
136 AGGAIGGAKYQDRQSNTIRWDSPMYADKFSIDAAVGAGDKAGLGA  
184 GDDYWGGIAAHYKLGPLQLDAAYEGNRNIEAEGQTWENNTYLVGV  
231 QGWFENGISFFAQYKYMEADASNGVNEKQDAMSAGLMYTTGDWQ  
277 YKLGAAANFDLERDGGKTLNNTSDDVVSQAQIMYFVDPSAVLYARAR  
321 MNDFNEGLDGLDDAARWTSGTNGDYNEYSVGVEYY

### 3. Amino acid sequences of W136F

1 DGANSDAAKEYLTKDSFSYEVYGIIAMQAAYRDYDSGDAKQDDNL  
 46 GGMQLNNESRIGFRGKKQFANFEPTFIWQIEGGYVDPSFGGEGAG  
 91 LGERDTFVGFESASWGQVRLGRVLTMPYELVDWPASN PGLGDVYD  
 \*136  
 136 FGGAIGGAKYQDRQSNTIRWDSPMYADKFSIDAAVGAGDKAGLGA  
 184 GDDYWGGIAAHYKLGPLQLDAAYEGNRNIEAEGQTWENNTYLVGV  
 231 QGWFENGISFFAQYKYMADASNGVNEKQDAMSAGLMYTTGDWQ  
 277 YKLGYAANFDLERDGGKTLSENTSDDVVSAQIMYFVDPSAVLYARAR  
 321 MNDFNEGLDGLDDAARWTSGTNGDYNEYSVGVEYY

### 4. Amino acid sequences of W136R

1 DGANSDAAKEYLTKDSFSYEVYGIIAMQAAYRDYDSGDAKQDDNL  
 46 GGMQLNNESRIGFRGKKQFANFEPTFIWQIEGGYVDPSFGGEGAG  
 91 LGERDTFVGFESASWGQVRLGRVLTMPYELVDWPASN PGLGDVYD  
 \*136  
 136 RGGAIGGAKYQDRQSNTIRWDSPMYADKFSIDAAVGAGDKAGLGA  
 184 GDDYWGGIAAHYKLGPLQLDAAYEGNRNIEAEGQTWENNTYLVGV  
 231 QGWFENGISFFAQYKYMADASNGVNEKQDAMSAGLMYTTGDWQ  
 277 YKLGYAANFDLERDGGKTLSENTSDDVVSAQIMYFVDPSAVLYARAR  
 321 MNDFNEGLDGLDDAARWTSGTNGDYNEYSVGVEYY

## 5. Amino acid sequences of W136D

1 DGANSDAAKEYLTKDSFSYEVYGIIAMQAAYRDYDSGDAKQDDNL  
46 GGMQLNNE SRIGFRGKKQFANFEPTFIWQIEGGYVDPSFGGEGAG  
91 LGERDTFVGFESASWGQVRLGRVLTMPYELVDWPASN PGLGDVYD  
\*136  
136 DGGAIGGAKYQDRQSNTIRWDSPMYADKFSIDAAVGAGDKAGLGA  
184 GDDYWGGIAAHYKLGPLQLDAAYEGNRNIEAEGQ TWENNTYLVGV  
231 QGWFENGISFFAQYKYMEADASNGVNEKQDAMSAGLMYTTGDWQ  
277 YKLGYAANFDLERDGTKLSNTSDDVVSAQIMYFVDPSAVLYARAR  
321 MNDFNEGLDGLDDAARWTSGTNGDYNEYSVGVEYY



# APPENDIC E

## SUPPORTING INFORMATIONS

### 1. Identification of *V. harveyi* chitoporin by mass spectrometry

MASYLKKSLLATAITGMMFSGSAFADGANSDAKEYLTKDSFSYEVYGIAMQAAYRDY P1  
DSGDAKQDDNLGGMQLNNSRIGFRGKKQFANFEPTFIWQIEGGYVDPSPFGGEGAGLG  
ERDTFVGFESASWGQVRLGRVLTPMYELVDWPASNPLGDVYDWGGAIGGAKYQDR P2 P3  
QSNTIRWDSPMYADKFSIDAAVGAGDKAGLGAGDDYWGGIAAHYKLGPLQLDAAYEGN P4 P5 P6  
RNIEAEGQTWENNTYLGVGQGWFFENGISFFAQYKMEADASNGVNEKQDAMSAGLMY P7  
TTGDWQYKLGYAANFDLERDGK P8&P9  
TLNNTSDDVVSAQIMYFVDPSAVLYARARMNDFNEG  
LDGLDDAARWTSGTNGDYNEYSVGVEYYF

**Figure S1** Identification of *V. harveyi* chitoporin by mass spectrometry. Tryptic peptides were prepared from the outer membrane fraction extracted with 2% (w/v) SDS, followed by 3% (v/v) octyl-POE by in-gel digestion method. The peptides were resolved by nano-LC/MS. The resultant monoisotopic masses were subjected to Mascot search using the NCBI Nr database for protein identification. Sequences underlined (P1-P9) are identical to nine internal peptides in the translated sequence of *V. harveyi* chitoporin identified in this study.

## 2. Liposome swelling assay

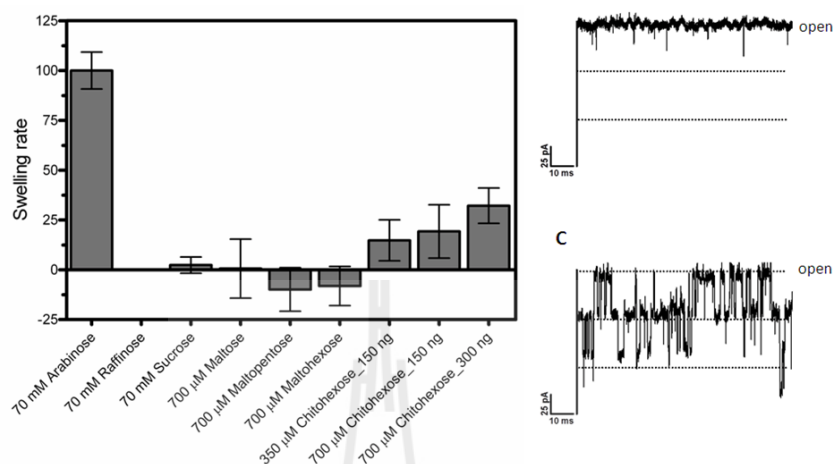


**Figure S2** Liposome swelling assays. Multilamellar liposomes, prepared as described in the text, were reconstituted with purified *VhChiP* (150 or 300 ng). The isotonic concentration was defined as the concentration of raffinose was added into the proteoliposome suspension that did not cause change in absorbance at 500 nm for a period of 60 s. Permeation of different types of sugars through *VhChiP* reconstituted liposomes were then tested. A) The swelling rates were normalized, with the rate of swelling in arabinose set to 100%. Values presented are averages of 4-6 independent experiments. B) BLM measurement of *VhChiP* ion current with the isotonic concentration of raffinose (70 mM) added. C) BLM measurement of *VhChiP* in the presence of 70 mM raffinose and 200 mM chitohexaose.

### 3. Effects of concentrations of small chitosugars on ion current blockages

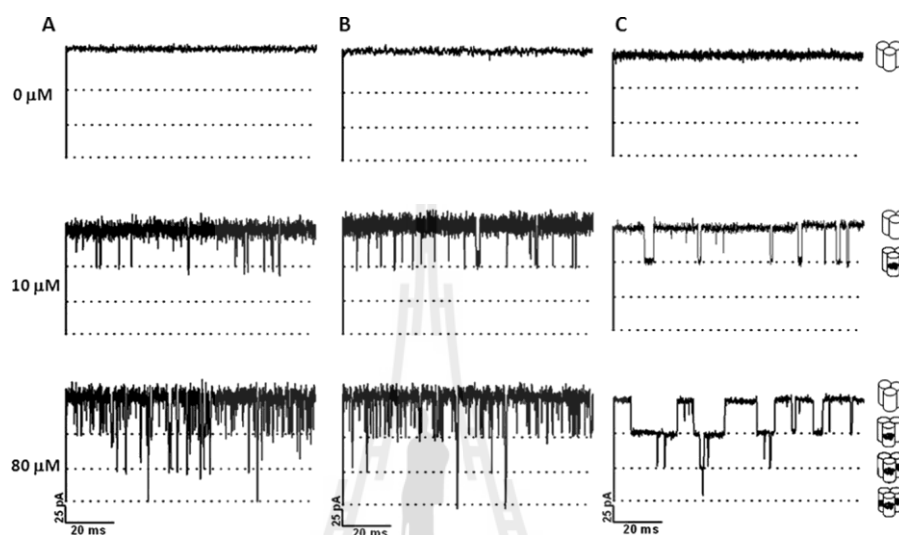


**Figure S3** Effect of concentration of small chitosugars on ion current blockages. A single channel of *VhChiP* was reconstituted into artificial lipid bilayers. A. Chitotriose, B. Chitotetraose and C. Chitopentaose were titrated on the *cis*-side. The ion current traces were recorded at +100 mV, T = 22 °C.

#### 4. Effect on ion currents of chitooligosaccharide diffusion into chitoporin

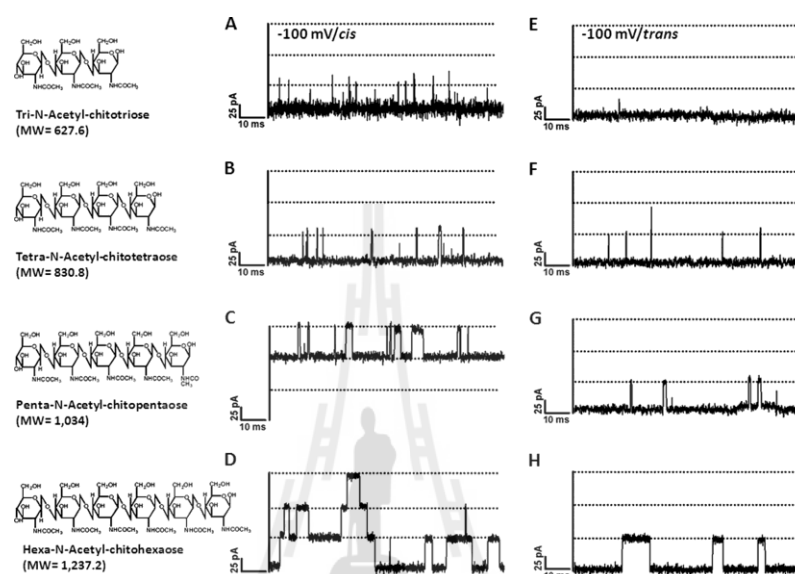


**Figure S4** Ion current blockages in presence of small sugar. A single trimeric channel of *VhChiP* was inserted in an artificial membrane. Chitooligosaccharides of various sizes were then added to a final concentration of 5  $\mu\text{M}$  on either the *cis*-side (A-D) or *trans*-side (E-H) of the chamber. A and E, chitotriose; B and F, chitotetraose; C and G, chitopentaose; D and H, chitohexaose. Ion current fluctuations were monitored for 120 s at applied potentials of  $\pm 100$  mV. Here, only ion traces for a potential of -100 mV are presented.

## 5. Ionic selectivity

5.1 Channel selectivity. Zero-current membrane potentials ( $V_m$ ) vs. the ratio of salt concentrations on *trans*- and *cis*-side addition of KCl bulk solution for *VhChiP* channel (WT).

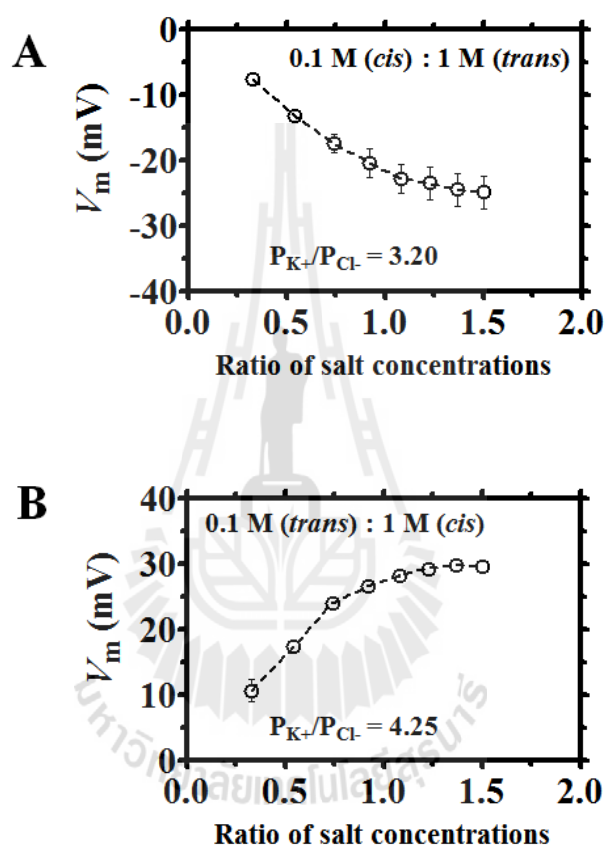


**Figure S5** Selectivity of *VhChiP* channel (WT). Plot of the zero-current membrane potentials ( $V_m$ ) vs. the ratio of the salt concentrations gradient on *trans*- and *cis*-side of KCl. A) High concentration of 1 M KCl was on *trans*-side and B) High concentration of 1 M KCl was on *cis*-side of the chamber. Increasing ratio of salt concentration reached 1.5 M was titrated with 3 M KCl on *trans*- or *cis*-side. The curves were fitted to the equation of Goldman-Hodgkin.

### 5.2 Ionic selectivity measurement for *VhChiP* (WT) and its mutant (W136A and W136F)

To quantify the selectivity the zero-current membrane potential was measured. Membranes were formed in a solution of 0.1 M KCl supplemented with 20 mM Hepes (pH 7.5) and the protein (WT, W136A, and W136F) was added onto both sides of the chamber, and the increase of membrane conductance due to insertion of pores was observed with the electrometer. As this measurement requires a multitude of channel we inserted many channels. After waiting for multiple insertion. After reaching a conductance of at least 0.18 nS (WT), 0.21 nS (W136A), or 0.2 nS (W136F) (corresponding to insertion of 100 channels) the instrumentation was switched to the measurement of the zero-current membrane potential, and a KCl gradient was established by adding 3 M KCl (20 mM Hepes, pH 7.5) solution to *cis*-side of the membrane (connected to ground electrode). The zero-current membrane voltage reached its final value after 5-10 min (constant value) and was analysed using the Goldman-Hodgkin equation (Benz *et al.*, 1979).

5.3 Table S1 shows the ionic selectivity of WT and its mutant. Single channel insertion was performed as describe in 5.2.

| <b>Protein</b> | <b>Ratio of salt concentrations (KCl, M)</b> | <b><math>V_m</math> (mV)</b> | <b><math>P_{K^+}/P_{Cl^-}</math></b> |
|----------------|--|------------------------------|--------------------------------------|
| 1) WT          | 0.1 ( <i>trans</i> ) : 0.5 ( <i>cis</i> )    | +26.1                        | 3.75                                 |
| 2) W136A       | 0.1 ( <i>trans</i> ) : 0.5 ( <i>cis</i> )    | +25.4                        | 3.63                                 |
| 3) W136F       | 0.1 ( <i>trans</i> ) : 0.5 ( <i>cis</i> )    | +27.3                        | 4.02                                 |

5.3 Plot between zero-current membrane potentials ( $V_m$ ) and the ratio of salt concentrations on *cis*-side addition of KCl bulk solution for WT and its mutant

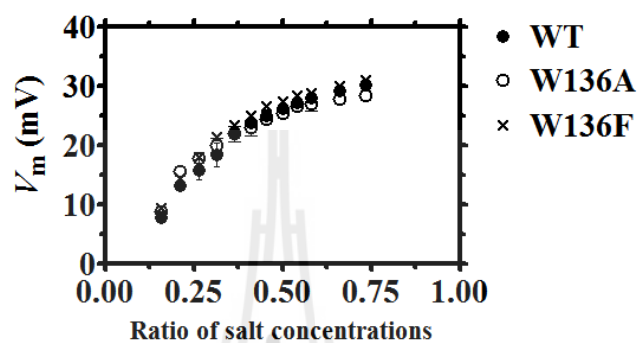


**Figure S6** Zero-current membrane potentials ( $V_m$ ) vs. the ratio of salt concentrations on *cis*-side addition of KCl bulk solution for WT and its mutant. Increasing ratio of salt concentration reached 0.75 M was titrated with 3 M KCl on *cis*-side. The curves were fitted to the equation of Goldman-Hodgkin.

**6. Adigram representing asymmetrical values of the energy barriers required for the chitohexaose binding and releasing from the binding affinity site localized within the *VhChiP* and its mutant pores**

6.1 The energy barriers obtained from  $k_{on}$  for chitohexaose on *cis* or *trans* side addition of mutated *VhChiP* (W136A, W136F, W136R, and W136D) compare to *its* wild type (WT) pores

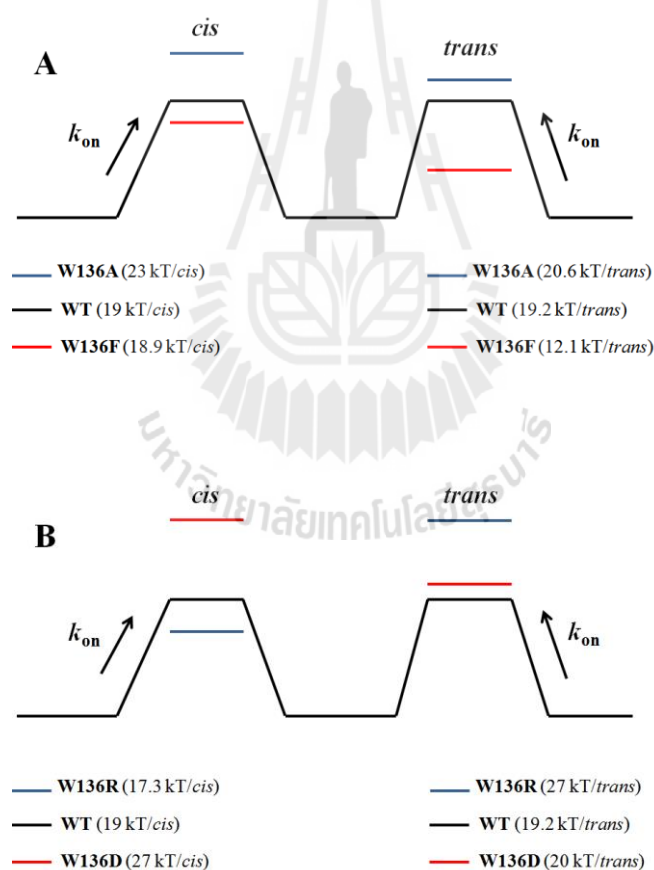


**Figure S7** The energy barriers obtained from  $k_{on}$  for chitohexaose on *cis* or *trans* side addition of A) W136A and W136F and B) W136R and W136D compare to its wild type (WT) pores.

6.2 The energy barriers obtained from  $k_{\text{off}}$  for chitohexaose on *cis* or *trans* side addition of mutated *VhChiP* (W136A, W136F, W136R, and W136D) compare to *its* wild type (WT) pores

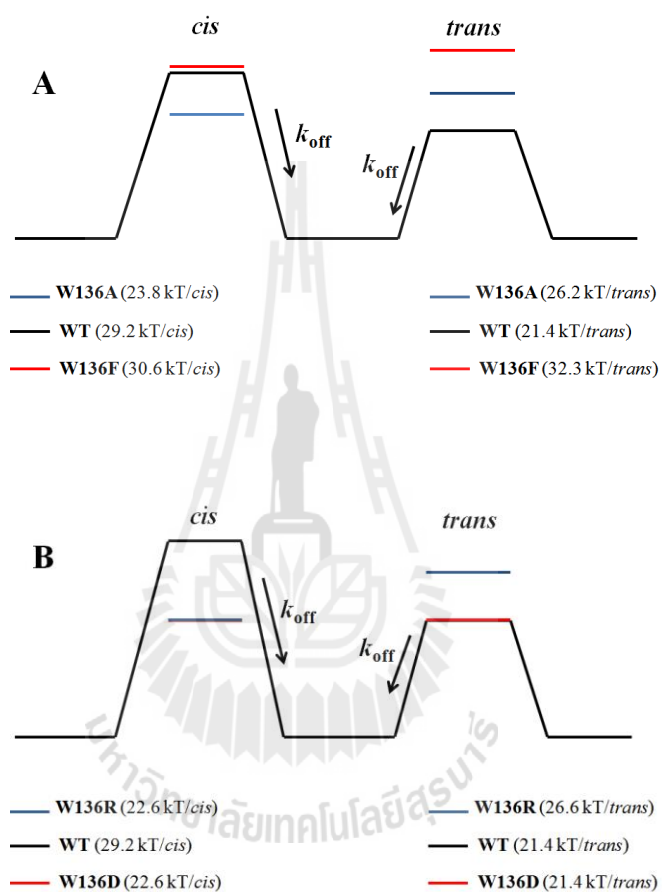


**Figure S8** The energy barriers obtained from  $k_{\text{off}}$  for chitohexaose on *cis* or *trans* side addition of A) W136A and W136F and B) W136R and W136D compare to its wild type (WT) pores.

## 6.3 Arrhenius plot of conductance as a function of temperature from 5-30 °C

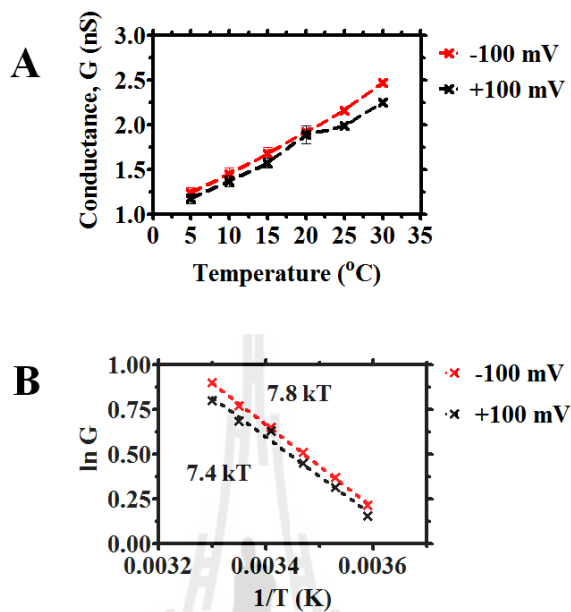


**Figure S9** Arrhenius plot of conductance as a function of temperature from 5 to 30  $^{\circ}\text{C}$  gave a linear slope with an energy barrier of about 7.8 kT ( $-100$  mV) and 7.4 kT ( $+100$  mV). The experiment carried out in 1 M KCl/20 mM Hepes (pH 7.5), with applied voltages of  $\pm 100$  mV.

**7. Table S2** the dissociation constants ( $K_D$ ) of *VhChiP* (WT) and its mutant with chitooligosaccharides (GlcNAc<sub>5</sub>-GlcNAc<sub>1</sub>) using Fluorescence Spectroscopy.

| Protein  | Ligands             | Nonpolar, Hydrophobic   |        |        |                                   |         |           |                     |        |        |
|----------|---------------------|-------------------------|--------|--------|-----------------------------------|---------|-----------|---------------------|--------|--------|
|          |                     | $K_D$ ( $\mu\text{M}$ ) |        |        | $K$ ( $1/K_D$ , $\text{M}^{-1}$ ) |         |           | $\Delta G$ (kJ/mol) |        |        |
|          |                     | pH 4.0                  | pH 6.0 | pH 7.4 | pH 4.0                            | pH 6.0  | pH 7.4    | pH 4.0              | pH 6.0 | pH 7.4 |
| 1) WT    | GlcNAc <sub>5</sub> | -                       | 4.34   | 0.29   | -                                 | 230,000 | 3,400,000 | -                   | -29.9  | -36.5  |
|          | GlcNAc <sub>4</sub> | -                       | 3.39   | 1.16   | -                                 | 290,000 | 860,000   | -                   | -30.6  | -33.0  |
|          | GlcNAc <sub>3</sub> | -                       | 29.84  | 1.91   | -                                 | 30,000  | 520,000   | -                   | -25.3  | -31.9  |
|          | GlcNAc <sub>2</sub> | -                       | -      | n.d.   | -                                 | -       | n.d.      | -                   | -      | n.d.   |
|          | GlcNAc <sub>1</sub> | -                       | -      | n.d.   | -                                 | -       | n.d.      | -                   | -      | n.d.   |
| 2) W136A | GlcNAc <sub>5</sub> | -                       | -      | n.d.   | -                                 | -       | n.d.      | -                   | -      | n.d.   |
|          | GlcNAc <sub>4</sub> | -                       | -      | n.d.   | -                                 | -       | n.d.      | -                   | -      | n.d.   |
|          | GlcNAc <sub>3</sub> | -                       | -      | n.d.   | -                                 | -       | n.d.      | -                   | -      | n.d.   |
|          | GlcNAc <sub>2</sub> | -                       | -      | -      | -                                 | -       | -         | -                   | -      | -      |
|          | GlcNAc <sub>1</sub> | -                       | -      | -      | -                                 | -       | -         | -                   | -      | -      |
| 3) W136F | GlcNAc <sub>5</sub> | -                       | -      | 0.81   | -                                 | -       | 1,200,000 | -                   | -      | -34.0  |
|          | GlcNAc <sub>4</sub> | -                       | -      | 1.56   | -                                 | -       | 640,000   | -                   | -      | -32.4  |
|          | GlcNAc <sub>3</sub> | -                       | -      | 3.21   | -                                 | -       | 310,000   | -                   | -      | -30.7  |
|          | GlcNAc <sub>2</sub> | -                       | -      | 3.32   | -                                 | -       | 300,000   | -                   | -      | -30.6  |
|          | GlcNAc <sub>1</sub> | -                       | -      | 13.39  | -                                 | -       | 75,000    | -                   | -      | -27.2  |
| Protein  | Ligands             | Polar Acidic            |        |        |                                   |         |           |                     |        |        |
|          |                     | $K_D$ ( $\mu\text{M}$ ) |        |        | $K$ ( $1/K_D$ , $\text{M}^{-1}$ ) |         |           | $\Delta G$ (kJ/mol) |        |        |
|          |                     | pH 4.0                  | pH 6.0 | pH 7.4 | pH 4.0                            | pH 6.0  | pH 7.4    | pH 4.0              | pH 6.0 | pH 7.4 |
| 4) W136D | GlcNAc <sub>5</sub> | -                       | 4.14   | -      | -                                 | 240,000 | -         | -                   | -30.1  | -      |
|          | GlcNAc <sub>4</sub> | -                       | 5.28   | -      | -                                 | 190,000 | -         | -                   | -29.5  | -      |
|          | GlcNAc <sub>3</sub> | -                       | 12.2   | -      | -                                 | 82,000  | -         | -                   | -27.4  | -      |
|          | GlcNAc <sub>2</sub> | -                       | 25.73  | -      | -                                 | 39,000  | -         | -                   | -25.6  | -      |
|          | GlcNAc <sub>1</sub> | -                       | 49.15  | -      | -                                 | 20,000  | -         | -                   | -24.0  | -      |
| Protein  | Ligands             | Polar Basic             |        |        |                                   |         |           |                     |        |        |
|          |                     | $K_D$ ( $\mu\text{M}$ ) |        |        | $K$ ( $1/K_D$ , $\text{M}^{-1}$ ) |         |           | $\Delta G$ (kJ/mol) |        |        |
|          |                     | pH 4.0                  | pH 6.0 | pH 7.4 | pH 4.0                            | pH 6.0  | pH 7.4    | pH 4.0              | pH 6.0 | pH 7.4 |
| 5) W136R | GlcNAc <sub>5</sub> | -                       | 6.77   | -      | -                                 | 150,000 | -         | -                   | -28.9  | -      |
|          | GlcNAc <sub>4</sub> | -                       | 10.53  | -      | -                                 | 95,000  | -         | -                   | -27.8  | -      |
|          | GlcNAc <sub>3</sub> | -                       | 32.23  | -      | -                                 | 31,000  | -         | -                   | -25.1  | -      |
|          | GlcNAc <sub>2</sub> | -                       | 69.44  | -      | -                                 | 14,000  | -         | -                   | -23.3  | -      |
|          | GlcNAc <sub>1</sub> | -                       | 105.3  | -      | -                                 | 9500    | -         | -                   | -22.2  | -      |

The dissociation binding constants ( $K_D$ ,  $\mu\text{M}$ ) was obtained from the Stern-Volmer Eq. 2.4 and converted to the equilibrium binding constants ( $K$ ,  $\text{M}^{-1}$ ) as inversion as  $1/K_D$ . The Gibbs free energy ( $\Delta G$ ) was calculated from the Eq. 2.8, where R is the ideal gas constant (8.314 J/K/mol); T is temperature (T = 298 K); and n.d. is non-detection.

## **APPENDIC F**

### **PUBLICATIONS**

#### **Publication outputs:**

1. Suginta, W., Mahendran, K. R., Chumjan, W., Hajjar, E., Schulte, A., Winterhalter, A., Weingart, H. (2010). Molecular analysis of antimicrobial agent translocation through the membrane porin BpsOmp38 from an ultraresistant *Burkholderia pseudomallei* strain. *Biochim. Biophys. Acta.* 1808(6):1552-1559.
2. Suginta, W., Chumjan, W., Mahendran, K. R., Janning, P., Schulte, A., Winterhalter, M. (2013) Molecular uptake of chitooligosaccharides through chitoporin from the marine bacterium *Vibrio harveyi*. *PLoS ONE* 8, e55126.
3. Suginta, W., Chumjan, W., Mahendran, K. R., Schulte, A., Winterhalter, M. (2013) Chitoporin from *vibrio harveyi*: a channel with exceptional sugar specificity. *J. Biol. Chem.* 288, 11038-11046.

#### **In preparations**

4. Suginta, W., Schulte, A., Mahendran, K. R., Aunkham, A., Chumjan, W., Winterhalter, M. (2014). Chitoporin from *Vibrio harveyi*: Effects of transmembrane voltage and *N*-acetyl functionality of chitin oligosaccharides on translocation.

5. Chumjan, W., Winterhalter, M., Schulte, A., Suginta, W., (2014). Effect of the central constriction lumen on the ion transport and chitohexaose translocation through the chitoporin channel from marine bacterium *Vibrio harveyi*.





## Molecular analysis of antimicrobial agent translocation through the membrane porin BpsOmp38 from an ultraresistant *Burkholderia pseudomallei* strain

Wipa Suginta<sup>a,\*</sup>, Kozhinjampara R. Mahendran<sup>b</sup>, Watcharin Chumjan<sup>a</sup>, Eric Hajjar<sup>c,1</sup>, Albert Schulte<sup>a</sup>, Mathias Winterhalter<sup>b</sup>, Helge Weingart<sup>b,\*</sup>

<sup>a</sup> Biochemistry-Electrochemistry Research Unit, Schools of Chemistry and Biochemistry, Institute of Science, Suranaree University of Technology, Nakhon Ratchasima 30000, Thailand

<sup>b</sup> School of Engineering and Science, Jacobs University Bremen, D-28759 Bremen, Germany

<sup>c</sup> Istituto Officina dei Materiali/CNR UOS SLACS and Department of Physics, University of Cagliari, I-09042 Monserrato, Italy

### ARTICLE INFO

#### Article history:

Received 10 August 2010  
Received in revised form 27 October 2010  
Accepted 28 October 2010  
Available online 13 November 2010

#### Keywords:

Black lipid membrane reconstitution  
*Burkholderia pseudomallei*  
Meloidosis  
Outer membrane protein  
Porin

### ABSTRACT

*Burkholderia pseudomallei* (*Bps*) is a Gram-negative bacterium that causes melioidosis, an infectious disease of animals and humans common in northern and north-eastern parts of Thailand. Successful treatment of melioidosis is difficult due to intrinsic resistance of *Bps* to various antibacterial agents. It has been suggested that the antimicrobial resistance of this organism may result from poor permeability of the active compounds through porin channels located in the outer membrane (OM) of the bacterium. In previous work, a 38-kDa protein, named "BpsOmp38", was isolated from the OM of *Bps*. A topology prediction and liposome-swelling assay suggested that BpsOmp38 comprises a  $\beta$ -barrel structure and acts as a general diffusion porin. The present study employed black lipid membrane (BLM) reconstitution to demonstrate the single-channel conductance of the trimeric BpsOmp38 to be  $2.7 \pm 0.3$  nS in 1 M KCl. High-time resolution BLM measurements displayed ion current blockages of seven antimicrobial agents in a concentration-dependent manner with the translocation on-rate ( $k_{on}$ ) following the order: norfloxacin > ertapenem > ceftazidime > cefepime > imipenem > meropenem > penicillin G. The dwell time of a selected antimicrobial agent (ertapenem) decayed exponentially with increasing temperature. The energy barrier for the ertapenem binding to the affinity site inside the BpsOmp38 channel was estimated from the Arrhenius plot to be 12 kT and for the ertapenem release to be 13 kT at +100 mV. The BLM data obtained from this study provide the first insight into antimicrobial agent translocation through the BpsOmp38 channel.

© 2010 Elsevier B.V. All rights reserved.

### 1. Introduction

*Burkholderia pseudomallei* (*Bps*) is a soil-dwelling Gram-negative bacterium commonly found in Southeast Asia and Northern Australia and a cause of a deadly disease of mammalian species termed melioidosis [1–4]. Patients infected with *Bps* usually develop skin ulcers, visceral abscesses, pneumonia and septicemia that imperatively require immediate antimicrobial treatment to avoid fatal progression of the disease. Very often, antimicrobial treatment is quite a challenge due to the high intrinsic broad spectrum resistance that most *Bps* strains exhibit towards a broad spectrum of antimicrobial agents including but not limited to  $\beta$ -lactam antibiotics, aminoglycosides, macrolides, and cephalosporins [1–4]. Due to the high incidence of drug resistance and very high virulence, *Bps* is regarded a potential bioterrorism and warfare agent [5]. As such, this organism has been listed by the US Centre for Disease Control and Prevention as a

category B health hazard [6,7]. Clinical and security concerns associated with *Bps* have justified intensive research in attempt to address the structural and functional organization of this pathogen as a prelude to the design of novel and efficacious anti-*Bps* therapeutic agents. Most of ongoing studies include characterization of biological and pathophysiological aspects of the agent, unraveling the mechanisms of genomic plasticity and evolution, as well as understanding the molecular mechanisms underlying drug resistance. The publication of the sequences of the entire *Bps* genome [8], as well as data from drug susceptibility testing [9–12], and recent reports on *Bps* vaccines [13–15] are important developments in the search for an effective anti-melioidosis treatment.

Current scientific evidence suggests that *Bps* successfully utilizes the strategy of genetic evolution, modified protein expression and/or mutation more than most other bacteria. These features underscore the ability of the pathogen to establish troublesome resistance against many antimicrobial agents. Some of the mechanisms of drug resistance include: alteration of intracellular drug action sites, generation of enzymes for the modification and/or complete degradation of drug molecules within the cytosol, and restriction of intracellular drug accumulation through impaired uptake and/or enhanced drug efflux [16–19].

\* Corresponding authors.

E-mail addresses: [wipa@sut.ac.th](mailto:wipa@sut.ac.th) (W. Suginta), [h.weingart@jacobs-university.de](mailto:h.weingart@jacobs-university.de) (H. Weingart).

<sup>1</sup> Present address: Biozentrum University of Basel, SIB Swiss Institute of Bioinformatics, 4056 Basel, Switzerland.

In the present study, we addressed limitation of cellular drug uptake which in a number of other bacteria is associated with reduced molecular transport of the active compounds through bacterial outer membrane protein (Omp) channels. Also known as porins, Omp channels are typical  $\beta$ -barrel protein structures that independently or as oligomeric units are inserted into the outer lipid bilayer of the bacterial cell wall to form pores through which extracellular species can diffuse and gain access to the periplasmic space and cytosol [20–22]. Membrane trafficking via porins has been elegantly measured at molecular level using the black lipid membrane (BLM) technique [23–25]. In BLM experiments, the parameter measured is the voltage-induced charge flow through an artificial lipid bilayer membrane that separates two electrolyte compartments and one that has the study porin artificially inserted. Recordings of the transmembrane current at microsecond time resolution enable visualization of insertions of the porin in their open state as stepwise increases in the signal. Movement of individual drug/other molecules through a stably open unit is detected by means of transient current fluctuations derived from physical channel blockade during the residence time of compounds traveling through the porin. Mechanistically, bacterial cells can counteract the influx of drug molecules through reduction of the total number of porins in their outer membrane, a decrease in the cross-sectional dimension of the protein channels, and/or through modification of the electrostatics and/or hydrophobicity of the pore interior through point mutations of the amino acids lining the protein pores. Quantitative correlation of the entry of specific drug molecules with a firm structural and predictive computational analysis may lead to a better understanding of the molecular basis of antimicrobial agent permeability, facilitating the design of effective drugs that have greater penetrating power [26].

While functional [27–32] and computational [33–35] BLM studies focused on membrane drug permeation have been performed on a number of bacterial porins, no similar research has investigated analogous proteins from clinically important *Bps* strains. In previous work, an Omp with an apparent molecular weight (MW) of 38 kDa, referred to as *BpsOmp38*, was isolated from the *Bps* cell wall [36,37]. Topology prediction and molecular modeling suggested that *BpsOmp38* has a  $\beta$ -barrel structure, a feature that is common among membrane porins. Subsequently, a liposome-swelling assay on this protein confirmed its channel-forming properties [37]. In the present study, a detailed functional characterization of the *BpsOmp38* porin by BLM-based single ion-channel analysis is described. Ion current measurements were carried out in the absence and in the presence of seven different antimicrobial agents as additional diffusing species in the membrane-bathing electrolyte. The differences in the ability of the selected drugs to move through open *BpsOmp38* pores and their kinetic behavior are discussed in the context of molecular drug/porin interactions.

## 2. Materials and methods

### 2.1. *BpsOmp38* expression and purification

The *E. coli* strain BL21 (DE3) Omp8 was a gift from Ralf Koebnik, Laboratoire Génomique et Développement des Plantes, Université de Perpignan via Domitia, Montpellier, France. This strain of *E. coli* does not express the major outer membrane proteins LamB, OmpA, OmpC and OmpF [38]; it was experimentally transformed with the recombinant plasmid pET23d.*BpsOmp38*. Purification of the recombinant *BpsOmp38* followed a modified version of protocols described by Garavito and Rosenbusch [39] and Rosenbusch [40]. In brief, transformed cells were grown at 37 °C in Luria–Bertani (LB) liquid medium containing 100  $\mu$ g/ml ampicillin. At an OD<sub>600</sub> reading of 0.5, IPTG (isopropyl  $\beta$ -D-thiogalactoside) was added to a final concentration of 0.4 mM. Cell growth was continued for a further 6 h and then cells

were harvested by centrifugation at 2948  $\times$  g for 10 min. The cell pellet was resuspended in buffer containing 20 mM Tris–HCl, pH 8.0, 2.5 mM MgCl<sub>2</sub>, 0.1 mM CaCl<sub>2</sub>, 10  $\mu$ g/ml DNase I and 10  $\mu$ g/ml RNase A and then disrupted using a high-pressure homogenizer (Emulsi-Flex-C3, Avestin Europe, Mannheim, Germany). The recombinant *BpsOmp38* was further extracted from the peptidoglycan layer using sodium dodecyl sulfate (SDS)-containing solutions based on a procedure reported by Lugtenberg and Alphen [41]. Briefly, SDS was added to the cell suspension to a final concentration of 2% (v/v) and incubation was carried out for 1 h at 60 °C with gentle shaking. The crude extract was then centrifuged at 39,636  $\times$  g for 60 min at 4 °C. The pellet, which at this stage included the cell envelopes, was resuspended in 20 mM phosphate buffer, pH 7.4 (PBS), containing 0.125% (v/v) octyl-POE (*n*-octyl-polyoxyethylene; ALEXIS Biochemicals, Lausanne, Switzerland). The suspension was incubated at 37 °C with gentle shaking for 60 min and then centrifuged at 109,564  $\times$  g at 4 °C for 40 min. The new pellet, now rich in outer membranes, was resuspended in 20 mM phosphate buffer, pH 7.4 containing 3% (v/v) octyl-POE and the suspension incubated at 37 °C with shaking at 250 rpm for 1 h to solubilize the porin. Insoluble material was removed by centrifugation at 109,564  $\times$  g at 20 °C for 40 min and the porin-rich supernatant concentrated using Amicon Ultra-15 centrifugal filter devices with a nominal MW limit of 30 kDa (Millipore, Schwalbach, Germany). Amicon centrifugal filters were also used to exchange the original preparation buffer with 20 mM PBS, containing 1% (v/v) octyl-POE. Aliquots of the final protein sample were used for absorbance measurement at 280 nm for the determination of protein concentration using NanoDropT 1000 Spectrophotometer (Thermo Fisher Scientific, Wilmington, DE, USA) and for SDS-polyacrylamide gel electrophoresis (SDS-PAGE) for the assessment of sample purity.

### 2.2. Lipid bilayer measurements and single-channel analysis

The following chemicals were used: NaCl, KCl, MES, *n*-pentane, and hexadecane (Sigma-Aldrich, Hamburg, Germany); ceftazidime, norfloxacin, and penicillin G (Sigma-Aldrich); cefepime, imipenem, meropenem, and ertapenem (Basilea Pharmaceutica Ltd., Basel, Switzerland); and 1,2-diphytanoyl-*sn*-glycero-3-phosphatidylcholine (DPhPC) (Avanti Polar Lipids, Alabaster, AL, USA). Double distilled and deionized water was used to prepare chemical reagents and the freshly made solutions passed through a 0.4- $\mu$ m filter. The drug stock solutions for translocation experiments were prepared with 1 M KCl in electrolyte buffer (20 mM phosphate buffer, pH 7.0 or in 20 mM HEPES, pH 8.0).

Lipid bilayer measurements and single-channel analysis were performed as described elsewhere [27–32]. Briefly, a cell with a 40–60  $\mu$ m diameter aperture in a 15- $\mu$ m-thick Teflon partition provided a two-compartment black lipid membrane (BLM) chamber and two silver–silver chloride electrodes at either side of the dividing wall allowed voltage control of solvent-free planar lipid bilayers that were formed using a solution of DPhPC in pentane. Low levels of the study *BpsOmp38* channel were introduced to the *cis* or *trans* side of the bilayers by adding the protein stock solution of about 1–2  $\mu$ g/ml containing 1% (v/v) octyl-POE (ALEXIS, Switzerland). In the trials addressing the temperature dependence of drug translocation, a peltier element (Dagan Corporation, Minneapolis, MN, USA) was used for accurate temperature regulation of the BLM chamber. At an applied transmembrane voltage of +50 mV, spontaneous channel insertion was usually obtained within a few minutes after adding the protein solution. Conductance measurements were performed using an Axopatch 200B amplifier (Molecular Devices, Sunnyvale, CA, USA) in the voltage clamp mode and the internal filter at 10 kHz. Amplitude, probability, and single-channel analyses were performed using pClamp v.10.0 software (Molecular Devices). Control experiments (refer to Supplementary S3, upper left recording) showed no

dependence of the *BpsOmp38* conductance and open channel noise on the presence of the buffer alone.

Black lipid bilayer measurements with *BpsOmp38* from an earlier preparation with mass spectrometry (MS) identification (Supplementary S1) established that the single-channel conductance of the targeted reconstituted protein channel is about  $2.7 \pm 0.3$  nS in 1 M KCl. A channel of identical conductance also routinely appeared when freshly formed solvent-free DPhPC bilayer membranes were exposed to the protein prepared by the procedure described in the preceding section. Accordingly, translocation of drug molecules was analyzed in recordings of this particular channel. Another channel that frequently incorporated during the BLM experiments was not used for the translocation studies after its small conductance (0.3 nS in 1 M KCl) and MS data suggested it was a maltoporin.

### 2.3. Porin homology modeling

The structural model of recombinant *BpsOmp38* was built based upon the Modeller suite of programs [42]. Initially, several iterations of the PSI-BLAST protein sequence search program in the pdb database were performed to allow detection of remote homologues of the *BpsOmp38* porin. Only the templates with non-redundant structures were kept and further used for building the homology model. Such templates included the pdb codes 3K1B (OmpF), 2IXX (OmpC), 1E54 (Omp32), 1OSM (Ompk36) and 3A2R (PorB). A multiple-sequence alignment revealed a complete coverage of the homology sequence, although only about 24% sequence identity was observed between the *BpsOmp38* and the template amino acid residues. Fifty structural models of the *BpsOmp38* trimers were further generated by the Modeller program, from which the "representative model" was defined as the one that minimized both the overall 'Modeller objective function' and the 'Dope score evaluation function'. Finally, the "final best model" was assessed with the energetic based validation suite ProQ [43] and the geometric based PROCHECK, with the latter showing only 2.8% of Ramachandran disallowed regions and absence of close (or "bad") contacts.

### 3. Results and discussion

We have previously reported the recombinant expression of the *BpsOmp38* gene in *E. coli* BL21 Origami (DE3) cells [36,37]. The recombinant *BpsOmp38* protein, which was in the form of inclusion bodies, was further refolded into trimeric form using 10% (w/v) Zwittergent™ 3-14. In the present study, the *BpsOmp38* gene, including a 20-amino acid signal peptide fragment, was subcloned into a pET23d(+) vector so it could be incorporated and fully expressed as a fully functional trimeric protein in the cell wall of the mutant *E. coli* BL21 (DE3) Omp8 strain. After extraction by 2% SDS and solubilization in 1% (v/v) octyl-POE, SDS-PAGE analysis demonstrated migration of the extracted porin as a protein band with an apparent MW of 100 kDa (Fig. 1A, lane 2). This was assumed to be the trimeric form of *BpsOmp38*. Upon heat treatment at 100 °C for 10 min, the presumed trimer was denatured and a new band with apparent MW of 35 kDa appeared as expected for the *BpsOmp38* monomer (Fig. 1A, lane 3).

When *BpsOmp38* was reconstituted in stable DPhPC lipid bilayers, the study protein (porin) behaved like an ion channel and allowed a specific current flow under controlled voltage application. Single trimeric *BpsOmp38* units in the bilayer membrane showed a characteristic conductance of  $2.7 \pm 0.3$  nS in 1 M KCl/20 mM HEPES pH 8.0 but the channels were prone to close at high transmembrane potentials (above  $\pm 100$  mV). A typical membrane current recording that was obtained for a single trimeric *BpsOmp38* channel at an elevated transmembrane potential of +150 mV is shown in Fig 1B. Within the time span of a few seconds, the fully open *BpsOmp38* channel changed sequentially by a three-step process into the fully closed state. This process appeared as a three-stage decrease in conductance signal and confirmed once again the trimeric channel organization that had already been suggested by the SDS-PAGE gel analysis (Fig. 1A). The biological relevance of the successive closure of the individual units of multimeric bacterial porins is poorly understood, bearing in mind that, *in vivo*, the potential difference across the bacterial outer membrane is usually negligible. On the other hand, parameters such as pH, ion composition of the internal and external

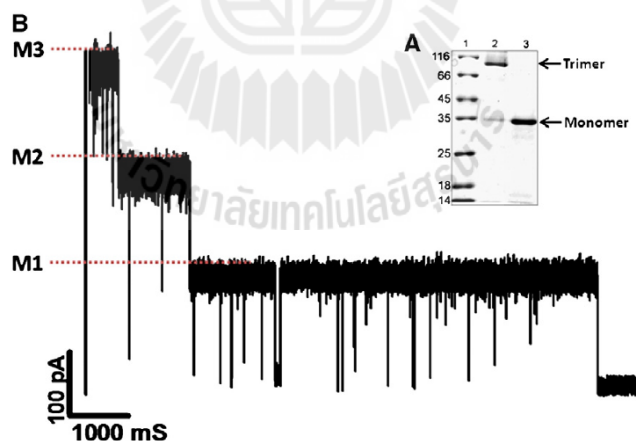
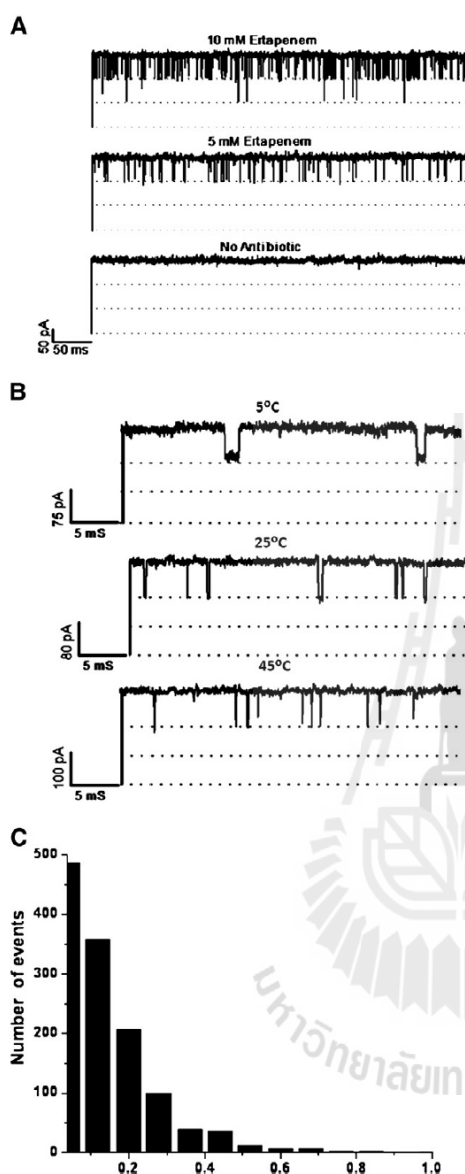


Fig. 1. Trimeric *BpsOmp38* porin from *Burkholderia pseudomallei*. The recombinant protein was expressed in a mutant *E. coli* BL21 (DE3) Omp8 strain lacking major intrinsic porins, isolated by sodium dodecyl sulfate-extraction and then solubilized by 1% (v/v) octyl-POE in 1 M KCl/20 mM HEPES, pH 8.0. A. Sodium dodecyl sulphate-polyacrylamide gel electrophoresis analysis of recombinant *BpsOmp38*. Track 1: low molecular weight protein markers (PageRuler, Fermentas Inc., USA); Track 2: intact *BpsOmp38* trimers under non-denaturing conditions; Track 3: *BpsOmp38* subunit after denaturing condition at 100 °C for 10 min. B. A single-channel recording of the *BpsOmp38* reconstituted in solvent-free DPhPC membranes. A three-step closure was induced by increasing the applied voltage to +150 mV.



**Fig. 2.** Kinetic analysis of antimicrobial agent translocation through *BpsOmp38*. **A.** Effect of ertapenem concentrations. No blockage event was detected when a single trimeric channel was recorded in the absence of antimicrobial agents, whereas complete blockage events were observed as a direct proportion to increased concentrations of ertapenem from 2.5, 5, 7.5, and 10 mM. Here, only 5 and 10 mM concentrations are presented. **B.** Effect of temperature. An increased number of blockage events were observed upon increases in temperature from 5, 10, 15, 20, 25, 30, 35, 40, and 45 °C. On the other hand, the dwell time of ertapenem translocation decreased exponentially with increasing temperatures. Here, only the BLM recordings at 5, 25 and 45 °C are presented. The single-channel recordings were recorded at +100 mV. Similar ion blockage patterns were also seen with +50 mV (not shown). **C.** Dwell time histogram. Ertapenem (10 mM) was added on the *cis* side of the lipid membranes. The average dwell time was obtained when the data was fitted using the standard exponential curve fit available in pClampfit v10.0.

**Table 1**  
Kinetic analysis of antibiotic translocation through the *BpsOmp38* channel.

| Antibiotic    | $k_{on}$ ( $s^{-1} M^{-1}$ ) | $k_{off}$ ( $s^{-1}$ ) | $K$ ( $M^{-1}$ ) |
|---------------|------------------------------|------------------------|------------------|
| Penicillin G  | n.d. <sup>a</sup>            | n.d.                   | n.d.             |
| Meropenem     | 25                           | 6700                   | 0.004            |
| Imipenem      | 150                          | 6700                   | 0.02             |
| Cefepime      | 1300                         | 5500                   | 0.24             |
| Ceftazidime   | 4200                         | 7000                   | 0.60             |
| Ertapenem     | 8200                         | 6900                   | 1.2              |
| Norfloraxacin | 300,000                      | 10,000                 | 30               |

<sup>a</sup> n.d. represents non-detectable event.

cell milieu and pressure influence, to a certain extent, the membrane potential and response to variations of these factors may contribute to the physiological significance of channel closing.

To study the translocation of drug molecules through the isolated porin, a potential was applied across the incorporating lipid membranes at which reconstituted *BpsOmp38* channels predominantly existed in their fully open state. Ion current blockages through the open channels were then analyzed after applying the selected antimicrobial agent to either the *cis* or *trans* side of the bilayer. Drug translocation trials were performed with a set of antimicrobial agents including three  $\beta$ -lactam antibiotics (penicillin G, meropenem, imipenem), two cephalosporins (cefepime, ceftazidime), one fluoroquinolone (norfloraxacin) and one carbapenem (ertapenem) (refer to Supplementary S2 for chemical structures). With the exception of penicillin G, all the test antimicrobial agents interacted with the *BpsOmp38* channel in such a way that spontaneous fast fluctuations of the BLM membrane current were induced. Overall, the number of current deflections in the recording of certain length varied linearly with concentrations that were independent of the type of antibiotic tested. Ertapenem, for example, produced a consistent response as shown in Fig. 2A. In high-time resolution current recordings, the

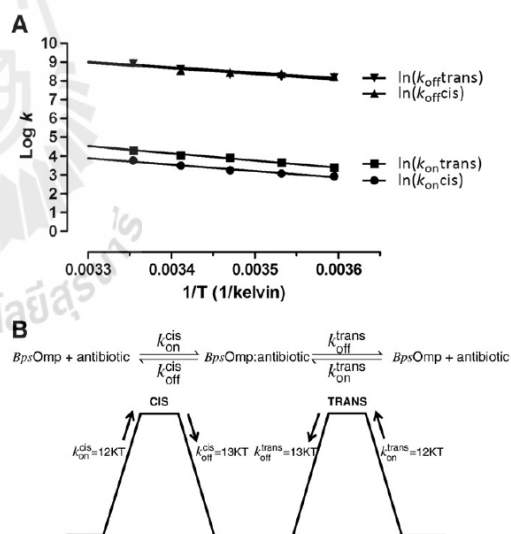


**Fig. 3.** Arrhenius plots for the ertapenem translocation through *BpsOmp38* protein pores. **A.** The logarithmic values of the on-rate and off-rate constants obtained from both *cis* and *trans* sides were plotted as a function of temperature. **B.** A diagram representing symmetrical values of the energy barriers required for ertapenem binding and releasing from most likely the identical affinity site localized within the *BpsOmp38* pore.



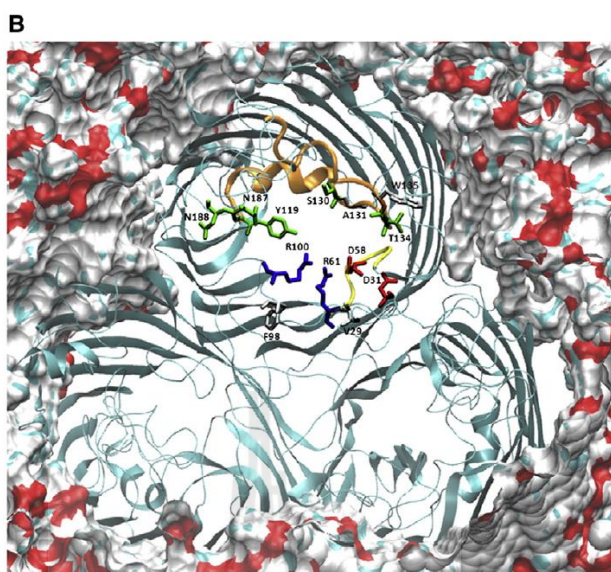


Fig. 4 (continued).

higher number of blocking events than when the same amount of the substrate was added to the *cis* side. Black lipid bilayer measurements taken between 5 and 45 °C in the presence and absence of the substrate demonstrated that temperature had a strong impact on the rate of ertapenem translocation through the *BpsOmp38* channel (Fig. 2B). At non-physiologically low temperature of 5 °C, relatively few membrane current blockages with rather long blocking times of over 1 ms were observed. Increasing the temperature to 45 °C elevated the frequency of current deflections while decreasing the dwell time ( $\tau$ ) of the penetrating molecules. Average  $\tau$  values for defined conditions in terms of temperature and concentration were obtained through a statistical analysis of raw BLM data and a single-exponential fitting of blockage time histograms as shown in Fig. 2C for ertapenem interaction with *BpsOmp38* measured at 25 °C. The average  $\tau$  of ertapenem molecules inside the *BpsOmp38* channel decreased exponentially with increasing temperature, did not appear to depend on the concentration of the antibiotic, nor was it influenced by the side of the BLM chamber to which the antimicrobial agent was added. Taken together, these observations support the existence of a single affinity site for the ertapenem molecules in the *BpsOmp38* channel. The rates of channel entry and exit are critical factors in the net flux of an antibiotic through a bacterial Omp pore. The BLM-based observation of the molecular interaction of ertapenem with the *BpsOmp38* channel at various temperatures and concentrations allowed calculation of: i) the drug binding kinetics and the second-order on-rate constant  $k_{on}$  ( $M^{-1} s^{-1}$ ), ii) the first-order off-rate constant  $k_{off}$  ( $s^{-1}$ ), and iii) the equilibrium binding constant  $K$  (the ratio of  $k_{on}/k_{off}$ ;  $M^{-1}$ ). Table 1 gives a comprehensive list of the three parameters  $k_{on}$ ,  $k_{off}$  and  $K$  for all seven antimicrobial agents whose translocation through the *BpsOmp38* channel was investigated in the present study (refer to Supplementary S3 for blockage characteristics of the ion flow through *BpsOmp38* by representatives of each class of the antimicrobial agents). Note that ion blockage by ertapenem applied to the *cis* side of the lipid membrane at a transmembrane potential +100 mV occurred with  $k_{on} = 8200 M^{-1} s^{-1}$  and a binding

constant of about  $1.2 M^{-1}$ . These values reasonably agree with those for the interaction of ertapenem with the major *Enterobacter aerogenes* Omp36 [30]. Furthermore, the off-rates did not vary significantly for this panel of antimicrobial agents, while a ranking of  $k_{on}$  and  $K$  saw the three  $\beta$ -lactam antibiotics with rather low values that were clearly at the bottom end, the two cephalosporin drugs at the middle, and carbapenem and fluoroquinolone antibiotics at top positions. Greater values of  $k_{on}$  and  $K$  indicated that translocation of the newer class of drugs through the *BpsOmp38* pore took place more rapidly.

Temperature dependence measurements were used to calculate the free energy profile of transporin antibiotic permeation. For ertapenem, the effective energy barriers ( $E$ ) to reach and cross the internal binding site of a *BpsOmp38* channel from the *cis* ( $E_{on,cis}$ ) or *trans* ( $E_{on,trans}$ ) side of the bilayer were estimated from the typical Arrhenius plots (Fig. 3A). The analysis of the relevant plots revealed that effective energy barriers  $E_{on,cis}$  and  $E_{on,trans}$ , representing the binding of ertapenem to the affinity site of a *BpsOmp38* protein pore at +100 mV transmembrane voltage, were estimated to be 12 kT. The Arrhenius plots for the off rates, which allowed calculation of the effective energy barriers  $E_{off,cis}$  and  $E_{off,trans}$  for the ertapenem release from the affinity site of the *BpsOmp38* channel at +100 mV, were 13 kT (see Fig. 3B). Estimation of symmetrical values of the energy barriers required for ertapenem binding and release from *cis*-to-*trans* side and from *trans*-to-*cis* side further supports a single affinity site inside the *BpsOmp38* channel as earlier on suggested.

The homology model of the porin *BpsOmp38* was built based on five different templates obtained from homologous Gram-negative bacterial porins with non-redundant structures (refer to Materials and methods). Despite an observed low-sequence identity (~24%), the overall fold of the generated *BpsOmp38* trimers was found to be conserved. The alignment in Fig. 4A shows that the target sequence is completely covered by the different templates and that a few insertions and deletions are all found in the extracellular loops except for the small protrusion of a four-residue loop in the middle of the

second strand of each monomer (see Fig. 4B). This small protrusion was also reported in the previously characterized Omp32 [44].

The BpsOmp38 model was compared with the structure of the porin OmpF, for which the structure–function relationship of antibiotic translocation has been extensively studied [34]. Compared with OmpF, however, the amino acid sequences of various regions that participate in pore-forming properties were found to be different. These include the L3 loop that forms the constriction region of the channel, the arginine residues at the mouth of the OmpF channel, and the basic cluster in the anti-L3 side. In the case of the BpsOmp38 channel, more acidic residues are observed instead in such regions. Within the known key residues of OmpF that were aligned with BpsOmp38, segments with conserved or amino acid substitutions are highlighted as shown in Fig. 4A.

Fig. 4B is a graphic representation of the modeled BpsOmp38 trimeric structure, when incorporated into phospholipid bilayer membranes. Highlights indicate an obstructing internal protrusion, as well as the polar to acidic character of certain channel wall residues that point towards the lumen of the pore. It is predictable that the substitutions from OmpF to BpsOmp38 of the residues: K16V29, V20D31, K80F108, D113S130, F118W135, R167N187, and R168N188 may have an effect on drug transport through the BpsOmp38 porin (see Fig. 4B). However, this hypothesis has to be confirmed by a combined approach, including microbiological assays, site-directed mutations and biophysical measurements, together with molecular dynamic simulations of antibiotic transport as previously described for OmpF [34,35].

In conclusion, the present study demonstrates, for the first time, the ion-channel properties of the outer membrane porin BpsOmp38 derived from the highly virulent and drug resistant bacterium *B. pseudomallei*. High-time resolution analysis of different classes of antimicrobial agents provided initial insights into the transport mechanisms of antimicrobial agents through the BpsOmp38 channel. We highly recommend further studies that base on thoughtfully genetically engineered BpsOmp38 and those that exploit joint applications of structural, functional and computational assays to develop highly efficacious drugs against clinical melioidosis.

#### Acknowledgments

This research was financially supported by the Alexander von Humboldt Foundation (Germany) through the Alexander von Humboldt Fellowships for Experienced Researchers, the Thailand Research Fund (Grant no: RMU5380055). This was supplemented by Suranaree University of Technology (Grant no: SUT 1-102-52-24-02) to WS and by the EU Grant MRTN-CT-2005-019335 (translocation) to EH.

#### Appendix A. Supplementary data

Supplementary data to this article can be found online at doi:10.1016/j.bbame.2010.10.018.

#### References

- [1] W.J. Wiersinga, T. van der Poll, N.J. White, N.P. Day, S.J. Peacock, Melioidosis: insights into the pathogenicity of *Burkholderia pseudomallei*, *Nat. Rev. Microbiol.* 4 (2006) 272–282.
- [2] S.J. Peacock, Melioidosis, *Curr. Opin. Infect. Dis.* 19 (2006) 421–428.
- [3] P. Aldhous, Tropical medicine: melioidosis? Never heard of it..., *Nature* 434 (2005) 692–693.
- [4] A.C. Cheng, B.J. Currie, Melioidosis: epidemiology, pathophysiology, and management, *Clin. Microbiol. Rev.* 18 (2005) 383–416.
- [5] J.B. Woods, Antimicrobials for biological warfare agents, in: L.L. Lindler, F.J. Lebeda, G.W. Korch (Eds.), *Biological Weapons Defense: Infectious Diseases and Counter Bioterrorism*, Humana Press Inc., Totowa, 2005, pp. 285–315.
- [6] Centers for Disease Control and Prevention. Bioterrorism Agents/Diseases, [www.bt.cdc.gov/agent/agentlist-category.asp](http://www.bt.cdc.gov/agent/agentlist-category.asp).
- [7] National Center for Zoonotic, Vector-Borne, and Enteric Diseases, Melioidosis, [www.cdc.gov/nczved/divisions/dfbmd/diseases/melioidosis](http://www.cdc.gov/nczved/divisions/dfbmd/diseases/melioidosis).
- [8] M.T.G. Holden, R.W. Titball, S.J. Peacock, A.M. Cerdeño-Tárraga, T. Atkins, L.C. Crossman, T. Pitt, C. Churcher, K. Mungall, S.D. Bentley, M. Sebailia, N.R. Thomson, N. Bason, I.R. Beacham, K. Brooks, K.A. Brown, N.F. Brown, G.L. Challis, I. Cherevach, T. Chillingworth, A. Cronin, B. Crosssett, P. Davis, D. DeShazer, T. Feltwell, A. Fraser, Z. Hance, H. Hauser, S. Holroyd, K. Jagels, K.E. Keith, M. Maddison, S. Moule, C. Price, M.A. Quail, E. Rabinowitsch, K. Rutherford, M. Sanders, M. Simmonds, S. Songsivilai, K. Stevens, S. Tumapa, M. Vesaratchaveit, S. Whitehead, C. Yeats, B.G. Barrell, P.C.F. Oyston, J. Parkhill, Genomic plasticity of the causative agent of melioidosis, *Burkholderia pseudomallei*, *Proc. Natl. Acad. Sci. USA* 101 (2004) 14240–14245.
- [9] L.A. Trunck, K.L. Probst, W. Wuthiekanun, A. Tuanyok, S.M. Beckstrom-Sternberg, J.S. Beckstrom-Sternberg, S.J. Peacock, P. Keim, S.W. Dow, H.P. Schweizer, Molecular basis of rare aminoglycoside susceptibility and pathogenesis of *Burkholderia pseudomallei* clinical isolates from Thailand, *PLoS Negl. Trop. Dis.* 3 (2009) e0000519.
- [10] S. Kanthawong, K. Nazmic, S. Wongratanaachewina, J.G.M. Bolscher, V. Wuthiekanun, S. Taweekaisupapong, In vitro susceptibility of *Burkholderia pseudomallei* to antimicrobial peptides, *Int. J. Antimicrob. Agents* 34 (2009) 309–314.
- [11] R. Karunakaran, S.D. Puthucherry, *Burkholderia pseudomallei*: in vitro susceptibility to some new and old antimicrobials, *Scand. J. Infect. Dis.* 39 (2007) 858–861.
- [12] F.M. Thibault, E. Hernandez, D.R. Vidal, M. Girardet, J.-D. Cavallo, Antibiotic susceptibility of 65 isolates of *Burkholderia pseudomallei* and *Burkholderia mallei* to 35 antimicrobial agents, *J. Antimicrob. Chemother.* 54 (2004) 1134–1138.
- [13] Y. Hara, R. Mohamed, S. Nathan, Immunogenic *Burkholderia pseudomallei* outer membrane proteins as potential candidate vaccine targets, *PLoS ONE* 4 (2009) e6496.
- [14] C. Druar, F. Yu, J.L. Barnes, R.T. Okinaka, N. Chantrata, S. Beg, C.W. Stratilo, A.J. Olive, C. Soltes, M.L. Russell, D. Limmathurotsakul, R.E. Norton, S.X. Ni, W.D. Picking, P.J. Jackson, D.I. Stewart, V. Tsvetnitsky, W.L. Picking, J.W. Cherwonogrodzky, N. Kethesana, S.J. Peacock, E.J. Wiersma, Evaluating *Burkholderia pseudomallei* Bip proteins as vaccines and Bip antibodies as detection agents, *FEMS Immunol. Med. Microbiol.* 52 (2008) 78–87.
- [15] A. Haque, K. Chu, A. Easton, M.P. Stevens, E.E. Galyov, T. Atkins, R. Titball, G.J. Bancroft, A live experimental vaccine against *Burkholderia pseudomallei* elicits CD4+ T cell-mediated immunity, priming T cells specific for 2 type III secretion system proteins, *J. Infect. Dis.* 194 (2006) 1241–1248.
- [16] J.A. Torres, M.V. Villegas, J.P. Quinn, Current concepts in antibiotic-resistant Gram-negative bacteria, *Experts Rev. Anti-Infect. Ther.* 5 (2007) 833–843.
- [17] A. Kumar, H.P. Schweizer, Bacterial resistance to antibiotics: active efflux and reduced uptake, *Adv. Drug Deliv. Rev.* 57 (2005) 1486–1513.
- [18] K. Poole, Mechanisms of bacterial biocide and antibiotic resistance, *J. Appl. Microbiol.* 92 (2002) 555–645.
- [19] B.G. Spratt, Resistance to antibiotics mediated by target alterations, *Science* 264 (1994) 388–393.
- [20] S. Galdiero, M. Galdiero, C. Pedone, Beta-barrel membrane bacterial proteins: structure, function, assembly and interaction with lipids, *Curr. Protein Pept. Sci.* 8 (2007) 63–82.
- [21] H. Nikaido, Molecular basis of bacterial outer membrane permeability revisited, *Microbiol. Molec. Biol. Rev.* 67 (2003) 593–656.
- [22] G.E. Schulz, The structure of bacterial outer membrane proteins, *Biochim. Biophys. Acta Biomembr.* 1565 (2002) 308–317.
- [23] H. Weingart, M. Petrescu, M. Winterhalter, Biophysical characterization of in- and efflux in Gram-negative bacteria, *Curr. Drug Targ.* 9 (2008) 789–796.
- [24] H.T. Tien, A.L. Ottova, The lipid bilayer concept and its experimental realization: from soap bubbles, kitchen sink, to bilayer lipid membranes, *J. Membr. Sci.* 189 (2001) 83–117.
- [25] M. Winterhalter, Black lipid membranes, *Curr. Opin. Colloid Interface Sci.* 5 (2000) 250–255.
- [26] J.-M. Pages, C.E. James, M. Winterhalter, The porin and the permeating antibiotic: a selective diffusion barrier in Gram-negative bacteria, *Nat. Rev. Microbiol.* 6 (2008) 893–903.
- [27] K.R. Mahendran, E. Hajjar, T. Mach, M. Lovelle, A. Kumar, I. Sousa, E. Spiga, H. Weingart, P. Gameiro, M. Winterhalter, M. Ceccarelli, Molecular basis of enrofloxacin translocation through OmpF, an outer membrane channel of *Escherichia coli*—when binding does not imply translocation, *J. Phys. Chem. B* 114 (2010) 5170–5179.
- [28] K.R. Mahendran, M. Kreir, H. Weingart, N. Fertig, M. Winterhalter, Permeation of antibiotics through *Escherichia coli* OmpF and OmpC porins: screening for influx on a single-molecule level, *J. Biomol. Screen.* 5 (2010) 302–307.
- [29] K.R. Mahendran, C. Chimerel, T. Mach, M. Winterhalter, Antibiotic translocation through membrane channels: temperature-dependent ion current fluctuation for catching the fast events, *Eur. Biophys. J.* 38 (2009) 1141–1145.
- [30] C.E. James, K.R. Mahendran, A. Molitor, J.-M. Bolla, A.N. Bessonov, M. Winterhalter, J.-M. Pagès, How  $\beta$ -lactam antibiotics enter bacteria: a dialogue with the porins, *PLoS ONE* 4 (2009) e5453.
- [31] T. Mach, P. Neves, E. Spiga, H. Weingart, M. Winterhalter, P. Ruggerone, M. Ceccarelli, P. Gameiro, Facilitated permeation of antibiotics across membrane channels—interaction of the quinolone moxifloxacin with the OmpF channel, *J. Am. Chem. Soc.* 130 (2008) 13301–13309.
- [32] E.M. Nestorovich, C. Danelon, M. Winterhalter, S.M. Bezrukov, Designed to penetrate: time-resolved interaction of single antibiotic molecules with bacterial pores, *Proc. Natl. Acad. Sci. USA* 99 (2002) 9789–9794.
- [33] M. Ceccarelli, C. Danelon, A. Laio, M. Parrinello, Microscopic mechanism of antibiotic translocation through a porin, *Biophys. J.* 87 (2004) 58–64.
- [34] E. Hajjar, K.R. Mahendran, A. Kumar, A. Bessonov, M. Petrescu, H. Weingart, P. Ruggerone, M. Winterhalter, M. Ceccarelli, Bridging timescales and length scales: from macroscopic flux to the molecular mechanism of antibiotic diffusion through porins, *Biophys. J.* 98 (2010) 569–575.

- [35] S. Pezeshki, C. Chimerel, A.N. Bessonov, M. Winterhalter, U. Kleinekathöfer, Understanding ion conductance on a molecular level: an all-atom modeling of the bacterial porin OmpF, *Biophys. J.* 97 (2009) 1898–1906.
- [36] J. Siritapetawee, H. Prinz, C. Krittanai, W. Suginta, Expression and refolding of Omp38 from *Burkholderia pseudomallei* and *Burkholderia thailandensis*, and its function as a diffusion porin, *Biochem. J.* 384 (2004) 609–617.
- [37] J. Siritapetawee, H. Prinz, W. Samosornsuk, R.H. Ashley, W. Suginta, Functional reconstitution, gene isolation and topology modelling of porins from *Burkholderia pseudomallei* and *Burkholderia thailandensis*, *Biochem. J.* 377 (2004) 579–587.
- [38] A. Prilipov, P.S. Phale, P. Van Gelder, J.P. Rosenbusch, R. Koebnik, Coupling site-directed mutagenesis with high-level expression: large scale production of mutant porins from *E. coli*, *FEMS Microbiol. Lett.* 163 (1998) 65–72.
- [39] R.M. Garavito, J.P. Rosenbusch, Isolation and crystallization of bacterial porin, *Methods Enzymol.* 125 (1986) 309–328.
- [40] J.P. Rosenbusch, Characterization of the major envelope protein from *Escherichia coli*. Regular arrangement on the peptidoglycan and unusual dodecyl sulfate binding, *J. Biol. Chem.* 249 (1974) 8019–8029.
- [41] B. Lugtenberg, L. Van Alphen, Molecular architecture and functioning of the outer membrane of *Escherichia coli* and other gram-negative bacteria, *Biochim. Biophys. Acta* 737 (1983) 51–115.
- [42] N. Eswar, B. Webb, M.A. Marti-Renom, M.S. Madhusudhan, D. Eramian, M.Y. Shen, U. Pieper, A. Sali, Comparative protein structure modeling using MODELLER, *Curr. Protoc. Protein Sci.* (2007), Chapter 2, Unit 2.9.
- [43] B. Wallner, A. Elofsson, Can correct protein models be identified? *Protein Sci.* 12 (2003) 1073–1086.
- [44] K. Zeth, K. Diederichs, W. Welte, H. Engelhardt, Crystal structure of Omp32, the anion-selective porin from *Comamonas acidovorans*, in complex with a periplasmic peptide at 2.1 Å resolution, *Structure* 15 (2000) 981–992.



# Molecular Uptake of Chitooligosaccharides through Chitoporin from the Marine Bacterium *Vibrio harveyi*

Wipa Suginta<sup>1\*</sup>, Watcharin Chumjan<sup>1</sup>, Kozhinjampara R. Mahendran<sup>2</sup>, Petra Janning<sup>3</sup>, Albert Schulte<sup>1</sup>, Mathias Winterhalter<sup>2</sup>

**1** Biochemistry-Electrochemistry Research Unit, Schools of Chemistry and Biochemistry, Institute of Science, Suranaree University of Technology, Nakhon Ratchasima, Thailand, **2** School of Engineering and Science, Jacobs University Bremen, Bremen, Germany, **3** Department of Chemical Biology, Max-Planck Institute of Molecular Physiology, Dortmund, Germany

## Abstract

**Background:** Chitin is the most abundant biopolymer in marine ecosystems. However, there is no accumulation of chitin in the ocean-floor sediments, since marine bacteria *Vibrios* are mainly responsible for a rapid turnover of chitin biomaterials. The catabolic pathway of chitin by *Vibrios* is a multi-step process that involves chitin attachment and degradation, followed by chitooligosaccharide uptake across the bacterial membranes, and catabolism of the transport products to fructose-6-phosphate, acetate and NH<sub>3</sub>.

**Principal Findings:** This study reports the isolation of the gene corresponding to an outer membrane chitoporin from the genome of *Vibrio harveyi*. This porin, expressed in *E. coli*, (so called *VhChiP*) was found to be a SDS-resistant, heat-sensitive trimer. Immunoblotting using anti-ChiP polyclonal antibody confirmed the expression of the recombinant ChiP, as well as endogenous expression of the native protein in the *V. harveyi* cells. The specific function of *VhChiP* was investigated using planar lipid membrane reconstitution technique. *VhChiP* nicely inserted into artificial membranes and formed stable, trimeric channels with average single conductance of  $1.8 \pm 0.13$  nS. Single channel recordings at microsecond-time resolution resolved translocation of chitooligosaccharides, with the greatest rate being observed for chitohexaose. Liposome swelling assays showed no permeation of other oligosaccharides, including maltose, sucrose, maltopentaose, maltohexaose and raffinose, indicating that *VhChiP* is a highly-specific channel for chitooligosaccharides.

**Conclusion/Significance:** We provide the first evidence that chitoporin from *V. harveyi* is a chitooligosaccharide specific channel. The results obtained from this study help to establish the fundamental role of *VhChiP* in the chitin catabolic cascade as the molecular gateway that *Vibrios* employ for chitooligosaccharide uptake for energy production.

**Citation:** Suginta W, Chumjan W, Mahendran KR, Janning P, Schulte A, et al. (2013) Molecular Uptake of Chitooligosaccharides through Chitoporin from the Marine Bacterium *Vibrio harveyi*. PLOS ONE 8(1): e55126. doi:10.1371/journal.pone.0055126

**Editor:** Daniel J. Muller, Swiss Federal Institute of Technology Zurich, Switzerland

**Received:** November 14, 2012; **Accepted:** December 18, 2012; **Published:** January 29, 2013

**Copyright:** © 2013 Suginta et al. This is an open-access article distributed under the terms of the Creative Commons Attribution License, which permits unrestricted use, distribution, and reproduction in any medium, provided the original author and source are credited.

**Funding:** This work is financially supported by the Thailand Research Fund (contract no. RMUS380055). WS was a Humboldt fellow under the Alexander von Humboldt Fellowship for Experienced Researchers, The Alexander von Humboldt Foundation, Germany. WC was funded by the Commission of Higher Education, Ministry of University Affairs (MUA), Thailand through a CHE-PHD-SW scholarship (contract no 60/2550). MW acknowledges funding through WI 2278/18-1 of the Deutsche Forschungsgemeinschaft (DFG). The funders had no role in study design, data collection and analysis, decision to publish, or preparation of the manuscript.

**Competing Interests:** The authors have declared that no competing interests exist.

\* E-mail: wipa@sut.ac.th

## Introduction

Chitin, a  $\beta$ -1,4-linked homopolymer of *N*-acetylglucosamine (GlcNAc), is the most abundant polysaccharide in marine ecosystems, because it is a major component of the shells of crustaceans and marine zoo-plankton. It has been estimated that multi-million tons of chitin-containing substances are produced annually in the aquatic biosphere [1]. However, there is no substantial accumulation of chitin on the ocean floor. This is because of bioconversion of this mass of biomaterials, primarily by marine bacteria of the family *Vibrionaceae* [2]. These bacteria utilize chitinous materials very efficiently, converting them into organic compounds that then can be used as nitrogen and carbon sources.

The catabolic cascade of chitin utilization by marine *Vibrios* has been demonstrated elegantly in *Vibrio fischeri* [3–8] and *V. cholerae* [9,10]. The cascade incorporates a large number of genes and

enzymes, which are orchestrated in a complex signal transduction pathway [9,11]. Roseman and co-workers previously identified chitoporin (ChiP) from *V. fischeri* [12] and suggested that it acts as a chitooligosaccharide-specific channel, based on their findings that expression of native ChiP was significantly induced when the *V. fischeri* cells were grown in the presence of chitooligosaccharides (GlcNAc<sub>2-6</sub>). A null mutant of *V. fischeri* ChiP also showed an impaired growth in the culture supplemented with chitotriose. Phylogenetic analysis of marine bacteria of the *Vibrionaceae* family identified a *chiP* gene in 16 out of 19 species [13]. Such results indicate that this protein is well conserved within this family. DNA microarray expression profiles further confirmed that expression of the *chiP* gene in *V. cholerae* responded positively to chitin oligosaccharides and that the genes responsible for chitin degradation are under the stringent control of the *chiS* regulon [6,13].

Although ChiP was identified more than a decade ago, its physiological function as a chitooligosaccharide-specific channel remains unproved. Here, we report cloning and recombinant expression of chitoporin (referred to as *Vh*ChiP) from the marine bacterium *V. harveyi* (formerly *V. carchariae*) type strain 650. The physicochemical properties of *Vh*ChiP were determined using a planar black lipid membrane (BLM) reconstitution technique. High-time resolution single channel current recordings, together with liposome swelling assays, provide strong evidence that *Vh*ChiP is a highly specific channel for the molecular uptake of chitin oligosaccharides.

## Methods

### Ethics Statement

The anti-rabbit polyclonal antibody production procedure was approved by the Animal Care Commission of Suranaree University of Technology. Two adult (8-week-old) female rabbits were purchased from the Animal Caring Center, Mahidol University, Bangkok, Thailand. The rabbit was housed in a standard animal facility under conditions of controlled temperature (25°C) and photoperiod (a 12:12-hour light/dark schedule), with food and water provided ad libitum.

### Bacterial strains and vectors

*V. harveyi* type strain 650 was a marine isolate from Greek sea bass and was a gift from Professor Brian Austin, Heriot-Watt University, Edinburgh, United Kingdom. *E. coli* strain DH5 $\alpha$  was used for routine cloning and plasmid preparations. pGEM<sup>®</sup>-T easy vector used for subcloning purpose was a product of Promega (Promega Pte Ltd, Singapore Science Park I, Singapore). The pET23d(+) expression vector and *E. coli* mutant strain BL21(DE3) Omp8 Rosetta were gifts from Professor Dr. Roland Benz, Jacobs University Bremen, Germany. The *E. coli* mutant was genetically engineered to have defective genes encoding the major outer membrane porins: OmpA, OmpC, OmpF and LamB [14] and was therefore suitable for production of recombinant porin.

### Gene identification, cloning and sequencing

A BlastP search using chitoporin from *V. furnissei* (UniProtKB/TrEMBL entry: Q9KK91 and ref. 12) as protein template identified putative chitoporins from several marine bacteria in family *Vibrionaceae*, including a hypothetical protein VIB-HAR\_01269 (accession number YP\_001444474) from *V. harveyi* type strain ATCC BAA-1116 BB120. Therefore, specific oligonucleotides were designed from the hypothetical gene of the BAA-1116 BB120 strain in order to obtain the gene encoding chitoporin from our laboratory strain (*V. harveyi* type strain 650). Genomic DNA was prepared from this bacterium using PureLink<sup>™</sup> Genomic DNA Kits (Invitrogen, Gibbstai Company Ltd., Bangkok, Thailand) and used as the DNA template for PCR amplification. The oligonucleotides used for amplification were 5'-ATAC-CATGCGTCTTACCTAAAGAAAAG-3' for the forward primer and 5'-AACCTCGAGTTAGAAGTAGTATTCAA-CAC-3' for the reverse primer. The PCR product was of the expected size (1.1 kbp) and was cloned into pET23d(+) expression vector using *Nco* I and *Xho* I cloning sites (sequences underlined) following the protocol supplied by the manufacturer. Nucleotide sequences of sense and anti-sense strands of the PCR fragment were determined by automated sequencing (First BASE Laboratories Sdn Bhd, Selangor Darul Ehsan, Malaysia).

### Recombinant expression and protein purification

*E. coli* BL21 (DE3) Omp8 Rosetta host strain was transformed with the plasmid pET23d(+)/*chiP*. Expression and preparation of the recombinant ChiP followed the protocols described by Garavito and Rosenbusch [15] and Rosenbusch [16]. In brief, transformed cells were grown at 37°C in Luria-Bertani (LB) liquid medium containing 100  $\mu\text{g mL}^{-1}$  ampicillin and 25  $\mu\text{g mL}^{-1}$  kanamycin. At an OD<sub>600</sub> reading of 0.5–0.7, IPTG (isopropyl  $\beta$ -D-thiogalactoside) was added to a final concentration of 0.5 mM. Cell growth was continued for a further 6 h and cells were then harvested by centrifugation at 4,500 $\times$ g at 4°C for 20 min. The cell pellet was resuspended in a buffer containing 20 mM Tris-HCl, pH 8.0, 2.5 mM MgCl<sub>2</sub>, 0.1 mM CaCl<sub>2</sub>, 10  $\mu\text{g mL}^{-1}$  DNase I and 10  $\mu\text{g mL}^{-1}$  RNase A. Cells were lysed on ice by sonication for 10 min (30% duty cycle; amplitude setting 20%) using a Sonopuls Ultrasonic homogenizer with a 6-mm-diameter probe. The recombinant *Vh*ChiP was extracted from the peptidoglycan layer with sodium dodecyl sulphate (SDS) based on the method of Lugtenberg and Alphen [17]. Briefly, SDS was added to the cell suspension to a final concentration of 2% (v/v) and incubation was carried out for 1 h at 60°C with gentle shaking. The crude extract was then centrifuged at 40,000 $\times$ g for 60 min at 4°C. The pellet, which at this stage included the cell envelopes, was re-suspended in 20 mM phosphate buffer, pH 7.4, containing 0.125% (v/v) octyl-POE (n-octyl polyoxyethylene; ALEXIS Biochemicals, Lausanne, Switzerland), using a Potter-Elvehjem homogenizer. The suspension was incubated at 37°C with gentle shaking for 1 h and then centrifuged at 100 000 $\times$ g at 4°C for 40 min. The new pellet, now rich in outer membranes, was resuspended in 20 mM phosphate buffer, pH 7.4 containing 5% (v/v) octyl-POE and the suspension incubated at 37°C for 60 min. Insoluble material was removed by centrifugation at 100,000 $\times$ g at 20°C for 40 min. After exchange of the detergent to 0.2% (v/v) LDAO (lauryldimethylamine oxide; Sigma-Aldrich Pte. Ltd., Singapore) by dialysis, the *Vh*ChiP-rich sample was subjected to ion-exchange chromatography using a Hitrap Q HP prepacked column (5 $\times$ 1 mL) connecting to an AKTA Prime plus FPLC system (GE Healthcare Life Sciences, Life Sciences Instruments, ITS (Thailand) Co., Ltd., Bangkok, Thailand). Bound proteins were eluted with a linear gradient of 0–1 M KCl in the phosphate buffer, containing 0.2% (v/v) LDAO. Purity of the eluted proteins was confirmed by SDS-PAGE. Fractions containing only *Vh*ChiP were pooled and the protein concentration was determined using the Pierce BCA protein assay kit (Bio-Active Co., Ltd., Bangkok, Thailand).

### Antibody production and immunological analysis

Production of anti-*Vh*ChiP antiserum was carried out using an in-gel method. Outer membrane fraction extracted by 5% (v/v) octyl-POE was applied to eight wells in parallel on an 8% polyacrylamide gel. Following electrophoresis and Coomassie Blue staining, the proteins were resolved into two bands. The upper band, just above 40 kDa, was identified by mass spectrometry as *E. coli* OmpN, while the lower band, slightly below 40 kDa, was chitoporin (*Vh*ChiP). The lower bands were excised from the gels, combined (ca. 80  $\mu\text{g}$  protein) and homogenized in 200  $\mu\text{L}$  PBS, pH 7.4, then emulsified with 500  $\mu\text{L}$  Freund's complete/incomplete adjuvant (Pierce). The emulsified mixture was injected subcutaneously into a female white rabbit to produce *Vh*ChiP antiserum. Antibody titres and cross-reactivities against other membrane proteins, including *E. coli* OmpF, *E. coli* OmpN and *Burkholderia pseudomallei* Omp38 were checked by Western blotting. Signals representing antibody-protein interaction were detected with HRP-conjugated IgG using the enhanced chemiluminescence method (ECL, Amersham, UK). Anti-OmpN serum was prepared

Chitoporin from *Vibrio harveyi*

**Figure 1. Alignment of the putative *V. harveyi* chitoporin sequence with other sugar-specific porins.** Amino acid sequences of *V. furnissii* chitoporin (Q9KK91), *E. coli* LamB or maltoporin (P02943), and *S. typhimurium* ScrY (P22340) were retrieved from the SwissProt/UniProtKB protein databases, aligned using “CLUSTALW” algorithm in the DNASTAR package, and displayed in Genedoc. The secondary structure of VhChiP was constructed by ESPrnt v. 2.2 according to the structure of *Delphinus acidovorans* Omp32 (pdb 2GFR and ref 37). The residues that are aligned with Y6, Y41, Y118, W74, W358, and W420 of *E. coli* LamB are shaded in magenta. Green shading refers to amino residues conserved within the four sequences.  $\beta$ -strands are represented as green lines with an arrow. doi:10.1371/journal.pone.0055126.g001

using purified *E. coli* OmpN, its titres and cross-reactivities being tested in the same way as the VhChiP antiserum.

For expression of native VhChiP, a 5-mL overnight culture of *V. harveyi* 650 grown in marine medium [18] was transferred to a 2-L flask containing 500 mL of marine medium. The cells were grown at 30°C with agitation until OD<sub>600</sub> reached 0.6, then 1% (wet w/v) colloidal chitin was added to induce chitoporin expression. Aliquots of 1 mL of cell culture were taken at various time points (1, 2, 3, 4, 5, and 6 h). Cell pellets collected after centrifugation were solubilized in 5× SDS-gel loading buffer, and then analyzed by SDS-PAGE, followed by western blotting.

#### Black lipid bilayer measurements and single channel analysis

Black lipid bilayer (BLM) measurements and single channel analysis were performed as described elsewhere [19–24]. The lipid bilayer cuvette consisted of two chambers with a 25  $\mu$ m-thick Teflon film sandwiched in between. The latter had a small aperture of 60–100  $\mu$ m in diameter across which a virtually solvent free planar lipid bilayer was formed. The chambers were filled with electrolyte solution and an electrode (Ag/AgCl electrodes; World Precision Instruments, Sarasota, FL) immersed on either side of the Teflon film. The electrolyte used was 1 M KCl adjusted to pH 7.5, and buffered by 20 mM HEPES. 1,2-Diphytanoyl-sn-glycero-3-phosphatidylcholine (DPhPC; Avanti Polar Lipids, Alabaster, AL) lipid was used for lipid bilayers formation. In order to form the bilayer first the aperture was pre-painted with 1  $\mu$ L of 1% (v/v) hexadecane in pentane (Sigma Aldrich). One of the electrodes

was used as ground (*cis*) whereas the other electrode was connected (*trans*) to the headstage of an Axopatch 200B amplifier (Axon Instruments, Foster City, CA). Trimeric VhChiP channel (50–100 ng mL<sup>-1</sup>) was added to the *cis* side of the lipid membrane. At applied transmembrane potentials of  $\pm$ 200 mV, a single channel was frequently inserted within a few minutes. The protein solution in the chamber was gently diluted out by multiple additions of the working electrolyte to prevent multiple insertions. Single channel current measurements were performed with an Axopatch 200B amplifier (Molecular Devices, Sunnyvale, CA, U.S.A.) in the voltage clamp mode, with the internal filter set at 10 kHz. Amplitude, probability, and single channel analyses were performed using pClamp v.10.0 software (all from Molecular Devices, Sunnyvale, CA).

To investigate sugar translocation, a chito oligosaccharide was added to either the *cis* or the *trans* side of the chamber to a final concentration of 80  $\mu$ M. Occlusions of ion flow observed as a result of sugar diffusion through the inserting channel were usually recorded for 2 min. To see the effect of sugar translocation on individual subunit blockages, discrete concentrations of chito hexaose (1, 120, and 400  $\mu$ M) were tested.

#### Liposome swelling assay

Trimeric VhChiP channel was reconstituted into liposomes as described previously [25,26]. *E. coli* total lipid extract was used to form liposomes and 15% dextran (MW 40,000) was entrapped in the liposomes. The size of the formed liposomes was checked using a Nano-ZS ZEN3600 zetasizer. The isotonic solute concentration

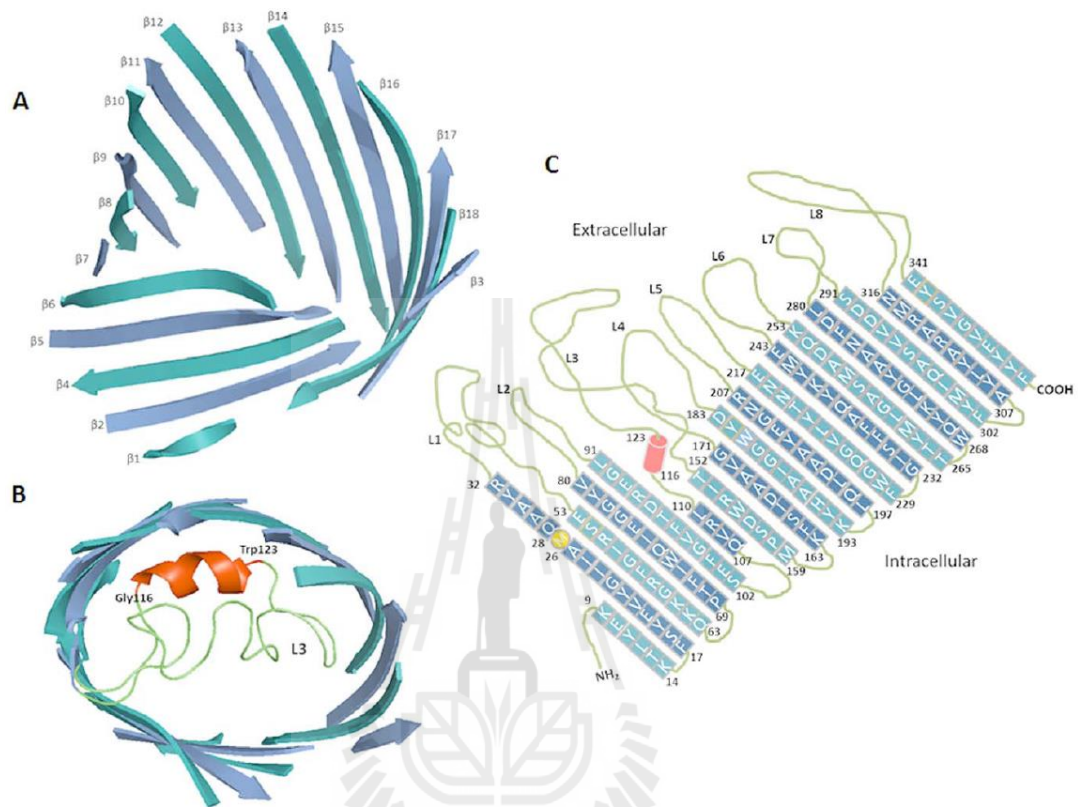


**Figure 2. The Swiss-Model 3D-structure of *V. harveyi* chitoporin.** A) Side view of a ribbon representation of VhChiP. The homology structure was constructed by the SWISS-MODEL program using an automated mode (<http://swissmodel.expasy.org/>). The x-ray structure of *D. acidovorans* Omp32 (pdb 2GFR) was selected as structure template (see texts). B) Top view of the modeled structure, showing L3 as the pore-confining loop with a short helix consisting 8 amino acids (G116-W123) presented in red. C) Transmembrane domains of VhChiA were depicted based on the homology structure (Fig. 2A–B) and the structure-based alignment (Fig. 1). doi:10.1371/journal.pone.0055126.g002

was determined with different concentrations of raffinose solution (prepared in 20 mM HEPES buffer, pH 7.5) added into the protoliposome suspension. The value obtained for isotonic concentration of raffinose was used as an approximation to facilitate the adjustment of isotonic concentrations for different solutes. Twenty microliters of liposome or proteoliposome solution was diluted into 500  $\mu$ L of the isotonic test solution in a 1-mL cuvette and mixed manually. The initial swelling rate upon addition of the isotonic sugar solutions (maltose, sucrose, maltopentaose, maltohexaose, and chitohexaose) was monitored using a UV-Vis spectrophotometer with the wavelength set at 500 nm. The absorbance change over the first 60 sec was used to estimate the swelling rate ( $s^{-1}$ ) following the equation:  $\Phi = (1/A_i)dA/dt$ , in which  $\Phi$  is the swelling rate,  $A_i$  the initial absorbance, and  $dA/dt$  the rate of absorbance absorbance change during the first 60 s. The swelling rate of each sugar was normalized by setting the rate of arabinose (MW 150.14 Da) to 100%. Values presented are averages obtained from four to six determinations. Protein-free liposomes and proteoliposomes without sugars were used as negative controls.

## Results

### Gene isolation, cloning, sequence analysis and transmembrane topology

The availability of the complete genome sequence of *V. harveyi* type strain ATCC BAA-1116 BB120 in the GenBank® database enabled us to identify an open reading frame that encodes a hypothetical chitoporin (ChiP). To isolate the gene encoding ChiP from the genome of the closely related species *V. harveyi* type strain 650, specific oligonucleotide primers were designed, based on the identified *chiP* gene from the BAA-1116 BB120 strain. The full-length *chiP* cDNA was amplified by the PCR technique. The nucleotide sequence of the identified gene comprises 1,125 bps, which was translated to a putative polypeptide of 375 amino acids, including the 25-aa signal sequence. The theoretical mass of the full-length VhChiP was 41,089.10 Da, with a predicted  $pI$  of 4.09. BLAST searching of the translated VhChiP sequence gave high-score hits with putative chitoporin of several species in the family *Vibrionaceae* in the SwissProt/UniProtKB database.

VhChiP shows low sequence identity (<20%) with other functionally characterized outer membrane porins, such as *E. coli*

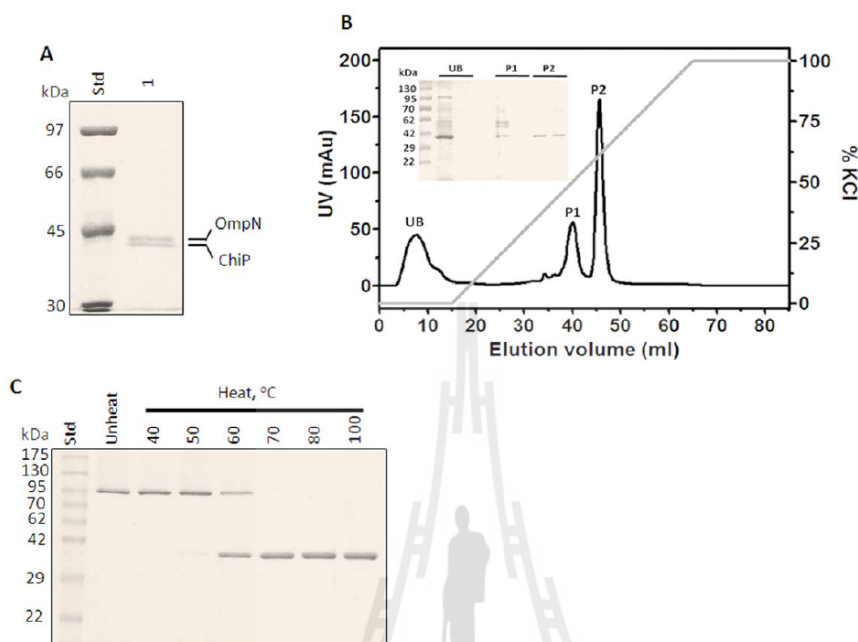


**Figure 3. SDS-PAGE analysis of *V. harveyi* chitoporin.** A) SDS-PAGE of outer membrane proteins extracted with 2% (w/v) SDS, followed by 5% (v/v) octyl-POE. *E. coli* OmpN and *VhChiP* bands were identified by mass spectrometry. B) Chromatographic profile of *VhChiP* purification with a Hitrap Q HP prepacked column (5 × 1 mL) connecting to an AKTA Prime plus FPLC system. The column was eluted with a linear gradient of 0–1 M KCl. SDS-PAGE analysis of unbound (UB) and bound fractions P1 and P2 is shown in an inset. C) Heat stability of *VhChiP*. The purified *ChiP* was subjected to different temperatures (40–100 °C) and then run on a 10% polyacrylamide gel.  
doi:10.1371/journal.pone.0055126.g003

OmpF (P02931), *E. coli* OmpC (P06996), *E. coli* OmpA (P0A910), *E. coli* OmpN (P47747), *Pseudomonas fluorescens* OprD (Q3LAG8), and *Neisseria gonorrhoeae* PorB (Q5XKX0). Fig. 1A presents amino acid sequence alignment of *VhChiP* with chitoporin from *V. fischeri* (accession number 09KK91) [12], *E. coli* LamB or maltoporin (maltose-specific porin) (P02943) [27], and *Salmonella typhimurium* ScrY (sucrose-specific porin) (P22340) [28]. The sequence identity of *VhChiP* with *V. fischeri* chitoporin is 40%, while it shows remarkably low identity with other sugar-specific porins: LamB (15.3%), and ScrY (12.9%). It is also only 15.7% identical to a carbohydrate-selective porin *Pseudomonas aeruginosa* OprB [29,30]. In LamB, six aromatic residues (Y6, Y41, W74, F229, W358 and W420) located in the pore lumen form a polar track, which aids ion and sugar transport [31–34]. Y118, on the other hand, controls the central constriction of the LamB channel [35,36].

Sequence alignment (Fig. 1) shows that the residues Y6, Y41, W74, W358 and W420 of LamB are well aligned with Y78, Y118, W151, F435 and W482, respectively, of ScrY. In marked contrast, *VhChiP* displays substantial sequence dissimilarities with both LamB and ScrY. Only two residues in LamB (W74 and W358) are aligned with F64 and Y310 of *VhChiP*. Furthermore, Y118 of LamB shows no match with any aromatic residue of *VhChiP*, which indicates that the functionality of pore constriction by Y118, as found in LamB, is governed by a different residue located elsewhere in the *VhChiP* sequence.

Submission of the putative sequence of *VhChiP* through the Swiss-Model database generated a structural model of *VhChiP* (Fig. 2) using *Delftia acidovorans* Omp32 as template (pdb 2GFR) [37]. Compared with all porins with known 3D-structures, *VhChiP* is closest to Omp32 with sequence identity of 20.5%. Fig. 1 shows the secondary structural features of *VhChiP*, which are similar to those of most Gram negative bacterial porins, with 18  $\beta$ -strands forming a barrel structure (Fig. 2A). These predicted 18 anti-parallel  $\beta$ -strands make up only 16 putative membrane-spanning domains, as strand  $\beta$ 2 is connected with  $\beta$ 3 and forms the first transmembrane domain, whereas strand  $\beta$ 1 with  $\beta$ 18 are part of the last domain (Figs. 1 and 2A). The predicted transmembrane topology (Fig. 2C) indicates considerable irregularity of the extracellular loops (L1–L3), while the eight periplasmic turns are short and of similar length. The longest extracellular loop (L3), comprising 41 amino acids (G111→N151), lies between strands  $\beta$ 7 and  $\beta$ 8. A typical right-handed  $\alpha$ -helix is found at the early part of L3 at positions P116 to W123 (Fig. 2B). This loop, known as a pore-confined loop, is responsible for the size-selectivity of sugar-specific porins (LamB and ScrY) [28,31] and general diffusion porins [38,39].

#### Recombinant expression, purification and mass identification

After the correct nucleotide sequence was confirmed, the full-length *chiP* DNA obtained from PCR amplification was cloned into pET23D(+) expression vector, which was ready to be

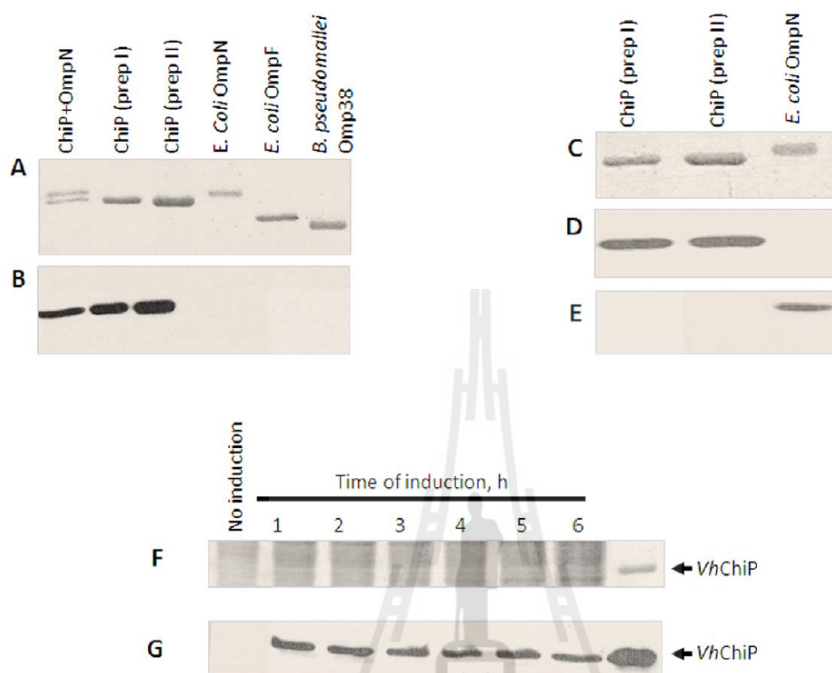


**Figure 4. Immunoblot analysis of *V. harveyi* chitoporin.** A–B: Cross-reactivity of *VhChiP* antiserum with other outer membrane porins. A. Coomassie blue-stained SDS-polyacrylamide gel, and B. The corresponding immunoblot detected with anti *VhChiP* antibody. C–D: Cross-reactivity of *VhChiP* and *E. coli* OmpN with anti *VhChiP* and anti OmpN antibodies. C. Coomassie blue-stained SDS-polyacrylamide gel, D. and E. The corresponding immunoblots showing cross-reactivity with anti *VhChiP* antiserum, and anti OmpN antiserum, respectively. F–G: Endogenous expression of chitoporin in *V. harveyi* F. Coomassie blue-stained SDS-polyacrylamide gel, and G. Immunoblot of cell lysate of *V. harveyi* cultured in the presence of 1% (w/v) colloidal chitin at various times of 1–6 h. doi:10.1371/journal.pone.0055126.g004

expressed in *E. coli* BL21(DE3) Omp8 Rosetta strain. The recombinant protein was expressed with the 25-amino acid *N*-terminal signal sequence attached, to aid protein targeting to the bacterial cell envelope. After proteolytic removal of the signal sequence, the mature *VhChiP* contains 350 amino acid residues and has a predicted MW of 38,508.97 Da. After cell-wall extraction by SDS, following 0.125% (v/v), and then 5% (v/v) octyl-POE, the solubilized fraction contained enriched *VhChiP* and a contaminant, which was later identified as *E. coli* OmpN. SDS-PAGE analysis (Fig. 3A) revealed two major protein bands. The upper band migrated close to 40 kDa and the lower band migrated to slightly lower than 40 kDa. Identification of tryptic peptides by high resolution ESI MS gave a primary hit with gi | 3273514 porin OmpN from *E. coli* for the higher MW band, while the lower protein band was identified as gi|28897534 putative chitoporin from *V. parahaemolyticus* RIMD 2210633, as well as gi|153834464 outer membrane protein from *V. harveyi* HY01, and gi|156973567 hypothetical protein from *V. harveyi* ATCC BAA-1116. Given that no functionally-identified chitoporin of the *V. harveyi* species is available in the NCBI database, we assume that the identified peptides of the lower MW protein were derived from chitoporin (see Fig. S1: nine tryptic peptides are unambiguously identified within the internal segments of the putative *VhChiP* sequence).

After several attempts to remove OmpN contamination, we discovered that OmpN was solubilized in 5% octyl-POE, but not in 3%. Therefore, later batches of *VhChiP* were prepared in 3% octyl-POE so that OmpN remained in the precipitate. To obtain highly purified *VhChiP* for functional characterization, the detergent-extracted *VhChiP* was further purified by ion exchange chromatography using a HiTrap DEAE FF column. Fig. 3B shows a chromatographic profile from *VhChiP* purification. After removal of the unbound fraction ('UB'), the bound proteins were then eluted in two peaks ('P1' and 'P2') when a linear gradient of 0–1 M KCl was applied. SDS-PAGE analysis shows that *VhChiP* was in the second peak (P2) and the protein was purified to homogeneity (Fig. 3B, inset) by ion-exchange chromatography. The pooled sample from peak P2 was heat-treated at different temperatures for 10 min, and then analyzed by SDS-PAGE. Fig. 3C shows migration of the purified *VhChiP* to above 95 kDa, corresponding to the trimeric form, when unheated (lane 1). The trimer remained intact when the temperature was raised to 40°C, but began to dissociate at 50°C. At 60°C, more than half of the *VhChiP* trimers were dissociated to monomers and at 70°C or above, no trimers remained. These results indicate that *VhChiP* is a heat-sensitive, SDS-stable trimer; each subunit has apparent MW of approximately 39 kDa, consistent with the predicted MW of the translated polypeptide lacking the signal sequence.

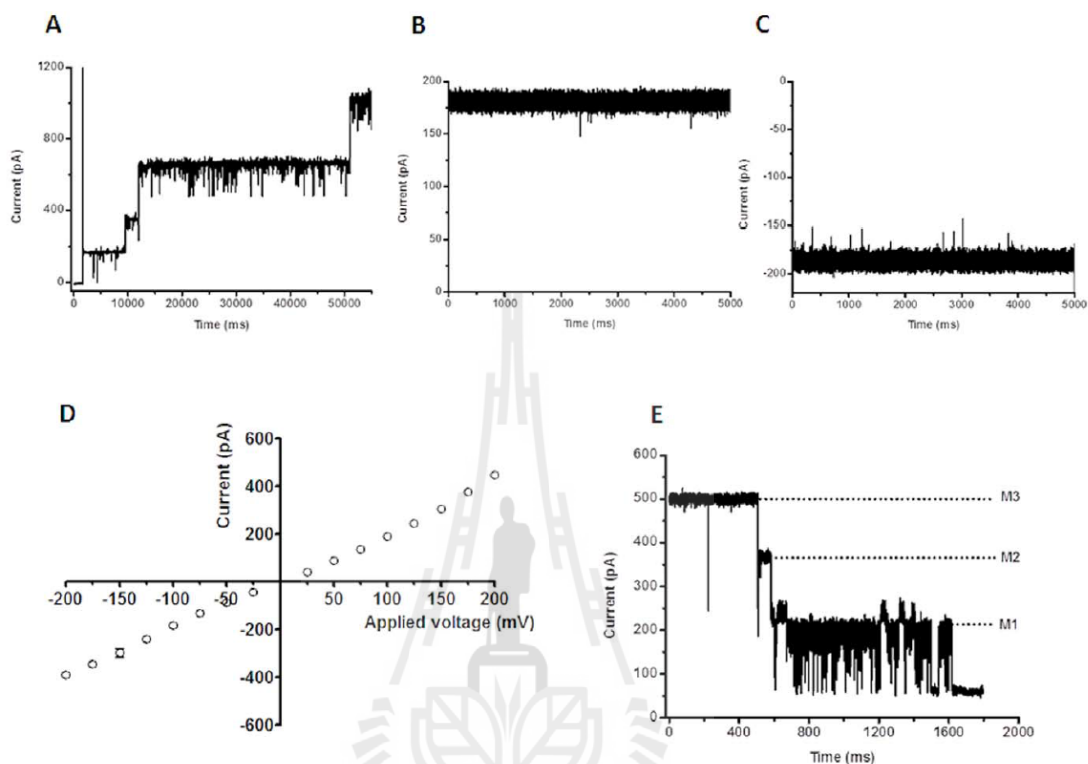


**Figure 5. Single channel recordings of chitoporin in artificial lipid membranes.** Trimeric VhChiP was expressed in *E. coli* BL21 (DE3) Omp8 Rosetta mutant, lacking major intrinsic porins. The protein was isolated by SDS-extraction, and then solubilized with 3% (v/v) octyl-POE. The protein was further purified by ion exchange chromatography as described in the text. The BLM measurements were carried out in the electrolyte containing 1 M KCl in 20 mM HEPES, pH 7.5. The protein was added on the *cis* side of the chamber. A. Multiple insertions of VhChiP were induced at an applied potential of +100 mV. B. Typical ion current trace of a single channel at fully-open state of VhChiP at applied voltage of +100 mV; and C. at -100 mV. The ion currents were normally recorded for a period of 120 s. D. Analysis of current-voltage (I-V) relationship. The average current values were obtained by stepwise ramping of the potential, preformed in triplicate. E. Three-step closure, induced by increasing the applied voltage to +200 mV. doi:10.1371/journal.pone.0055126.g005

#### Immunoblotting and endogenous expression of VhChiP

To ensure that the recombinant protein obtained was chitoporin and not contaminating OmpN, which was co-expressed by the *E. coli* host strain Omp8 Rosetta, polyclonal antibodies against OmpN and VhChiP were raised independently. Fig. 4A shows a Coomassie Blue stained gel of different porins, corresponding to the immunoblot with anti-VhChiP antiserum (Fig. 4B). It is clear that the antibody recognized only the VhChiP band (Fig. 4A lower band and lanes 2 and 3), but not *E. coli* OmpN (lane 1, upper band and lane 4), *E. coli* OmpF (lane 5) and *B. pseudomallei* Omp38 (lane 6). The results suggest no cross reactivity of anti-VhChiP antibody with other porins. Fig. 4C-E further confirmed that there was no cross-reactivity of the anti-VhChiP serum with OmpN and anti-*E. coli* OmpN serum with VhChiP. Anti-VhChiP serum recognized only VhChiP (Fig. 4D, lanes 1 and 2), and correspondingly, anti-OmpN serum reacted only with OmpN (Fig. 4E, lane 3).

To determine whether expression of native chitoporin in *V. harveyi* type strain 650 was controlled by the chitin-induced operon, expression profiles of VhChiP were evaluated after the bacterial cells were grown in the presence of chitin. Fig. 4F shows a

Coomassie stained gel of the cell lysates prepared at different times of induction, while Fig. 4G shows the corresponding immunoblot with anti-VhChiP antibody. It is seen that the antibody reacted with the protein bands in the position of purified VhChiP when the cells were exposed to 1% (w/v) colloidal chitin for 1 h or more. No positive signal was detected in the lysate prepared from the cells grown in the absence of chitin. We also observed chitoporin expression in the *V. harveyi* cells after induction with crystalline  $\alpha$ -chitin, but the signals were not as strong as when colloidal chitin was used (data not shown).

#### Single channel properties of VhChiP and chitin oligosaccharide translocation

The pore-forming properties of VhChiP were investigated at the molecular level using a planar lipid bilayer (BLM) set-up for ion current recordings. The signals for functional analysis were acquired on application of a small potential across two Ag/AgCl wires, one either side of an artificial bilayer of diphytanoylphosphatidylcholine (DPhPC) in 1 M KCl (pH 7.5), and the parallel measurement of the electrostatically driven ion (current) flow through the normally non-conducting lipid membrane, on the

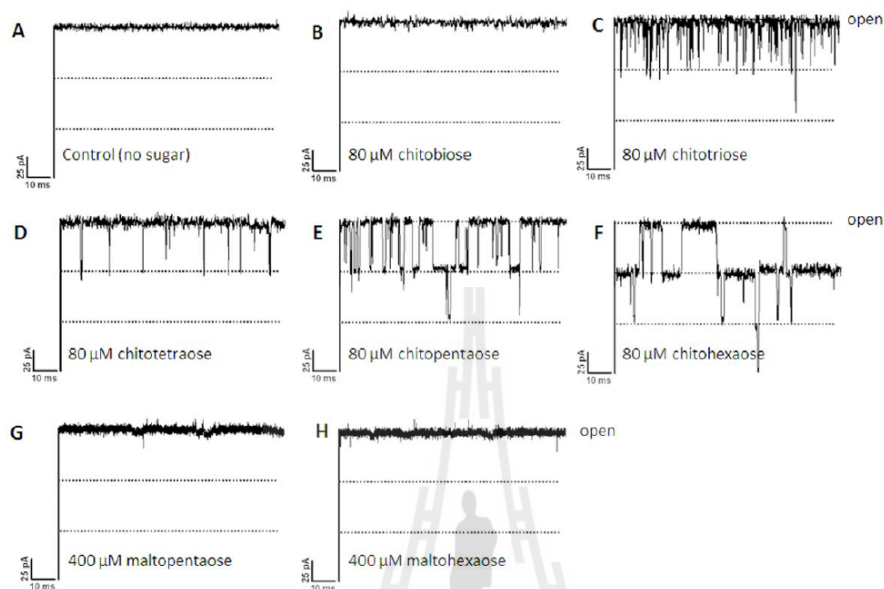


**Figure 6. Effect of chitooligosaccharides on chitoporin ion currents.** A single channel of *Vh*ChiP was inserted in the artificial membrane in A, a fully open state. Then, chitooligosaccharide: chitobiose, -triose, -tetraose, -pentaose, and -hexaose were added on the *cis* side of the chamber to a final concentration of 80  $\mu\text{M}$ . Control recordings were made with maltopentaose and maltohexaose at a concentration of 400  $\mu\text{M}$ . Ion current fluctuations were monitored for 120 s at applied voltages of  $\pm 100$  mV. Here, only ion traces for +100 mV are presented. doi:10.1371/journal.pone.0055126.g006

inclusion of single pore-forming units. Reconstitution of trimeric *Vh*ChiP into a previously formed lipid bilayer membrane was reproducibly obtained through the addition of a small amount of the purified protein to the bulk phase of the membrane-bathing KCl solution on one or other side of the bilayer. Membrane insertions of *Vh*ChiP were visible in the continuous current recordings as well-defined, step-like increases of about  $\pm 180$  pA per protein entity at  $\pm 100$  mV transmembrane potential (Fig. 5A). At higher concentrations of *Vh*ChiP ( $\mu\text{g mL}^{-1}$ ) added in the measuring buffer, multiple insertions of *Vh*ChiP were frequently seen and the resultant current traces displayed numerous fluctuations due to transient channel closures. However, the addition of much lower concentrations of added protein ( $< 1$   $\text{ng mL}^{-1}$ ) resulted in the incorporation of a single protein molecule in more constantly open state and this was the favored situation for inspecting the *Vh*ChiP single channel conductance and chitin oligosaccharide translocation. Figure 5B and 5C are characteristic examples of membrane current recordings (5 s out of 120 s measuring time) from individual *Vh*ChiP trimers inserted in a DPhPC bilayer in 1 M KCl under applied transmembrane potentials of +100 and  $-100$  mV, respectively. The traces indicate that the inserted *Vh*ChiP channel is fully open, with a stable ionic current over the time of recording. Occasionally transient current deflections occur as one of the three subunits apparently closes and opens rapidly in a stochastic manner. In multiple measurements, single reconstituted trimeric *Vh*ChiP channels showed an average conductance of  $1.8 \pm 0.13$  nS ( $n = 50$ ) in 1 M KCl (pH 7.5). As with many other bacterial porins, currents through DPhPC-incorporated *Vh*ChiP pores followed Ohm's Law, being directly proportional to the applied voltage over the range  $\pm 200$  mV

(Fig. 5D). Finally, *Vh*ChiP channels showed the typical voltage gating properties of bacterial porins and closed in a characteristic three-step fashion upon abrupt application of higher voltages (Fig. 5E). The threshold potential (critical voltage) inducing the trimeric closure of the channels was found to be  $\pm 150$  mV, while at less than or equal to 100 mV the channels were not affected by gating perturbations and so were suitable for studies on chitin oligosaccharide translocation.

Chitoporin has been proposed to facilitate the movement of chitin degradation products from the extracellular into the periplasmic space of marine *Vibrios* [12,13] before they are further transported to the cytoplasm and used as an energy source. To test this function we performed experiments to investigate the effects of chitooligosaccharides of various sizes (see Fig. S2 for the chemical structure of chitobi-, tri-, tetra-, penta-, and hexaose) on fully-open pores of *Vh*ChiP in artificial phospholipid bilayer membranes. Fig. 6 shows current recordings from single *Vh*ChiP channels with all the tested chitooligosaccharides (Fig. 6A–F) as well as those acquired in comparative trials with the structurally related maltopentaose and maltohexaose (Fig. 6G and H). With no chitosugars in the measuring buffer (Fig. 6A), the ion current through a fully open *Vh*ChiP trimer was stable and the standard value of  $\sim 180$  pA was measured with a transmembrane potential of +100 mV. The response of the system to the addition of the set of chitosugars was diverse. For instance, no transient decreases were observed when the reconstituted *Vh*ChiP was exposed to chitobiose (Fig. 6B). The current traces obtained had, however, slightly greater noise levels than controls without added solute. In marked contrast, the presence of higher MW chitosugars ( $\text{GlcNAc}_{4,5,6}$ ) in the solution on the *cis* side of the membrane

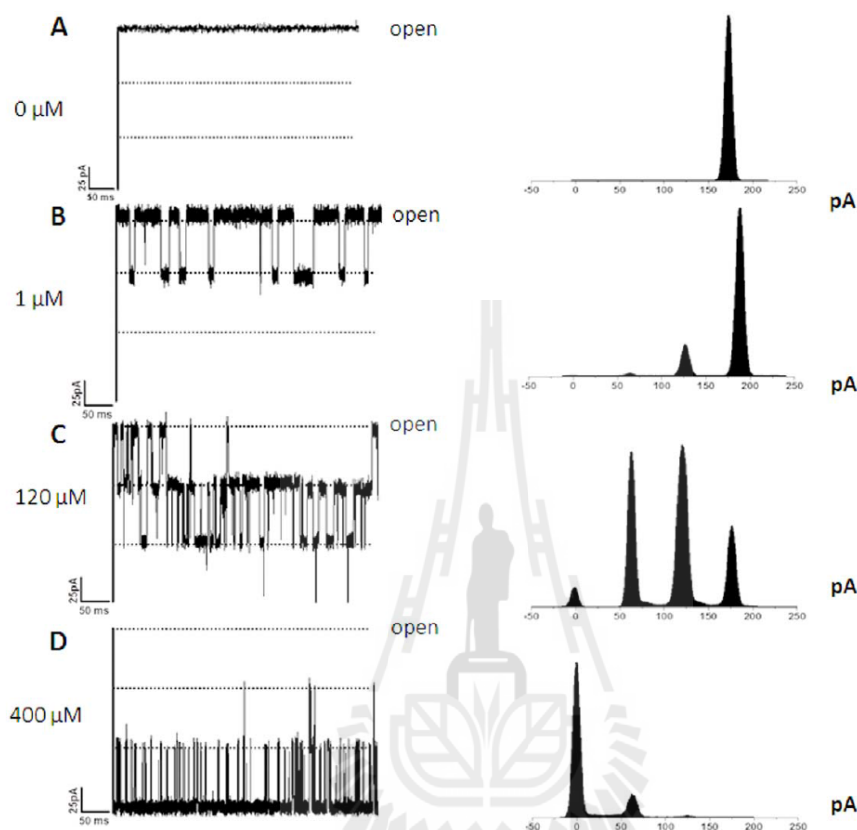


**Figure 7. Effects of chitohexaose diffusion on subunit closure.** The fully open *Vh*ChiP channel was exposed to different concentrations of chitohexaose (A–D). Right panel: the original traces displaying ion current blockade. Left panel: the corresponding frequency/current histograms, reflecting discrete changes in the subunit conductance upon sugar diffusion through the channel. doi:10.1371/journal.pone.0055126.g007

produced clear short-lived downward current deflections (Fig. 6C to F). These correspond to the time-resolved blockade of the trimeric pores of *Vh*ChiP by individual chito-oligosaccharide molecules that physically obstruct the channels in course of contact. Occlusion of ion flow during sugar diffusion apparently occurred as a reversible process by which each of the brief current decreases was caused by a single sugar molecule entering the *Vh*ChiP channel and leaving it very shortly later. Characteristic current traces for 80  $\mu$ M chitotriose and chitotetraose showed that no more than one of the three subunits of a *Vh*ChiP trimer was blocked by such chitosugars, the other two remaining unaffected during that period (Fig. 6C and D). The frequency of the single subunit blockades was considerably higher for the triose than for the tetraose. At the same concentration, diffusion of chitopentaose also caused two-subunit blockade (Fig. 6E) and with chitohexaose, even blockade of all three channel subunits could be observed (Fig. 6F). Chito-oligosaccharides were also added into the solution on the *trans* side of the bilayer membrane. As with sugar supplementation on the *cis* side, distinct channel blockades were observed in the corresponding membrane current recordings; however, for the same solute concentration the blocking effect was

slightly less pronounced. The magnitude of the sugar-induced current depressions is the same for all compounds, corresponding to the quantized blockade of individual subunits; however, the shorter the oligosaccharide, the shorter the time of current blockage. Importantly, the exposure of single *Vh*ChiP channels to maltopentaose and maltohexaose did not cause the transient drops of ion flow that were observed with the chitosugars, even when five times higher concentrations (400  $\mu$ M) of the maltosugars were used (Fig. 6G and H, respectively).

BIM trials with different chitosugars identified chitohexaose to be most potent in terms of pore obstruction (Fig. 6). Chitohexaose was thus chosen for evaluating the concentration dependence of chitosugar-induced *Vh*ChiP blockade. Membrane current recordings were taken for the same single channel, while the chitohexamer concentration was progressively increased from 0  $\mu$ M to 1, 120 and 400  $\mu$ M, respectively. Fig. 7 shows the original membrane current measurements (A–D, left panel) together with a statistical analysis of the raw data as current magnitude histograms (A–D, right panel). Clearly, the open probability of the channel decreases with increased concentrations of the sugar. On addition of 1.0  $\mu$ M chitohexaose to the *cis* side of the chamber, the protein

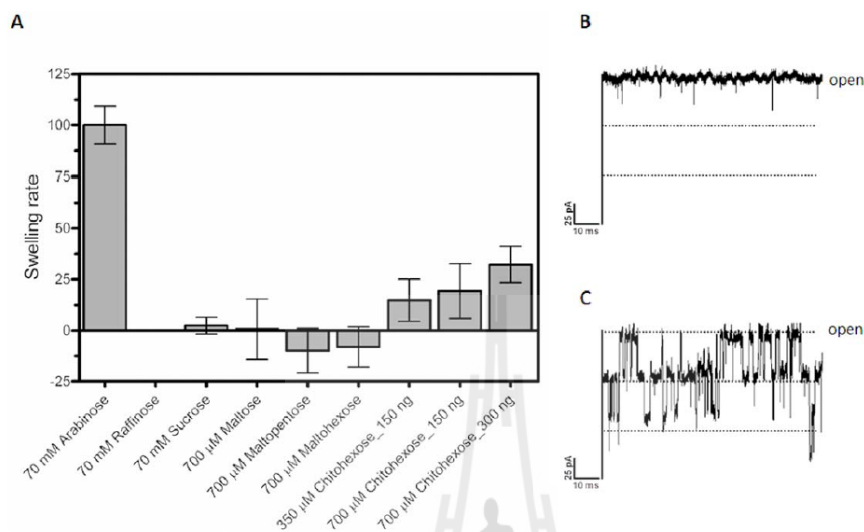


**Figure 8. Liposome swelling assays.** Multilamellar liposomes, prepared as described in the text, were reconstituted with purified *VhChiP* (150 or 300 ng). The isotonic concentration was defined as the concentration of raffinose added into the proteoliposome suspension that did not cause change in absorbance at 500 nm for a period of 60 s. Permeation of different types of sugars through *VhChiP* reconstituted liposomes were then tested. A) The swelling rates were normalized, with the rate of swelling in arabinose set to 100%. Values presented are averages of 4–6 independent experiments. B) BLM measurement of *VhChiP* ion current with the isotonic concentration of raffinose (70 mM) added. C) BLM measurement of *VhChiP* in the presence of 70 mM raffinose and 200 μM chitohexaose. doi:10.1371/journal.pone.0055126.g008

channel instantaneously transformed from being constantly fully open (Fig. 7A) to a state in which one subunit of *VhChiP* was temporarily occluded (Fig. 7B). This is shown by a decrease of the channel conduction by one-third of the full conductance. As its concentration was raised to 120 μM (Fig. 7C), the sugar began to occupy two subunits, decreasing the conductance by two-thirds. At this concentration, occupation of the third subunit was periodically observed, with the channel conductance reduced to zero. At 400 μM chitohexaose (Fig. 7D), two of the three subunits were constantly blocked, and the effect of increased chitohexaose concentration on the third subunit was apparent. The probability of complete closure of the trimeric channel was approx. 0.8, indicating that the *VhChiP* channel was nearly saturated by chitohexaose at this concentration.

The most likely explanation for the short-term inhibition by chitoooligosaccharides of ion conduction by *VhChiP* is that these molecules permeate the membrane through *VhChiP*. Bulk entry of chitoooligosaccharides into proteoliposomes containing *VhChiP* was therefore investigated by liposome swelling measurements.

#### Assay of sugar permeation by liposome swelling

High resolution ion conductance measurements were complemented by proteoliposome swelling assays, which determined the permeation of sugar molecules through *VhChiP* channels reconstituted into liposomes. Diffusion rates of sugars through *VhChiP* channels determined by these assays indicate influx of solutes into the proteoliposomes. The liposome swelling can be visualized by recording changes in the scattering signal of the liposome solution, using a spectrophotometer. Under isotonic conditions, the scattering signal remains constant throughout the measuring time, indicating neither swelling nor shrinking of the proteoliposomes. In the case of a solute permeation into the proteoliposomes, the

total solute concentration inside the vesicles rises, driving the influx of water through the channels and swelling is detected as a decrease in absorbance. It is important to note that the rates of swell provide relative numbers to assess how the translocation varies from one sugar to the other. Here, we used raffinose, a branched sugar (MW 504.42) that is unable to diffuse through the porins and arabinose, a small sugar (MW 150.13) that always permeates through the channel, for comparison. Fig. 8A is an illustration of the swelling of liposomes exposed to chitohexaose, which was the sugar found to be the most potent channel blocker in membrane current measurements. The swelling rates in raffinose, sucrose, maltose, maltopentaose and maltohexaose are included for comparison. When normalized to the swelling rate of arabinose (set to 100%), only chitohexaose at low concentrations (350 and 700 μM) was found to permeate through *VhChiP*, and increases of internal osmolality occurred in a concentration-dependent manner. Fig. 8B is *VhChiP* single-channel current measurements in the presence of raffinose. The raffinose alone did not cause channel blockage at up to 70 mM, while further addition of a much lower concentration of the chitohexaose (200 μM) to the same bilayer, after the negative results with the raffinose were obtained, immediately produced current deflections (Fig. 8C). Observable swelling of the proteoliposomes apparently reflects permeation of chitohexaose through the embedding *VhChiP* pores in the lipid vesicles, but was not significant with other sugars.

#### Discussion

The chitin catabolic cascade of *Vibrios* is a complex system that involves a cluster of genes in the chitin-induced *GlcNAc<sub>2</sub>* operon, which is stringently controlled by a two-component chitin sensor/

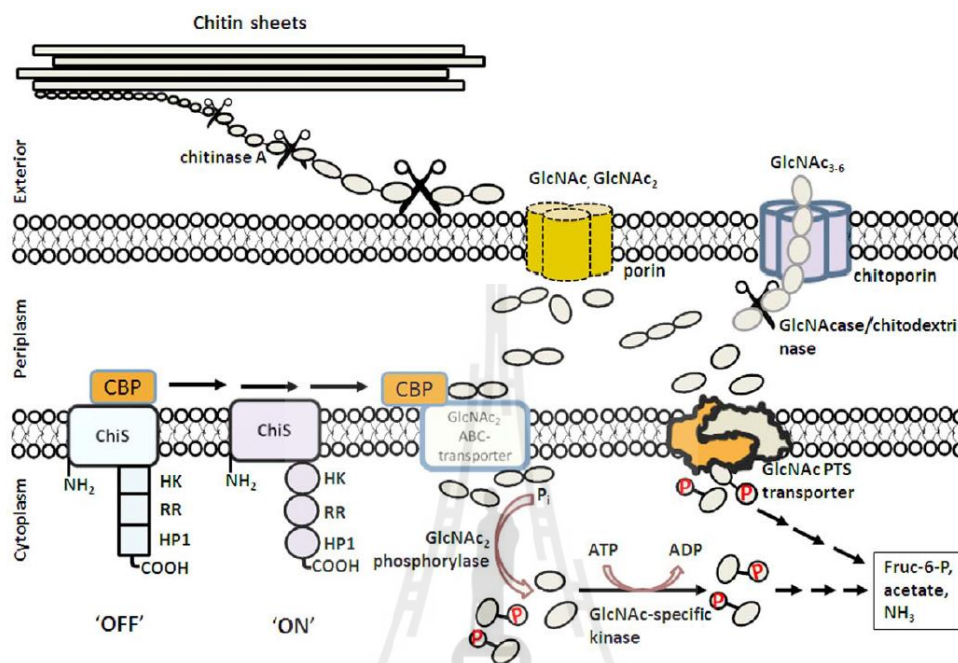


**Figure 9. Model of the chitin degradation cascade of the marine bacterium *Vibrio harveyi*.** The model was reconstructed from the chitinolytic cascade proposed by Li and Roseman [6]. After chitin degradation by chitinase, the chitin fragments are transported through the outer membrane by diffusion through porin or chitoporin, depending on their sizes. Further enzymatic degradation takes place in the periplasm, producing GlcNAc and GlcNAc<sub>2</sub>. Binding of GlcNAc<sub>2</sub> to CBD activates the ChiS sensor, producing transcription of the genes under control of the GlcNAc<sub>2</sub> catabolic operon. GlcNAc is translocated to the cytoplasm by the GlcNAc PTS system, while GlcNAc<sub>2</sub> is transported through the inner membrane by the GlcNAc<sub>2</sub> ABC permease. Both products are phosphorylated, and finally converted to Fructose-6-P, acetate and NH<sub>3</sub>. doi:10.1371/journal.pone.0055126.g009

histidine kinase (also referred to as ChiS sensor) [6,13]. Fig. 9 summarizes the multiple-step process in the chitin degradation pathway, which involves: i) Chitin binding. Traces of chitooligosaccharides in the surrounding microenvironment are suggested to act as a chemoattractant that triggers adhesion of the bacteria to the surface of chitin-containing particles [3,40]. ii) Chitin degradation. Secretion of chitinases leads to partial degradation of chitin to chitooligosaccharides on the extracellular side of the bacterial cell wall. Endochitinases (mainly chitinase A) were shown to mostly be responsible for chitin degradation [5,41]. iii) Molecular uptake of chitooligosaccharides. Chitin degradation products presumably permeate the outer membrane of the bacteria through a substrate-specific porin (referred to as “chitoporin or ChiP” [6,9]). iv) Further breakdown of chitooligosaccharides. In the periplasm,  $\beta$ -*N*-acetylglucosaminidase [42] and chitodextrinase [43] degrade the translocated chitin fragments to GlcNAc and GlcNAc<sub>2</sub>. GlcNAc<sub>2</sub> generated in the periplasm is crucial as it binds to the chitin binding protein (CBP) that is usually attached to ChiS at the outer part of the inner membrane. Dissociation of CBP upon binding to GlcNAc<sub>2</sub> successively activates the ChiS sensor, which in turn up-regulates expression of the genes that comprise the *chiS* regulon [6,13]. v) Active transport of GlcNAc and GlcNAc<sub>2</sub> into cytoplasm. GlcNAc<sub>2</sub> is transported through the inner membrane by the GlcNAc<sub>2</sub> ABC-type permease [44], whereas GlcNAc is transported by the phosphoenolpyruvate transferase system (PTS) [45,46]. vi) Generation of metabolic intermediates. Upon arrival

in the cytoplasm, individual dimers are phosphorylated by the cytoplasmic GlcNAc<sub>2</sub> phosphorylase as follows: GlcNAc<sub>2</sub> + P<sub>i</sub> = GlcNAc-6-P + GlcNAc [7]. GlcNAc from the ABC transport system is phosphorylated by a specific GlcNAc kinase [47]. Alternatively, PTS converts GlcNAc to GlcNAc-6-P, concurrently with translocation. As a result, the final forms of intracellular intermediates are fructose-6-P, acetate and NH<sub>3</sub>, which can readily be metabolized as carbon and nitrogen sources for the cells.

Although the chitin degradation pathway of *Vibrios* has been generally accepted [3–7], some key issues remain to be clarified concerning the functionality of the proteins involved in the pathway, of which chitoporin is an example. Chitoporin was first identified in *V. furnissii* in 2000 [12]. However, its distinctive function as a chitooligosaccharide-specific channel has not been demonstrated hitherto. To understand the specificity of oligosaccharide transport through the outer membrane, it is necessary to establish the physiological role of this protein. In this study, *V. harveyi* was selected as the source organism for two reasons. First, the mechanisms underlying chitin degradation by chitinase A and *N*-acetylglucosaminidases from *V. harveyi* have been studied in detail by our group [48–52]. Second, *V. harveyi* is a fast-growing bioluminescent bacterium through its adaptive ability to grow under anaerobic and respiratory conditions. Therefore, *V. harveyi* contributes significantly to a rapid turnover of chitin in marine ecosystems. It sometimes causes a fascinating phenomenon called

'milky seas', in which, during the night, a uniform blue glow is emitted from the seawater. Some glows cover nearly 6,000 square miles of deep oceans. *Ipsa facto*, the chitin utilization machinery of *V. harveyi* is expected to work efficiently.

*VhChiP* was successfully cloned and the recombinant gene expressed in the *E. coli* system, as verified by mass-spectrometry (Fig. S1) and immunoblotting (Fig. 4A–E). Detection of endogenous expression of chitoporin when the *V. harveyi* cells were grown on chitin-containing medium suggests that the *chiP* gene is regulated by the same control system (the *chiS* regulon, refs 6,13) as the *chi A* gene. We demonstrated previously that in *V. harveyi* expression of the *Chi A* gene was strongly induced by chitin [41].

Single channel recordings revealed that *VhChiP* would insert readily into the artificial membranes and behaved as a pore-forming component with a characteristic trimeric closure when high external membrane potentials were applied (Fig. 5). Its structural homology with other porins (Fig. 2) strongly suggests that *VhChiP* has 16  $\beta$ -stranded transmembrane domains, 8 extracellular loops and 8 periplasmic turns, as is observed for most bacterial porins [38–39,53].

BLM current measurements with high time-resolution were used to demonstrate the interaction of chitooligosaccharides with *VhChiP*. These are interpreted as indicating oligosaccharide translocation, confirming the specific function of *VhChiP* as a chitooligosaccharide-specific porin. The channel was found to interact with the chitosugars to various extents, depending on the sizes and the types of the sugars (Fig. 6). The observation of no fluctuation of ion current on the addition of chitobiose can be explained by the fact that this disaccharide could not permeate through the *VhChiP* channel; it may require a general diffusion porin as already described earlier (see Fig. 9). Alternatively, it may permeate so fast that the residence time is too small to lead to well-resolved blocking events. In contrast, the *VhChiP* channel was much more sensitive to higher-MW chitosugars (GlcNAc<sub>3–6</sub>). The channel blocking behavior (Figs. 6 and 7) is comparable to the blockage of maltoporin by maltooligosaccharides [19] and also reflects a common characteristic of substrate-specific channels, in which higher-MW oligosaccharides are preferred substrates [32,54].

BLM measurements revealed no response of *VhChiP* to maltopentaose and maltohexaose even at a concentration five-fold greater than that of the chitosugars (Fig. 6). The results of liposome swelling assays additionally confirmed insignificant permeation of other sugars, including raffinose, maltose and sucrose (Fig. 9). These data indicate the high selectivity of the *ChiP* porin towards chitooligosaccharides. The low sequence identity of between *VhChiP* and other sugar-specific porins (less than 20%)

(Fig. 1) also demonstrates no detailed structural similarity. *VhChiP* appears to be exceptionally specific for chitohexaose, as ion current fluctuation, representing the blockage of individual subunits, was detected at sugar concentrations as low as 125 nM (not shown). The sugar-channel interaction was even stronger at higher concentrations, almost fully blocking all three subunits. Taken together, the results suggest that *VhChiP* is a chitooligosaccharide-specific porin. Detailed characterization of channel specificity and binding kinetics towards different chitooligosaccharides has been the subject of our ongoing investigations.

In summary, we employed biochemical assays, together with high-time resolution single channel recordings to address, for the first time, the pore-forming property of chitoporin from the representative *V. harveyi*. The isolated *ChiP* was found to be highly specific for chitooligosaccharides. The data obtained from this study, therefore, establish the fundamental role of chitoporin in the chitin degradation pathway as the molecular gateway that the marine *Vibrios* employ to efficiently uptake chitooligosaccharides into the cellular interior in order to utilize them as a sole source of energy.

#### Accession number

The nucleotide sequence of *V. harveyi* chitoporin has been deposited in the EMBL Nucleotide Sequence Database under accession number HF558985.

#### Supporting Information

**Figure S1 Identification of *V. harveyi* chitoporin by mass spectrometry.** Tryptic peptides were prepared from the outer membrane fraction extracted with 2% (w/v) SDS, followed by 5% (v/v) octyl-POE by in-gel digestion method. The peptides were resolved by nano-LC/MS. The resultant monoisotopic masses were subjected to Mascot search using the NCBI nR database for protein identification. Sequences underlined (P1–P9) are identical to nine internal peptides in the translated sequence of *V. harveyi* chitoporin identified in this study. (TIF)

**Figure S2 Chemical structure of chitin oligosaccharides and maltooligosaccharides.** (TIF)

#### Author Contributions

Conceived and designed the experiments: WS. Performed the experiments: WS WC PJ. Analyzed the data: WS KRM AS MW. Contributed reagents/materials/analysis tools: WS MW. Wrote the paper: WS KRM AS MW.

#### References

- Jeuniaux C, Voss-Foucart MF (1991) Chitin biomass and production in the marine environment. *Biochem Syst Ecol* 19:347–356.
- Zobell CE, Rittenberg SC (1938) The occurrence and characteristics of chitinolytic bacteria in the sea. *J Bacteriol* 35:275–287.
- Yu C, Lee AM, Bassler BL, Roseman S (1991) Chitin utilization by marine bacteria. A physiological function for bacterial adhesion to immobilized carbohydrates. *J Biol Chem* 266:24260–24267.
- Bassler BL, Gibbons PJ, Yu C, Roseman S (1991) Chitin utilization by marine bacteria. Chemotaxis to chitin oligosaccharides by *Vibrio fujisii*. *J Biol Chem* 266:24268–24275.
- Keyhani NO, Roseman S (1999) Physiological aspects of chitin catabolism in marine bacteria. *Biochim Biophys Acta* 1473:108–122.
- Li X, Roseman S (2004) The chitinolytic cascade in *Vibrios* is regulated by chitin oligosaccharides and a two-component chitin catabolic sensor/kinase. *Proc Natl Acad Sci USA* 101:627–631.
- Park JK, Keyhani NO, Roseman S (2000) Chitin catabolism in the marine bacterium *Vibrio fujisii*. Identification, molecular cloning, and characterization of A N, N'-diacetylchitinobiose phosphorylase. *J Biol Chem* 275:33077–33083.
- Bassler BL, Yu C, Lee CYC, Roseman S (1991) Chitin utilization by marine bacteria. Degradation and catabolism of chitin oligosaccharides by *Vibrio fujisii*. *J Biol Chem* 266:24276–24286.
- Hunt DE, Gevers D, Vahora NM, Polz MF (2008) Conservation of the chitin utilization pathway in the *Vibrionaceae*. *Appl Environ Microbiol* 74:44–51.
- Pruzzo C, Vezzulli L, Colwell RR (2008) Global impact of *Vibrio cholerae* interactions with chitin. *Environ Microbiol* 10:1400–1410.
- Jung BO, Roseman S, Park JK (2008) The central concept for chitin catabolic cascade in marine bacterium, *Vibrios*. *Macromol Res* 16:1–15.
- Keyhani NO, Li XB, Roseman S (2000) Chitin catabolism in the marine bacterium *Vibrio fujisii*. Identification and molecular cloning of a chitoporin. *J Biol Chem* 275:33068–33076.
- Meibom KL, Li XB, Nielsen AT, Wu CY, Roseman S, et al. (2004) The *Vibrio cholerae* chitin utilization program. *Proc Natl Acad Sci USA* 101:2524–2529.
- Prilipov A, Phale PS, Van Gelder P, Rosenbusch JP, Koebnik R (1998) Coupling site-directed mutagenesis with high-level expression: large scale production of mutant porins from *E. coli*. *FEMS Microbiol Lett* 163:65–72.
- Garavito RM, Rosenbusch JP (1986) Isolation and crystallization of bacterial porin. *Methods Enzymol* 125:309–328.

16. Rosenbusch JP (1974) Characterization of the major envelope protein from *Escherichia coli*. Regular arrangement on the peptidoglycan and unusual dodecyl sulfate binding. *J Biol Chem* 249:8019–8029.
17. Lugtenberg B, Van Alphen L (1983) Molecular architecture and functioning of the outer membrane of *Escherichia coli* and other gram-negative bacteria. *Biochim Biophys Acta* 737:51–115.
18. Dando RT, Young EPS (1990) In The NCIMB catalogue of strains: Growth media, p. 172, Aberdeen University Press, Aberdeen.
19. Bezrukov SM, Kullman L, Winterhalter M (2000) Probing sugar translocation through maltoporin at the single channel level. *FEBS Lett* 476:224–228.
20. Schwarz G, Danelon C, Winterhalter M (2003) On translocation through a membrane channel via an internal binding site: kinetics and voltage dependence. *Biophys J* 84:2990–2998.
21. Danelon C, Brando T, Winterhalter M (2003) Probing the orientation of reconstituted maltoporin channels at the single-protein level. *J Biol Chem* 278:35542–35551.
22. Kullman L, Winterhalter M, Bezrukov SM (2002) Transport of maltodextrins through maltoporin: a single-channel study. *Biophys J* 82:803–812.
23. Mahendran KR, Chimere C, Mach T, Winterhalter M (2009) Antibiotic translocation through membrane channels: temperature-dependent ion current fluctuation for catching the fast events. *Eur Biophys J* 38:1141–1145.
24. Van Gelder P, Dumas F, Winterhalter M (2000) Understanding the function of bacterial outer membrane channels by reconstitution into black lipid membranes. *Biophys Chem* 85:153–167.
25. Luckey M, Nikaïdo H (1980) Diffusion of solutes through channels produced by phage lambda receptor protein of *Escherichia coli*: inhibition by higher oligosaccharides of maltose series. *Biochem Biophys Res Commun* 93:166–171.
26. Yoshimura F, Nikaïdo H (1985) Diffusion of beta-lactam antibiotics through the porin channels of *Escherichia coli* K-12. *Antimicrob Agents Chemother* 27:84–92.
27. Clément JM, Hofnung M (1981) Gene sequence of the lambda receptor, an outer membrane protein of *E. coli* K12. *Cell* 27:507–514.
28. Forst D, Welte W, Wacker T, Diederichs K (1998) Structure of the sucrose-specific porin ScrY from *Salmonella typhimurium* and its complex with sucrose. *Nat Struct Biol* 5:37–46.
29. Wylie JL, Worobec EA (1994) Cloning and nucleotide sequence of the *Pseudomonas aeruginosa* glucose-selective OprB porin gene and distribution of OprB within the family *Pseudomonadaceae*. *Eur J Biochem* 220:505–512.
30. Trias J, Rosenberg EY, Nikaïdo H (1988) Specificity of the glucose channel formed by protein D1 of *Pseudomonas aeruginosa*. *Biochim Biophys Acta* 938:493–496.
31. Schirmer T, Keller TA, Wang YF, Rosenbusch JP (1995) Structural basis for sugar translocation through maltoporin channels at 3.1 Å resolution. *Science* 267:512–514.
32. Dumas F, Koebnik R, Winterhalter M, Van Gelder P (2000) Sugar transport through maltoporin of *Escherichia coli*. Role of polar tracks. *J Biol Chem* 275:19747–19751.
33. Dutzler R, Schirmer T, Karplus M, Fischer S (2002) Translocation mechanism of long sugar chains across the maltoporin membrane channel. *Structure* 10:1273–1284.
34. Denker K, Orlik F, Schiffler B, Benz R (2005) Site-directed mutagenesis of the greasy slide aromatic residues within the LamB (maltoporin) channel of *Escherichia coli*: effect on ion and maltopentaose transport. *J Mol Biol* 352:534–550.
35. Orlik F, Andersen C, Benz R (2002) Site-directed mutagenesis of tyrosine 118 within the central constriction site of the LamB (maltoporin) channel of *Escherichia coli*. II. Effect on maltose and maltooligosaccharide binding kinetics. *Biophys J* 83:309–321.
36. Orlik F, Andersen C, Benz R (2002) Site-directed mutagenesis of tyrosine 118 within the central constriction site of the LamB (Maltoporin) channel of *Escherichia coli*. I. Effect on ion transport. *Biophys J* 82:2466–2467.
37. Zeth K, Diederichs K, Welte W, Engelhardt H (2000) Crystal structure of Omp32, the anion-selective porin from *Comamonas acidovorans*, in complex with a periplasmic peptide at 2.1 Å resolution. *Structure* 8:981–992.
38. Koebnik R, Locher KP, Van Gelder P (2000) Structure and function of bacterial outer membrane proteins: barrels in a nutshell. *Mol Microbiol* 37:239–253.
39. Nikaïdo H (1992) Porins and specific channels of bacterial outer membranes. *Mol Microbiol* 6:435–442.
40. Bassler BL, Gibbons PJ, Yu C, Roseman S (1991) Chitin utilization by marine bacteria. Chemotaxis to chitin oligosaccharides by *Vibrio furnissii*. *J Biol Chem* 266:24268–24275.
41. Suginta W, Robertson PA, Austin B, Fry SC, Fothergill-Gilmore LA (2000) Chitinases from *Vibrio*: activity screening and purification of chiA from *Vibrio carchariae*. *J Appl Microbiol* 89:76–84.
42. Keyhani NO, Roseman S (1996) The chitin catabolic cascade in the marine bacterium *Vibrio furnissii*. Molecular cloning, isolation, and characterization of a periplasmic beta-N-acetylglucosaminidase. *J Biol Chem* 271:33425–33432.
43. Keyhani NO, Roseman S (1996) The chitin catabolic cascade in the marine bacterium *Vibrio furnissii*. Molecular cloning, isolation, and characterization of a periplasmic chitodextrinase. *J Biol Chem* 271:33414–33424.
44. Bouma CL, Roseman S (1996) Sugar transport by the marine chitinolytic bacterium *Vibrio furnissii*. Molecular cloning and analysis of the glucose and N-acetylglucosamine permeases. *J Biol Chem* 271:33457–33467.
45. Bouma CL, Roseman S (1996) Sugar transport by the marine chitinolytic bacterium *Vibrio furnissii*. Molecular cloning and analysis of the mannose/glucose permease. *J Biol Chem* 271:33468–33475.
46. Keyhani NO, Wang LX, Lee YC, Roseman S (1996) The chitin catabolic cascade in the marine bacterium *Vibrio furnissii*. Characterization of an N,N'-diacetyl-chitobiose transport system. *J Biol Chem* 271:33409–33413.
47. Park JK, Wang LX, Roseman S (2002) Isolation of a glucosamine-specific kinase, a unique enzyme of *Vibrio cholerae*. *J Biol Chem* 277:15573–15578.
48. Suginta W, Vongsuwan A, Songsiririthigul C, Prinz H, Estibeiro P, et al. (2004) An endochitinase A from *Vibrio carchariae*: cloning, expression, mass and sequence analyses, and chitin hydrolysis. *Arch Biochem Biophys* 424:171–180.
49. Suginta W, Vongsuwan A, Songsiririthigul C, Svasti J, Prinz H (2005) Enzymatic properties of wild-type and active site mutants of chitinase A from *Vibrio carchariae*, as revealed by HPLC-MS. *FEBS J* 272:3376–3386.
50. Suginta W, Songsiririthigul C, Koldaj A, Opassin R, Svasti J (2007) Mutations of Trp275 and Trp397 altered the binding selectivity of *Vibrio carchariae* chitinase A. *Biochim Biophys Acta* 1770:1151–1160.
51. Songsiririthigul C, Pantoom S, Aguda AH, Robinson RC, Suginta W (2008) Crystal structures of *Vibrio harveyi* chitinase A complexed with chitooligosaccharides: implications for the catalytic mechanism. *J Struct Biol* 162:491–499.
52. Suginta W, Chuenark D, Mizuhara M, Fukamizo T (2010) Novel beta-N-acetylglucosaminidases from *Vibrio harveyi* 650: cloning, expression, enzymatic properties, and subsite identification. *BMC Biochem* 11:40.
53. Schirmer T (1998) General and specific porins from bacterial outer membranes. *J Struct Biol* 121:101–109.
54. Hilty C, Winterhalter M (2001) Facilitated substrate transport through membrane proteins. *Phys Rev Lett* 86:5624–5627.

## Chitoporin from *Vibrio harveyi*, a Channel with Exceptional Sugar Specificity

Received for publication, January 17, 2013, and in revised form, February 26, 2013. Published, JBC Papers in Press, February 27, 2013, DOI 10.1074/jbc.M113.454108

Wipa Suginta<sup>1</sup>, Watcharin Chumjan<sup>2</sup>, Kozhinjampara R. Mahendran<sup>5</sup>, Albert Schulte<sup>3</sup>, and Mathias Winterhalter<sup>5,3</sup>

From the <sup>1</sup>Biochemistry-Electrochemistry Research Unit, Schools of Chemistry and Biochemistry, Institute of Science, Suranaree University of Technology, Nakhon Ratchasima 30000, Thailand and the <sup>5</sup>School of Engineering and Science, Jacobs University Bremen, 28759 Bremen, Germany

**Background:** *Vibrio harveyi* chitoporin (VhChiP) was recently identified as a pore-forming channel responsible for chito-oligosaccharide uptake through the outer membrane of *V. harveyi*.

**Results:** Kinetic analysis revealed that VhChiP was several orders of magnitude more active than other known sugar-specific porins.

**Conclusion:** VhChiP is a channel with exceptional sugar specificity.

**Significance:** The high activity of VhChiP reflects an evolutionary adaptation required for *V. harveyi* to thrive under extreme aquatic conditions.

Chitoporin (VhChiP) is a sugar-specific channel responsible for the transport of chito-oligosaccharides through the outer membrane of the marine bacterium *Vibrio harveyi*. Single channel reconstitution into black lipid membrane allowed single chitosugar binding events in the channel to be resolved. VhChiP has an exceptionally high substrate affinity, with a binding constant of  $K = 5.0 \times 10^6 \text{ M}^{-1}$  for its best substrate (chitohexaose). The on-rates of chitosugars depend on applied voltages, as well as the side of the sugar addition, clearly indicating the inherent asymmetry of the VhChiP lumen. The binding affinity of VhChiP for chitohexaose is 1–5 orders of magnitude larger than that of other known sugar-specific porins for their preferred substrates. Thus, VhChiP is the most potent sugar-specific channel reported to date, with its high efficiency presumably reflecting the need for the bacterium to take up chitin-containing nutrients promptly under turbulent aquatic conditions to exploit them efficiently as its sole source of energy.

*Vibrio harveyi* is a Gram-negative, bioluminescent, marine bacterium of the family Vibrionaceae. It is found free-living in tropical marine waters and also commensally as a component of the gut microflora of marine animals. The bacterium is both a primary and an opportunistic pathogen of marine animals, triggering a lethal disease called luminous vibriosis (1), which affects marine fish and prawn-farming operations worldwide (2, 3). *V. harveyi* is a fast growing bacterium under both aerobic and anaerobic conditions. Accordingly, it can cause the “milky seas” effect, in which a uniform blue glow is emitted from the

seawater and which is apparent during the night. Sometimes the glow covers nearly 16,000 km<sup>2</sup>.

In marine ecosystems, chitin-containing substances are major sources of carbon and nitrogen for marine vibrios. The catabolic cascade of chitin utilization has been proposed to be a complex system, involving a large number of genes that are orchestrated under the stringent control of the chitin-induced operon (4). In brief, the multistep chitin degradation pathway involves (i) chitin sensing and degradation; (ii) chito-oligosaccharide uptake into the periplasm; (iii) degradation of the transported products to GlcNAc and GlcNAc<sub>2</sub>, which are then transported farther into the cytoplasm; and (iv) conversion of GlcNAc intermediates to Fru-6-P and NH<sub>3</sub><sup>+</sup>, which are metabolized for energy production and biosynthesis (5–7).

Chitoporin was initially identified in the marine bacterium *Vibrio furnissii* as part of the chitin catabolic cascade. Its function was partially revealed by gene knockdown and GlcNAc<sub>2</sub> uptake assays (8). Later, the gene encoding chitoporin was also identified in the genome of other marine bacteria, such as *Vibrio cholera* and *Shewanella* spp. (6, 9, 10). However, the specific function of chitoporin as a sugar-specific channel had never been clearly elucidated. We recently employed black lipid membrane (BLM)<sup>4</sup> reconstitution and liposome swelling assays to demonstrate that chitoporin from *V. harveyi* (VhChiP) is a pore-forming channel that performs highly specific translocation of chito-oligosaccharides (11). In the present study, we focused on the kinetic evaluation of single chito-oligosaccharide translocation through a single VhChiP. Detailed assessment of the kinetic parameters suggested that VhChiP acts as a highly specific channel, interacting with chito-oligosaccharides, especially chitohexaose, down to nanomolar concentrations.

### EXPERIMENTAL PROCEDURES

**Vectors and Bacterial Strains**—A cDNA fragment of 1.1 kilobase pairs corresponding to the full-length VhChiP gene was

<sup>1</sup> Humboldt Fellow supported by an Alexander von Humboldt Fellowship for Experienced Researchers from the Alexander von Humboldt Foundation (Bonn, Germany). To whom correspondence should be addressed: Suranaree University of Technology, 111 University Ave., Nakhon Ratchasima 30000, Thailand. Fax: 66-44-226-187; E-mail: wipa@sut.ac.th.

<sup>2</sup> Supported by CHE-PhD-SW Scholarship Contract 60/2550 from the Commission of Higher Education, Ministry of University Affairs (Bangkok, Thailand).

<sup>3</sup> Supported by Deutsche Forschungsgemeinschaft (DFG) Grant WI 2278/18-1.

<sup>4</sup> The abbreviations used are: BLM, black lipid membrane; VhChiP, *V. harveyi* chitoporin.

### Kinetics of Sugar Translocation through Chitoporin

cloned into the Novagen expression vector pET-23d(+) (Merck). *Escherichia coli* host strain BL21(DE3) Omp8 Rosetta was a kind gift from Professor Dr. Roland Benz (Jacobs University Bremen, Bremen, Germany). This *E. coli* strain was genetically engineered to carry defective genes encoding the major outer membrane porins OmpA, OmpC, OmpF, and Lamb, making it suitable for production of an exogenous porin (12).

**Recombinant Expression and Protein Purification**—The *E. coli* BL21(DE3) Omp8 Rosetta host strain was transformed with plasmid pET-23d(+)/VhChiP. Expression and preparation of recombinant VhChiP were performed following the protocols described by Garavito and Rosenbusch (13) and Rosenbusch (14). In brief, transformed cells were grown at 37 °C in LB liquid medium containing 100 µg/ml ampicillin and 25 µg/ml kanamycin. At  $A_{600} = 0.5\text{--}0.7$ , isopropyl  $\beta$ -D-thiogalactopyranoside was added to a final concentration of 0.5 mM. Cell growth was continued for an additional 6 h, and cells were then harvested by centrifugation at  $4500 \times g$  for 20 min at 4 °C. The cell pellet was resuspended in buffer containing 20 mM Tris-HCl (pH 8.0), 2.5 mM MgCl<sub>2</sub>, 0.1 mM CaCl<sub>2</sub>, 10 µg/ml DNase I, and 10 µg/ml RNase A. Cells were lysed by sonication on ice for 10 min (30% duty cycle, amplitude setting of 20%) using a SONOPULS ultrasonic homogenizer with a 6-mm diameter probe. Recombinant VhChiP was extracted from the peptidoglycan layer with SDS based on the method of Lugtenberg and Van Alphen (15). Briefly, SDS was added to the cell suspension to a final concentration of 2% (w/v), and incubation was carried out for 1 h at 60 °C with gentle shaking. The crude extract was then centrifuged at  $40,000 \times g$  for 60 min at 4 °C. The pellet, which at this stage included the cell envelopes, was resuspended in 20 mM phosphate buffer (pH 7.4) containing 0.125% (v/v) *n*-octylpolyoxyethylene (Alexis Biochemicals, Lausanne, Switzerland) using a Potter-Elvehjem homogenizer. The suspension was incubated at 37 °C with gentle shaking for 1 h and then centrifuged at  $100,000 \times g$  for 40 min at 4 °C. The new pellet, now rich in outer membranes, was resuspended in 20 mM phosphate buffer (pH 7.4) containing 3% (v/v) *n*-octylpolyoxyethylene, and the suspension was incubated at 37 °C for 60 min. Insoluble material was removed by centrifugation at  $100,000 \times g$  for 40 min at 20 °C. After exchange of the detergent with 0.2% (v/v) lauryldimethylamine oxide (Sigma-Aldrich) by dialysis, the VhChiP-rich sample was subjected to ion exchange chromatography using a HiTrap Q HP prepacked column (5 × 1 ml) connected to an ÄKTAprime Plus FPLC system (GE Healthcare). Bound proteins were eluted with a linear gradient of 0–1 M KCl in phosphate buffer containing 0.2% (v/v) lauryldimethylamine oxide. The purity of the eluted proteins was confirmed by SDS-PAGE. Fractions containing only VhChiP were pooled, and the protein concentration was determined using the Pierce BCA protein assay kit (Bio-Active Co., Ltd., Bangkok, Thailand).

**BLM Measurements and Single Channel Analysis**—BLM measurements and single channel analysis were performed following the methods described previously (16–23). Briefly, the lipid bilayer cuvette consisted of two chambers separated by a 25-µm-thick Teflon film. The latter had a small aperture of 60–100 µm in diameter, across which a virtually solvent-free planar lipid bilayer was formed. The chambers were filled with electrolyte solution and Ag/AgCl electrodes (World Precision

Instruments, Sarasota, FL) immersed on either side of the Teflon film. The electrolyte solution used was 1 M KCl buffered with 20 mM HEPES (adjusted to pH 7.5). 1,2-Diphytanoyl-*sn*-glycero-3-phosphatidylcholine (Avanti Polar Lipids, Alabaster, AL) was used for lipid bilayer formation. To form the bilayer, the aperture was first pre-painted with 1 µl of 1% (v/v) hexadecane in pentane (Sigma-Aldrich). One of the electrodes (*cis*) was used as the ground electrode, whereas the other (*trans*) was connected to the headstage of an Axopatch 200B amplifier (Axon Instruments, Foster City, CA). The trimeric VhChiP channel (50–100 ng/ml) was always added to the *cis* side of the lipid membrane. At applied transmembrane potentials of +200 and –200 mV, a single channel was frequently inserted within a few minutes. The protein solution in the chamber was gently diluted by sequential additions of the working electrolyte to prevent multiple insertions. To investigate sugar translocation, chitoooligosaccharides of various lengths (chitotriose (GlcNAc<sub>3</sub>), chitotetraose (GlcNAc<sub>4</sub>), chitopentaose (GlcNAc<sub>5</sub>), or chitohexaose (GlcNAc<sub>6</sub>)) were titrated on the *cis* side or, in separate experiments, on the *trans* side of the membrane. In some experiments, the sugar was titrated on one side and finally diluted, followed by titration on the opposite side. These experiments were tedious, but yielded consistent results.

A fully open channel of the VhChiP trimer was titrated with discrete concentrations of chitosugar until saturated, typically from nanomolar to micromolar concentrations, although the suitable range of sugar concentrations depended upon which sugar was being studied. Occlusions of ion flow observed as a result of sugar diffusion through the inserted channel were usually recorded for 120 s at transmembrane potentials of +50, –50, +100, and –100 mV. Single channel current measurements were performed with an Axopatch 200B amplifier in the voltage clamp mode, with the internal filter set at 10 kHz. Amplitude, probability, and single channel analyses were performed using pCLAMP version 10.0 software (Molecular Devices, Sunnyvale, CA).

**Estimation of Binding Constants**—The equilibrium binding constant ( $K$ , M<sup>–1</sup>) was estimated from the reduction of the ion conductance in the presence of increasing concentrations of sugar using Equation 1 (24, 25),

$$\frac{G_{\max} - G_{[c]}}{G_{\max}} = \frac{I_0 - I_{[c]}}{I_0} = K \cdot c / (1 + K \cdot c) \quad (\text{Eq. 1})$$

where  $G_{\max}$  is the average conductance of the fully open VhChiP channel,  $G_{[c]}$  is the average conductance at a given concentration of a chitosugar ( $[c]$ ),  $I_0$  is the initial current through the fully open channel in the absence of sugar, and  $I_{[c]}$  is the current at a particular sugar concentration. The quality of the data is readily seen by inverting Equation 1 into a so-called Lineweaver-Burk plot ( $((G_{\max} - G_{[c]})/G_{\max})^{-1}$  versus  $([c]^{-1})$ ). Single channel analysis was performed to calculate the rates of association and dissociation. The off-rate ( $k_{\text{off}}$ , s<sup>–1</sup>) was obtained from Kullman *et al.* (19) (Equation 2),

$$k_{\text{off}} = 1/\tau_c \quad (\text{Eq. 2})$$

where  $\tau_c$  is the average residence (dwell) time (s<sup>–1</sup>) of the sugar molecule in the channel. The on-rate ( $k_{\text{on}}$ , M<sup>–1</sup>·s<sup>–1</sup>) is given by  $k_{\text{on}} = K \cdot k_{\text{off}}$ .

### Kinetics of Sugar Translocation through Chitoporin

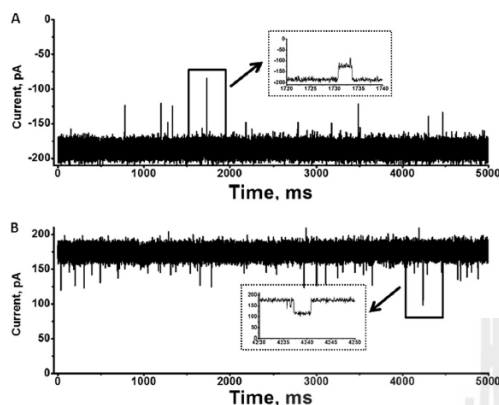


**FIGURE 1. Single trimeric channel recordings of chitoporin in artificial lipid membranes.** The BLM measurements were carried out in electrolyte solution containing 1 M KCl in 20 mM HEPES (pH 7.5). Purified VhChiP was added on the *cis* side of the chamber. Shown are typical ion current traces of a single VhChiP channel in the fully open state at applied potentials of +100 mV (A) and -100 mV (B). The ion currents were normally recorded for a period of 120 s, but representative traces of 5000-ms duration are presented. *Insets*, recordings with an expanded time scale of transient gating at +100 and -100 mV.

### RESULTS

**Single Channel Properties**—As described under “Experimental Procedures,” purified VhChiP was incorporated into solvent-free lipid bilayers, and single channel conductance was estimated to be  $1.8 \pm 0.13$  nanosiemens ( $n = 50$ ). Fig. 1 (A and B) presents representative current recordings showing current amplitudes of around  $\pm 180$  pA over 5 s. At applied voltages of +100 and -100 mV, the trimeric channels were fully open, with occasional transient gating (Fig. 1, *insets*). It is important to note that, under the given condition, the pre-inserted membranes were found to be stable, with some lasting beyond 7 h, making them suitable for the kinetic assessment of chito oligosaccharide translocation through the VhChiP pore.

**Channel Specificity**—Chito oligosaccharides of various sizes were added on either side of the chamber, and their ability to block ion current was quantified. Fig. 2 shows 100-ms-long recordings of chito oligosaccharide-induced current fluctuations at -100 mV. No blockage was visible when chitobiose was varied up to  $400 \mu\text{M}$  on either the *cis* or *trans* side or when the channel was exposed to maltodextrins (maltopentaose and maltohexaose) or raffinose (data not shown). In marked contrast, after the addition of  $5 \mu\text{M}$  chitosugars, we observed ion current blockages, which depended on the size of the sugar and the side of sugar addition. The ionic current blockages were observed at much greater frequency when the sugar was added on the *cis* side (Fig. 2, A–D) compared with the *trans* side (Fig. 2, E–H). For instance, current blockage by chitotriose was rarely visible with addition on the *trans* side, whereas significant blocking events were detected when same concentration of chitotriose was added on the *cis* side.

Starting with the *cis* side addition, chitotriose was found to partially interrupt the flow of ions, visible by statistical transient

reduction of the channel conductance by one-third (Fig. 2). Chitotriose (Fig. 2A), chitotetraose (Fig. 2B), and chitopentaose (Fig. 2C) blocked one monomer of the single trimeric channel, whereas increasing the sugar length to hexamer (Fig. 2D) resulted in the double and triple blocking of the single trimeric channel. Furthermore, chitohexaose exhibited the longest residence time, during which each sugar molecule remained entrapped before leaving the pore. This was clear from single channel analysis, which yielded an average residence time of  $6.0 \pm 0.7$  ms for the chitohexamer. This value decreased rapidly as the number of GlcNAc units in the polymer decreased from five ( $2.4 \pm 0.24$  ms) to four ( $0.33 \pm 0.08$  ms) and three ( $0.11 \pm 0.05$  ms).

**Effects of Applied Voltages on Sugar Translocation**—We further investigated the effect of applied voltages on sugar translocation from both the *cis* and *trans* sides at various concentrations. As shown in Fig. 3, channel blockage by chitohexaose occurred to a much greater extent for *cis* side addition compared with *trans* side addition. Considering *cis* side addition, the number of blocking events was obviously higher at -100 mV (Fig. 3, E–H) than at +100 mV (Fig. 3, A–D). This result was reversed with *trans* side addition (data not shown). In both cases, the frequency of blocking events increased with concentration. Fig. 3 (E–H) shows that at -100 mV/*cis*, chitohexaose at  $0.25 \mu\text{M}$  blocked only one subunit on average. Two subunits were blocked when the concentration was increased to  $1.25 \mu\text{M}$ , and finally, all three subunits were blocked at  $2.5 \mu\text{M}$ . Similar observations were made with +100 mV/*cis* (Fig. 3, A–D), although the frequency of blocking events was much lower.

Fig. 4 presents a detailed analysis of the original traces shown partially in Fig. 3. Plots of the number of blockade events/ (reflecting translocation rate) over a selected range of chitohexaose concentrations were examined for *cis* and *trans* side additions at +100 and -100 mV. The on-rates for chitohexaose moving through open pores decreased as follows: -100 mV/*cis* > +100 mV/*cis* > +100 mV/*trans* >> -100 mV/*trans* (Fig. 4A). The rates versus sugar concentrations from *cis*-to-*trans* yielded saturable curves, but the rates for *trans*-to-*cis* translocation did not reach saturation over the same concentration range.

Applied potentials also affected both  $\tau_o$ , the time that the monomeric protein channel remains open, and  $\tau_c$ , the time that the sugar resides within the monomer. As shown in Fig. 4 (B and C), each setting condition yielded different values of  $\tau_o$  and  $\tau_c$ . Nonetheless, all conditions showed a linear decay of  $\tau_o$  in a concentration-dependent manner, but  $\tau_c$  does not depend on the concentration.

**Rate of Sugar Penetration and Binding Affinity**—The characteristic substrate-specific channel activity of VhChiP was confirmed by enhancement of the on-rate of chitohexaose, relative to that of other oligosaccharides, and by its concentration dependence. As the concentration was increased above  $0.1 \mu\text{M}$ , the on-rate, reflected in the frequency of current blockages, increased, eventually reaching a plateau (Fig. 4A). Chitohexaose blocked the ion flow very efficiently even at nanomolar concentrations. A conductance histogram (Fig. 5A) shows a continuous increase in the level of monomeric blockage as the channel was titrated with chitohexaose from  $0.125 \mu\text{M}$  to  $2.5 \mu\text{M}$ . It is

## Kinetics of Sugar Translocation through Chitoporin

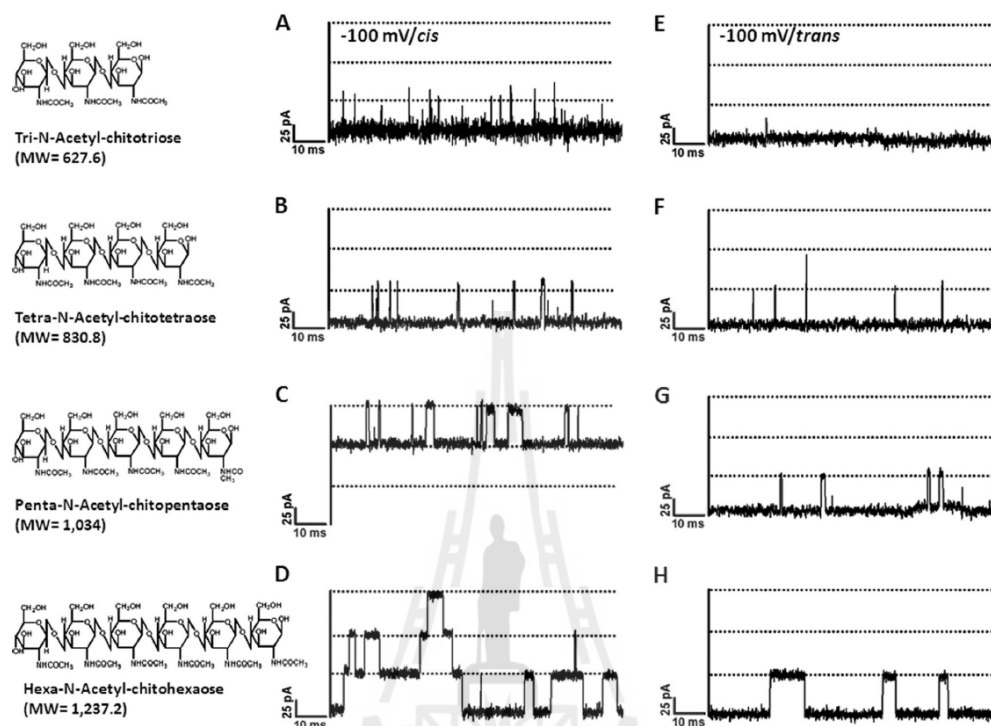


FIGURE 2. Effect on ion currents of chitoooligosaccharide diffusion into chitoporin. A single trimeric channel of *VhChiP* was inserted in an artificial membrane in a fully open state. Chitoooligosaccharides of various sizes were then added to a final concentration of  $5 \mu\text{M}$  on either the *cis* side (A–D) or *trans* side (E–H) of the chamber. A and E, chitotriose; B and F, chitotetraose; C and G, chitopentaose; D and H, chitohexaose. Ion current fluctuations were monitored for 120 s at applied potentials of +100 and –100 mV. Here, only ion traces for a potential of –100 mV are presented.

shown that the amplitude of the monomeric conductance at  $2.5 \mu\text{M}$  was not much greater than at the previous concentration. Fig. 5B displays the related power density spectra. The amplitudes of sugar-induced noise levels were elevated in proportion to the concentration of chitohexaose and correlated well with the levels of monomeric blockage shown in Fig. 5A.

Further quantitative analysis of the binding constants was carried out to access the channel affinity. Fig. 6 shows the binding curves of various chitosugars at +100 mV/*cis*. Fitting the curves using a nonlinear regression function derived from Equation 1 yielded typical Michaelis-Menten plots (26). The plot for chitohexaose is hyperbolic, as described above, and saturation was reached within  $5 \mu\text{M}$  (Fig. 6, inset). On the other hand, the binding curves of chitotriose, chitotetraose, and chitopentaose did not approach saturation even at  $40 \mu\text{M}$ . Transformation of these binding curves yielded linear double reciprocal plots (Lineweaver-Burk plots) as shown in Fig. 7. Fig. 7A shows the Lineweaver-Burk plots for chitotriose, chitotetraose, and chitopentaose at +100 mV/*cis*, whereas Fig. 7B shows the Lineweaver-Burk plots for chitohexaose at +100 mV/*cis* compared with –100 mV/*cis*. These Lineweaver-Burk plots allowed the binding constants ( $K$ ) to be determined as shown in Table 1. As shown in Table 1, the binding constant of chitohexaose was

found to be larger than those of other chitosugars at both +100 and –100 mV. The value of  $K$  decreased by several orders of magnitude as the polymer length decreased from  $\text{GlcNAc}_6$  to  $\text{GlcNAc}_5$  and  $\text{GlcNAc}_4$ . Clearly, the greater binding affinity of the *VhChiP* channel for chitohexaose was under the –100 mV/*cis* condition ( $K = (5.0 \pm 0.068) \times 10^6 \text{ M}^{-1}$ ). These kinetic data consistently show chitohexaose to be the best substrate for the *VhChiP* channel.

## DISCUSSION

Marine vibrios require uptake of chitin breakdown products for survival under the critical condition of there being no alternative source of carbon and nitrogen. The chitin catabolic cascade of these bacteria is therefore expected to function efficiently. Once chitin-containing nutrients are detected by the bacteria, a series of events brings the chitinous materials into the cells and metabolizes them as an energy source. Chitin is initially broken down by secreted chitinases (27–29). During chitin degradation, the resulting products are therefore locally enriched in the vicinity of the cells, ready to be rapidly transported through the bacterial outer membrane. Small chitin units ( $\text{GlcNAc}$  and  $\text{GlcNAc}_2$ ) are thought to pass through a general diffusion porin, but permeation of larger chitin oligo-

### Kinetics of Sugar Translocation through Chitoporin

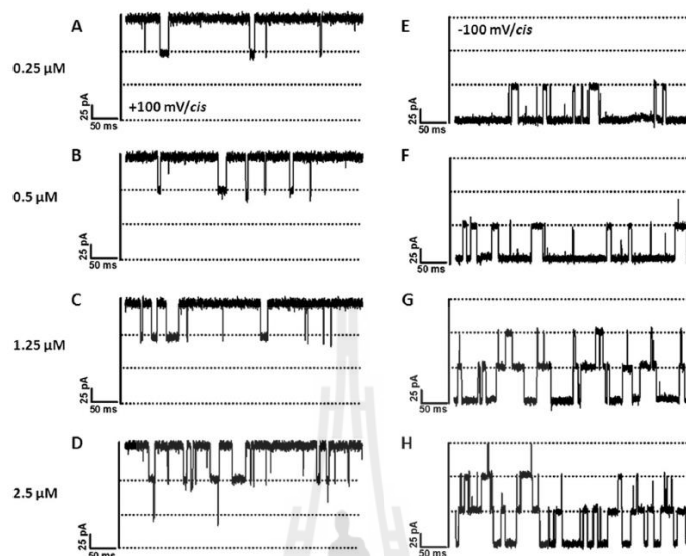


FIGURE 3. Effects of transmembrane potentials and sugar concentrations on ion currents. The fully open *VhChiP* trimeric channel was exposed to different concentrations of chitohexaose. Ion current blockages at +100 mV (A–D) and –100 mV (E–H) are shown. Here, we show the titration on the *cis* side.

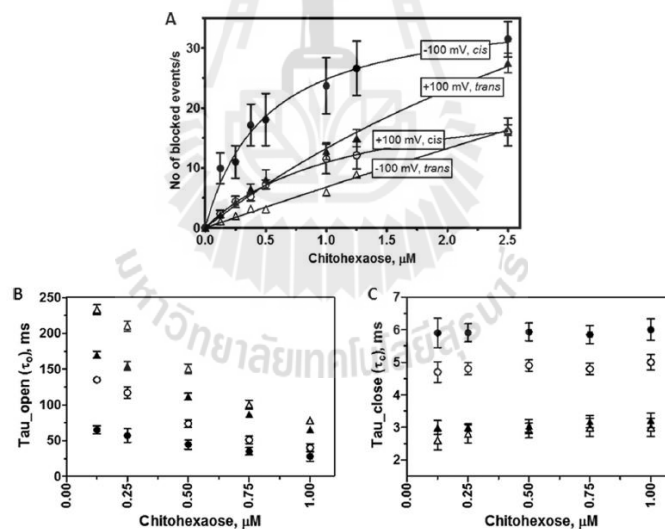


FIGURE 4. Analysis of ion current blockades at various transmembrane potentials and chitohexaose concentrations. A, plot of the number of binding events versus sugar concentrations, comparing +100 and –100 mV and *cis/trans* side potential application. B, plot of open times ( $\tau_{open}$ ) versus sugar concentrations. C, plot of residence times ( $\tau_{close}$ ) versus sugar concentrations. ●, –100 mV/*cis*; ○, +100 mV/*cis*; ▲, +100 mV/*trans*; △, –100 mV/*trans*.

saccharides is facilitated by specific channels, namely chitoporin (8, 30).

To resolve the uncertainty surrounding the function of chitoporin, we previously performed liposome swelling assays to demonstrate possible translocation of chitohexaose, but not

other non-chitooligosaccharides, through *VhChiP* (11). To quantify translocation, we employed the BLM reconstitution technique based on channel occlusion for ion current. When a *VhChiP* channel in the artificially formed membrane was exposed to various types of sugars, the channel responded only

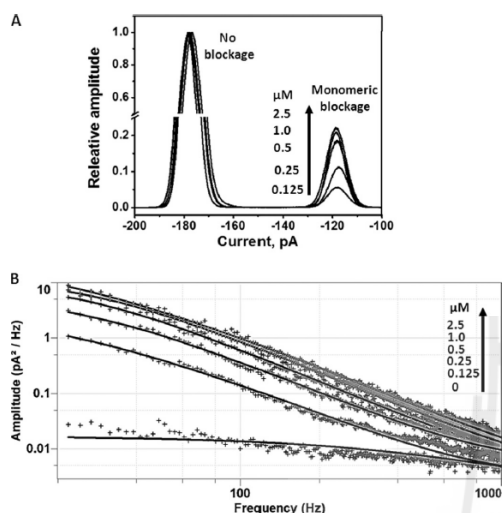


FIGURE 5. Concentration dependence of channel blockages. *A*, conductance histogram showing increased frequencies of monomeric blockages as chitoheptaose concentrations are increased. The monomeric blockages became steady when the sugar concentrations were above 1  $\mu\text{M}$ . *B*, power density spectra showing the effects of increasing concentrations of chitoheptaose on current noise levels. The spectra were fitted without control (the noise level at 0 M sugar) subtraction using the Lorentzian power 2 function available in Clampfit version 10.

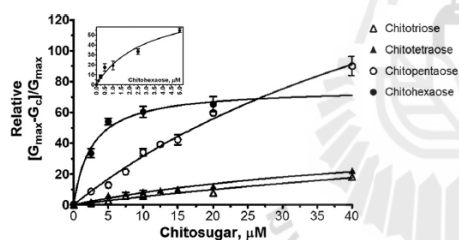


FIGURE 6. Binding of chitoheptaose to *VhChiP* compared with that of chitopentaose, chitotetraose, and chitotriose. The Michaelis-Menten plots were evaluated from the data acquired on the *cis* side at +100 mV. The values are averaged from the BLM data obtained in triplicate. The plots of  $(G_{\text{max}} - G_{\text{cis}})/G_{\text{max}}$  versus sugar concentrations (micromolar) were derived from Equation 1. The inset shows the plot for chitoheptaose at initial concentrations of 0–5  $\mu\text{M}$ .

to chitoooligosaccharides, with the degree of responsiveness increasing with greater chain length. The channel was most active with chitoheptaose, suggesting some channel specificity for this particular molecule. This observation was analogous to maltoporin-binding maltooligosaccharides, the most effective ligand for this channel being maltoheptaose (31, 32). Note that analysis of the sugar-induced blockages provides information on the presence of sugar in the channel with a residence time limit of 100  $\mu\text{s}$  of events/s. Faster events are not resolvable by this technique.

Regardless of the chain length, the probability of ion current blockade was greater with elevated concentrations of the chito-sugars. Fig. 8 represents selected current time traces showing

### Kinetics of Sugar Translocation through Chitoporin

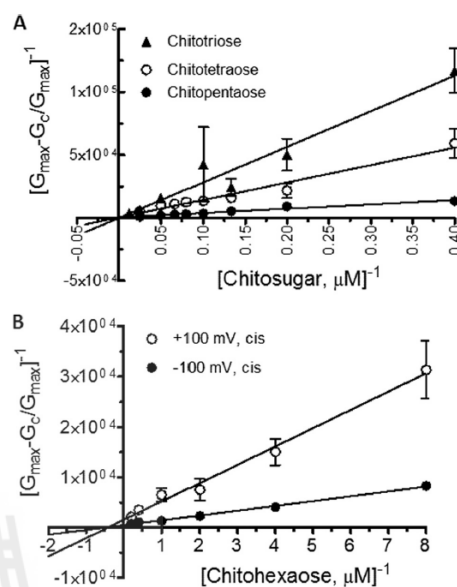


FIGURE 7. Lineweaver-Burk plots for different chitosugars. *A*, Lineweaver-Burk plots of chitotriose, chitotetraose, and chitopentaose at a concentration range of 2.5–40  $\mu\text{M}$ . The conditions for data analysis were +100 mV/*cis*. *B*, Lineweaver-Burk plots of chitoheptaose at +100 and –100 mV/*cis*. The equilibrium binding constant ( $K$ ) can be obtained directly by fitting the curves with a linear regression function as described under “Results.”

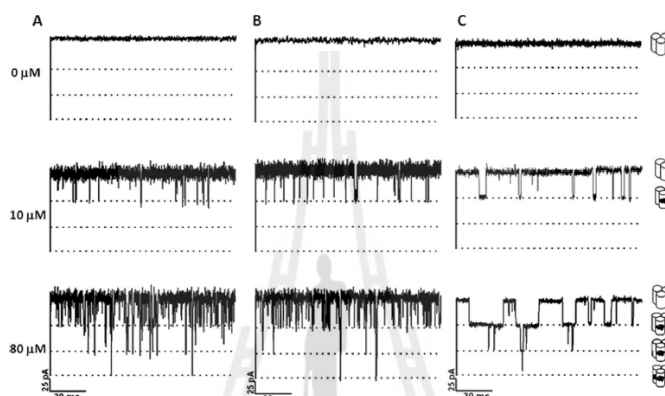
that, at 10  $\mu\text{M}$ , chitotriose (Fig. 8*A*), chitotetraose (Fig. 8*B*), and chitopentaose (Fig. 8*C*) blocked only the *VhChiP* monomer. The second and third subunits were subsequently blocked when the sugar concentration was raised to 80  $\mu\text{M}$ . The results suggest that *VhChiP* responded in a concentration-dependent manner not only toward chitoheptaose but also toward lower molecular weight chitosugars. However, much higher concentrations of these sugars were required to induce multiple blockages due to their poor affinity as shown in Table 1.

The rate of sugar interaction (Fig. 4*A*) with *VhChiP*, the residence time within the channel (Fig. 4*C*), and its binding affinity (Table 1) were found to be highly dependent on the polarity of the applied potential. Voltage-dependent sugar permeation through the *VhChiP* pore likely reflected transient dipole moments due to the existence of the *N*-acetamido (–NHCOCH<sub>3</sub>) groups of the multiple GlcNAc units that compose a chitoooligosaccharide chain. As a result, the sugar chains seem to orient themselves favorably for channel entrance with a negative potential on the *cis* side and an opposite potential on the other side. The much higher rate of sugar permeation from *cis*-to-*trans* over *trans*-to-*cis* clearly indicates intrinsic asymmetry of channel. In the case of maltoporin, channel asymmetry was also observed; however, the effect was opposite that seen with *VhChiP*. The frequency of sugar diffusion into maltoporin from *trans*-to-*cis* was found to be significantly higher than from *cis*-to-*trans* (17–19). Such results indicate that the molecular arrangement contributing to

## Kinetics of Sugar Translocation through Chitoporin

**TABLE 1**  
Substrate specificity of VhChiP

| Substrate     | +100 mV/cis                                       |   |   | −100 mV/cis                                       |   |   |
|---------------|---|---|---|---|---|---|
|               | Binding constant ( $K$ ) <sup>a</sup><br>$M^{-1}$ | On-rate constant ( $k_{on}$ )<br>$10^6 M^{-1} s^{-1}$ | Off-rate constant ( $k_{off}$ ) <sup>b</sup><br>$10^3 s^{-1}$ | Binding constant ( $K$ ) <sup>a</sup><br>$M^{-1}$ | On-rate constant ( $k_{on}$ )<br>$10^6 M^{-1} s^{-1}$ | Off-rate constant ( $k_{off}$ ) <sup>b</sup><br>$10^3 s^{-1}$ |
| Chitobiose    | ND <sup>c</sup>                                   |   |   | ND  |   |   |
| Chitotriose   | 220 ± 100   | 2.0 ± 0.2   | 9.0 ± 2.0   | 400 ± 150   | 5.0 ± 0.4   | 12.5 ± 2.5  |
| Chitotetraose | 2700 ± 700  | 10.0 ± 0.1  | 3.7 ± 0.11  | 5000 ± 850  | 15.2 ± 0.3  | 3.0 ± 0.40  |
| Chitopentaose | 15,000 ± 3000                                     | 25.5 ± 0.4  | 1.7 ± 0.13  |   |   |   |
| Chitohexaose  | 370,000 ± 140,000                                 | 78.0 ± 29.4   | 0.21 ± 0.02   | 500,000 ± 68,000                                  | 85.0 ± 1.4  | 0.17 ± 0.02   |

<sup>a</sup> The equilibrium binding constant ( $K$ ) was determined by the titration method according to Equation 1.<sup>b</sup> The on-rate constant ( $k_{on}$ ) was estimated from  $k_{on} = Kk_{off}$ . Because the residence time below 100  $\mu$ s could not be evaluated with confidence, we therefore estimated the  $k_{on}$  of chitotriose from the number of blocking events/s. The resultant off-rate constant, in this case, was cross-calculated from  $k_{off} = k_{on}/K$  instead.<sup>c</sup> ND, no detectable blocking events with this sugar.**FIGURE 8.** Effects of concentrations of small chitosugars on ion current blockages. A single channel of VhChiP was reconstituted into artificial lipid bilayers. Chitotriose (A), chitotetraose (B), and chitopentaose (C) were titrated on the *cis* side. Ion current blockages at +100 mV are presented.**TABLE 2**  
Comparison of the rates and the binding kinetics of VhChiP with those of other sugar-specific porins

| Channel type   | Substrate     | $K$<br>$M^{-1}$ | $k_{on}$<br>$10^6 M^{-1} s^{-1}$ | $k_{off}$<br>$10^3 s^{-1}$ | Ref.                     |
|--|---------------|-----------------|----------------------------------|----------------------------|--------------------------|
| VhChiP   | Chitohexaose  | 500,000         | 85.0                             | 0.17                       | This study               |
| <i>E. coli</i> maltoporin (LamB)                             | Maltotriose   | 4300            | 8.4                              | 1.95                       | Refs. 25, 33, 35, and 40 |
|  | Maltotetraose | 8100            | 6.1                              | 0.77                       |                          |
|  | Maltopentaose | 13,000          | 5.3                              | 0.43                       |                          |
|  | Maltohexaose  | 20,000          | 4.8                              | 0.24                       |                          |
|  | Maltoheptaose | 31,000          | 5.6                              | 0.18                       |                          |
| <i>Salmonella typhimurium</i> sucrose porin (ScrY)           | Sucrose       | 80              | 0.004                            | 0.05                       | Ref. 25                  |
| <i>Klebsiella oxytoca</i> cyclodextrin porin (CymA)          | Cyclodextrin  | 31,300          |                                  |                            | Ref. 38                  |
| <i>Pseudomonas putida</i> glucose-inducible porin (OprB)     | Glucose       | 9.1             |                                  |                            | Ref. 36                  |
| <i>Pseudomonas aeruginosa</i> glucose-inducible porin (OprB) | Glucose       | 2.6             |                                  |                            | Ref. 37                  |

GlcNAc-binding subsite(s) within the VhChiP lumen is completely different from that in maltoporin.

Kinetic analysis indicated that VhChiP interacted with chitooligosaccharides in a concentration-dependent manner. However, there is a discrepancy regarding the size of the sugars. On-rates increased almost linearly for chitotriose and chitotetraose as their concentrations were increased. Diffusion through the VhChiP channel in these cases was driven entirely by the concentration gradient, with weak interactions between the sugar and protein molecules. However, the binding affinity significantly increased if the sugar chain was longer. Binding of chitopentaose to chitoporin was of particular interest because the sugar did not just transiently block the ion passage but appeared to interact strongly with the channel subunits at −100

mV/cis, yielding a permanent reduction of the channel conductance to one-third of the full conductance when its concentrations exceeded 50 nM (see Fig. 2C as a representative trace at 5  $\mu$ M). As a result, we could not evaluate the binding constant of chitopentaose under this particular condition (Table 1). We do not yet completely understand why negative potentials strongly affect the permeation of chitopentaose. This will be a subject of our further investigation. Translocation of chitohexaose particularly involved specific substrate-protein interactions, resulting in Michaelis-Menten transport kinetics resembling those of previously reported sugar-specific porins, including maltoporin (LamB) (31–34), sucrose porin (ScrY) (25, 35), glucose-inducible porin (OprB) (36, 37), and cyclodextrin porin (CymA) (38, 39).

Our study revealed that chitohexaose is the most potent substrate of the *Vh*ChiP channel, as it blocked the ion flow even at nanomolar concentrations, and the monomeric subunit was already saturated below 1  $\mu\text{M}$ . In Table 2, we summarize the rate constants: the on-rate ( $k_{\text{on}}$ ) is by far the highest for chito-hexaose, whereas the off-rate ( $k_{\text{off}}$ ) is the lowest. Consequently, the resultant binding constant ( $K$ ) of  $5.0 \times 10^6 \text{ M}^{-1}$  is 1–5 orders stronger than the reported values for other analogs (25, 31, 35–40). According to the kinetic data in Table 2, *Vh*ChiP is the most active sugar-specific channel reported to date. A highly effective sugar transport machinery is considered to be crucial for *V. harveyi* to maintain the homeostatic balance that enables the bacterium to survive and thrive in extreme marine environments with a scarcity of the usual nutrients.

In conclusion, our quantification of the single channel turnover demonstrates the power of evolutionary pressure that drives marine bacteria (*V. harveyi* in our model study) to select for a highly active sugar-transporting system as a survival strategy in extreme aquatic environments. This mechanistic adaptation is not required by other bacteria that utilize glucose or sucrose as a common source of cellular energy.

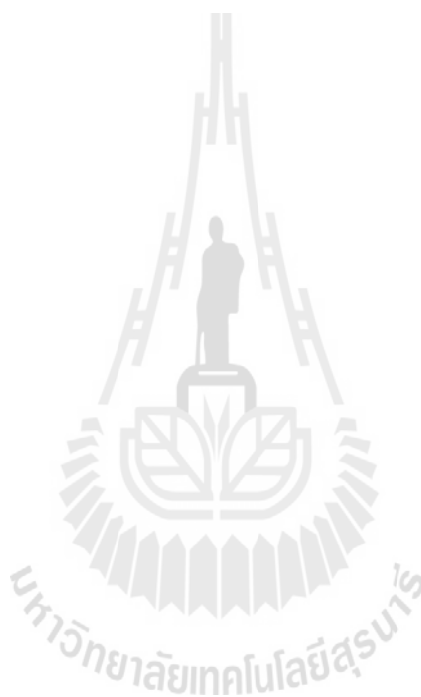
**Acknowledgment**—We thank Dr. David Apps (Centre for Integrative Physiology, School of Biomedical Sciences, The University of Edinburgh, Edinburgh, United Kingdom) for critical proofreading of this manuscript.

## REFERENCES

- Austin, B., and Zhang, X. H. (2006) *Vibrio harveyi*: a significant pathogen of marine vertebrates and invertebrates. *Lett. Appl. Microbiol.* 43, 119–124
- Liuxy, P. C., Lee, K. K., and Chen, S. N. (1996) Pathogenicity of different isolates of *Vibrio harveyi* in tiger shrimp, *Penaeus monodon*. *Lett. Appl. Microbiol.* 22, 413–416
- Actis, L. A., Tolmasky, M. E., and Crosa, J. H. (2011) *Vibriosis in Fish Diseases and Disorders: Viral, Bacterial and Fungal Infections* (Woo, P. T. K., and Bruno, D. W., eds) Vol. 3, 2nd Ed., pp. 570–605, CABI, Wallingford, United Kingdom
- Li, X., and Roseman, S. (2004) The chitinolytic cascade in vibrios is regulated by chitin oligosaccharides and a two-component chitin catabolic sensor/kinase. *Proc. Natl. Acad. Sci. U.S.A.* 101, 627–631
- Jung, B. O., Roseman, S., and Park, J. K. (2008) The central concept for chitin catabolic cascade in marine bacterium, *Vibrio*. *Macromol. Res.* 16, 1–15
- Hunt, D. E., Gevers, D., Vahora, N. M., and Polz, M. F. (2008) Conservation of the chitin utilization pathway in the Vibrionaceae. *Appl. Environ. Microbiol.* 74, 44–51
- Bassler, B. L., Yu, C., Lee, Y. C., and Roseman, S. (1991) Chitin utilization by marine bacteria. Degradation and catabolism of chitin oligosaccharides by *Vibrio furnissii*. *J. Biol. Chem.* 266, 24276–24286
- Keyhani, N. O., Li, X. B., and Roseman, S. (2000) Chitin catabolism in the marine bacterium *Vibrio furnissii*. Identification and molecular cloning of a chitoporin. *J. Biol. Chem.* 275, 33068–33076
- Meibom, K. L., Li, X. B., Nielsen, A. T., Wu, C. Y., Roseman, S., and Schoolnik, G. K. (2004) The *Vibrio cholerae* chitin utilization program. *Proc. Natl. Acad. Sci. U.S.A.* 101, 2524–2529
- Yang, C., Rodionov, D. A., Li, X., Laikova, O. N., Gelfand, M. S., Zagnitko, O. P., Romine, M. F., Obratsova, A. Y., Nealon, K. H., and Osterman, A. L. (2006) Comparative genomics and experimental characterization of *N*-acetylglucosamine utilization pathway of *Shewanella oneidensis*. *J. Biol. Chem.* 281, 29872–29885
- Suginta, W., Chumjan, W., Mahendran, K. R., Janning, P., Schulte, A., and Winterhalter, M. (2013) Molecular uptake of chito oligosaccharides through chitoporin from the marine bacterium *Vibrio harveyi*. *PLoS ONE* 8, e55126
- Prilipov, A., Phale, P. S., Van Gelder, P., Rosenbusch, J. P., and Koebnik, R. (1998) Coupling site-directed mutagenesis with high-level expression: large scale production of mutant porins from *E. coli*. *FEMS Microbiol. Lett.* 163, 65–72
- Garavito, R. M., and Rosenbusch, J. P. (1986) Isolation and crystallization of bacterial porin. *Methods Enzymol.* 125, 309–328
- Rosenbusch, J. P. (1974) Characterization of the major envelope protein from *Escherichia coli*. Regular arrangement on the peptidoglycan and unusual dodecyl sulfate binding. *J. Biol. Chem.* 249, 8019–8029
- Lugtenberg, B., and Van Alphen, L. (1983) Molecular architecture and functioning of the outer membrane of *Escherichia coli* and other gram-negative bacteria. *Biochim. Biophys. Acta* 737, 51–115
- Bezrukov, S. M., Kullman, L., and Winterhalter, M. (2000) Probing sugar translocation through maltoporin at the single channel level. *FEBS Lett.* 476, 224–228
- Schwarz, G., Danelon, C., and Winterhalter, M. (2003) On translocation through a membrane channel via an internal binding site: kinetics and voltage dependence. *Biophys. J.* 84, 2990–2998
- Danelon, C., Brando, T., and Winterhalter, M. (2003) Probing the orientation of reconstituted maltoporin channels at the single-protein level. *J. Biol. Chem.* 278, 35542–35551
- Kullman, L., Winterhalter, M., and Bezrukov, S. M. (2002) Transport of maltodextrins through maltoporin: a single-channel study. *Biophys. J.* 82, 803–812
- Mahendran, K. R., Chimere, C., Mach, T., and Winterhalter, M. (2009) Antibiotic translocation through membrane channels: temperature-dependent ion current fluctuation for catching the fast events. *Eur. Biophys. J.* 38, 1141–1145
- Van Gelder, P., Dumas, F., and Winterhalter, M. (2000) Understanding the function of bacterial outer membrane channels by reconstitution into black lipid membranes. *Biophys. Chem.* 85, 153–167
- Winterhalter, M. (2000) Black lipid membranes. *Curr. Opin. Colloid Interface Sci.* 5, 250–255
- Berkane, E., Orlik, F., Charbit, A., Danelon, C., Fournier, D., Benz, R., and Winterhalter, M. (2005) Nanopores: maltoporin channel as a sensor for maltodextrin and lambda-phage. *J. Nanobiotech.* 3, 3
- Benz, R., and Hancock, R. E. (1987) Mechanism of ion transport through the anion-selective channel of the *Pseudomonas aeruginosa* outer membrane. *J. Gen. Physiol.* 89, 275–295
- Andersen, C., Cseh, R., Schüle, K., and Benz, R. (1998) Study of sugar binding to the sucrose-specific ScRY channel of enteric bacteria using current noise analysis. *J. Membr. Biol.* 164, 263–274
- Nikaido, H. (1992) Porins and specific channels of bacterial outer membranes. *Mol. Microbiol.* 6, 435–442
- Suginta, W., Robertson, P. A., Austin, B., Fry, S. C., and Fothergill-Gilmore, L. A. (2000) Chitinases from *Vibrio*: activity screening and purification of *chiA* from *Vibrio carchariae*. *J. Appl. Microbiol.* 89, 76–84
- Suginta, W. (2007) Identification of chitin binding proteins and characterization of two chitinase isoforms from *Vibrio alginolyticus* 283. *Enzyme Microb. Technol.* 41, 212–220
- Keyhani, N. O., and Roseman, S. (1999) Physiological aspects of chitin catabolism in marine bacteria. *Biochim. Biophys. Acta* 1473, 108–122
- Hjerde, E., Lorentzen, M. S., Holden, M. T., Seeger, K., Paulsen, S., Bason, N., Churcher, C., Harris, D., Norbertczak, H., Quail, M. A., Sanders, S., Thurston, S., Parkhill, J., Willassen, N. P., and Thomson, N. R. (2008) The genome sequence of the fish pathogen *Aliivibrio salmonicida* strain LFI1238 shows extensive evidence of gene decay. *BMC Genomics* 9, 616
- Andersen, C., Jorby, M., and Benz, R. (1995) Evaluation of the rate constants of sugar transport through maltoporin (LamB) of *E. coli* from the sugar-induced current noise. *J. Gen. Physiol.* 105, 385–401
- Benz, R., Schmid, A., Nakae, T., and Vos-Scheperkeuter, G. H. (1986) Pore formation by LamB of *Escherichia coli* in lipid bilayer membranes. *J. Bacteriol.* 165, 978–986
- Van Gelder, P., Dumas, F., Bartoldus, I., Saint, N., Prilipov, A., Winterhal-

### Kinetics of Sugar Translocation through Chitoporin

- ter, M., Wang, Y., Philippsen, A., Rosenbusch, J. P., and Schirmer, T. (2002) Sugar transport through maltoporin of *Escherichia coli*: role of the greasy slide. *J. Bacteriol.* **184**, 2994–2999
34. Klebba, P. E. (2002) Mechanism of maltodextrin transport through LamB. *Res. Microbiol.* **153**, 417–424
35. Van Gelder, P., Dutzler, R., Dumas, F., Koebnik, R., and Schirmer, T. (2001) Sucrose transport through maltoporin mutants of *Escherichia coli*. *Protein Eng.* **14**, 943–948
36. Saravolac, E. G., Taylor, N. F., Benz, R., and Hancock, R. E. (1991) Purification of glucose-inducible outer membrane protein OprB of *Pseudomonas putida* and reconstitution of glucose-specific pores. *J. Bacteriol.* **173**, 4970–4976
37. Wylie, J. L., Bernegger-Egli, C., O'Neil, J. D., and Worobec, E. A. (1993) Biophysical characterization of OprB, a glucose-inducible porin of *Pseudomonas aeruginosa*. *J. Bioenerg. Biomembr.* **25**, 547–556
38. Pajatsch, M., Andersen, C., Mathes, A., Böck, A., Benz, R., and Engelhardt, H. (1999) Properties of a cyclodextrin-specific, unusual porin from *Klebsiella oxytoca*. *J. Biol. Chem.* **274**, 25159–25166
39. Orlik, F., Andersen, C., Danelon, C., Winterhalter, M., Pajatsch, M., Böck, A., and Benz, R. (2003) CymA of *Klebsiella oxytoca* outer membrane: binding of cyclodextrins and study of the current noise of the open channel. *Biophys. J.* **85**, 876–885
40. Hilty, C., and Winterhalter, M. (2001) Facilitated substrate transport through membrane proteins. *Phys. Rev. Lett.* **86**, 5624–5627



# CURRICULUM VITAE

**Name:** Watcharin Chumjan  
**Status:** Ph. D. Student in Biochemistry  
**Birthday:** 22<sup>nd</sup> September 1985  
**Place of Birth:** Sisaket, Thailand  
**Nationality:** Thai

## **Educations:**

- Academic year 2004, High school graduation  
Muangkhan Wittayakhom School, Sisaket, 33160
- Academic year 2007 B.Sc. (Chemistry)  
Valaya Alongkorn Rajabhat University, Pathumthani, GPA 3.57
- Academic year 2011, Start as Ph.D. student  
Schools of Chemistry and Biochemistry, Institute of Science, Suranaree  
University of Technology, Nakhon Ratchasima

## **Awards and Scholarships**

1. Commission of Higher Education, Ministry of University Affairs (MUA)  
through a Ph.D. sandwich scholarship program, Thailand, 2008-2011.
2. Deutscher Akademischer Austausch Dienst e.V. German Academic Exchange  
Service (DAAD scholarship), Germany, October 2013-Dezember 2014.